REFERENCE ONLY

UNIVERSITY OF LONDON THESIS

Degree PhD Year 2006 Name of Author FERREIRA, C. C.

UNIVERSITY COLLEGE LONDON

DEPARTMENT OF MECHANICAL ENGINEERING

MODELLING AND REAL-TIME SIMULATION OF AN ADVANCED MARINE FULL-ELECTRICAL PROPULSION SYSTEM

Author: César Leal Ferreira

Supervisor: Dr. Richard W. G. Bucknall

Degree: Doctor of Philosophy (PhD)

London, March 2006

ProQuest LLC
789 East Eisenhower Parkway
P.O. Box 1346
Ann Arbor, MI 48106-1346

Declaration

I declare that the work presented in this thesis is my own and the work of other persons is appropriately acknowledged.

César Leal Ferreira

ABSTRACT

Modelling and Real-Time Simulation of an Advanced Marine Full-Electrical Propulsion System

After being consolidated as the preferred propulsion system for cruise ships, integrated full electrical propulsion (IFEP) is now being considered as the natural choice for the future warship vessels. The United States and the United Kingdom are developing parallel projects in order to gain broad knowledge of this new propulsion technology.

The Royal Navy's Type 45 Destroyer, due to enter into service in 2007, will set the course by development and acquisition of practical experience for the Future Surface Combatant Ship (FSC) and the Future Aircraft Carrier (CVF) programmes, both envisaging the use of integrated full-electrical propulsion.

One main step towards this new technology is the computational simulation of each independent component and of the system as a whole, to de-risk and refine the design.

The present project aims to develop a computational model of an advanced marine integrated full-electrical propulsion system such as the one being proposed for the Royal Navy's Type 45 Destroyer.

The main focus is the development of new advanced electrical equipment models, which are the building blocks of the propulsion system, to be integrated with some existing models from various earlier investigations, to achieve an Integrated Full Electric Propulsion System Model.

Two particular aspects of this work are:

- The construction of an algorithm for the 15-phase induction motor capable of processing the resulting currents at the machine more precisely than the traditional *dq*-algorithms, taking into account eventual unbalances and faults in the voltage supply;
- The development of a Direct Torque and Flux Control algorithm for the 15-phase system, capable of maintaining the stability of the induction motor under severe transients, such as the crash-stop manoeuvring situation.

The work concludes by assessing the performance of the proposed advanced marine propulsion system predicting its likely behaviour across a number of important scenarios.

Table of Contents:

List of Figures

List of Tables

Nomenclature

In order of appearance in text:

i_{as}, i_{bs} and i_{cs}	instantaneous currents in the stator phases
v_{as}, v_{bs} and v_{cs}	instantaneous voltages in the stator phases
λ_{as}, λ_{bs} and λ_{cs}	instantaneous flux linkages in the stator phases
$\underline{\mathbf{i}}_s$	complex stator current vector
$i_{\alpha s}$ and $i_{\beta s}$	instantaneous currents transformed to the $\alpha\beta$ reference frame
I_m	magnitude of the phase currents
i_{ds} and i_{qs}	instantaneous currents transformed to the dq reference frame
$\mathbf{i}_{dqs}$	complex stator current vector represented in the dq reference frame
i_{0s}	zero-sequence current component
v_{ds}, v_{qs} and v_{0s}	instantaneous voltages at the stator transformed to the dq reference frame
v'_{dr}, v'_{qr} and v'_{0r}	instantaneous voltages at the rotor referred to the stator transformed to the dq reference frame
λ_{ds}, λ_{qs} and λ_{0s}	instantaneous flux linkages at the stator transformed to the dq reference frame
λ'_{dr}, λ'_{qr} and λ'_{0r}	instantaneous flux linkages at the rotor referred to the stator transformed to the dq reference frame
ϕ	flux linkage
T_{em}	electromagnetic torque
P	number of poles
p	number of pair of poles

θ	instantaneous rotor position (rad)
ω	instantaneous rotor speed (rad/sec)
ω_b	rated frequency of the system (rad/sec)
x_{ls}	stator leakage reactance
x_{lr}	rotor leakage reactance
x_m	mutual leakage reactance
l_{ls}	stator leakage inductance
l_{lr}	rotor leakage inductance
l_m	mutual leakage inductance
$V_{line\text{-}line}$	voltage measured between lines
$V_{line\text{-}neutral}$	voltage measured between line and neutral
rms	root mean square
r_s	stator resistance
h	width of hysteresis band

1.0 CHAPTER ONE – Introduction

1.1 Motivation

It was announced in November 2000 that the recently ordered Type 45 Daring Class Destroyers for the Royal Navy, due enter service in 2007, will be fitted with an Integrated Electric Propulsion (IEP) system. The Type 45's power and propulsion system will simultaneously provide the means to propel the ship and power the ship's services. The system will be a development on from that used in the Albion Class Landing Platform Docks, although probably still less sophisticated than the Integrated Full Electric Propulsion (IFEP) system planned for the Future Surface Combatant and Future Aircraft Carrier.

On the other side of the Atlantic Ocean, the American Integrated Power System (IPS) project takes a parallel course. The new generation of warships for the US Navy (New Amphibious Assault Ship Multi-Purpose LHD8, Multi-Mission Surface Combatant Ship DD(X), Future Aircraft Carrier CVNX and the New Attack Submarine Virginia Class) will form the basis of the "Electric Naval Force", based on the new technologies of electric propulsion [1].

In reality, IFEP is not simply being considered as a result of the natural evolution of propulsive technologies already in use, as the case of submarines and CODLAG ships (combined diesel-electric and gas turbine). In the existent technologies the electric system is mostly restricted to the machinery space, working together with mechanics, hydraulics, pneumatics and other equipments. The IFEP concept 'electrifies' the whole ship: propulsion and services, command and control, weapons and sensors, the concept suggests that the ship as a whole would be electric.

IFEP will impact on the composition and structure of the naval fleet. So it is being treated as one of the largest revolutions since the development of nuclear propulsion. The consequences of its implementation will be reflected in the design, manufacture, support and in the operational area, with the adoption of new philosophies to allow the full exploitation of the advantages provided by this kind of propulsion.

The investments on both sides of the Atlantic Ocean are significant because the expected benefits of this new technology are extremely promising. The main benefits are [2]:

- Reduced life cycle costs through

  - more efficient propulsion and electric power plant, reducing operational and maintenance costs;

  - improved reliability;

  - increased automation leading to reduced manning;

  - design flexibility causing reduced total acquisition cost.

- Improved survivability through

  - inherent modularity, which provides for redundant, distributed, reconfigurable power and propulsion systems;

  - signature reduction.

- Improved flexibility for upgrades over life (~ 50 years) by allowing

  - future installation of advanced weapons systems;

  - future propulsion system upgrades.

The modelling and simulation of equipment and system is a trend in the analysis and de-risking of this new technology. The functionality of the models allows assessment of dynamic performance, system transients, external impacts and bounds of operation [3]. Ultimately the modelling and simulation of the IFEP can provide technical knowledge to allow this novel technology to be applied in a shorter time frame with better control of the potentialities and risks involved.

1.2 Aim of the Investigation

The aim of this project is to develop a computer based System Model loosely based on the proposed Type 45 propulsion system using appropriate software modelling packages such as MATLAB/SIMULINK SimPowerSystems and High Level Languages such as VISUAL FORTRAN.

Some sub-System Models are already in existence such as the WR21 ICR gas turbine, propeller and ship from earlier modelling studies making it possible to avoid the need to model some components from fundamentals.

Having defined the aim it is possible to identify the objectives:

- To consider the Software and Hardware needs in order to choose the more adequate package to be used;
- To develop and validate an Advanced Induction Motor model having 15 phases;
- To develop and validate an PWM Converter with 15 phases arranged in three channels, comprising rectifier, DC link, inverter and dynamic braking resistance;
- To establish a control strategy in order to investigate the performance of each control method;
- To develop and validate the model algorithms;
- To assess and adapt the existing models of the GTA (Gas Turbine Alternator), governor, AVR (Automatic Voltage Regulator), Propeller and Ship to allow integration with the new developed models;
- To develop and validate an integrated System Model comprising all the component models;
- To analyse issues of stability and torque pulsations in the motor drive chain;
- To analyse issues for different operating scenarios (steady-state, transient and faulted operation);
- To draw conclusions and make recommendations about the way forward for the improvement of the resulting System Model;
- To briefly consider (having into perspective the limitations of the System Model) the probable difficulties that will arise during the implementation of an actual IFEP design.

1.3 Background – Setting the Scene

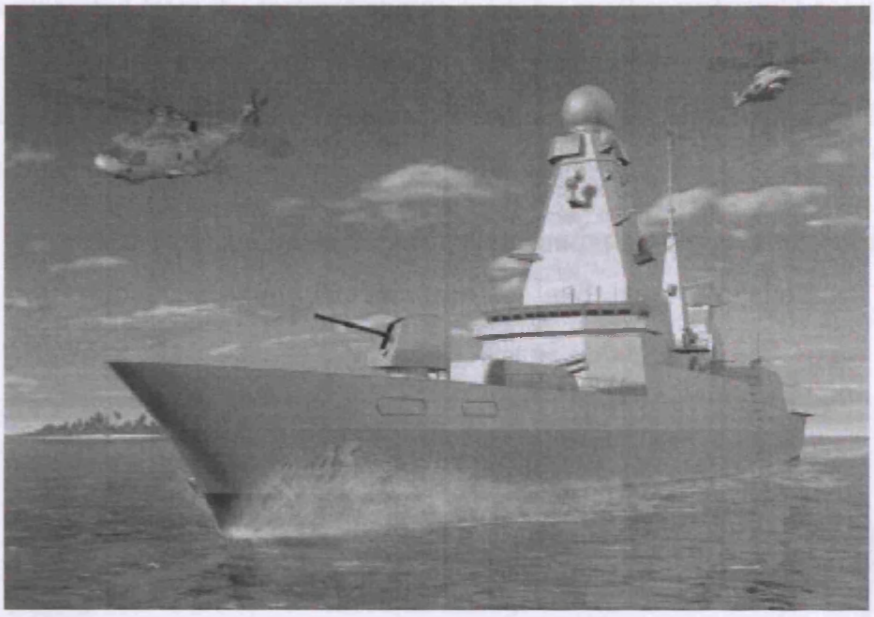

Figure 1: Destroyer Type 45 [4]

The Type 45 Destroyers will have a two-unit twin-shaft configuration, each unit having a Rolls Royce/Northrop Grumman WR-21 ICR gas turbine generator and alternator unit in the forward engine room and a 20MW electric induction motor in the aft engine room.

The fuel-efficient WR-21 Intercooled Recuperated (ICR) marine gas turbine is based upon Rolls Royce's Trent family of commercial aircraft engines, and is the culmination of a nine-year, £300 million development programme funded by the US, British and French navies. Each gas turbine, rated at 25 MW, powers a 21 MW synchronous alternator. Together with two 2 MW diesel generators they will occupy the forward engine room compartment.

ALSTOM Power Conversion had been selected to supply the remainder of the integrated electric power/propulsion system architecture, with the order for the equipment for an initial three ships expected to be worth around £40 million. The scope of supply includes 20 MW advanced induction motors, commercially-based Pulse Width Modulated Converter drives with three five-channel banks, 20 MW alternators, 2 MW diesel generators, ships service transformers, and the power system controls.

Most of the equipment will be in the aft engine room compartment, which is separated from the forward engine room by another watertight compartment to reduce vulnerability from battle damage. The prime units in the aft compartment will be two advanced induction motors each generating 20 MW with a Pulse Width Modulated Converter drive arranged in three five-channel banks.

ALSTOM will also be providing the high voltage switchboard, ship services transformer, dynamic braking resistor and High Voltage/Low Voltage harmonic filters.

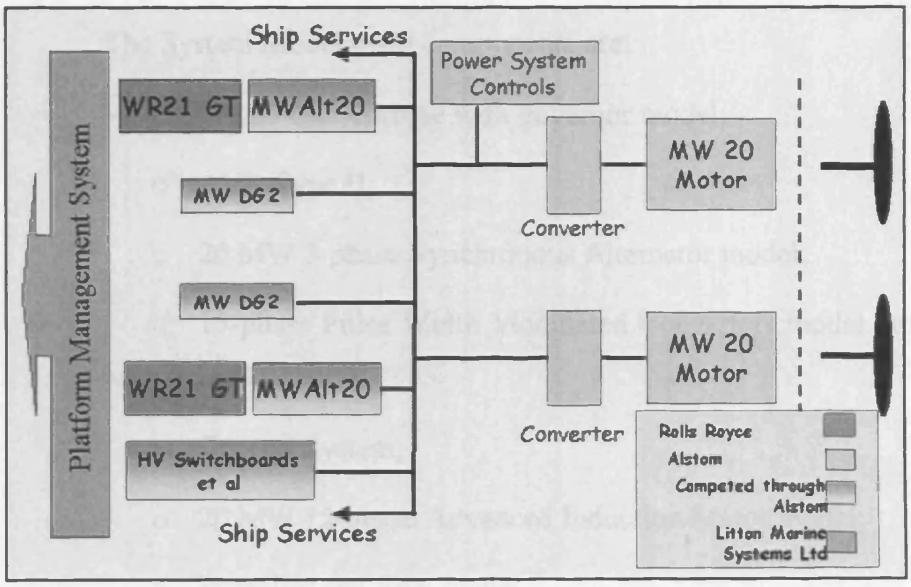

Figure 2: Type 45 – Simplified Line Diagram [5]

1.4 Structure of the Thesis – Preview of the Chapters

Regardless of the software and hardware used for simulation of a system, the simulation process will have the following steps:

1. Definition of a simplified model of the system (flow chart for example);
2. Production of mathematical descriptions of each component of the system, development and validation of subsystem models;
3. Combination of all individual subsystems and subsequent validation of the resulting complete System Model, setting up all physical parameters;

4. Running the System Model to obtain numeric results; and

5. Analysis of results.

The fidelity [6] is an important issue to be considered in large scale system modelling. One must have in mind the purpose to which the results are to be put, before deciding on an appropriate level of fidelity for individual components. An inappropriate choice may lead either to misleading output from the System Model, or to an extended execution time with no real benefit in terms of information content of the results.

The System Model main components are:

- WR21 Gas Turbine with governor model;
- AVR Type II;
- 20 MW 3-phase Synchronous Alternator model;
- 15-phase Pulse Width Modulated Converters model (arranged in Channels);
- Control System;
- 20 MW 15-phase Advanced Induction Motor model;
- Propeller and Ship model.

The models of the WR21 Gas Turbine with Alternator, Propeller and Ship are already available from previous works [7]. This project will focus primarily on the modelling of the Advanced Induction Motor, PWM Converter and Control System, followed by the construction of an integrated System Model combining the available subsystems.

The flow chart of figure 3 shows a simplified approach of the modelling procedure implemented for one propulsion line. Note that the lines connecting the Alternator, Converter Channels and Induction Motor have arrows in both ends (even though it is not an adequate symbol in a flow chart) depicting electrical connections, where currents can flow in both directions.

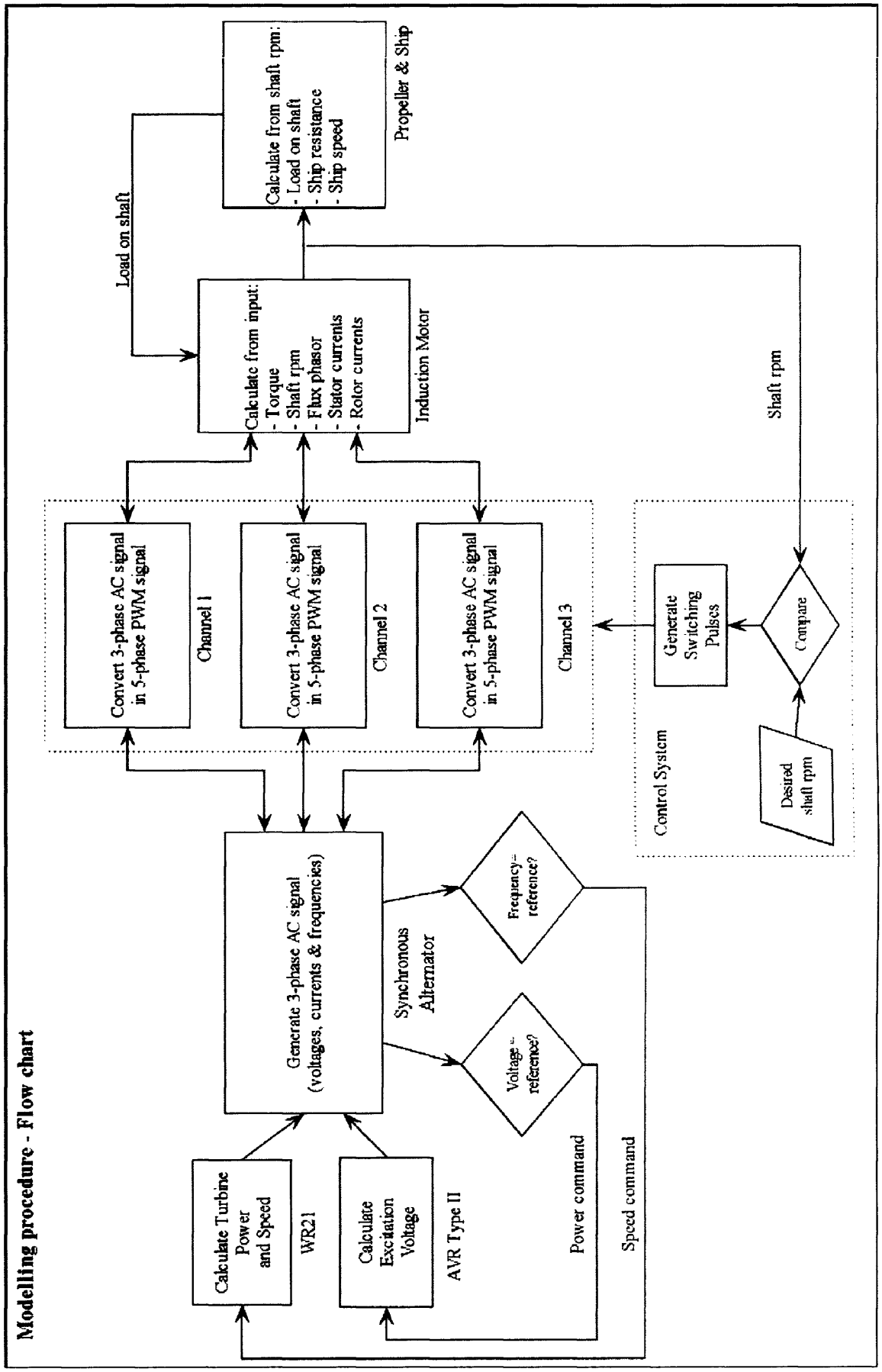

Figure 3: Modelling procedure – flow chart

The strategy to accomplish the proposed System Model, following the steps 2 to 5 (mentioned before) will be discussed in the next Chapters, as follows:

- In Chapter Two considerations are made about the simulation Software and Hardware, in order to choose the more adequate package to be used in the development of the project, considering a range of available options, and using a decision matrix process;
- In Chapter Three a 15-phase Advanced Induction Motor model is developed and validated, by assessing theory, choosing reference frame and algorithm;
- In Chapter Four a PWM Converter with 15 phases is developed and validated; the Converter is to be arranged in three channels, comprising rectifier, DC link, inverter and braking resistance;
- In Chapter Five a control strategy is defined, a control method is chosen and an algorithm based on the choice is developed and validated;
- In Chapter Six the existing subsystem models of the AVR, Gas Turbine with governor, Propeller and Ship are assessed and adapted, if necessary, to allow integration with the created new models;
- In Chapter Seven an integrated System Model is put together comprising all the subsystem models (existing and new ones); issues of stability and torque pulsation are analysed, and means to reduce torque ripples increasing system stability are proposed;
- In Chapter Eight the results of running the System Model simulation under different scenarios, in steady-state, transient and faulted operation, are presented and analysed;
- Finally, in Chapter Nine, general conclusions are presented, assessing the benefits of the project; considerations are made about probable difficulties that will arise during the implementation of an actual IFEP design and recommendations are proposed, about the way forward for the future improvements of the System Model.

2.0 CHAPTER TWO – Simulation Software and Hardware

2.1 Introduction

The technology used for simulation has changed significantly over the years. The objective of this introduction is to give a brief historic overview on this evolution. The first simulators were Analog devices, based on ordinary differential equations and block diagrams. The idea was to model a system in terms of ordinary differential equations and then make a physical device (using, for example, gear boxes and cams) that obeys the equations. The physical system was initialized with proper initial values and its development over time would mimic the system of interest. The simulation of an ordinary differential equation could be accomplished by using integrators and function generators [8].

The development of digital computers has led to a different approach to simulation. There are basically two different methods to perform those numerical solutions, one using Ordinary Differential Equations and the other using Differential Algebraic Equations [8].

In Ordinary Differential Equations the unknown element is a function, rather than a number, in which the known information relates that function to its derivatives. Frequently algebraic constraints have to be considered in the differential equation, the resulting system being called Differential Algebraic Equations. These methods were well known when digital simulators emerged in the 1960s, even so this new application prompted research in this particular field of numerical mathematics [8].

By 1967 there were more than 23 different simulation programs available. A system could basically be described in three different ways: by interconnection of blocks (as in MIDAS and DYNASAR); by mathematic expressions (as in MIMIC and DSL/90); and by conventional programming construct (as in FORTRAN and PASCAL).

Prototype graphical environments were designed in the mid 1970s using a cathode ray tube and light pen for drawing block diagrams. However, graphical modelling was not widely used until modern workstations and PCs with raster graphics became generally available.

The matrix environments MATLAB and MATRIX X, which appeared in the 1980s, were provided with modelling tools. SystemBuild, which was integrated with MATRIX X, appeared in 1984. SIMULINK, originally named SIMULAB I, which was integrated with MATLAB, appeared in 1991. A new PC based system VisSim appeared in 1990. The ACSL Graphics Modeller was introduced in 1993.

The analog-computing paradigm, which is requirement of explicit state models, is a fundamental limitation of block diagram modelling. The blocks have a unidirectional data flow from inputs to outputs. As a consequence it is not a simple task to build model libraries using only block diagram languages.

It is possible to design modelling environments that are very user friendly by restricting the domain of the models. A large number of tools of this type have been developed in several branches of engineering. A model can be assembled simply by connecting components from predefined libraries. The idea is to relieve the user from model development by providing ready-made models or model components, which can be assembled to a complete system model.

SIMPLORER[9] is an example of simulation and design package specific for power electronics and drive technology. 'Ansoft' released the version 4.0, with integral graphical interface and electric machine libraries, in 1998. SIMPLORER links to various tools, such as MATLAB/SIMULINK. It has power devices, standard electronic components and function blocks (including common structures for rectifiers and inverters, supplies and loads, control elements, motor and transformer models).

MODELICA[10], based on Dynamic Modelling Language (DYMOLA), is another software intended for modelling within many application domains such as electrical circuits, multi-body systems, drive trains, hydraulics, thermodynamic systems, chemical processes etc. With its version 1.0 finished in September 1997, it was based on physical modelling procedure (each subsystem is modelled by balances of mass, energy and momentum and material equations), and supports several formalisms: ordinary differential equations, differential-algebraic equations, bond graphs, finite state automata, and Petri nets.

Power System Blockset (recently renamed SimPowerSystems) [11] is another example of simulation package. Developed by Hydro-Quebec Research Institute and Mathworks, the version 1.0 was released in 1998. It was intended to provide a design tool that allows scientists and engineers to build models that simulate power systems using the Simulink environment, allowing a model to be built using click and drag procedures. Since Simulink uses MATLAB as the computational engine, the designer can also use its other toolboxes in the project.

2.2 Requirements of the Simulation Package

The list of desirable characteristics of the simulation package (software and hardware) can be summarized in two items: low cost and high practicality. Considering that this project has limited funds, the cost (or availability) will be a decisive factor. However, in order to allow a more comprehensive overview of the available options, especially in the software market, a more detailed assessment for selection will be followed, and a wider range of criteria considered, as follows:

a. Availability of software;

b. Availability of bibliographic reference;

c. Availability of add-ons for real-time simulation;

d. Practicality;

e. Algorithm; and

f. Previous works related with ship propulsion.

2.3 Hardware Requirement

The natural choice for a simulation problem today is the use of digital computers, due to the current state of the art, flexibility and simplicity offered by these equipments.

The PC platforms are widespread, and today it is cheap to purchase a PC with high speed processor and proper memory size, necessary to cope with the high amount of data involved in a simulation with a low/medium level of detailing. For more advance level of complexity, which generates massive amount of data

handling, there are possible hardware upgrades to the PC platform, which allow parallel processing.

Since the hardware platform adopted will be the PC, it constrains the range of simulation software available although there are many PC based options. It will be necessary to methodically search, evaluate and decide the best software environment to perform simulations using a PC platform.

2.4 Software Selection

Software for specific domain is very easy to use if the problem fits the tool directly. It is however often very difficult to modify the tools and add new features, therefore it is necessary to choose a package that allows creation of custom made blocks but also permits the calling of external executable files, in order to enable the creation and compiling of subroutines in FORTRAN or C++ for example.

At this point it is necessary to choose the software that will be used, to allow the performing of the next steps in this work. The options are many, but a comparison will be carried out between Simplorer, SimPowerSystems and Modelica, which are the ones having more references in technical literature and better availability.

A decision analysis tool (weighted matrixes) is employed to support the selection process. It is important to qualify this as a tool used in support of the analysis and decision making process, not as a replacement for it.

The technical expertise and professional experience of a design team and their resources are the more important bases to achieve a final decision. A proper assessment only could be carried out by a user or a team with reasonable experience in such environments. Since it is currently not possible regarding this work, the weighted decision matrix will be used.

The first step in the decision-making process using weighted matrix is the adoption of a selection criteria. They are, from the more to the less important:

a. Availability of software:

MATLAB/Simulink with SimPowerSystems toolbox was already available at the Department of Mechanical Engineering

(University College London); Simplorer and Modelica both have demonstration versions available through the Internet.

b. Availability of bibliographic reference:

The following result was obtained using the search mechanism "Google" to find Internet pages in English with the described key words, in October 28th, 2002:

- "Power System Blockset" (old name of SimPowerSystems) – 1180 pages;
- "Simplorer" – 1640 pages; and
- "Modelica" – 2520 pages.

Searching the virtual bookshop "Amazon" it was found one book about Modelica, and no books specifically about SimPowerSystems or Simplorer.

There were 3820 pages found with the key words "Simulink; Electric; Simulation" and one book specifically about modelling of electric systems using Simulink, which is the background of SimPowerSystems.

c. Availability of add-ons for real-time simulation:

The speed of simulation is an important issue; since comparison between performances of each software alone is not available at the moment, other criteria have to be analysed, which is the availability of add-ons (hardware and software) to accelerate the processing speed.

Since Simulink is a very popular tool for simulation, there are a number of resources to cut down its running time.

d. Practicality:

All three software have graphic interfaces, drag-and-drop feature, library of electric components, etc. Despite the lack of practical experience (at the moment this assessment was made) they all seemed to be equally user friendly.

e. Algorithm:

Modelica is the one with the most modern algorithm, based on physical modelling procedure. It allows a highly realistic approach of simulation and allows more "fashionable" formalisms, as the bond graph for example.

f. Previous works in the same field:

Mathworks, the developers of SimPowerSystems, is working together with the British Ministry of Defence[12], through a consultancy contract, to develop and validate mathematical models of electrical system and propulsion for the next generation of warships; there is no news of similar work being done among the other software developers.

At this point it is possible to build a decision-making matrix:

	Weight	Simplorer	Simplorer weighted	SPS	SPS weighted	Modelica	Modelica weighted
Software	10.0	8.0	80.0	10.0	100.0	8.0	80.0
Documentation	10.0	6.5	65.0	7.0	70.0	10.0	100.0
Add-ons	8.0	6.0	48.0	10.0	80.0	6.0	48.0
Practicality	8.0	10.0	80.0	10.0	80.0	10.0	80.0
Algorithm	6.0	6.0	36.0	6.0	36.0	10.0	60.0
Previous works in the same field	5.0	5.0	25.0	10.0	50.0	5.0	25.0
Total			**334.0**		**416.0**		**393.0**

Table 1: Software choice matrix

The final result favours SimPowerSystems, which is thus the chosen software. Since the final score of Modelica was narrowly in second place, it is worthwhile trying to evaluate it in the future.

2.5 Conclusions

The choice of hardware is a PC platform. The specification of the computer available is: PC notebook with microprocessor Intel Pentium III 650 MHz, Random Access Memory (RAM) of 192 Kbytes and Operational System Windows 2000.

This actually is not the more adequate choice, but is the achievable within the budget constraints. The ideal PC platform to perform computer simulation would have high clock speed microprocessor and plenty of RAM, to allow satisfactory simulation run time. Commercial computers are available with clock speed in excess of 2 GHz and RAM of 512 Kbytes, and would be a better PC based platform.

The choice of software is the MATLAB/Simulink version 6.5 Release 13, installed with SimPowerSystems toolbox, an upgrade from the version 5.2 that was available at the Department of Mechanical Engineering (University College London).

3.0 CHAPTER THREE – Induction Motor Development

3.1 Introduction – Theory

Algorithms to simulate three-phase induction motors are well known and widely available in technical literature. The algorithm construction is dependant on the reference frame chosen (see more details about reference frame theory in the Appendix "A", page 126).

Consequently a simpler reference frame leads to a less complex algorithm. Although it may be advantageous to have an uncomplicated algorithm, in order to speed-up simulation, it is necessary to understand the implications in accuracy, to guarantee a reliable model.

3.1.1. Algorithm using *dq* reference frame

SimPowerSystems has a library of electric components that contains an Asynchronous Machine model to simulate the behaviour of an induction motor. The core of this block was modelled in Simulink, using *dq* transformation. It is a very simple and fast algorithm; however reference [12] points out the following precautions to be taken when using it:

- "Use the stationary reference frame if the stator voltages are either unbalanced or discontinuous and the rotor voltages are balanced (or zero);

- "Use the rotor reference frame if the rotor voltages are either unbalanced or discontinuous and the stator voltages are balanced;

- "Use either the stationary or synchronous reference frames if all voltages are balanced and continuous."

In fact, since the algorithm doesn't take into account the zero-sequence component, it is very likely that any kind of unbalance will result in imprecision on the results. The algorithm therefore only will be practical to deal with balanced phases.

3.1.2. Algorithm using *dq0* reference frame

There are lots of bibliographic references dealing with *dq0* reference frame, making it very popular for modelling purposes. Reference [13] presents an

algorithm very similar to the one used in SimPowerSystems, but including the zero-sequence component. This makes the model slightly more complex, but it also makes it more complete and theoretically allows a more accurate simulation of unbalanced condition, although the simulation run time is a bit longer.

The equations for an induction machine using *dq0* reference frame are [13]:

- **Stator and rotor voltage equations:**

$$v_{ds} = \frac{p}{\omega_b}\lambda_{ds} + \frac{\omega}{\omega_b}\lambda_{qs} + r_s \cdot i_{ds}$$

$$v_{qs} = \frac{p}{\omega_b}\lambda_{qs} + \frac{\omega}{\omega_b}\lambda_{ds} + r_s \cdot i_{qs}$$

$$v_{0s} = \frac{p}{\omega_b}\lambda_{0s} + r_s \cdot i_{0s}$$

$$v'_{dr} = \frac{p}{\omega_b}\lambda'_{dr} - \left(\frac{\omega - \omega_r}{\omega_b}\right)\lambda'_{qr} + r'_r \cdot i'_{dr}$$

$$v'_{qr} = \frac{p}{\omega_b}\lambda'_{qr} + \left(\frac{\omega - \omega_r}{\omega_b}\right)\lambda'_{dr} + r'_r \cdot i'_{qr}$$

$$v'_{0r} = \frac{p}{\omega_b}\lambda'_{0r} + r'_r \cdot i'_{0r} \qquad (1)$$

Where $\omega = 0$ in the stationary reference frame, $\omega = \omega_s$ (synchronous speed) in the synchronous reference frame and $\omega = \omega_r$ (rotor speed) in the rotor reference frame.

- **Flux linkage equations:**

$$\begin{bmatrix} \phi_{ds} \\ \phi_{qs} \\ \phi_{0s} \\ \phi'_{dr} \\ \phi'_{qr} \\ \phi'_{0r} \end{bmatrix} = \begin{bmatrix} l_{ls}+l_m & 0 & 0 & l_m & 0 & 0 \\ 0 & l_{ls}+l_m & 0 & 0 & l_m & 0 \\ 0 & 0 & l_{ls} & 0 & 0 & 0 \\ l_m & 0 & 0 & l'_{lr}+l_m & 0 & 0 \\ 0 & x_m & 0 & 0 & l'_{lr}+l_m & 0 \\ 0 & 0 & 0 & 0 & 0 & l'_{lr} \end{bmatrix} \begin{bmatrix} i_{ds} \\ i_{qs} \\ i_{0s} \\ i'_{dr} \\ i'_{qr} \\ i'_{0r} \end{bmatrix} \qquad (2)$$

- **Torque equations:**

$$T_{em} = \frac{3}{2} \cdot \frac{P}{2\omega_b} \left(\lambda'_{qr} i'_{dr} - \lambda'_{dr} i'_{qr} \right) = \frac{3}{2} \cdot \frac{P}{2\omega_b} \left(\lambda_{ds} i_{qs} - \lambda_{qs} i_{ds} \right)$$

$$T_{em} = \frac{3}{2} \cdot \frac{P}{2\omega_b} \cdot x_m \left(i'_{dr} i_{qs} - i'_{qr} i_{ds} \right) \tag{3}$$

3.1.3. Algorithm using *matrix operations*

The algorithm using *matrix operations*, or natural reference frame, offers more difficulties in the modelling process compared to the previous ones. The availability of bibliographic reference is considerably inferior if compared to *dq0* reference frame for example. Reference [14] proposes a FORTRAN program based on Runge-Kutta-Gill algorithm.

Theoretically the simulation using the *matrix* algorithm will produce the more reliable results, since there is no mathematical transformation of reference frame involved.

The equations for a three-phase induction machine using *matrix operations* are [14]:

- **Stator and rotor voltage equations:**

$$\mathrm{v}_s = [v_s] = [v_{as} \quad v_{bs} \quad v_{cs}]^T$$

$$\mathrm{v}_r = [v_r] = [v_{ar} \quad v_{br} \quad v_{cr}]^T$$

$$\mathrm{i}_s = [i_s] = [i_{as} \quad i_{bs} \quad i_{cs}]^T$$

$$\mathrm{i}_r = [i_r] = [i_{ar} \quad i_{br} \quad i_{cr}]^T$$

And:

$$\mathrm{x}_{ss} = [x_{ss}] = \begin{bmatrix} x_{ls} + x_m & -0.5 \cdot x_m & -0.5 \cdot x_m \\ -0.5 \cdot x_m & x_{ls} + x_m & -0.5 \cdot x_m \\ -0.5 \cdot x_m & -0.5 \cdot x_m & x_{ls} + x_m \end{bmatrix}$$

$$x_{rr} = [x_{rr}] = \begin{bmatrix} x_{lr} + x_m & -0.5 \cdot x_m & -0.5 \cdot x_m \\ -0.5 \cdot x_m & x_{lr} + x_m & -0.5 \cdot x_m \\ -0.5 \cdot x_m & -0.5 \cdot x_m & x_{lr} + x_m \end{bmatrix}$$

$$x_{sr} = [x_{sr}] = x_m \begin{bmatrix} \cos\theta & \cos(\theta + 2\pi/3) & \cos(\theta - 2\pi/3) \\ \cos(\theta - 2\pi/3) & \cos\theta & \cos(\theta + 2\pi/3) \\ \cos(\theta + 2\pi/3) & \cos(\theta - 2\pi/3) & \cos\theta \end{bmatrix}$$

$$G_{sr} = [G_{sr}] = x_m \begin{bmatrix} -\sin\theta & -\sin(\theta + 2\pi/3) & -\sin(\theta - 2\pi/3) \\ -\sin(\theta - 2\pi/3) & -\sin\theta & -\sin(\theta + 2\pi/3) \\ -\sin(\theta + 2\pi/3) & -\sin(\theta - 2\pi/3) & -\sin\theta \end{bmatrix}$$

$$x_{rs} = [x_{sr}]^T;\ G_{ss} = [0];\ G_{rr} = [0];\ G_{rs} = [G_{sr}]^T \qquad (4)$$

Then:

$$v_s = [r_s].[i_s] + [x_{ss}].p.[i_s] + [x_{sr}].p.[i_r] + \omega_r.[G_{sr}].[i_r]$$

$$v_r = [r_r].[i_r] + [x_{rs}].p.[i_s] + [x_{rr}].p.[i_r] + \omega_r.[G_{rs}].[i_s] \qquad (5)$$

- **Torque equations:**

$$T_{em} = [I]^T[G][I] \text{ where } [I] = [i_{as} \quad i_{bs} \quad i_{cs} \quad i_{ar} \quad i_{br} \quad i_{cr}]$$

$$T_{em} = \frac{2}{3\sqrt{3}} \omega_b [\lambda_{as}(i_{bs} - i_{cs}) + \lambda_{sb}(i_{cs} - i_{as}) + \lambda_{sc}(i_{as} - i_{bs})] \qquad (6)$$

3.1.4. Modelling with selected algorithms

Three different models of three-phase induction motor fed from a sinusoidal constant voltage source were developed and tested representing each different reference frame and algorithm mentioned above, i.e.:

Model name	Reference frame used in algorithm
dq_im_model	*dq* reference frame (built with SimPowerSystems components)
dq0_im_model	*dq0* reference frame (built with Simulink blocks)
matrix_im_model	*matrix operations* (built with Simulink blocks and FORTRAN subroutine)

Table 2: Models created to compare performance of reference frames

The SimPowerSystems/Simulink representation of the models are presented in the Appendix "B", page 135. The output waveforms of each models has been compared with available data from reference [14], to promote validation.

3.2 Requirements of IM Model

3.2.1. Selection of Algorithm

A decision analysis tool (weighted matrixes) is again employed to support a selection process to decide which algorithm best complies with the requirements of the Induction Motor Model. The requirements are (from the more to the less important):

a. Accuracy of torque and speed applied to the shaft:

The torque and speed results obtained running the three different models under the same parameters were very similar, disregarding reference frame and algorithm, even with unbalanced voltage supply.

b. Accuracy of stator and rotor currents:

Running the models with balanced phases resulted in similar values for stator and rotor currents disregarding reference frame and algorithm.

When a small percentage of voltage unbalance was applied in the stator phases, the **"dq_im_model"** and the **"dq0_im_model"** responded with an almost proportional percentage of current

unbalance on the stator, when the **"matrix_im_model"** responded with a considerably higher percentage of unbalance.

According to reference [15] the response that presents more similarity with the actual system is the **matrix_im_model's** one.

c. Simulation speed:

Running six seconds of simulation time, in discrete mode, with time step of 0.0001 seconds, using the same hardware platform, led to the following:

- **"dq_im_model"** took 6.7 seconds to run;
- **"dq0_im_model"** took 8.0 seconds to run; and
- **"matrix_im_model"** took 47.0 seconds to run.

d. Compatibility with SimPowerSystems:

Since SimPowerSystems is the chosen software tool, it is important to have a model compatible or adaptable to work in this environment.

"dq_im_model" was totally built with SimPowerSystems blocks, therefore is 100 % compatible; **"dq0_im_model"** was built in Simulink, which is the background of SimPowerSystems, and so is compatible with small adaptations.

"matrix_im_model" was built in FORTRAN, and then compiled to become a subroutine of Simulink; consequently it is compatible, despite needing the larger amount of work to make the necessary adaptations.

e. Flexibility to changes:

All models can be changed, but the **"matrix_im_model"** requires a more laborious process, since it needs to be programmed in FORTRAN and then compiled into a Simulink subroutine.

f. Lower complexity:

"dq_im_model" is the less and **"matrix_im_model"** is the more complex.

g. Availability of literature:

"**dq_im_model**" and "**dq0_im_model**" have plenty of bibliographic reference available, due to the popularity of these reference frames in control applications. "**matrix_im_model**" have considerably less availability.

Then the decision-making matrix will be:

	Weight	dq_im_model	dq_im_model weighted	dq0_im_model	dq0_im_model weighted	matrix_im_model	abc_im_model weighted
Accuracy Torque/Speed	10.0	10.0	100.0	10.0	100.0	10.0	100.0
Accuracy Currents	10.0	4.0	40.0	4.0	40.0	9.5	95.0
Simulation Speed	5.0	10.0	50.0	8.0	40.0	5.0	25.0
Compatibility with SPS	5.0	10.0	50.0	9.0	45.0	8.0	40.0
Flexibility to Changes	4.0	8.0	32.0	10.0	40.0	6.0	24.0
Lower Complexity	3.0	8.0	24.0	9.0	27.0	7.0	21.0
Available Literature	3.0	10.0	30.0	10.0	30.0	7.0	21.0
Total			**326.0**		**322.0**		**326.0**

Table 3: Reference frame choice matrix

The final scores were very close in value, meaning in practice that any model could be used with almost the same result. The main difference in performance was verified when running under unbalanced condition. In that case, it is useful to analyse more deeply the consequences of a miscalculation of unbalanced currents.

3.2.2. Response under unbalanced voltage supply

Polyphase AC induction motors are designed to use a balanced voltage supply [15]. When the voltage of each phase is unequal, the effect is equivalent to the introduction of a "negative sequence voltage" having a rotation opposite to that occurring with balanced voltages (i.e 'positive sequence').

This negative sequence voltage produces in the air gap of the machine a flux rotating opposite to the direction of rotation of the rotor, tending to create high currents in the stator windings. A small negative sequence voltage may produce, in the stator windings, currents considerably in excess of those present under balanced voltage conditions.

A relatively small unbalance in voltage may cause a considerable increase in temperature rise. In the phase with the highest current, the percentage increase in temperature rise will be approximately twice the square of the percentage of voltage unbalance [16].

The increase in losses and consequently the increase in the average heating of the whole winding will be slightly lower than the winding with the highest current. To determine the effect of unbalanced phase voltages on motor performance, reference [15] proposes a practical method:

- The percentage of voltage unbalance is calculated through the formula:

$$\% \text{ Volts Unbalance} = \frac{\text{Max. volts deviation from avg. volts}}{\text{avg. volts}} \times 100 \quad (7)$$

- Then the obtained value is entered in the following diagram to find the resultant current:

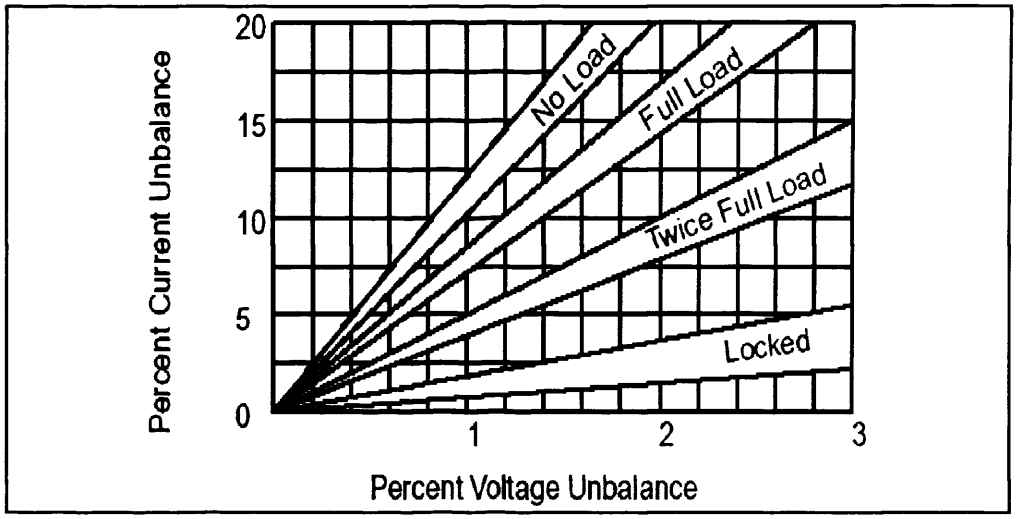

Figure 4: Percentage of voltage unbalance x percentage of current unbalance graph [15]

The models "**dq_im_model**", "**dq0_im_model**" and "**matrix_im_model**" were tested with one unbalanced phase with 206 V rms and the other two with 200 V rms. Using the practical method:

Avg. volts = (206 + 200 + 200)/3 = 202 V

Max. volts deviation = 206 – 202 = 4 V

% Volts Unbalance = 100 x 4 / 202 ≅ 2%

From the diagram (at full load) => Current Unbalance ≅ 15%

From the simulation the following results were found:

- "**dq_im_model**" => Avg current = (4.50 + 4.10 + 4.20)/3 ≅ 4.27 A

  Current Unbalance = (4.50 – 4.27)/4.27 ≅ 5.4%

- "**dq0_im_model**" => Avg current = (4.50 + 4.10 + 4.20)/3 ≅ 4.27 A

  Current Unbalance = (4.50 – 4.27)/4.27 ≅ 5.4%

- "**matrix_im_model**" => Avg current = (5.00 + 4.00 + 4.10)/3 ≅ 4.37 A

  Current Unbalance = (5.00 – 4.37)/4.37 ≅ 14.4%

The "**dq_im_model**" performed poorly, as expected, since zero-sequence components are not considered in its algorithm.

The "**dq0_im_model**" however performed similarly to the "**dq_im_model**", largely indicating that the mathematical implementation of the zero-sequence current was not enough to cope with the unbalance. It managed to produce a smoother and more realistic waveform, although it did not alter much the magnitudes of the resulting currents.

The "**matrix_im_model**" is the one that achieved a result closer to the obtained with the practical formulation.

In fact Smith [14] points out that "the vast majority of methods has taken the *dq* representation of machines as the basis of computer simulation models and as such has constrained derived solutions to balanced operation, which not only severely limits the scope of many practical problems that may be studied but also impairs the accuracy of these solutions since absolute balanced conditions rarely apply." This is particularly true in inverter driven motors.

The obtained results are meaningful, and give support to select the *matrix algorithm* for modelling a 15-phase Induction Motor model, especially useful in a fidelity level where the unbalanced voltage supply must be considered.

However due to the inherent speed advantage, the *dq* algorithm should be used in parallel to develop a simpler 15-phase Induction Motor model. This would provide significant benefit where faster simulation is required and voltage unbalance is not an issue.

3.3 Modelling Method and Model Development

The Advanced Induction Motor that will be used in the Type 45 propulsion system consists of a 15-phase machine, each phase with its own positive and negative connection, without grounding. This means that some changes have to be made in the algorithm adopted to simulate the 3-phase machine, with the stator arrangement represented by figure 5, in order to characterize the arrangement of figure 6.

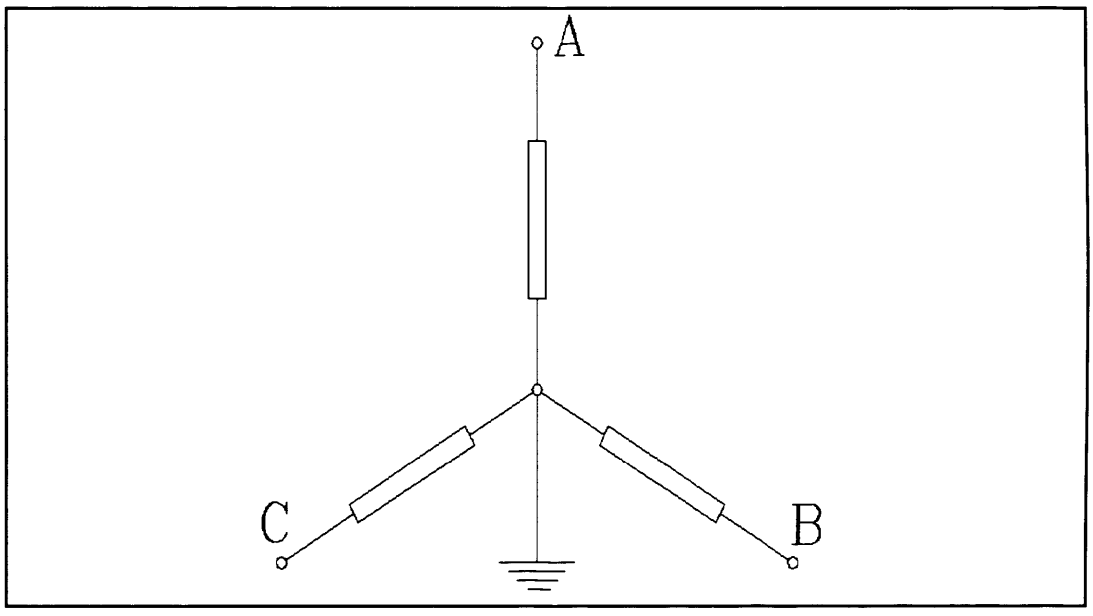

Figure 5: Three phases grounded

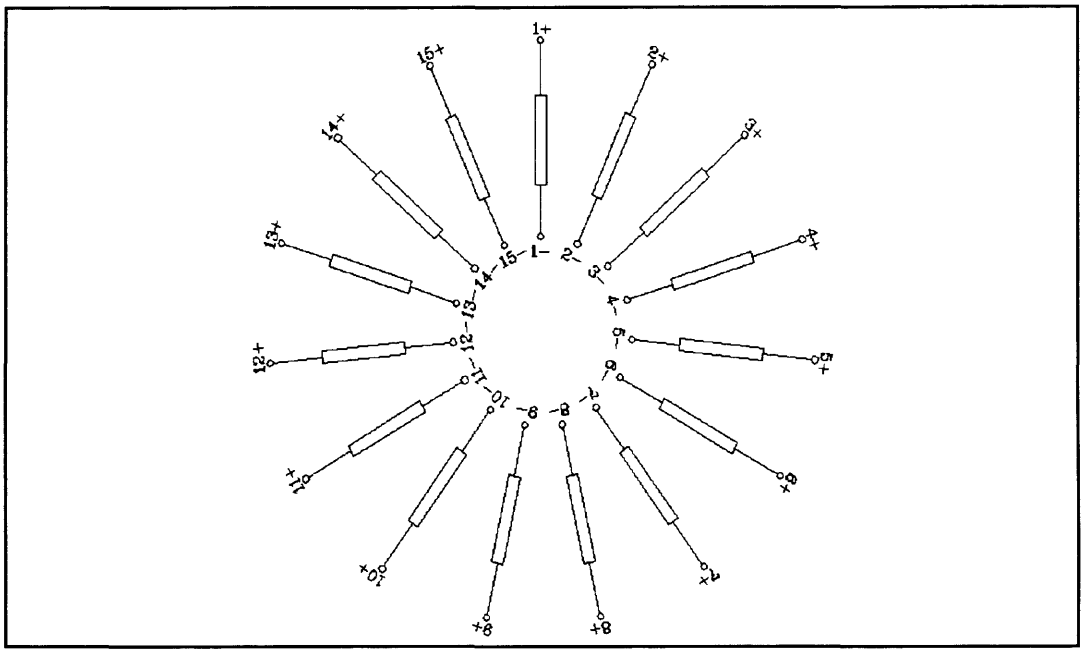

Figure 6: Fifteen phases ungrounded

3.3.1. Development of a 15-phase Matrix Algorithm

Taking the set of equations (4), for three-phase system, and making the adequate mathematical manipulations to conform to the 15-phase system result in the following:

- **Stator and rotor voltage equations:**

$$v_1 = v_{1+} - v_{1-};\ v_2 = v_{2+} - v_{2-} \quad \ldots \quad v_{15} = v_{15+} - v_{15-}$$

$$\mathrm{v}_s = [v_s] = [v_{1s} \quad v_{2s} \quad \ldots \quad v_{15s}]^T$$

$$\mathrm{v}_r = [v_r] = [v_{1r} \quad v_{2r} \quad \ldots \quad v_{15r}]^T$$

$$\mathrm{i}_s = [i_s] = [i_{1s} \quad i_{2s} \quad \ldots \quad i_{15s}]^T$$

$$\mathrm{i}_r = [i_r] = [i_{1r} \quad i_{2r} \quad \ldots \quad i_{15r}]^T$$

and

$$\mathrm{x}_{ss}=\begin{bmatrix} x_{ls}+x_m & \cos\left(\frac{2\pi}{15}\right)\cdot x_m & \cdots & \cos\left(\frac{14\pi}{15}\right)\cdot x_m & \cos\left(\frac{-14\pi}{15}\right)\cdot x_m & \cdots & \cos\left(\frac{-2\pi}{15}\right)\cdot x_m \\ \cos\left(\frac{-2\pi}{15}\right)\cdot x_m & x_{ls}+x_m & \cdots & \cos\left(\frac{12\pi}{15}\right)\cdot x_m & \cos\left(\frac{14\pi}{15}\right)\cdot x_m & \cdots & \cos\left(\frac{-4\pi}{15}\right)\cdot x_m \\ \vdots & \vdots & \ddots & \vdots & \vdots & \vdots & \vdots \\ \cos\left(\frac{-14\pi}{15}\right)\cdot x_m & \cos\left(\frac{-12\pi}{15}\right)\cdot x_m & \cdots & x_{ls}+x_m & \cos\left(\frac{2\pi}{15}\right)\cdot x_m & \cdots & \cos\left(\frac{14\pi}{15}\right)\cdot x_m \\ \cos\left(\frac{14\pi}{15}\right)\cdot x_m & \cos\left(\frac{-14\pi}{15}\right)\cdot x_m & \cdots & \cos\left(\frac{-2\pi}{15}\right)\cdot x_m & x_{ls}+x_m & \cdots & \cos\left(\frac{12\pi}{15}\right)\cdot x_m \\ \vdots & \vdots & \vdots & \vdots & \vdots & \ddots & \vdots \\ \cos\left(\frac{2\pi}{15}\right)\cdot x_m & \cos\left(\frac{4\pi}{15}\right)\cdot x_m & \cdots & \cos\left(\frac{-14\pi}{15}\right)\cdot x_m & \cos\left(\frac{-12\pi}{15}\right)\cdot x_m & \cdots & x_{ls}+x_m \end{bmatrix}$$

$$\mathrm{x}_{rr}=\begin{bmatrix} x_{lr}+x_m & \cos\left(\frac{2\pi}{15}\right)\cdot x_m & \cdots & \cos\left(\frac{14\pi}{15}\right)\cdot x_m & \cos\left(\frac{-14\pi}{15}\right)\cdot x_m & \cdots & \cos\left(\frac{-2\pi}{15}\right)\cdot x_m \\ \cos\left(\frac{-2\pi}{15}\right)\cdot x_m & x_{lr}+x_m & \cdots & \cos\left(\frac{12\pi}{15}\right)\cdot x_m & \cos\left(\frac{14\pi}{15}\right)\cdot x_m & \cdots & \cos\left(\frac{-4\pi}{15}\right)\cdot x_m \\ \vdots & \vdots & \ddots & \vdots & \vdots & \vdots & \vdots \\ \cos\left(\frac{-14\pi}{15}\right)\cdot x_m & \cos\left(\frac{-12\pi}{15}\right)\cdot x_m & \cdots & x_{lr}+x_m & \cos\left(\frac{2\pi}{15}\right)\cdot x_m & \cdots & \cos\left(\frac{14\pi}{15}\right)\cdot x_m \\ \cos\left(\frac{14\pi}{15}\right)\cdot x_m & \cos\left(\frac{-14\pi}{15}\right)\cdot x_m & \cdots & \cos\left(\frac{-2\pi}{15}\right)\cdot x_m & x_{lr}+x_m & \cdots & \cos\left(\frac{12\pi}{15}\right)\cdot x_m \\ \vdots & \vdots & \vdots & \vdots & \vdots & \ddots & \vdots \\ \cos\left(\frac{2\pi}{15}\right)\cdot x_m & \cos\left(\frac{4\pi}{15}\right)\cdot x_m & \cdots & \cos\left(\frac{-14\pi}{15}\right)\cdot x_m & \cos\left(\frac{-12\pi}{15}\right)\cdot x_m & \cdots & x_{lr}+x_m \end{bmatrix}$$

$$\mathrm{x}_{sr}=x_m\begin{bmatrix} \cos\theta & \cos\left(\theta+\frac{2\pi}{15}\right) & \cdots & \cos\left(\theta+\frac{14\pi}{15}\right) & \cos\left(\theta-\frac{14\pi}{15}\right) & \cdots & \cos\left(\theta-\frac{2\pi}{15}\right) \\ \cos\left(\theta-\frac{2\pi}{15}\right) & \cos\theta & \cdots & \cos\left(\theta+\frac{12\pi}{15}\right) & \cos\left(\theta+\frac{14\pi}{15}\right) & \cdots & \cos\left(\theta-\frac{4\pi}{15}\right) \\ \vdots & \vdots & \ddots & \vdots & \vdots & \vdots & \vdots \\ \cos\left(\theta-\frac{14\pi}{15}\right) & \cos\left(\theta-\frac{12\pi}{15}\right) & \cdots & \cos\theta & \cos\left(\theta+\frac{2\pi}{15}\right) & \cdots & \cos\left(\theta+\frac{14\pi}{15}\right) \\ \cos\left(\theta+\frac{14\pi}{15}\right) & \cos\left(\theta-\frac{14\pi}{15}\right) & \cdots & \cos\left(\theta-\frac{2\pi}{15}\right) & \cos\theta & \cdots & \cos\left(\theta+\frac{12\pi}{15}\right) \\ \vdots & \vdots & \vdots & \vdots & \vdots & \ddots & \vdots \\ \cos\left(\theta+\frac{2\pi}{15}\right) & \cos\left(\theta+\frac{4\pi}{15}\right) & \cdots & \cos\left(\theta-\frac{14\pi}{15}\right) & \cos\left(\theta-\frac{12\pi}{15}\right) & \cdots & \cos\theta \end{bmatrix}$$

$$G_{sr} = x_m \begin{bmatrix} -\sin\theta & -\sin\left(\theta+\frac{2\pi}{15}\right) & \cdots & -\sin\left(\theta+\frac{14\pi}{15}\right) & -\sin\left(\theta-\frac{14\pi}{15}\right) & \cdots & -\sin\left(\theta-\frac{2\pi}{15}\right) \\ -\sin\left(\theta-\frac{2\pi}{15}\right) & -\sin\theta & \cdots & -\sin\left(\theta+\frac{12\pi}{15}\right) & -\sin\left(\theta+\frac{14\pi}{15}\right) & \cdots & -\sin\left(\theta-\frac{4\pi}{15}\right) \\ \vdots & \vdots & \ddots & \vdots & \vdots & \vdots & \vdots \\ -\sin\left(\theta-\frac{14\pi}{15}\right) & -\sin\left(\theta-\frac{12\pi}{15}\right) & \cdots & -\sin\theta & -\sin\left(\theta+\frac{2\pi}{15}\right) & \cdots & -\sin\left(\theta+\frac{14\pi}{15}\right) \\ -\sin\left(\theta+\frac{14\pi}{15}\right) & -\sin\left(\theta-\frac{14\pi}{15}\right) & \cdots & -\sin\left(\theta-\frac{2\pi}{15}\right) & -\sin\theta & \cdots & -\sin\left(\theta+\frac{12\pi}{15}\right) \\ \vdots & \vdots & \vdots & \vdots & \vdots & \ddots & \vdots \\ -\sin\left(\theta+\frac{2\pi}{15}\right) & -\sin\left(\theta+\frac{4\pi}{15}\right) & \cdots & -\sin\left(\theta-\frac{14\pi}{15}\right) & -\sin\left(\theta-\frac{12\pi}{15}\right) & \cdots & -\sin\theta \end{bmatrix}$$

$$x_{rs} = [x_{sr}]^T;\ G_{ss} = [0];\ G_{rr} = [0];\ G_{rs} = [G_{sr}]^T \tag{8}$$

The algorithm for the 3-phase motor, comprising the block that calls the FORTRAN subroutine, can be adapted using the above formulation, to represent the 15-phase machine. The new subroutine is presented in the Appendix "C", page 145.

3.3.2. Development of a 15-phase *dq* Algorithm

In the 15-phase *dq* algorithm the equations (1) and (2) are kept the same, and equation (3) becomes:

$$T_{em} = \frac{15}{2} \cdot \frac{P}{2\omega_b} \cdot x_m \left(i'_{dr} i_{qs} - i'_{qr} i_{ds} \right) \text{N.m} \tag{9}$$

The equations (3) and (5) from Appendix "A" have a new format to support the 15-phase input, where $\gamma = 2\pi/15$, as follows:

$$\begin{bmatrix} i_{\alpha s} \\ i_{\beta s} \end{bmatrix} = \frac{2}{15} \begin{bmatrix} 1 & \cos(\gamma) & \cos(2\gamma) & \cdots & \cos(13\gamma) & \cos(14\gamma) \\ 0 & \sin(\gamma) & \sin(2\gamma) & \ldots & \sin(13\gamma) & \sin(14\gamma) \end{bmatrix} \begin{bmatrix} i_{1s} \\ i_{2s} \\ \vdots \\ i_{15s} \end{bmatrix} \tag{10}$$

$$\begin{bmatrix} i_{1s} \\ i_{2s} \\ \vdots \\ i_{15s} \end{bmatrix} = \begin{bmatrix} 1 & 0 \\ \cos(\gamma) & \sin(\gamma) \\ \cos(2\gamma) & \sin(2\gamma) \\ \vdots & \vdots \\ \cos(13\gamma) & \sin(13\gamma) \\ \cos(14\gamma) & \sin(14\gamma) \end{bmatrix} \begin{bmatrix} i_{\alpha s} \\ i_{\beta s} \end{bmatrix} \tag{11}$$

The algorithm for the 3-phase motor can be adapted using the above formulation, to represent the 15-phase machine. The new subroutine is presented in the Appendix "D", page 150.

3.4 Validation

The validation can be done by comparison with demonstration models available in the SimPowerSystems toolbox of Simulink.

The toolbox was developed by the software company Mathworks Inc. in conjunction with TEQSIM International Inc., a sublicense of Hydro-Quebec. The initial assumption is that the individual component models and the demonstration models available in the toolbox produce valid results, which could be used to assess and validate new models.

The demonstration model 'psbpwm.mdl' was created by Louis-A. Dessaint and R. Champagne, from the École de Technologie Superieure (Montréal, Canada) [12]. It comprises a three-phase motor rated at 3 HP, 220 V, 1725 rpm fed by a sinusoidal PWM inverter. The base frequency of the sinusoidal reference wave is 60 Hz while the triangular carrier wave's frequency is set to 1980 Hz.

The PWM inverter is built entirely with standard Simulink blocks. Its output goes through Controlled Voltage Source blocks before being applied to the Asynchronous Machine block's stator windings. The machine's rotor is short-circuited. Its stator leakage inductance is set to twice its actual value to simulate the effect of a smoothing reactor placed between the inverter and the machine.

The load torque applied to the machine's shaft is constant and set to its nominal value of 11.9 N.m. The motor is started from stall. The speed set point is 1.0 pu, or 1725 rpm. This speed is reached after 0.9 s.

The line voltage fundamental component at the machine's stator terminals is calculated using a Fourier's transformer block, and the result was 220.5 Volts rms. The results for stator current at phase 'A', rotor speed and electromagnetic torque are presented in figure 7 and will be the reference for the validation process.

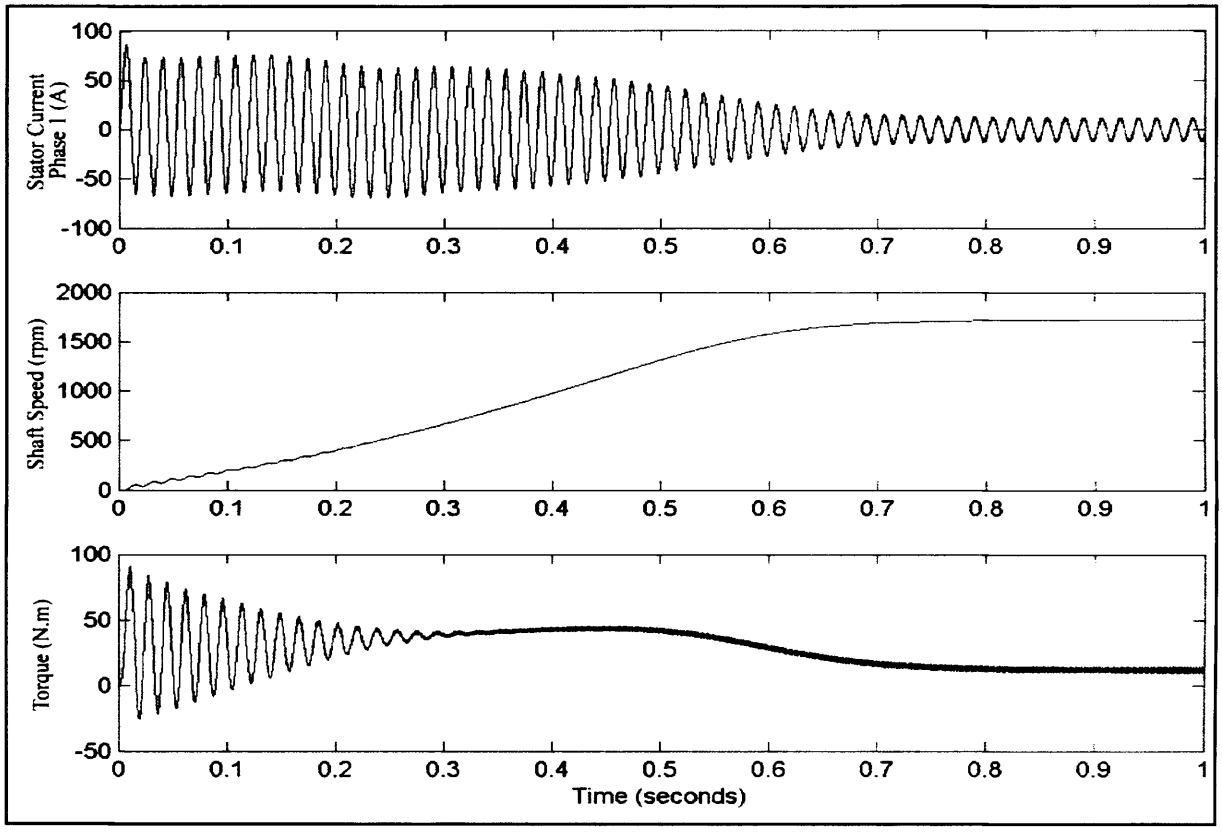

Figure 7: Reference for validation – 'psbpwm.mdl' results

The created 15-phase models, using *dq reference frame* and *matrix operations,* were fitted in the 'psbpwm.mdl' system, keeping all the parameters and conditions unchanged. Now, due to the higher number of phases, the line voltage fundamental component at the machine's stator terminals was 52.95 Volts rms for both models. The results for stator current at phase 'A', rotor speed and electromagnetic torque are presented in figures 8 and 9.

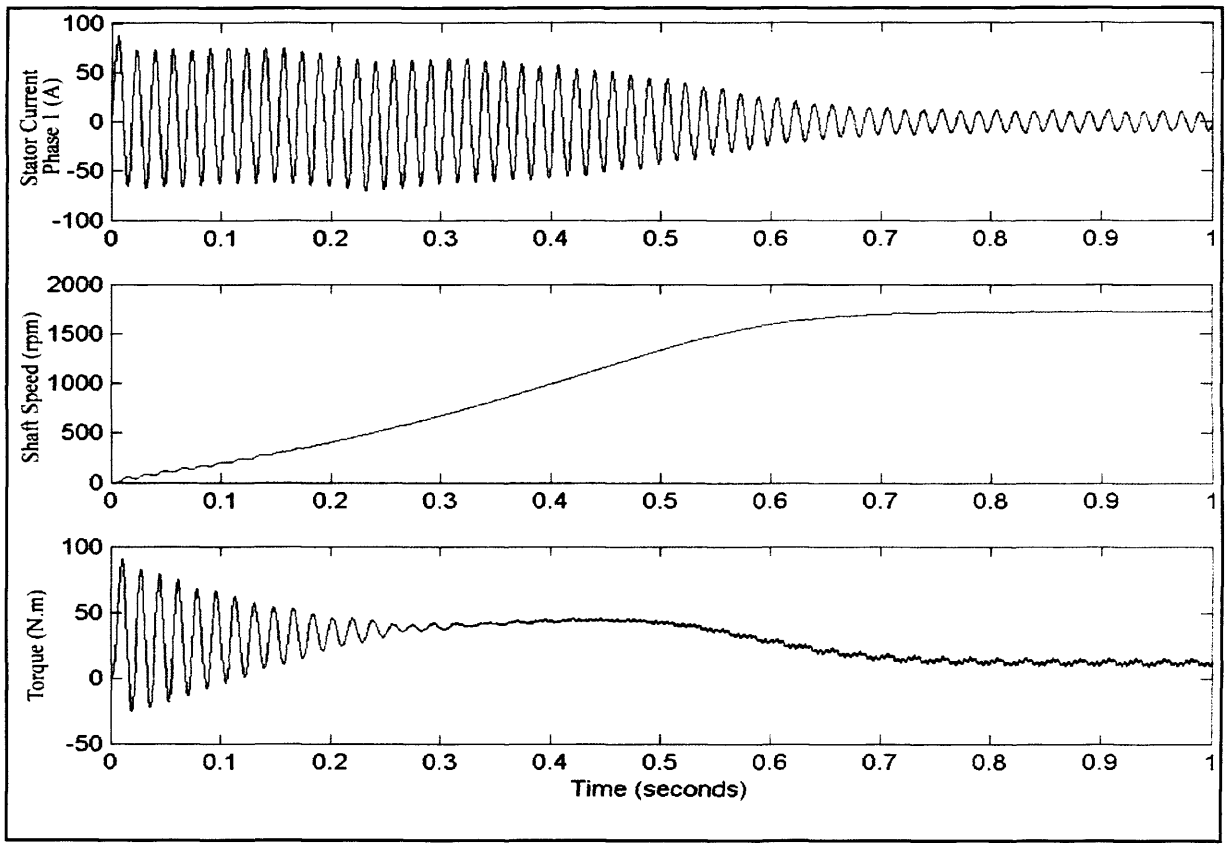

Figure 8: Results for 'psbpwm.mdl' with 15-phase *dq* model fitted

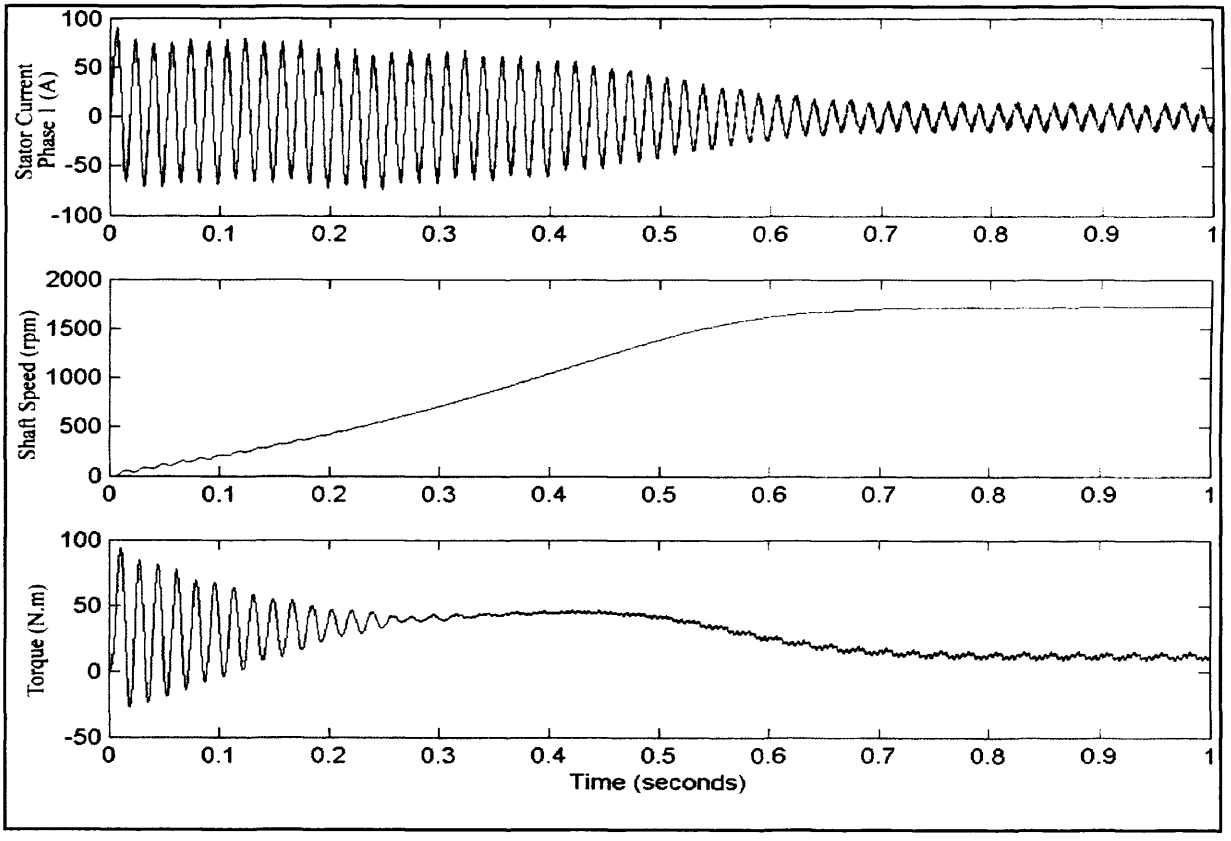

Figure 9: Results for 'psbpwm.mdl' with 15-phase matrix model fitted

By comparing the resulting curves (figures 8 and 9) with the reference (figure 7) it is possible to realise the similarity of shapes. Even though the ripples on torque being more prominent in figures 8 and 9 at the steady-state region, having a slightly different shape compared to the reference in figure 7, it is understandable due the increased number of phases compared to the reference.

The resulting line voltage is also coherent with the new number of phases, as we can appreciate by using the trigonometric relationships:

3-phase: 1208 between lines

$$V_{line-neutral} = \frac{V_{line-line}}{2 \cdot \sin\left(\frac{120°}{2}\right)} \tag{12}$$

$$V_{line-neutral} = \frac{220.5}{2 \cdot \sin\left(\frac{120°}{2}\right)} = 127.3 \text{ Volts rms}$$

15-phase: 248 between lines

$$V_{line-neutral} = \frac{V_{line-line}}{2 \cdot \sin\left(\frac{24°}{2}\right)} \tag{13}$$

$$V_{line-line} = 2 \cdot \sin\left(\frac{24°}{2}\right) \cdot V_{line-neutral}$$

$$V_{line-line} = 2 \cdot \sin\left(\frac{24°}{2}\right) \cdot 127.3 = 52.93 \text{ Volts rms}$$

Since there is no availability of actual data from a real 15-phase induction motor, the models can only have a restricted validation.

3.5 Conclusions

A 15-phase matrix model was developed using induction motor theory without making use of reference frame transformation. Its algorithm is based in mathematical matrix manipulation, what represents a heavy processing load to the hardware platform.

The matrix model has the advantage of calculating more precisely stator and rotor current when voltage unbalance is present. It has the disadvantage of requiring longer simulation run time.

A 15-phase *dq*-model was developed using reference frame transformation to simplify the mathematical equations, by transforming the differential equations, with time varying inductances, into differential equations with constant inductances.

The *dq*-model has the advantage of requiring shorter simulation run time, but it is not very accurate to calculate stator and rotor currents under voltage unbalance condition.

Both models were validated to simulate stator and rotor currents, shaft speed and electromagnetic torque when submitted to a balanced 15-phase supply voltage.

To perform the validation under unbalanced voltage supply it would be necessary the availability of measurement data of an actual polyphase induction motor.

4.0 CHAPTER FOUR – PWM Converter Development

4.1 Introduction

The Advanced Induction Motors of the Type 45 Destroyer will be controlled by the latest technology PWM System, the ALSTOM VDM 25000. The advantages of a PWM Converter are described at the 1998 International Conference on Electric Ship (Benatmane, [17]):

"A PWM Converter was selected over a Load Commutated Inverter (LCI) or Cycloconverter for numerous reasons. Since a PWM Converter does not require a synchronous motor to maintain a controlled load commutation, the advantages of an induction motor become available with the PWM drive."

"The PWM Converter provides the ability to control the waveform for a more sinusoidal shape. This reduces harmonics resulting in lower motor noise than is possible with other converters. Other advantages of PWM converters over LCI and cycloconverters are a higher, more constant power factor for better efficiency, constant harmonic frequencies to ease any supply filtering required and smaller size and weight."

4.2 Requirements of PWM Converter Model

The Converter to be fitted in the Type 45 propulsion system comprises three separate channels, each supplying five phases. Each channel has:

- One six pulse rectifier, with four thyristors in each leg;
- One DC link, comprising inductors and capacitors;
- One inverter, comprising five H bridges with five IGBTs in each H bridge leg;
- Dynamic braking resistance.

A simplified schematic diagram is presented in figure 10 [18]:

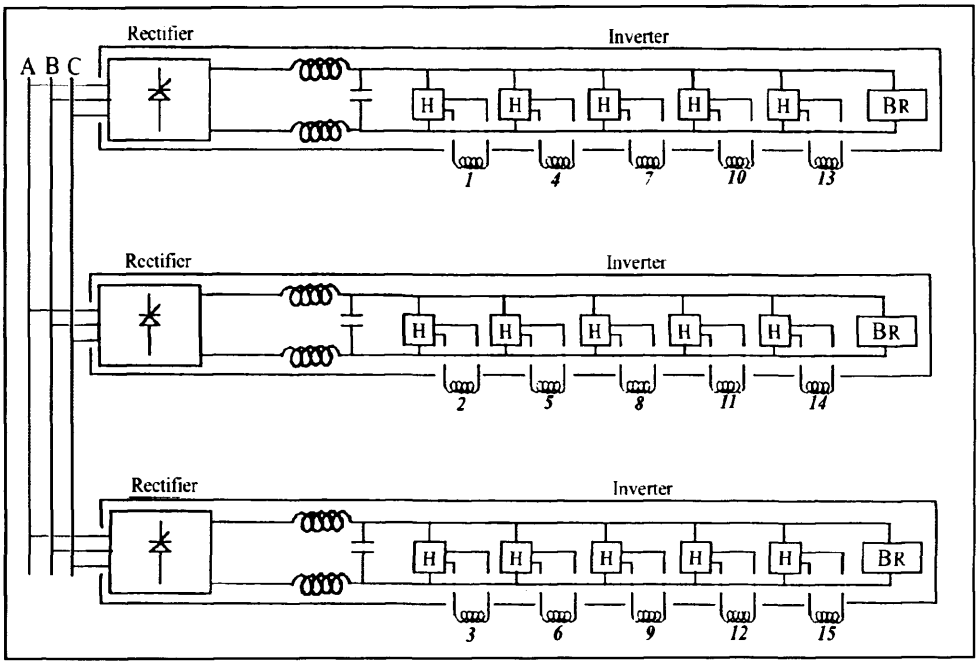

A, B and C – AC supply voltage	BR – Dynamic Braking Resistance
H – H bridge IGBTs	1,2,3 ... 15 – Induction motor phases

Figure 10: Fifteen-phase PWM Converter [18]

4.3 Modelling Method – Development

The components of a PWM Converter are available in the SymPowerSystems three-phase elements toolbox. Obviously the 15-phase Inverter is not a standard function and has been developed from the basic elements.

The rectifier can be modelled using the Universal Bridge element from the toolbox by selecting the number of bridge arms as three, ports configuration as input terminals and choosing the thyristors as the power electronic device. For simplicity the parameters for each leg of the Rectifier can be the equivalent-resistance and equivalent-inductance of the five thyristors in series.

A customized inverter can be built combining the same Universal Bridge element from the toolbox by selecting the number of bridge arms as one, port configuration as output terminal and choosing the IGBTs as the power electronic device. For simplicity each leg of the H Bridges can be represented by only one

equivalent IGBT in the model, since it will provide virtually the same response during the simulation.

The Simulink diagram of the PWM Converter is presented in the Appendix "E", page 154.

4.4 Validation

The 15-phase Inverter, part of the PWM Converter, especially created to provide the 15-phase voltage to the Induction Motor, needed to be validated. It was done by comparing its simulation results with the SimPowerSystems 3-phase inverter block, called 'Universal Bridge'.

Again it will be used the initial assumption that the models available in the toolbox produce valid results, which could be used to assess and validate new models.

The 'psbbridges.mdl' is a demonstration model of an AC-DC-AC converter, which illustrates the use of Universal Bridge. It was developed by G. Sybille (from Hydro-Québec) [12] and comprises a 60 Hz voltage source, feeding a 50 Hz, 50 kW load through an AC-DC-AC converter. The 600V, 60 Hz voltage obtained at the secondary of the Wye/Delta transformer is first rectified by a six pulse diode bridge.

The filtered DC voltage is applied to an IGBT two-level inverter generating 50 Hz. The IGBT inverter uses PWM with 2 kHz carrier frequency. The circuit is discretised at a sample time of 2 μs. The load voltage is regulated at 1 pu (380 V rms) by a PI voltage regulator using abc_to_dq and dq_to_abc transformations.

In this particular simulation the steady state is reached at time = 0.04 seconds. The harmonics generated by the inverter around multiples of 2 kHz are filtered by the LC filter. The peak value of the load voltage is 537 V (380 Vrms). In steady state the mean value of the modulation index is m = 0.80 and the mean value of the DC voltage is 778 V. The fundamental component of 50 Hz voltage buried in the chopped inverter voltage is therefore:

$$V_{ab} = V_{max} \times \frac{\sqrt{3}}{2} \times \frac{\sqrt{2}}{2} \times (Modulation\ index) = \quad 778 * 0.612 * 0.80 =$$

381 V *rms*

The results for DC rectified voltage, line-to-line inverted voltage between phases A and B, line-to-line load voltage between phases A and B and modulation index are presented in figure 11 and will be the reference for the validation process.

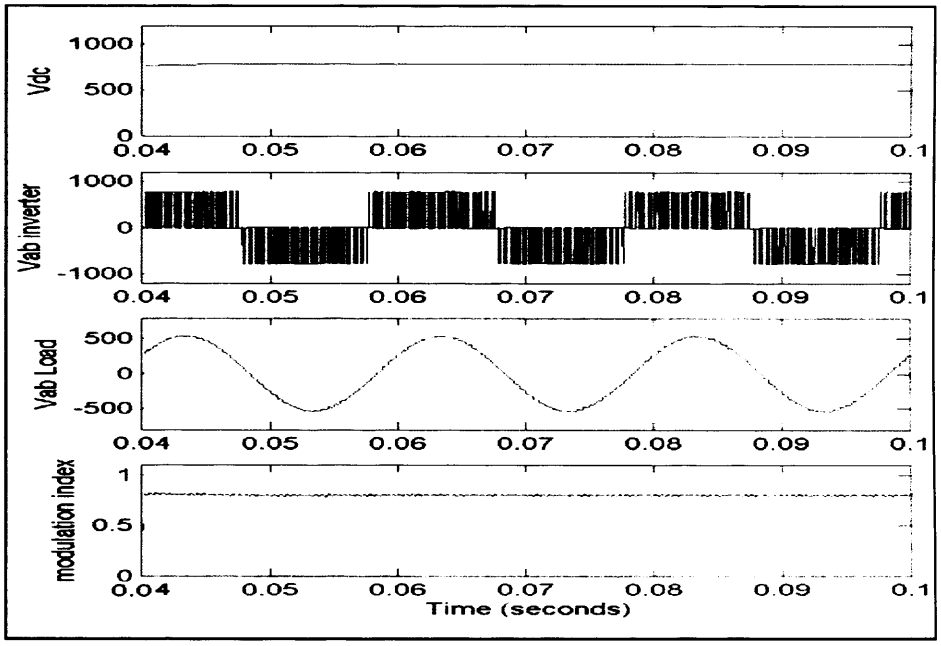

Figure 11: Reference for validation – Results for 'psbbridges.mdl'

The created customized inverter was fitted in the 'psbbridges.mdl' model, keeping all the parameters and conditions unchanged. The results are shown in figure 12:

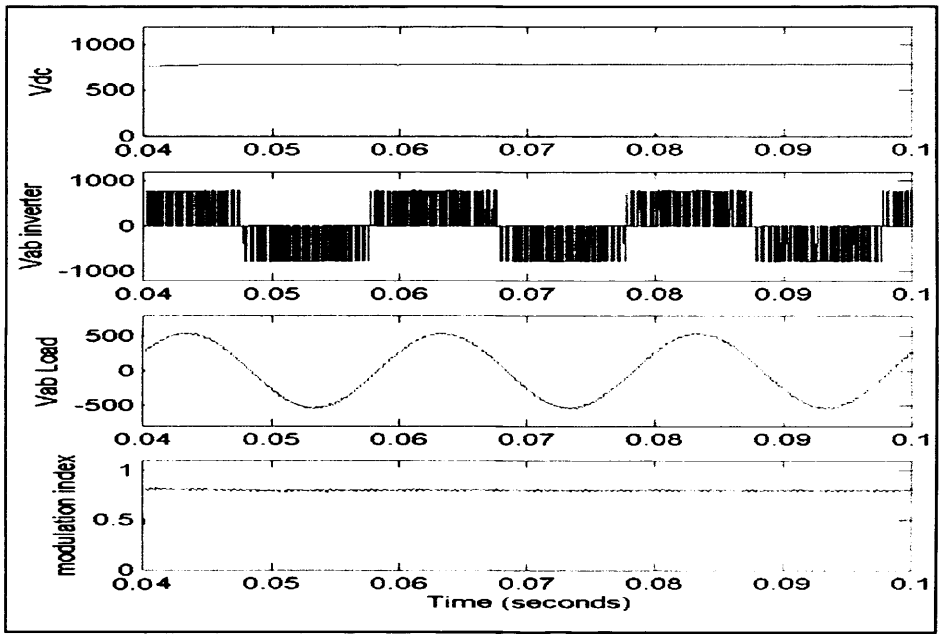

Figure 12: Results for 'psbbridges.mdl' with the customized inverter

Comparing the resulting curves in figure 12 with the reference in figure 11 is possible to identify the similarity of shapes, meaning that the 15-phase inverter operates adequately, generating the correct switching sequence, therefore it is possible to consider the customized inverter validated.

4.5 Conclusions

The PWM Converter comprising rectifier, DC link, inverter and dynamic braking resistance was developed.

The inverter block needed to be customized, in order to have 15 phases, and therefore had to be validated. The validation was successfully performed by comparison with the response of a standard three-phase inverter block from the SimPowerSystems toolbox; therefore the PWM Converter was developed and validated to drive the 15-phase Advanced Induction Motor model.

The actual design of the PWM Converter comprises harmonic filters in each phase of the inverter. The need of such filters in a medium fidelity model (such as the present one) is uncertain and its ratings are unknown. For these reasons they are omitted. Further work can be done to include such filters and analyse the impact on the system.

The adequate operation of the PWM Converter is dependent on the switching pulses input, which commands the generation of the correct waveform. It is a function of the control system and is the subject of the next chapter.

5.0 CHAPTER FIVE – Control Strategy

5.1 Introduction

There are a number of methods to control induction motors with a variable speed drive (VSD). Basically two physical quantities describe the state of the rotor shaft: torque and speed. To control the flow of energy it is necessary, therefore, to control both these quantities [19].

In practice, either one of them is controlled: the system is classified as "torque control" or as "speed control". When the VSD operates in torque control mode, the speed is determined by the load. Likewise, when operated in speed control, the torque is determined by the load [19].

The existing methods can be classified according to the principle in:

1) Scalar Control;

2) Field-Oriented Control; and

3) Direct Torque and Flux Control.

In addition there is a classification according the existence of feedback information from sensor measuring physical variables:

1) Closed-loop Control (with feedback); and

2) Open-loop Control (without feedback).

5.1.1. Scalar Control Methods

Scalar control methods can be open loop or closed loop. The most popular open loop scalar control is obtained using constant stator Voltage/Frequency ratio, which means the combination of changes in voltage and frequency applied to the stator in order to obtain a resulting constant torque. Figure 13 exemplifies the configuration of an open loop V/f control.

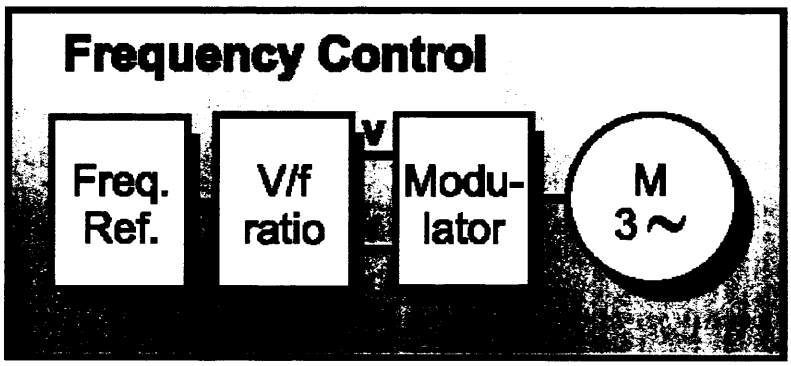

Figure 13: Constant V/f Control [19]

Both voltage and frequency reference are fed into a modulator, which simulates an AC sine wave and feeds this to the motor's stator windings. This Pulse Width Modulation (PWM) technique utilises the fact that there is a rectifier towards the mains and the intermediate DC voltage is kept constant. The inverter controls the motor in the form of a PWM pulse train dictating both the voltage and frequency [19].

Closed loop scalar control has basically the same configuration, but with a feedback from the motor, which can be a speed or torque measurement. This data is fed into the control processor, which calculates the error and then defines the adjustments to the voltage/frequency controls.

With this technique field orientation of the motor is not considered. Instead, frequency and voltage are the main control variables and are applied directly to the stator windings. In today's practice, scalar control is being overtaken by more modern vector control methods, which result is much better dynamic performance [20].

5.1.2. Field-Oriented Control Methods

In the field-oriented method torque is controlled indirectly, through a flux-vector electronic controller. There are basically two kinds of field-oriented control (FOC):

1) Direct FOC; and

2) Indirect FOC.

In the Direct FOC, the knowledge of the orientation and magnitude of the field vector is obtained by measuring the air-gap flux through sensors. They could be Hall sensors, flux sensing coils or taps on the stator winding. However sensors of the air-gap are inconvenient [20] as they spoil the ruggedness of the induction motor. They are imprecise and fragile, and it is the main drawback of this method.

To preclude the use of air-gap sensors, in the Indirect FOC the orientation and magnitude of the field vector is obtained indirectly, by measuring the rotor speed and angular position relative to the stator field, which are then applied to a computer model.

The electronic controller of a flux-vector drive creates electrical quantities (voltage, current and frequency), which are the controlling variables fed into a modulator to produce the PWM supply voltage. Figure 14 exemplifies the configuration of a field-oriented control.

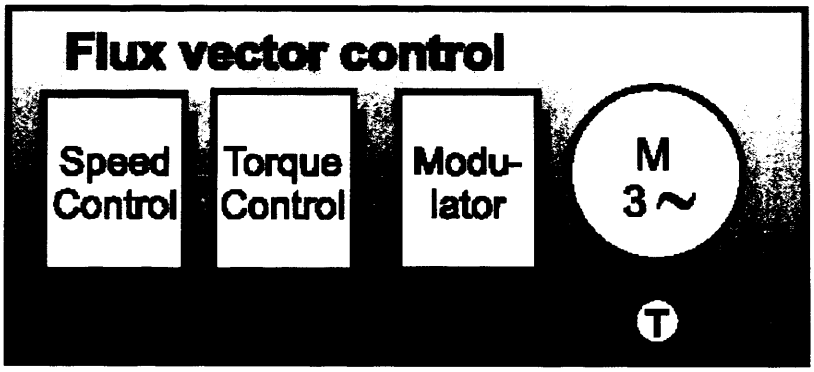

Figure 14: Field-Oriented Control [19]

The strategy in a field-oriented method is to avoid perturbing the rotor flux linkage when responding to a change in torque. To achieve a high level of torque response and speed accuracy, the feedback device is required to measure either the air-gap flux or the rotor speed and angular position. This is what makes the FOC typically a closed loop device.

5.1.3. Direct Torque and Flux Control Methods

In the Direct Torque and Flux Control (DTFC) the controlling variables are magnetising flux and electromagnetic torque. The control is obtained trough a selection of consecutive states of the inverter feeding the induction motor.

Reaction of the rotor flux vector is slower than the stator flux vector therefore with the application of appropriate voltage vectors, associated with individual inverter states, it is possible to adjust the magnitude of the stator flux and manipulate the angle between the stator and the rotor flux vectors.

Since the torque developed in the motor is proportional to the sine of the angle between the two fluxes, the magnetic field and torque of the motor can simultaneously be controlled [20]. Figure 15 exemplifies the configuration of a DTFC.

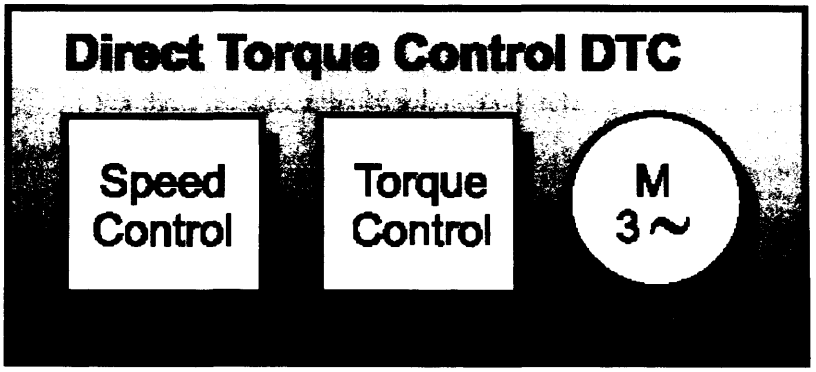

Figure 15: Direct Torque and Flux Control [19]

The main advantages of the DTFC are:

- No need of modulator, to generate the PWM pulses, and
- No need of tachometer or position encoder, to feedback the speed or position of the rotor.

DTFC is typically an open loop control system that relies on the information calculated using a sophisticated mathematically modelled motor inserted into the control algorithm.

Additional advantage of precluding the need of a modulator is the optimization of the switching pattern.

5.2 Requirements of Control System

In industrial motors, where required rotor speeds are mostly constant, the environment highly controllable and the maintenance personal easily accessible, the most important requirement would probably be the energy efficiency, for economic reasons.

In a warship's propulsion system the scenario is different compared to the industrial environment, and therefore there are other priorities:

- Environment at sea is extremely unpredictable;
- Operational profile of a warship comprises abundant changes of speed;
- Personal on board is kept to a minimum and therefore maintenance is restricted;
- Combat scenarios are chaotic and extremely demanding for the ship systems.

For these reasons, robustness and fault-tolerance of the control system are absolute priorities.

"Robust control refers to the control of unknown plants with unknown dynamics subject to unknown disturbances [21]". The key issue with robust control systems is uncertainty and how the control system can deal with this problem. One of the techniques to develop a robust control is 'Adaptive Control'.

An Adaptive Control system sets up observers for each significant state variable in the system. The system can adjust each observer to account for time varying parameters of the system. In an adaptive system, there is always a dual role of the control system. The output is to be brought closer to the desired input while, at the same time, the system continues to learn about changes in the system parameters [21], therefore it is a control system that adjusts the response from conditions detected during the operation.

Fault-tolerant control (FTC) is an emerging area in automatic control. Automated systems are vulnerable to faults. Defects in sensors, actuators, in the process itself, or within the controller, can be amplified by the closed-loop control

systems, and faults can develop into malfunction of the loop. The closed-loop control action may hide a fault from being observed.

A situation is reached in which a fault eventually develops into a state where loop-failure is inevitable. A control-loop failure will easily cause the system being controlled to stop. Automation for safety-critical applications, where no failure could be tolerated, requires redundant hardware to facilitate fault recovery. Fail-operational systems are made insensitive to any single point component failure. Fail-safe systems make controlled shutdown to a safe state when a sensor measurement indicates a critical fault [22].

In contrast, fault-tolerant control systems employ redundancy in the plant and its automation system to make "intelligent" software that monitors behaviour of components and function blocks. Faults are isolated, and appropriate remedial actions taken to prevent that faults develop into critical failures. The overall FTC strategy is to keep plant availability and accept reduced performance when critical faults occur. One way of achieving fault-tolerance is to employ fault diagnosis schemes on-line [22].

Therefore robustness and fault-tolerance are first in scale of importance. There are also other requirements with different weight.

In second place is the reduction of torque ripples to minimise noise, making difficult the detection of the ship by the enemy and increasing its survivability.

In third place is the reduction of switching rate, which will increase the lifetime of the power electronics components, minimising maintenance stops.

In fourth place is the optimisation of motor performance requirement, which would increment the energy efficiency of the motor.

5.3 Selection of Control Method

5.3.1. FOC Realisation

The concept of field orientation was proposed by Hasse in 1969 and Blaschke in 1972 [20]. This method is the most popular and has wider utilisation in induction motor drives. Technical books and papers are profuse (references [13], [14]

and [23] for example); there are also papers dealing specifically with control of multi-phase machines using field-oriented control (i.e. references [24] and [25]). Alstom, the company that is developing the Advanced Induction Motor for the Type 45 Programme, utilises this method in its controllers.

The formulation presented in reference [13] was used as basis for the development of an algorithm and construction of a Simulink model of a 3-phase Field Oriented Controller. The desired angle for field orientation ρ can be computed using geometrical relations on the rotor flux:

$$\lambda'^{s}_{qr} = \frac{x'_r}{x_m}\lambda^{s}_{mq} - x'_{lr}\, i^{s}_{qs} \quad \text{and} \quad \lambda'^{s}_{qr} = \frac{x'_r}{x_m}\lambda^{s}_{mq} - x'_{lr}\, i^{s}_{qs}$$

$$\cos\rho = \frac{\lambda'^{s}_{dr}}{\left|\lambda'^{s}_{r}\right|} \quad \text{and} \quad \sin\rho = \frac{\lambda'^{s}_{qr}}{\left|\lambda'^{s}_{r}\right|} \tag{14}$$

The stator flux can be expressed in terms of only the stator currents and rotor flux linkages:

$$\lambda^{e}_{qs} = x'_s\, i^{e}_{qs} + \frac{x_m}{x'_r}\lambda'^{e}_{qr} \quad \text{and} \quad \lambda^{e}_{ds} = x'_s\, i^{e}_{ds} + \frac{x_m}{x'_r}\lambda'^{e}_{dr} \tag{15}$$

And the field-oriented stator currents are determined by converting the *abc* currents to *dq* stationary and then using the value of ρ:

$$i^{e}_{qs} = i^{s}_{qs}\cos\rho - i^{s}_{ds}\sin\rho \quad \text{and} \quad i^{e}_{ds} = i^{s}_{qs}\sin\rho + i^{s}_{ds}\cos\rho \tag{16}$$

At the end, the commanded values (indicated with *) for the *abc* stator voltages can be computed as follows:

$$\begin{aligned} v^{s*}_{qs} &= v^{e}_{qs}\cos\rho + v^{e}_{ds}\sin\rho \\ v^{s*}_{ds} &= v^{e}_{qs}\sin\rho + v^{e}_{ds}\cos\rho \\ \\ v^{*}_{as} &= v^{s*}_{qs} \\ v^{*}_{bs} &= -\frac{1}{2}v^{s*}_{qs} - \frac{\sqrt{3}}{2}v^{s*}_{ds} \\ v^{*}_{cs} &= -\frac{1}{2}v^{s*}_{qs} + \frac{\sqrt{3}}{2}v^{s*}_{ds} \end{aligned} \tag{17}$$

The complete diagram of the test model using 3-phase FOC is presented in the Appendix "F", page 156.

5.3.2. DTFC Realisation

Direct-torque-controlled induction motor drives were developed in 1985 by Depenbrock and Takahashi. However, at the present, Asea Brown Boveri Industry – ABB – is the first and seems to be the only company who have introduced (in 1995) a commercially available direct-torque induction motor drive [26]. It is indeed the most modern method of control, and therefore has less technical literature compared to the Field-Oriented method.

The formulation presented in reference [27] was used to build an algorithm and create a Simulink model of a 3-phase Direct Torque and Flux Controller. The principle of DTFC is the selection of appropriate voltage vector in the inverter, based on a stator equation in stator coordinates:

$$\frac{d\lambda_s}{dt} = v_s - r_s i_s$$

$$\Delta\lambda_s = \lambda_s - \lambda_{s0} = \int_0^{T_i} (v_s - r_s i_s)dt \approx v_s(i)T_i \qquad (18)$$

For the flux space-phasor in the first sector, the voltage vector selection is shown in the figure 16:

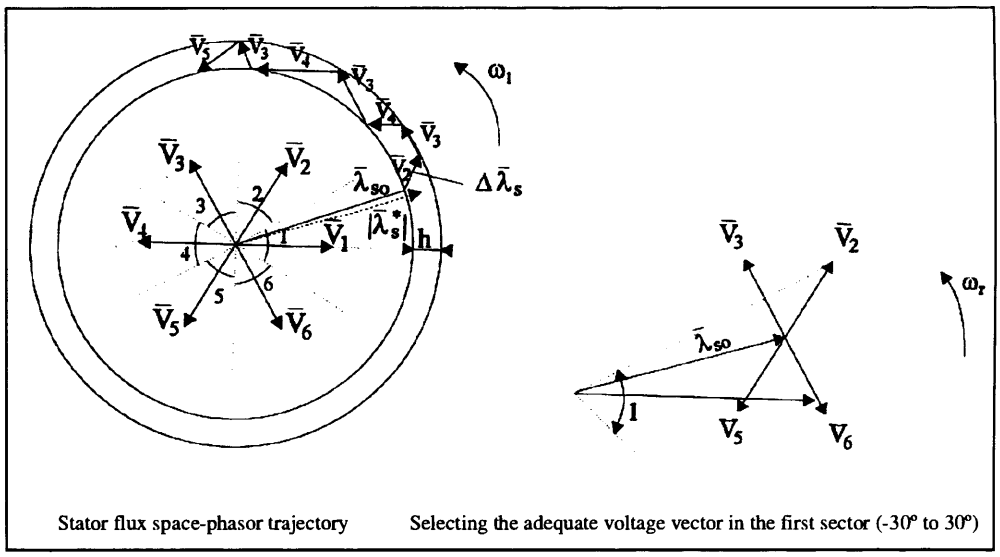

Stator flux space-phasor trajectory — Selecting the adequate voltage vector in the first sector (-30° to 30°)

Figure 16: Stator flux space-phasor diagram [26]

The torque can be varied by stator flux acceleration and deceleration in order to cancel the torque error. The flux acceleration will then cause an increase

in torque amplitude – vectors V_2 and V_3 – and the flux deceleration will cause a decrease in torque amplitude – vectors V_5 and V_6.

The flux amplitude can also be controlled. A voltage vector phase shifted by an angle larger than 90° with respect to the existing flux vector will increase flux amplitude – vectors V_2 and V_6. In contrast a vector with an angle less than 90° will decrease flux amplitude – vectors V_3 and V_5.

The complete table of optimal switching is [27]:

Vectors V_1 to V_6 are active switching vectors: (1 -1 -1); (1 1 -1); (-1 1 -1); (-1 1 1); (-1 -1 1) and (1 -1 1). Vectors V_0 and V_7 are zero switching vectors: (1 1 1) and (-1 -1 -1).							
$\theta_s(i)$		$\theta_s(1)$	$\theta_s(2)$	$\theta_s(3)$	$\theta_s(4)$	$\theta_s(5)$	$\theta_s(6)$
λ	T						
1	1	V_2	V_3	V_4	V_5	V_6	V_1
1	-1	V_6	V_1	V_2	V_3	V_4	V_5
0	1	V_0	V_7	V_0	V_7	V_0	V_7
0	-1	V_0	V_7	V_0	V_7	V_0	V_7
-1	1	V_3	V_4	V_5	V_6	V_1	V_2
-1	-1	V_5	V_6	V_1	V_2	V_3	V_4

Table 4: Optimal switching pattern – three-phase system

The hysteresis band is the region where the flux amplitude should be within, which have the width h in figure 16. The width of the hysteresis band will define the switching frequency of the voltage vector. A lower width will mean a higher frequency and vice-versa.

The stator flux has to be estimated to the optimum switching vector selection and for the calculation of the electromagnetic torque. Therefore a combined voltage-current model of the induction motor is a necessary component of the control algorithm. Once the stator flux is known, the expression for torque is:

$$T_{em} = \frac{3}{2} p\text{Real}(j\lambda_s i_s) \tag{19}$$

DTFC provides a very fast torque response by quickly changing the position of the stator flux-linkage space vector relative to the rotor flux-linkage space vector, or in other words, by quickly changing its speed [26].

The complete diagram of the test model using 3-phase DTFC is presented in the Appendix "G", page 158.

5.3.3. Further Considerations

The control methods previously described are not the only existent ones, but probably are the most popular. In the state they are presented previously, they are effective to control the motor in steady-state condition, but offer some restrictions to transient conditions.

FOC and DTFC methods can adjust the developed torque and selected magnetic flux, both in steady state and transient operating conditions [20], but in order to obtain an optimal adjustment with minimization of power losses and torque ripples (specially during transient mode) it is necessary to combine these control methods with other kind of dynamic control.

For that purpose it is used speed and position control systems with linear, variable structure and machine intelligence controllers [20].

Part of this study is assess which method would be the more appropriate to be used in the propulsion system under investigation, allowing the best response under steady state and transient conditions. Further developments then will be necessary when applying these techniques to the 15-phase induction motor.

5.3.4. Selection

A method of control has to be selected, in order to be fully developed into a 15-phase control system. As shown before, Scalar Methods are obsolete and today the Voltage/Frequency Controllers are only used in low performance applications [20]. Therefore the options available are the FOC and the DTFC.

In order to verify the adequacy (ability to follow the control strategy and compliance with the control requirements) of each control method to be applied on the propulsion system in study, Simulink representations (Appendixes "F" and "G") of each method were created based on proposed mathematical formulations existent in the technical literature, and their performance in a simple 3-phase system assessed and compared.

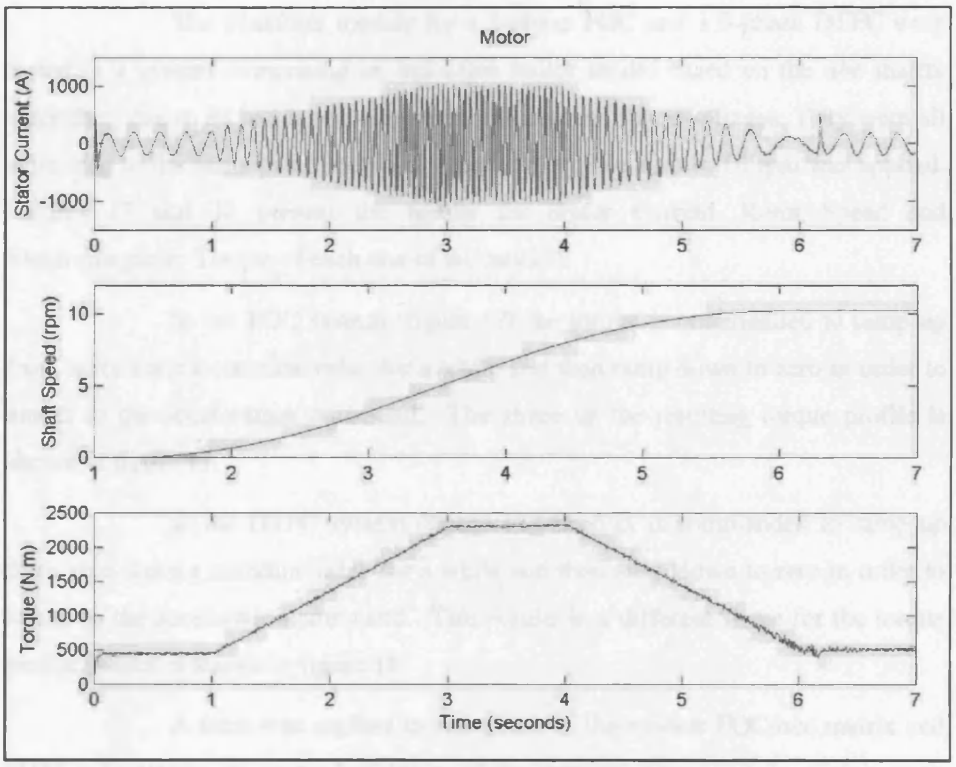

Figure 17: System with Field-Oriented Control

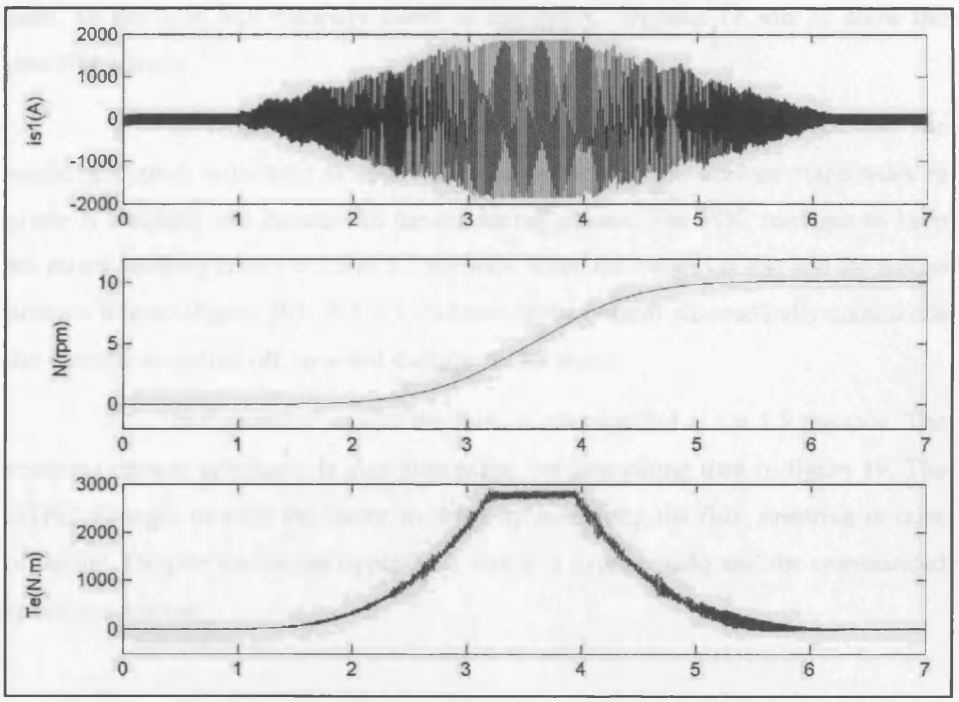

Figure 18: System with Direct Torque and Flux Control

The Simulink models for a 3-phase FOC and a 3-phase DTFC were tested in a system comprising an induction motor model based on the *abc* matrix algorithm, due to its better accuracy under unbalanced stator voltages. They were all submitted to the same parameters and acceleration from zero to 10 rpm was applied. Figures 17 and 18 present the results for Stator Current, Rotor Speed and Electromagnetic Torque of each one of the models.

In the FOC system (figure 17) the torque is commanded to ramp up from zero, keep a constant value for a while and then ramp down to zero in order to attend to the acceleration command. The shape of the resulting torque profile is shown in figure 17.

In the DTFC system (figure 18) the flux is commanded to ramp up from zero, keep a constant value for a while and then ramp down to zero in order to attend to the acceleration command. This results in a different shape for the torque profile, which is shown in figure 18.

A fault was applied to one phase of the models FOC/*abc* matrix and DTFC/*abc* matrix, to assess behaviour of the systems. Since simple models were used at this stage, there is no mechanism to provide the optimum response to the fault, so the fault will naturally result in instability. Figures 19 and 22 show the resulting curves.

In figures 19 and 20 the fault is applied at t = 3.5 seconds. The resulting current unbalance is noticeable due to decrease in current magnitudes in phase A (faulted) and increase in the remaining phases. The FOC manages to keep the motor working from t = 3.5 to 3.7 seconds, when the control is lost and the torque plunges to zero (figure 20). At t = 3.75 seconds the control automatically commands the currents to switch off, to avoid damage to the motor.

In figures 21 and 22 the fault is also applied at t = 3.5 seconds. The resulting current unbalance is also noticeable, but less strong than in figure 19. The DTFC manages to keep the motor working by increasing the flux, resulting in raise of torque. Despite the torque ripples, the motor is kept running and the commanded speed is achieved.

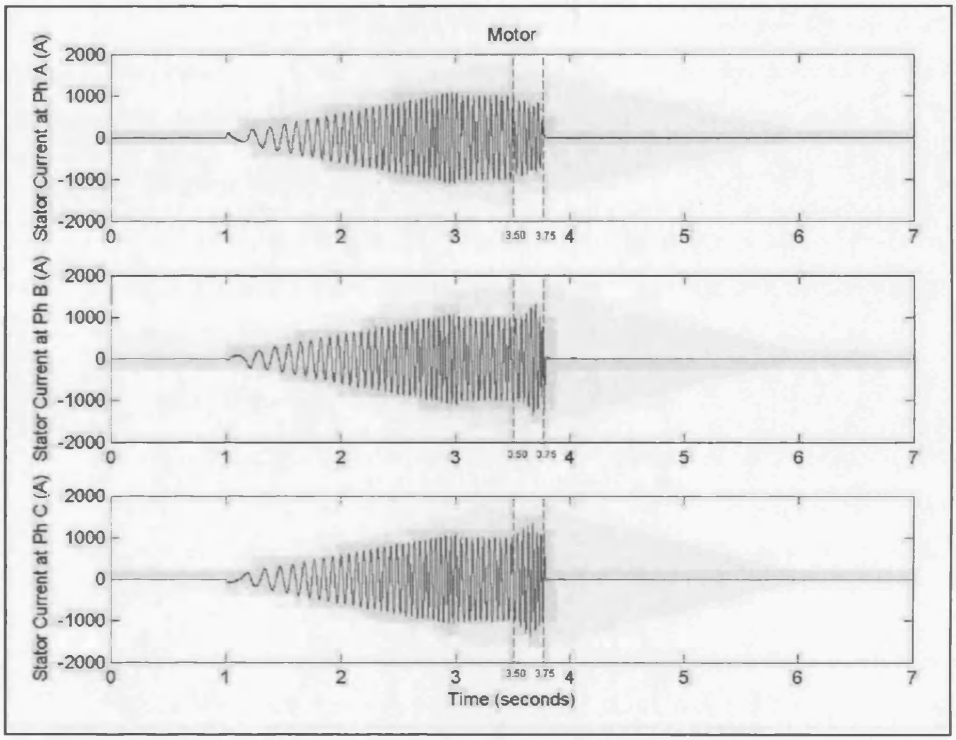

Figure 19: Stator current in System with FOC – one phase faulted at t = 3.5 sec

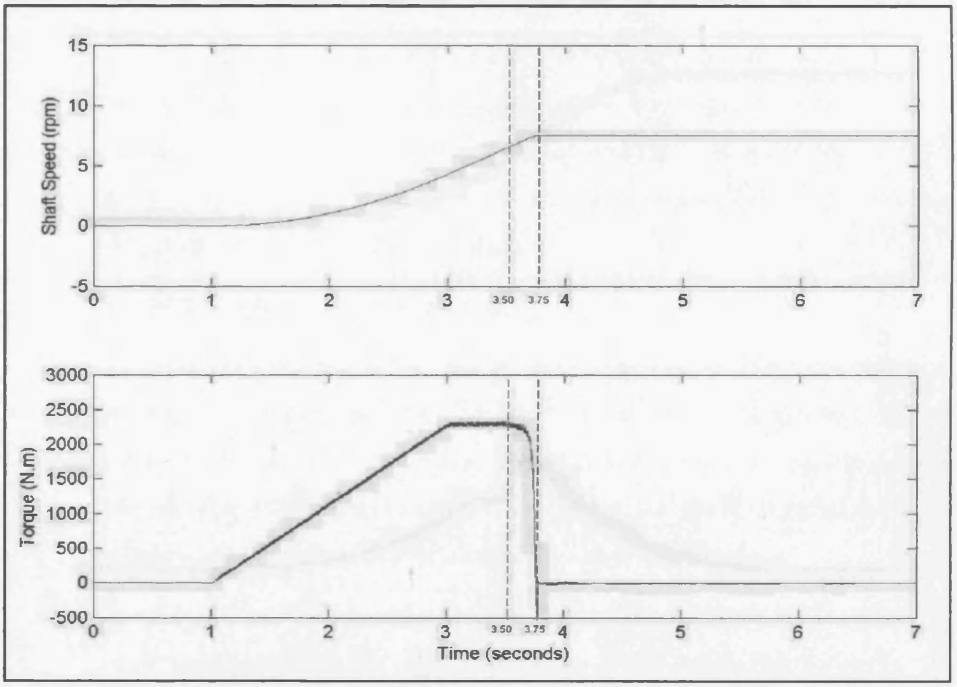

Figure 20: Motor output in System with FOC – one phase faulted at t = 3.5 sec

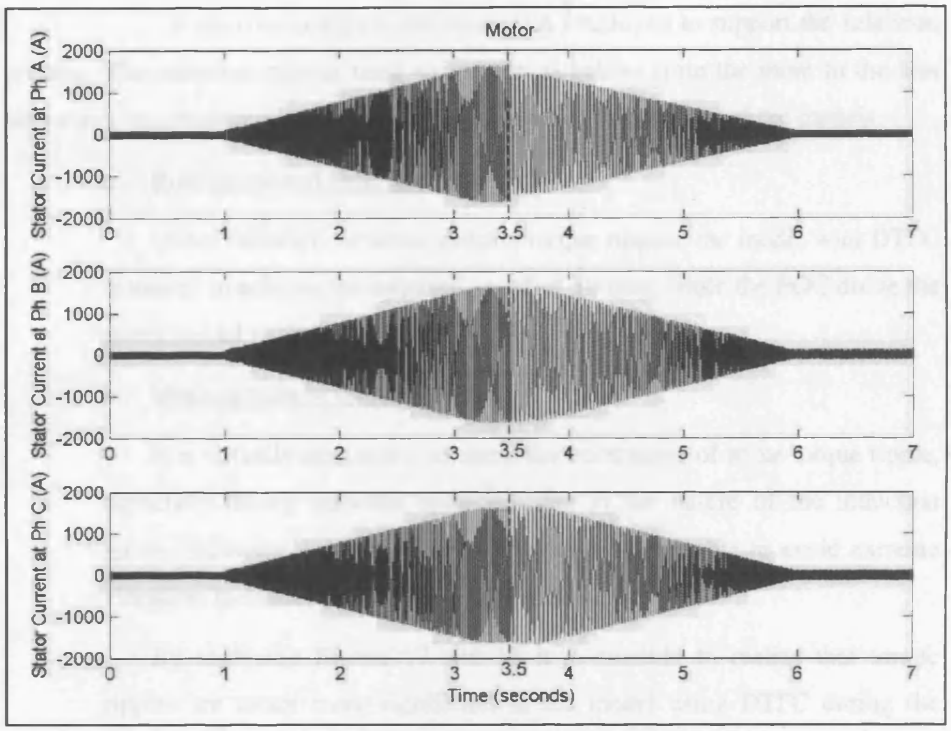

Figure 21: Stator current in System with DTFC – one phase faulted at t = 3.5 sec

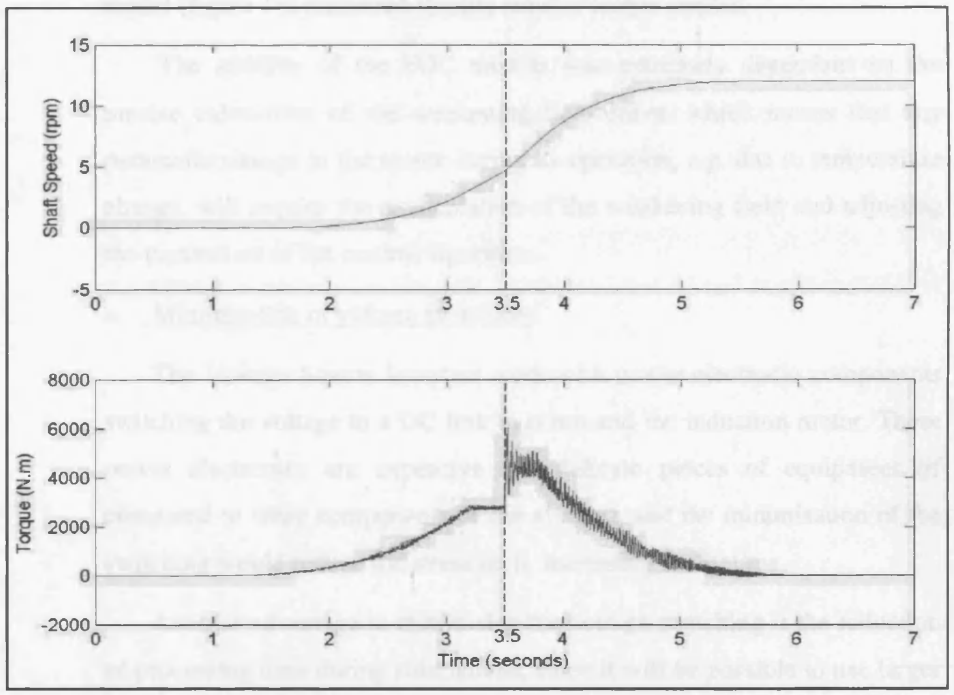

Figure 22: Motor output in System with DTFC – one phase faulted at t = 3.5 sec

A decision analysis tool was again employed to support the selection process. The selection criteria used are presented below, from the more to the less important, accompanied by comments regarding the performance of the models:

a. Robustness and fault-tolerance:

Under faulted conditions, despite torque ripples, the model with DTFC managed to achieve the required speed of 10 rpm, while the FOC drove the motor model to stall.

b. Minimisation of torque ripples:

It is virtually impossible to avoid the occurrence of some torque ripple, especially during transient response, due to the nature of the induction motor. However the minimisation of ripples is desirable to avoid extreme vibration, to reduce losses and minimise noise.

By analysing figures 17 and 18 it is possible to realize that torque ripples are much more significant in the model using DTFC during the transient mode, therefore in that particular aspect the FOC had better performance than the DTFC. After steady state was achieved the DTFC model (figure 18) presented slightly smaller torque ripples.

The stability of the FOC models was extremely dependant on the precise calculation of the weakening field curve, which means that any parameter change in the motor during its operation, e.g. due to temperature change, will require the recalculation of the weakening field and adjusting the parameters of the control algorithm.

c. Minimisation of voltage switching:

The Voltage Source Inverters work with power electronic components switching the voltage in a DC link to command the induction motor. These power electronics are expensive and delicate pieces of equipment (if compared to other components of the system), and the minimisation of the switching would reduce the stress on it, increasing its lifetime.

Another advantage in minimising the voltage switching is the reduction of processing time during simulations, since it will be possible to use larger sample time in the fixed-time discrete models.

To allow comparison the same sample time of $5x10^{-5}$ seconds was used for all models. The FOC models presented a rate of 6520 switches per second while the DTFC models presented a rate of 2105 switches per second (about 68% reduction).

d. Minimisation of stator current:

It is important in order to reduce losses and optimise the motor performance. The FOC responded better to this requirement. Since FOC have a modulator, it is possible to adjust frequency of the supply voltage. This means it is easier to control the slip, making the motor work at the optimum operational point and therefore minimising the stator currents.

e. Lower complexity:

The Simulink models under testing represent just the core of a complete control system algorithm. After choosing the control method, its implementation will imply in the construction of a more detailed algorithm, which should cope with every possible operational scenario.

For that reason it is a disadvantage to start from an already complex algorithm that will need to grow considerably during its implementation.

The DTFC is a more sophisticated concept, but has a simpler realisation – and consequently a simpler algorithm – if compared to FOC.

f. Availability of literature:

It is important to support the development and implementation of a complete algorithm. FOC has considerably more technical bibliography than DTFC, since it has been in the market for longer.

The resulting decision making matrix is:

	Weight	FOC	FOC weighted	DTFC	DTFC weighted
Robustness and fault-tolerance	10.0	7.0	70.0	9.0	90.0
Minimisation of torque ripples	10.0	8.0	80.0	8.0	80.0
Minimisation of voltage switching	5.0	5.0	25.0	8.0	40.0
Minimisation of stator current	5.0	10.0	50.0	7.0	35.0
Lower Complexity	3.0	6.0	18.0	10.0	30.0
Available Literature	3.0	10.0	30.0	5.0	15.0
Total			**273.0**		**290.0**

Table 5: Control choice matrix

Since the DTFC had a better score in the decision-making matrix and it is a more sophisticated and naturally robust algorithm, then it is the chosen method to be used in the building of a 15-phase controller to be fitted in the propulsion System Model.

5.4 Development of the 15-phase Control System

Having selected the control method, now it is necessary to build a control algorithm for the 15-phase induction motor. The principle is similar to the 3-phase DTFC tested previously; however instead of dividing the locus of the stator flux space-phasor in six sectors, it will be divided in 30 sectors, as shown in figure 23:

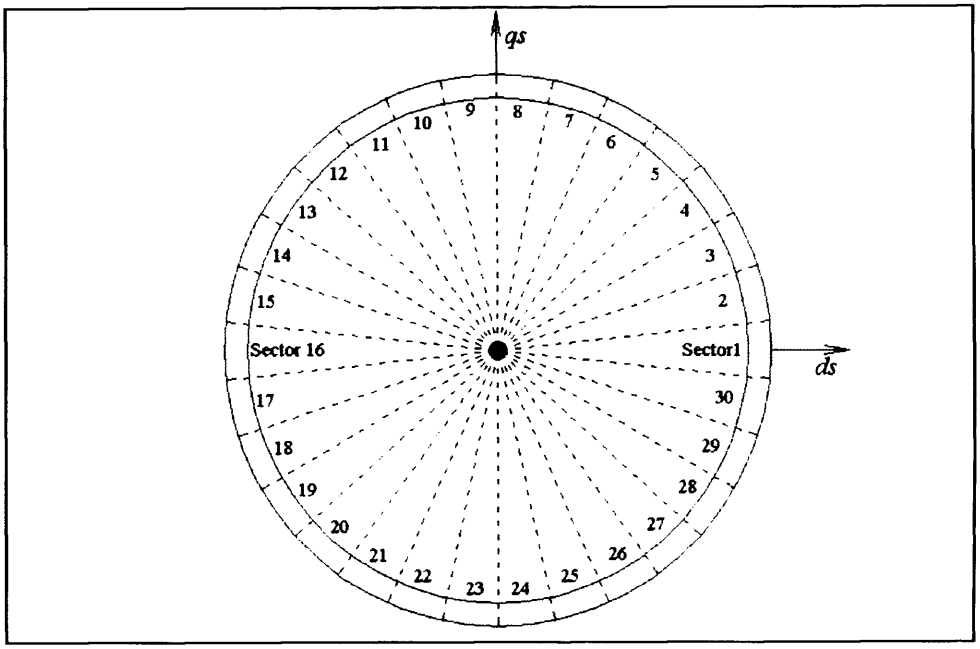

Figure 23: Stator flux space-phasor divided in 30 sectors

Now the table of optimal switching will be:

Vectors V_1 to V_{30} are active switching vectors: (1 1 1 1 -1 -1 -1 -1 -1 -1 -1 -1 -1 1 1 1); (1 1 1 1 -1 -1 -1 -1 -1 -1 -1 -1 -1 1 1 1); ... ; (1 1 1 -1 -1 -1 -1 -1 -1 -1 -1 -1 1 1 1 1) and (1 1 1 -1 -1 -1 -1 -1 -1 -1 -1 -1 1 1 1 1).

Vectors V_0 is the zero switching vector: (-1 -1 -1 -1 -1 -1 -1 -1 -1 -1 -1 -1 -1 -1 -1) or (1 1 1 1 1 1 1 1 1 1 1 1 1 1 1)

$\theta_s(i)$		$\theta_s(1)$	$\theta_s(2)$	$\theta_s(3)$	$\theta_s(4)$	$\theta_s(5)$	$\theta_s(6)$
λ	T						
1	1	V_6	V_7	V_8	V_9	V_{10}	V_{11}
1	-1	V_{26}	V_{27}	V_{28}	V_{29}	V_{30}	V_1
0	1	V_0	V_0	V_0	V_0	V_0	V_0
0	-1	V_0	V_0	V_0	V_0	V_0	V_0
-1	1	V_{11}	V_{12}	V_{13}	V_{14}	V_{15}	V_{16}
-1	-1	V_{21}	V_{22}	V_{23}	V_{24}	V_{25}	V_{26}

* Vectors V_1 to V_{30} are active switching vectors: (1 1 1 1 -1 -1 -1 -1 -1 -1 -1 -1 1 1 1); (1 1 1 1 -1 -1 -1 -1 -1 -1 -1 -1 -1 1 1 1); ... ; (1 1 1 -1 -1 -1 -1 -1 -1 -1 -1 -1 1 1 1 1) and (1 1 1 -1 -1 -1 -1 -1 -1 -1 -1 -1 1 1 1 1).
Vectors V_0 is the zero switching vector: (-1 -1 -1 -1 -1 -1 -1 -1 -1 -1 -1 -1 -1 -1 -1) or (1 1 1 1 1 1 1 1 1 1 1 1 1 1 1)

$\theta_s(i)$		$\theta_s(7)$	$\theta_s(8)$	$\theta_s(9)$	$\theta_s(10)$	$\theta_s(11)$	$\theta_s(12)$
λ	T						
1	1	V_{12}	V_{13}	V_{14}	V_{15}	V_{16}	V_{17}
1	-1	V_2	V_3	V_4	V_5	V_6	V_7
0	1	V_0	V_0	V_0	V_0	V_0	V_0
0	-1	V_0	V_0	V_0	V_0	V_0	V_0
-1	1	V_{17}	V_{18}	V_{19}	V_{20}	V_{21}	V_{22}
-1	-1	V_{27}	V_{28}	V_{29}	V_{30}	V_1	V_2

* Vectors V_1 to V_{30} are active switching vectors: (1 1 1 1 -1 -1 -1 -1 -1 -1 -1 -1 1 1 1); (1 1 1 1 -1 -1 -1 -1 -1 -1 -1 -1 -1 1 1 1); ... ; (1 1 1 -1 -1 -1 -1 -1 -1 -1 -1 -1 1 1 1 1) and (1 1 1 -1 -1 -1 -1 -1 -1 -1 -1 -1 1 1 1 1).
Vectors V_0 is the zero switching vector: (-1 -1 -1 -1 -1 -1 -1 -1 -1 -1 -1 -1 -1 -1 -1) or (1 1 1 1 1 1 1 1 1 1 1 1 1 1 1)

$\theta_s(i)$		$\theta_s(13)$	$\theta_s(14)$	$\theta_s(15)$	$\theta_s(16)$	$\theta_s(17)$	$\theta_s(18)$
λ	T						
1	1	V_{18}	V_{19}	V_{20}	V_{21}	V_{22}	V_{23}
1	-1	V_8	V_9	V_{10}	V_{11}	V_{12}	V_{13}
0	1	V_0	V_0	V_0	V_0	V_0	V_0
0	-1	V_0	V_0	V_0	V_0	V_0	V_0
-1	1	V_{23}	V_{24}	V_{25}	V_{26}	V_{27}	V_{28}
-1	-1	V_3	V_4	V_5	V_6	V_7	V_8

* Vectors V_1 to V_{30} are active switching vectors: (1 1 1 1 -1 -1 -1 -1 -1 -1 -1 -1 1 1 1); (1 1 1 1 -1 -1 -1 -1 -1 -1 -1 -1 1 1 1); ... ; (1 1 1 -1 -1 -1 -1 -1 -1 -1 -1 1 1 1 1) and (1 1 1 -1 -1 -1 -1 -1 -1 -1 -1 1 1 1 1).
Vectors V_0 is the zero switching vector: (-1 -1 -1 -1 -1 -1 -1 -1 -1 -1 -1 -1 -1 -1 -1) or (1 1 1 1 1 1 1 1 1 1 1 1 1 1 1)

$\theta_s(i)$		$\theta_s(19)$	$\theta_s(20)$	$\theta_s(21)$	$\theta_s(22)$	$\theta_s(23)$	$\theta_s(24)$
λ	T						
1	1	V_{24}	V_{25}	V_{26}	V_{27}	V_{28}	V_{29}
1	-1	V_{14}	V_{15}	V_{16}	V_{17}	V_{18}	V_{19}
0	1	V_0	V_0	V_0	V_0	V_0	V_0
0	-1	V_0	V_0	V_0	V_0	V_0	V_0
-1	1	V_{29}	V_{30}	V_1	V_2	V_3	V_4
-1	-1	V_9	V_{10}	V_{11}	V_{12}	V_{13}	V_{14}

* Vectors V_1 to V_{30} are active switching vectors: (1 1 1 1 -1 -1 -1 -1 -1 -1 -1 -1 1 1 1); (1 1 1 1 -1 -1 -1 -1 -1 -1 -1 -1 1 1 1); ... ; (1 1 1 -1 -1 -1 -1 -1 -1 -1 -1 1 1 1 1) and (1 1 1 -1 -1 -1 -1 -1 -1 -1 -1 1 1 1 1).
Vectors V_0 is the zero switching vector: (-1 -1 -1 -1 -1 -1 -1 -1 -1 -1 -1 -1 -1 -1 -1) or (1 1 1 1 1 1 1 1 1 1 1 1 1 1 1)

$\theta_s(i)$		$\theta_s(25)$	$\theta_s(26)$	$\theta_s(27)$	$\theta_s(28)$	$\theta_s(29)$	$\theta_s(30)$
λ	T						
1	1	V_{30}	V_1	V_2	V_3	V_4	V_5
1	-1	V_{20}	V_{21}	V_{22}	V_{23}	V_{24}	V_{25}
0	1	V_0	V_0	V_0	V_0	V_0	V_0
0	-1	V_0	V_0	V_0	V_0	V_0	V_0
-1	1	V_5	V_6	V_7	V_8	V_9	V_{10}
-1	-1	V_{15}	V_{16}	V_{17}	V_{18}	V_{19}	V_{20}

Table 6: Optimal switching pattern – 15-phase system

A simple *dq* model calculates the magnetising flux. The rotor speed is fed into a PI controller generating the torque command. These are the controlling variables that will define the switching pattern from the optimal switching table. The corresponding Simulink model using 15-phase DTFC is presented in the Appendix "H", page 160.

5.5 Validation

A simple system, combining 15-phase DTFC, motor, propeller and ship was put together to test and validate the newly developed control algorithm. The Simulink block diagram is presented in the Appendix "I", page 164.

The objective is to check if the motor follows the commands of the control system, producing a smooth shaft speed curve and torque pulsations within a tolerable limit. The resulting diagrams are presented in figure 24.

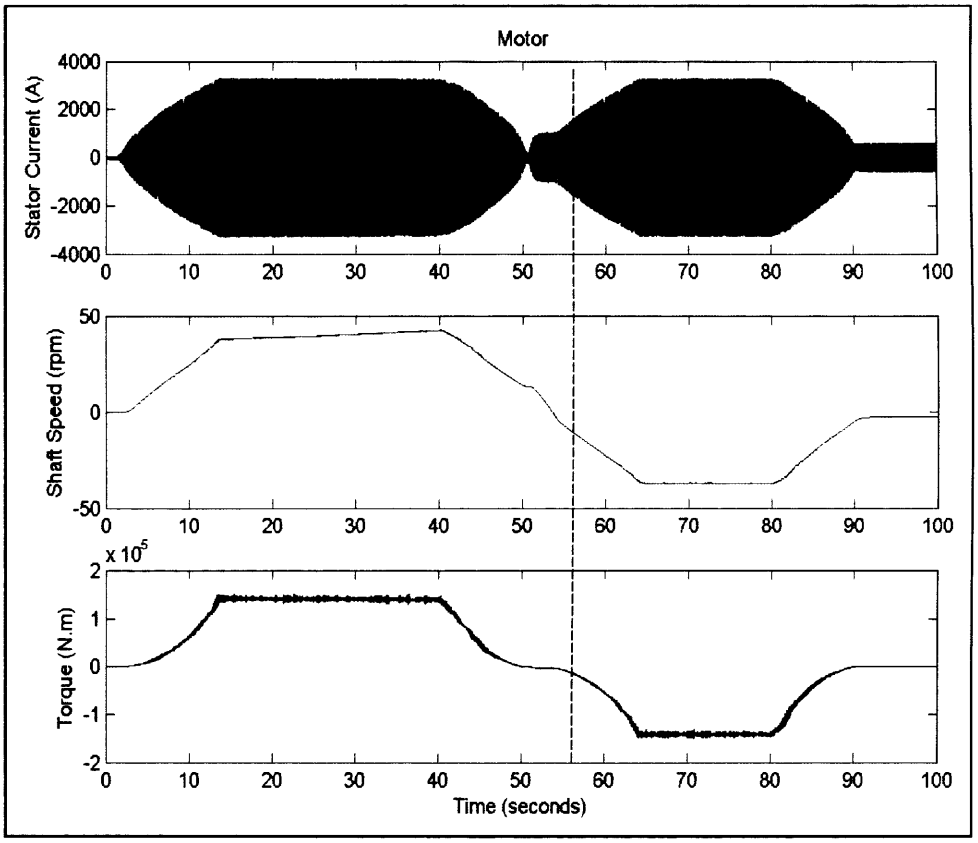

Figure 24: 15-phase DTFC test diagrams

The result is satisfactory. The shaft speed is varied from zero to 40 ahead, then to 40 astern, then to zero again. The speed variation is reasonably smooth and the torque ripples are minimal.

5.6 Conclusions

Two main methods of induction motor control were investigated: Field Oriented Control (FOC) and Direct Torque and Flux Control (DTFC).

3-phase models using each method were built, to analyse the performance of each system and the compliance with basic requirements, in special the robustness and fault-tolerance.

Each method has its advantages: FOC has the major benefit of being a well known fully documented control technique; DTFC benefits from being extremely fault-tolerant.

In warship propulsion system the ability to maintain the propulsive motor running despite adverse operational scenarios is an invaluable feature, which put the DTFC method on the lead during the decision process to select the control method.

A 15-phase Control algorithm based on DTFC method was developed; the model implemented in Simulink and validated to control a 15-phase Induction Motor model. The control system is consequently ready to be fitted in the System Model.

6.0 CHAPTER SIX – Assessment of Existing Models for Integration

6.1 Introduction – Description of Existing Models

The models available from previous works, which can be incorporated in the model of the Integrated Electric Propulsion System, are:

- AVR Type II
- WR21 Gas Turbine with Governor
- Propeller
- Ship

6.1.1. AVR Type II

The model of the Excitation System AVR Type II (or ST2A Excitation System Model) was developed by Konrad Ciaramella (Department of Mechanical Engineering – UCL – London) [7], based on the IEEE standard 421.5-1992 [27], and shown in figure 25:

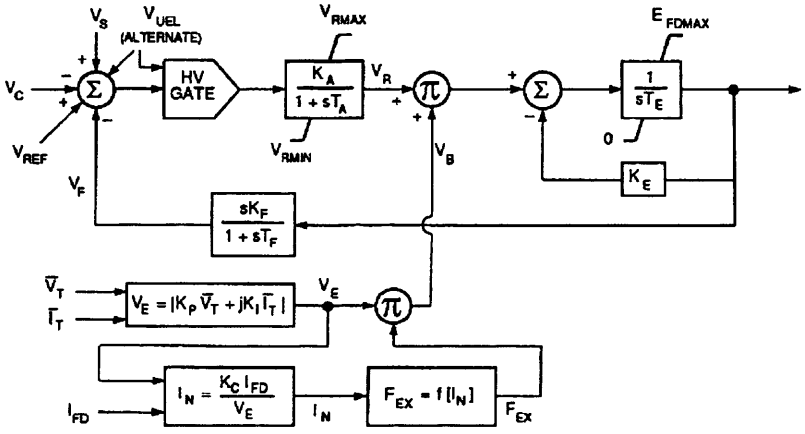

Figure 25: ST2A Excitation System

6.1.2. WR21 Gas Turbine and Governor

The models of the WR21 Gas Turbine and Governor were developed by Dr. Rajendra C. Patel (Department of Mechanical Engineering – UCL – London) [7] to represent an ICR Gas Turbine loosely based on the Rolls-Royce WR21. This design comprises: a low-pressure compressor and turbine; a high-pressure compressor and turbine; a free power turbine and a combustion chamber.

As actual data on the WR21 ICR is commercially restricted, the required characteristics curves for matching the turbine and compressor data have been extracted from the reference [29]. The turbine and compressor characteristics are given for values relative to certain designs parameters. This and other parameters, which are required by the matching procedure, are [7]:

Constant pressure specific heat of the air	1.005 KJ/(Kg.K)
Specific heat ratio of the air	1.4
Specific heat ratio of the gas	1.01
Ambient temperature	288 K
Cooling water temperature	283 K
Regenerator efficiency	0.9
Intercooler efficiency:	0.9
Mechanical efficiency of the LP shaft	0.99
Mechanical efficiency of the HP shaft	0.99
Pressure losses in the Intercooler, Regenerator and Combustion Chamber	2%

Table 7: Parameters of ICR Gas Turbine

For the given design values the LP and HP compressor characteristics, as well the LP, HP and FP turbine characteristics are given in the Appendix "J", page 165 [7].

6.1.3. Propeller

The propeller model was developed by R. D. Geertsma (Royal Netherlands Navy / University College London – 1999) [30]. The propeller model calculates the thrust and torque using speed and shaft revolutions. The required parameters are the propeller characteristic curves. In this case, it is necessary to use Beta to C_t and C_q curves to cover all four quadrants of operation.

The parameters from the Wageningen B5-75 propeller series were used, supplied by the Maritime Royal Institute of Netherlands [31].

The other parameters of the propeller model are the relative rotational efficiency and the wake fraction.

The efficiency of a propeller in open water (with no hull) is called open-water efficiency; the same propeller behind a hull has a different efficiency than in open water, called behind-hull efficiency. The ratio of behind-hull efficiency upon open-water efficiency is called relative rotational efficiency.

Wake fraction is the average deficiency reflected in the axial flow of the propeller plane caused by the wake of the ship hull.

Estimate values were selected:

- Relative rotational efficiency: 99% for positive ship speed and 100% for negative ship speed.
- Wake fraction: 0.03 for positive speed and 0 for negative speed.

6.1.4. Ship

The ship model was developed by R. D. Geertsma and P. Methven (Royal Netherlands Navy / University College London – 1999) [30]. It calculates the ship speed from propeller thrust. The fundamental input parameter is the power-speed curve of the ship. The other parameters are:

- Thrust deduction factor: it was estimated to be 0.06 for any ship speed.
- Ship mass: assumed 6200 ton.

6.2 Further Development - Real-Time Requirements

There are a number of software packages available to provide real-time capability to the MATLAB/Simulink environment. Real-Time Workshop is the add-on produced by MathWorks Inc. to use MATLAB/Simulink as front-end interface for editing graphic models in block-diagram format, which are afterwards used by the real-time module to generate the necessary code for real-time simulations on a single or more target processors.

The use of real-time simulator allows rapid prototyping of complex systems in particular, and testing of embedded systems in general [23].

The main requirement for the model in order to be compatible with the real-time capability is to have fixed step algorithm. As a result the continuous state blocks existent in the current models are to be replaced by the equivalent discrete state blocks.

This is an easy procedure regarding the integrator blocks, because its parameters don't need to be changed. However for the transfer function blocks the recalculation of all parameters is necessary, since they are dependent of the time step, given that continuous transfer functions are in the s-plane, and discrete transfer functions are in the z-plane.

There are several ways for mapping from the s-plane to z-plane. The most accurate one is using the relationship $z = e^{sT}$. Where:

T = Sampling time (sec/sample)

s = Location in the s-plane

z = Location in the z-plane

It is not possible to obtain transfer function in this way because the discrete-time transfer function would have more zeroes than poles, which is not realizable. Instead it is possible to use the bilinear transformation shown below [32]:

$$s = \frac{2}{T_s} \cdot \frac{z-1}{z+1} \qquad \text{(where Ts = Time step)} \qquad (20)$$

Other enviable characteristic to a real-time model is to have a time step of a proper size. A large time step can provide faster simulation; a small time step can provide more precise results; and an excessively small time step can produce accumulative roundness error: that's why balance has to be achieved.

The target value set for this work is 25 μs, which is the time step supported by a range of real-time hardware simulators commercially available.

6.3 Validation

Again it will be used the initial assumption that the models available in the toolbox SimPowerSystems produce valid results, which could be used to assess and validate new models.

6.3.1. Validation of the Excitation System AVR Type II:

The 'psbturbine.mdl' is a demonstration model of SimPowerSystems that illustrates the use of the synchronous machine associated with a turbine, governor and excitation system blocks. It was developed by Louis-A. Dessaint and R. Champagne (École de Technologie Superieure, Montréal), and comprises a three-phase generator connected to a network through a Delta-Wye transformer.

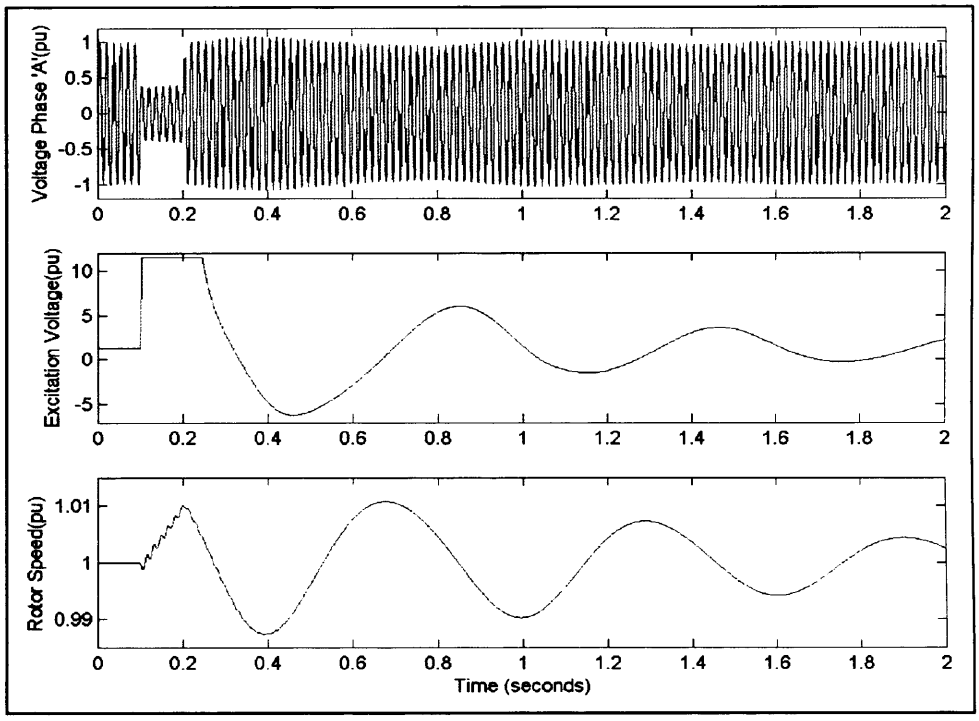

Figure 26: Reference for validation – Results for 'psbturbine.mdl'

In figure 26 is presented the simulation results of the model. At t = 0.1 second a three-phase to ground fault occurs on the low-voltage bus bar. The fault is cleared after 6 cycles (t = 0.2 s). The system is initialized in order to start in steady state with the generator supplying 1 pu of active power. As the rated values will not be important for the validation, all the response outputs were transformed to per unit.

The results, in per unit, of voltage on phase 'A' (high-voltage side of transformer), excitation voltage generate by the AVR and rotor speed are presented in figure 26 and will be the reference for the validation process.

The model uses an AVR Type I (IEEE standard), from the SimPowerSystems library, however it will be necessary to use an AVR Type II (or

ST2A Excitation System Model), which is the kind of excitation system present in the WR21 GTA, and, differently from the Type I, it utilises a phasor combination of the terminal voltage and terminal current to generate a model of the exciter power source.

The new excitation model was fitted in the 'psbturbines.mdl' model, keeping all the parameters and conditions unchanged. The gains and output limits of the new excitation model were set to match the parameters of the system. The resulting outputs are shown in figure 27:

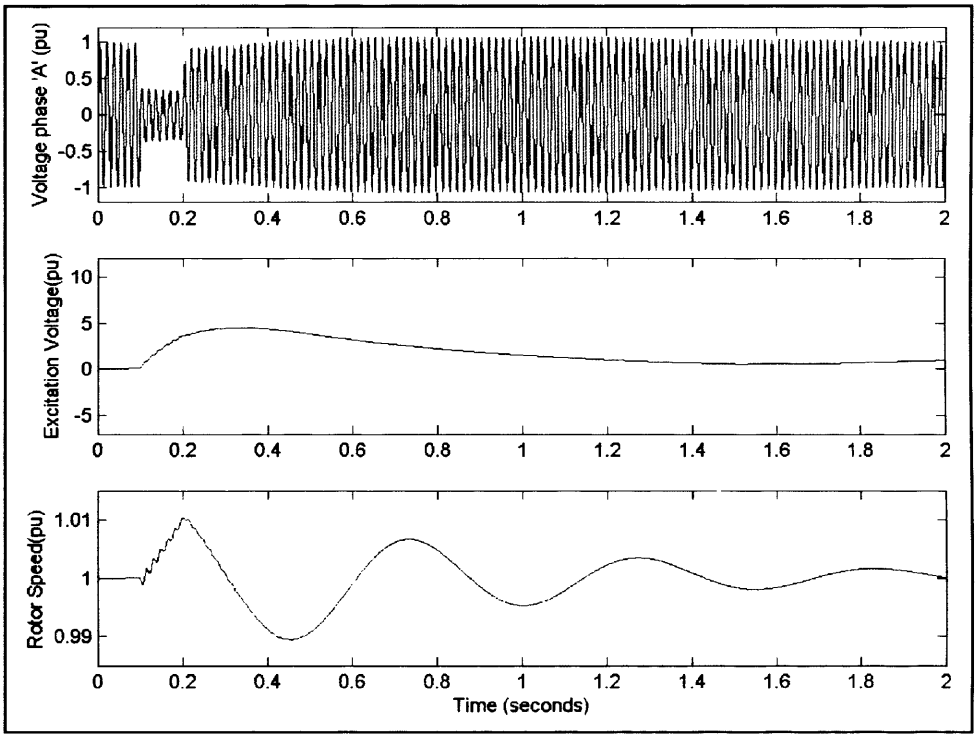

Figure 27: Results for 'psbturbine.mdl' with AVR Type II fitted

The differences comparing the resulting diagrams of the new model (figure 27) with the reference (figure 26) are clear. Since the AVR Type II has a different algorithm and utilises a combination of terminal voltages and currents, it is expected to achieve a result dissimilar from the AVR Type I, having superior performance. It can be confirmed realizing that voltage in phase A regains its value in less than 0.2 seconds in figure 27, differently from figure 26, where it takes approximately 1.4 seconds.

This is recognizable by the reduction in voltage oscillation after recovery from the fault; by the smooth variation of excitation voltage and by the tendency to 'easy the job' of the governor, making the speed move quickly and efficiently to the reference value of 1 pu.

As a result the AVR Type II model is validated to generate excitation for a synchronous generator model and regulate its voltage output to a constant reference value.

6.3.2. Validation of the WR21 Gas Turbine and Governor model

A SimPowerSystems model was used to represent the alternator (synchronous motor block), and therefore it is assumed that this component is already validated by Mathworks / Hydro-Quebec. Therefore the validation is to be focused on the Gas Turbine model.

The model 'psbturbine.mdl' presented previously is to be used as reference in the validation process again.

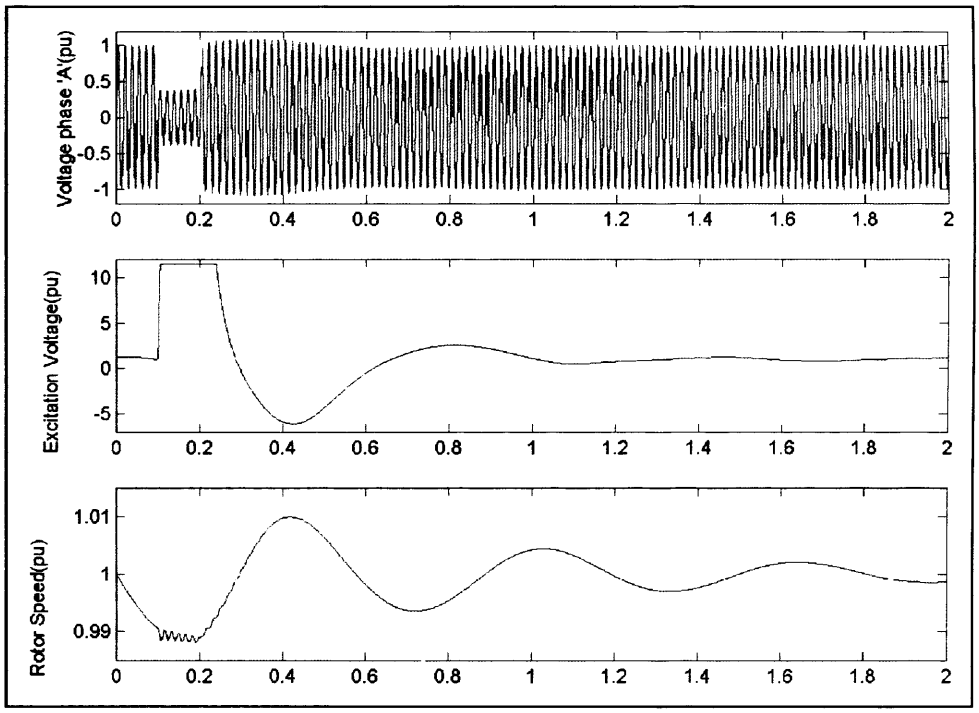

Figure 28: Results for 'psbturbine.mdl' with WR21 Gas Turbine model fitted

The WR21 Gas Turbine and Governor model was fitted in the 'psbturbines.mdl' System Model, keeping all the parameters and conditions unchanged. Since the link between the turbine and the alternator is set in per unit, there was no need to match the power rate of the turbine model with the alternator in SI. The resulting outputs are shown in figure 28.

Comparing the results (figure 28) with the reference (figure 26) it is possible to assume that the response of the system is coherent, due to better efficiency of the WR21 Gas Turbine Model and faster reaction of the new governor. Voltage in phase A regains its value in less than 0.8 seconds in figure 28, differently from figure 26, where it takes approximately 1.4 seconds. Rotor speed takes more time to increase in figure 28, due most likely to the higher inertia of the WR21 gas turbine.

Considering that the Intercooled Recuperated Gas Turbine is a very complex device, it demands a complex model to represent it adequately. Therefore other outputs of the simulation model have to be assessed in order to allow a proper validation (as for example the temperature and pressure in each stage during different operational conditions). Having no reliable source of data to compare is an obvious restriction and in effect makes impossible the progression of the validation.

In conclusion, the model of the WR21 Gas Turbine with Governor presents coherent results working in a valid ICR GT system, but it cannot be considered properly validated unless compared with actual data. It is suitable strictly for academic purposes, and therefore is to be considered having restricted validation.

6.3.3. Validation of the Propeller model

To validate the model, a comparison with the Robinson curves of a fixed-pitch propeller from Mikkola [33] was performed. The diagrams are presented in figures 29 and 30:

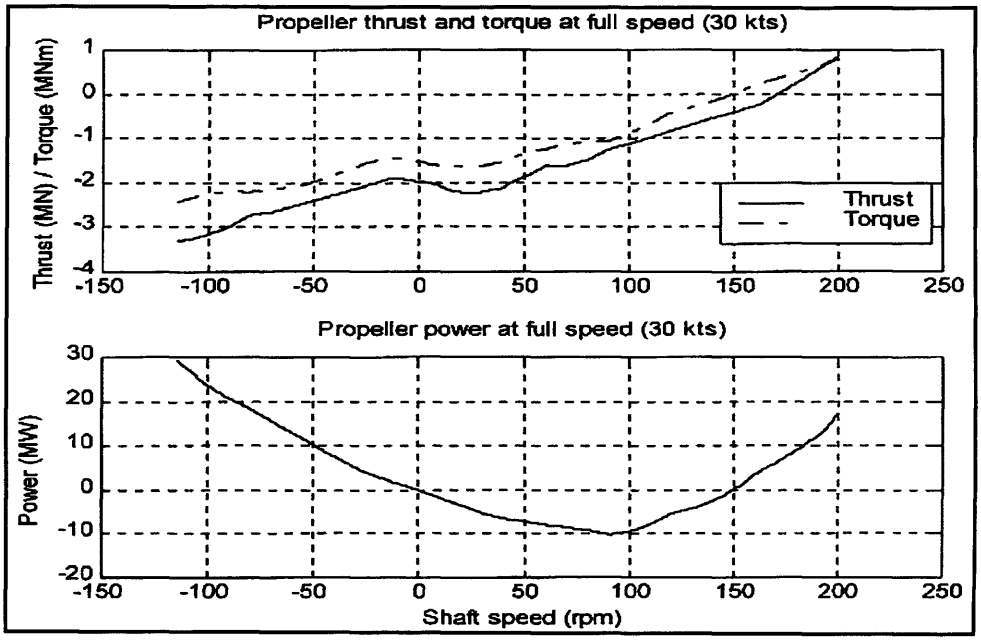

Figure 29: Reference curves for propeller model

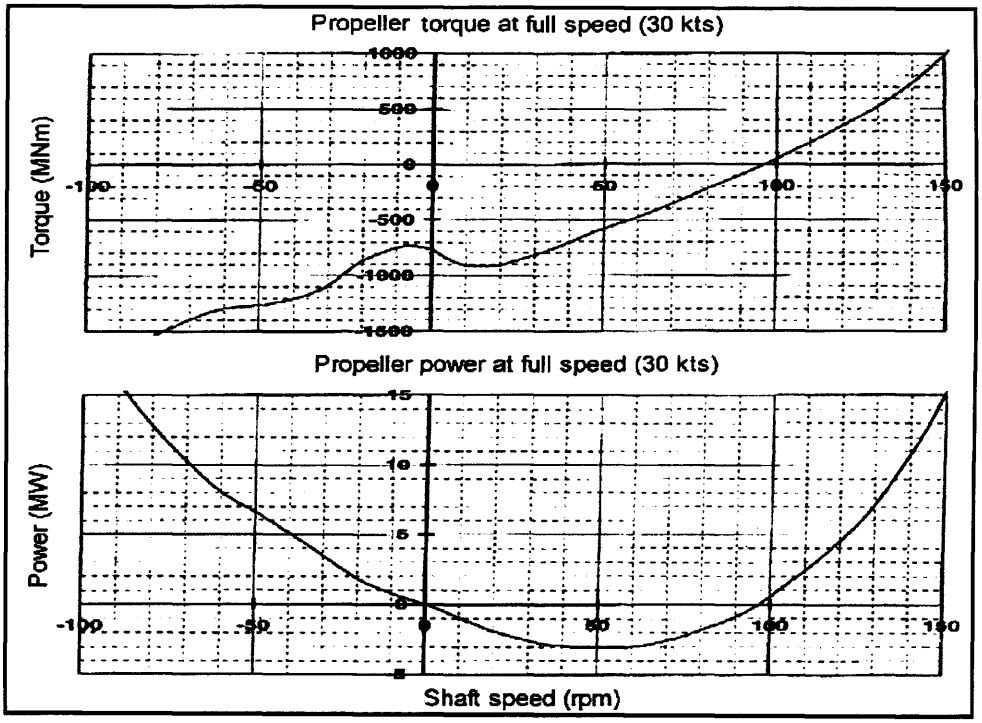

Figure 30: Actual curves of propeller model

In the diagrams torque is the momentum, or "rotational force", applied to the propellers and thrust is the reaction force generated by the ship when the propellers are turned to accelerate water backwards (or forwards). The comparison between figures 29 and 30 demonstrates the similarities between the two sets of curves. Although the propellers have different characteristics, it is possible to realise that the shape of curves produced by the model are coherent, therefore allowing the validation. But there are two important remarks about this validation:

- It depends on the characteristic curves, which are input data; therefore the model is validated to represent exclusively the Wageningen B5-75 propeller, and in order to simulate another propeller it is necessary to have the correspondent Beta to C_t and C_q curves available.
- Cavitation was not included in the characteristic curves and is an important effect to be considered. In order to have a precise simulation, it is necessary to take the cavitation effect into account.

It is important to point out that the propeller of the Type 45 ship has a different diameter, therefore the model had to be scaled in order to represent more properly the actual propeller.

6.3.4. Validation of the Ship model

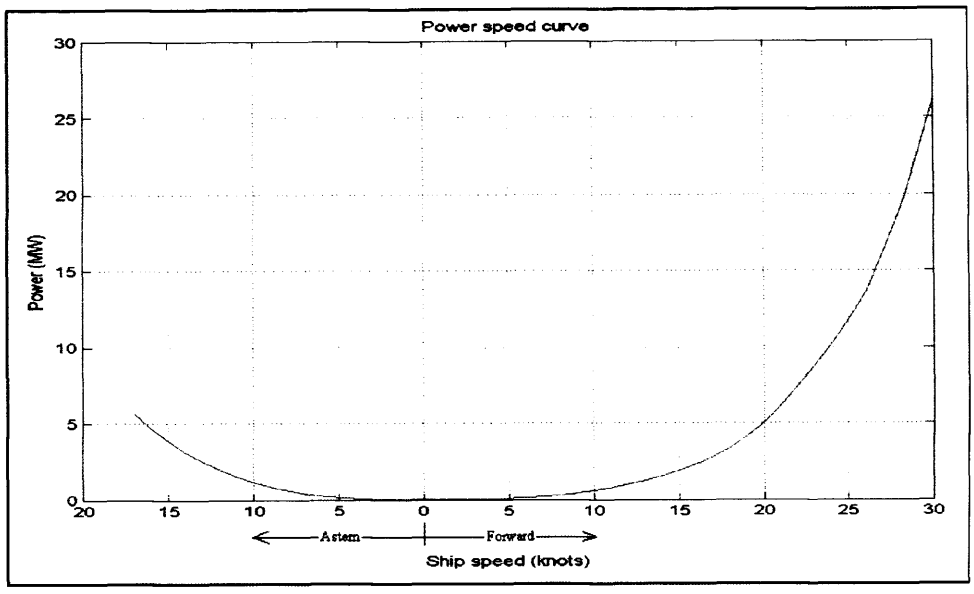

Figure 31: Power-speed curve of Ship Model

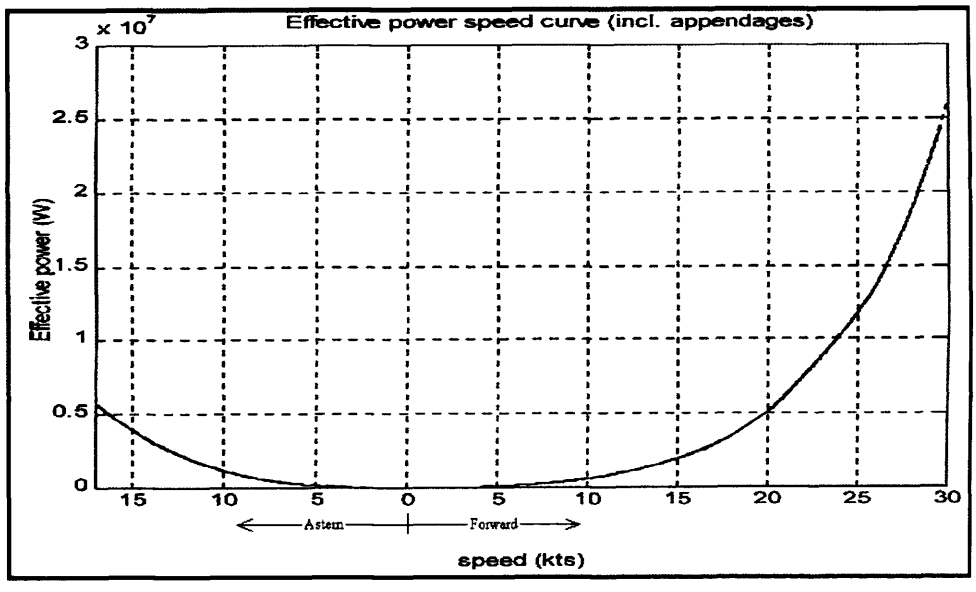

Figure 32: Power-speed curve of Royal Netherlands Navy Frigate [31]

The ship model performance is inherently dependent on the precision of the input parameters, therefore the validation of the model was done comparing the power-speed curve of the model (figure 31) with the Air Defence and Command Frigate of the Royal Netherlands Navy (figure 32). Since the curves are similar in

shape, the model is validated for academic purposes, to loosely simulate the ship response of a Frigate hull. Further validation would only be possible with availability of tow tank or full-scale tests data.

The remark about scaling is also applicable. The hull of the Type 45 ship has different dimensions and displacement, therefore the model had to be scaled in order to represent more properly the actual hull that displaces approximately 6200 ton.

6.4 Conclusions

The existing subsystems were developed in Simulink/SimPowerSystems, hence compatible with the new models. However they were modelled in continuous mode, with variable time step, what is incompatible with the real-time application. For that reason the subsystem models of the AVR Type II, WR21 Gas Turbine with Governor, Propeller and Ship were adapted, by transforming its continuous blocks into discrete blocks, in order to be integrated in the real-time System Model.

The validation of each model, performed in previous works, was reassessed. In this case lack of actual data still a disadvantage, which constrains the validation process and produces limitations in the reliability of the resulting outputs. Despite the limitations, the subsystem models produced consistent responses and are cleared to be used in the next developments of the present work.

All the described subsystem models are parameterized. Its pre-settings can be straightforwardly accessed and changed through pop-up windows by double-clicking on the subsystem block, in order to allow easy update in case more reliable data becomes available.

7.0 CHAPTER SEVEN – System Model Development

7.1 Introduction

After having the entire main components (or subsystems) ready and validated, it is possible to put together a larger System Model, representing the propulsion system, in order to perform the following investigations:

- Steady-state analysis
- Transient analysis – crash-stop manoeuvre
- Faulted electrical propulsion motor
- Large and small generator operating in parallel

This System Model, although representing a larger and more complex system, will still be a limited representation of reality. The composition of the System Model will be described next, followed by a summary of the limitations incorporated by the main subsystems.

7.2 Composition

The main subsystems put together to represent the System Model are:

- AVR Type II;
- WR-21 ICR Gas Turbine with Governor;
- 20 MW 4.16 KV Synchronous motor;
- Bus bar;
- Service Load;
- Rectifiers;
- DC Link (inductors and capacitors);
- Inverters;
- Dynamic Braking Resistance (resistors and IGBTs);

- Direct Torque and Flux Control System;
- Induction motor;
- Propeller; and
- Ship.

All these components, combined with connectors, switches, measurements, displays and other secondary blocks, are put together to represent one entire propulsive line, from one extreme end (the generation of electric power) to the other (the transformation of electric in mechanical power resulting in ship motion).

The flow chart of the System Model is presented in figure 3. The diagram of the resulting System Model is presented in the Appendix "K", page 171.

7.3 Limitations

The System Model of this project only represents one shaft line, although the actual system comprises two shaft lines interconnected. Consequently the influence of parallel operation with another shaft line (which is not negligible) is discarded in the present System Model.

The construction and simulation of a more complete System Model, having two shaft lines, is feasible since all the subsystems are available, but it would be necessary a more powerful hardware, to cope with a heavier model, and availability of more time to development and analysis.

The System Model also doesn't feature all the subsystems of an actual system. Secondary components, like circuit breakers, electric switches, line filters etc, are not included in order to achieve a lighter model, capable of running in small computers with a reasonable speed.

The limitations of each subsystem also have to be taken into account. They are summarized in the following table:

Model	Situation	Limitations
15-phase *dq*-reference Induction Motor	Validated	Only for balanced voltage operation & constant parameters (no iron-core saturation simulated for example).
15-phase *matrix*-algorithm Induction Motor	Validated	Only for balanced voltage operation & constant parameters (no iron-core saturation simulated for example). This model has the capability of processing unbalanced voltage supply, however no actual data was found to properly validate this capability.
15-phase Inverter	Validated	Only for constant parameters (parameters not affected by temperature changes for example).
AVR Type II	Validated	Tested only for Reference Voltage = 1 pu and Underexcitation Limiter Output of zero.
WR21 Gas Turbine and Governor	Validated	Simulation results dependent on input parameters, due to extensive use of Look-up tables. Actual parameters not available, therefore validation is good only to apply the model for academic purposes.
Propeller	Validated	Simulation results dependent on input parameters, due to extensive use of Look-up tables. Therefore it is validated only to represent the Wageningen B5-75 propeller. Cavitation effect not included.
Ship	Validated	Simulation results dependent on input parameters, due to extensive use of Look-up tables. Therefore it is validated only to loosely represent a 6200 ton Frigate. Effects of ship trim and balance not included.

Table 8: Summary of validation / limitations

The limitations, as expected, reflect in the reliability of the System Model. The correct input parameters and look-up tables would make possible a considerable improvement in the precision of outputs, strengthening the reliability. In order to achieve that a considerable effort was made to adequately gather and

estimate the necessary input parameters, as seen in the next topic. Nevertheless changing these parameters and look-up tables was made a straightforward procedure during the modelling process, in order to allow in the future the enhancement of outputs preciseness and trustworthiness.

7.4 Parameters Estimation for the System Model

The System Model under construction is loosely based on the Type 45 propulsion system; therefore it is desirable the use of parameters taken from the actual system. However it sill under development and most of the design data is not available or is classified.

In a visit to the Electric Ship Technology Demonstrator (ESTD) some general data, potentially useful for the simulation, was collected. The main ones are:

- Prime-mover (WR-21 GTA):
  - Power rate: 20 MW
  - Power factor: 0.9
  - Rated voltage: 4160 V
  - Rated frequency: 60 Hz
- AC Bus Bar:
  - Rated voltage: 4160 V
  - Rated current: 1100 A
  - Rated frequency: 60 Hz
- DC Bus Bar:
  - Rated voltage: 5600 V
  - Rated current: 1410 A
- Dynamic Braking Resistance:
  - Rated voltage: 0 - 5600 V
  - Rated current: 100 A rms
- Propulsion Motor:
  - Rated torque: 1.061 MNm (all range of speeds)

- Maximum speed ahead: 180 rpm
- Maximum speed astern: 90 rpm
- Number of phases: 15
- Number of poles: 12 (6 pairs)

Though it is useful information, it is not enough to provide full support for the simulation.

Another source of information is reference [24], which deals with the "Integrated Propulsion System" – IPS – Programme, the American version of the British IFEP Programme. It is possible to find a set of convenient parameters for the Synchronous Alternator, DC Link components and Advanced Induction Motor. Despite the programmes being slightly different, the parameters are practical for this project. They are:

- Synchronous Machine:
  - Stator resistance: 1.27×10^{-3} Ohms
  - Stator leakage inductance: 396×10^{-6} Henry
  - Stator d-axis magnetizing inductance: 2.79×10^{-3} Henry
  - Stator q-axis magnetizing inductance: 2.51×10^{-3} Henry
  - Field resistance referred to the stator: 401×10^{-6} Ohms
  - Field inductance referred to the stator: 227×10^{-6} Henry
  - Dampers d-axis resistance: 4.74×10^{-3} Ohms
  - Dampers d-axis leakage inductance: 69.8×10^{-6} Henry
  - Dampers q-axis resistance: 5.26×10^{-3} Ohms
  - Dampers q-axis leakage inductance: 157×10^{-6} Henry
  - Number of poles: 2
- AVR Type II:
  - Voltage regulator maximum output: 7.3 pu
  - Voltage regulator minimum output: 0 pu

- Excitation control system stabiliser gain: 0.03
- Voltage regulator gain: 400
- Voltage regulator time constant: 20 x 10^{-3} s
- Exciter constant, related to self excited field: 1.0
- Exciter time constant, integration rate associated with exciter: 0.8
- Excitation control system stabiliser time constant: 1.0

- DC Link:
  - Inductance: 3 x 10^{-3} Henry
  - Capacitance: 1 x 10^{-3} Faraday

- Advanced Induction Motor:
  - Stator resistance: 122 x 10-3 Ohms
  - Stator leakage inductance: 6.79 x 10-3 Henry
  - Rotor referred resistance: 35.7 x 10-3 Ohms
  - Rotor referred leakage inductance: 7.62 x 10-3 Henry
  - Magnetising inductance: 145 x 10-3 Henry
  - Rated Frequency: 15.0 Hz
  - Number of Poles: 12
  - Inertia constant*: 5 x 10^3 Kg.m^2

* Inertia constant estimated considering:

- Overall weight ~ 65 tonnes;
- External diameter ~ 2.5 m;

$$J = \frac{W \times D^2}{8 \times g} \approx \frac{65 \times 10^3 \times 2.5^2}{8 \times 9.81} \approx 5 \times 10^3 \, Kg.m^2$$

Reference [34] deals with dynamic braking resistor calculation, and can be used to establish the maximum value of the Brake resistance. The proposed formulation is:

$$R_{db1} = \frac{(V_d)^2}{P_b} \tag{21}$$

Where:

R_{db1} = Maximum allowable value for the dynamic brake resistor (ohms)

V_d = DC bus voltage the chopper module regulates

P_b = Peak breaking power in watts, which is:

$$P_b = \frac{J_T[\omega_b(\omega_b - \omega_0)]}{(t_3 - t_2)} \tag{22}$$

Where:

J_T = Total inertia reflected to the motor shaft (kg-m^2)

ω_b = Rated angular rotational speed (Rad/s)

ω_o = Angular rotational speed less than rated speed down to zero (Rad/s)

$t_3 - t_2$ = Deceleration time from ω_b to ω_o (seconds)

Therefore:

$J_T = 5000$ kg-m^2

$\omega_b = \frac{2 \times \pi \times 150}{60} = 15.71$ Rad/s

$\omega_o = 0$ Rad/s

$t_3 - t_2 = 35$ seconds

$$P_b = \frac{5000 \times (15.71 \times (15.71 - 0))}{35} = 35.26 \text{ kW}$$

$$R_{db1} = \frac{5600^2}{35260} = 889 \text{ Ohms}$$

The maximum total braking resistance is 889 Ohms, or $\frac{889}{3} = 296$ Ohms per Channel. The minimum resistance can be calculated using the rated values of voltage and current described before, which is $\frac{5600V}{100A} = 56$ Ohms per Channel.

The actual value must be selected within this range. If the value used is greater than the maximum, the drive can trip on DC bus overvoltage [34]. If it is smaller than the minimum, it can generate overcurrent.

At this point the list of parameters is adequate to proceed to the simulation, in order to validate the System Model. Any gap of unavailable data can be filled with the existing pre-settings of the SimPowerSystems toolbox.

The data can be adjusted and changed in the future, according to the simulation response, in order to fine-tune the system.

7.5 System Stability and Torque Pulsation

The most important dynamic effect on the System Model in the present context is the change in speed of the propeller shaft, and the consequential effect on torque[6]. Because of the fundamental principles of the Induction Motor, torque ripples will always be present, in particular during transient conditions.

One of the conditions to achieve a stable system is to keep the torque pulsation within a tolerable limit. Its effects on the system and its minimization are issues of great complexity, which involves mechanical, electrical and control aspects.

7.5.1. Mechanical Aspects

The mechanical consequences of torque pulsation are mostly vibration and noise. The normal way of reducing these unwished effects is by providing special flexible mountings to hold up the motor. Since the subject is out of scope, it will not be dealt in this work.

7.5.2. Electrical Aspects

Torque pulsations can cause instabilities to the electrical system. The inverter regulates the current waveform to adjust the electromagnetic flux, in order to maintain the torque pulsation within tolerable limits. Such regulation has the disadvantage that it makes the motor drive appear to have 'negative impedance': as the inverter voltage is reduced the DC link current will increase to maintain constant power, and vice-versa. This 'negative impedance' can result in loss of dynamic stability in the propulsion system [25].

One way of reducing the effect of this 'negative impedance' is by increasing the capacitance on the DC Link, allowing it to cope with more severe variations of the current. It has an effective result, but has also a drawback of introducing a big, expensive and unreliable component in the system [25].

Another way of addressing the problem is by incorporating a stabilization algorithm in the control system, which commands the torque in proportion to the filtered DC inverter voltage, improving the damping of the DC link. Reference [25], for example, proposes a non-linear control algorithm based on Field Oriented principle.

Due to lack of time to develop a stabilization algorithm, the System Model subject of this work will be fitted with a large capacitor at the DC Link, to address the effects of the 'negative impedance'.

7.5.3. Control Aspects

Since electromagnetic torque is proportional to rotor flux-linkage space-phasor multiplied by rotor current space-phasor (or, by the principle of action-reaction, proportional to stator flux-linkage space-phasor multiplied by stator current space-phasor) [26] it is possible to maintain the torque at a required value by increasing or decreasing flux magnitude.

In that case the sample time (or time step) of the simulation plays an important role. The shorter the sample time, the faster will be the selection of the optimum switching pattern to the inverter, in order to adjust the magnitude of the flux-linkage space-phasor and to control the produced torque, consequently reducing its ripples.

Small sample time requires heavier, faster and expensive hardware, to speed up the software processing. In an actual system, a reduction in the sample time can cause an increment in switching, due to more frequent changes in optimum patterns, and therefore submitting the IGBTs to increased stress.

The choice of control system also has influence in the torque ripple. Tests in Chapter Five have identified that FOC can have lower torque oscillations in transient mode and DTFC can have better response in steady-state.

The selected method, DTFC, actuate in the electromagnetic flux to control torque and command the speed. This actuation can be set to minimise flux or torque variation. The advantage of restricting the torque oscillation is fast torque response and very low steady-state torque ripple, but the drawback is the occurrence of large variation in stator flux magnitude and high current distortion [35]. For that

reason it is not practical setting up the DTFC to have a tight grip on the electromagnetic torque.

7.6 Conclusions

The System Model, comprising the subsystems studied in the previous Chapters of this work, loosely based on one line of the propulsion system of the Type 45 Royal Navy Destroyer, is developed but not yet validated.

In general the validation is done using comparison with actual data obtained from trials on physical systems, which would guarantee that the algorithms used for the simulation are able to mimic the reality. However the system that is being simulated is a novel one and it is still under development.

A good illustration of the major importance of availability of actual data is the ESTD itself, part of the Electric Warship Programme (the co-operative effort between France, United Stated and United Kingdom).

In order to demonstrate the electric propulsion technology applied to warship design, this physical demonstrator was built, comprising all the main equipments of the propulsion plant. One of the main objectives of the ESTD is equipment and system model validation, so that a set of validated models could be available for the assessment of future platform designs [36].

The present shortage of available data to validate the developed models is a major drawback for this project, but doesn't represent an ultimate obstacle. The alternative solution is to use available data from usual three-phase equipments and systems, doing the proper adaptations when necessary.

Even though there is lack of actual data to suitably perform the whole system validation, all the components are satisfactorily validated (with the described limitations) and therefore they are fit to be put together in a system.

The validation of the present System Model will be a result of analysis of the response under a number of scenarios, presented on Chapter Eight.

The issue of torque ripple minimization was also discussed in this Chapter, and its aspects analysed, which have straight relationship with system stability. Some torque oscillation is expected using DTFC, since a tight restriction on torque ripples would cause large variation in stator flux magnitude and high current distortion.

8.0 CHAPTER EIGHT – Results

8.1 Steady State Analysis

The goal of a steady state analysis is to find the value of variables after the system enters the steady state condition, when there are no further changes as the simulation time progresses. The assumption is that the run of the System Model will approach such a state if enough simulation time is provided and no parameters are changed.

To actually achieve such a state it is needed an outsized simulation time, due to long transient mode observed in the ship behaviour curves (resistance and speed).

Despite the difficulty, an approach to the steady-state analysis is performed and the resulting curves (for 80 and 130 rpm shaft speed) are presented in figures 33 to 38.

Figures 33 and 34 refer to simulation with control at a reference speed of 80 rpm and other parameters unchanged. The system reached a situation next to steady state after 390 seconds (simulation time).

Figures 35 and 36 refer to simulation with control at a reference speed of 130 rpm and other parameters unchanged. The system reached a situation next to steady state after 740 seconds (simulation time).

In figures 33 to 36 it is important to point out that ship resistance and speed still altering slightly, but this variation is almost negligible considering its effects on other system variables. In figures 34 and 36 it is noticeable that shaft speed has a small oscillation due to torque pulsation, but tends to stay around the pre-set value.

Since a complete steady state in the ship subsystem takes a long time to achieve, the System Model was altered to consider a constant load (much smaller than the ship load) being applied to the induction motor. The resulting outputs are presented in figures 37 to 40.

Comparing the resulting outputs it is possible to make some observations:

- The torque oscillation is always present, what is expected since the DTFC commands constant flux during the steady state mode; and
- The magnitudes of the torque and shaft speed oscillations are apparently proportional to the load torque applied to the induction motor.

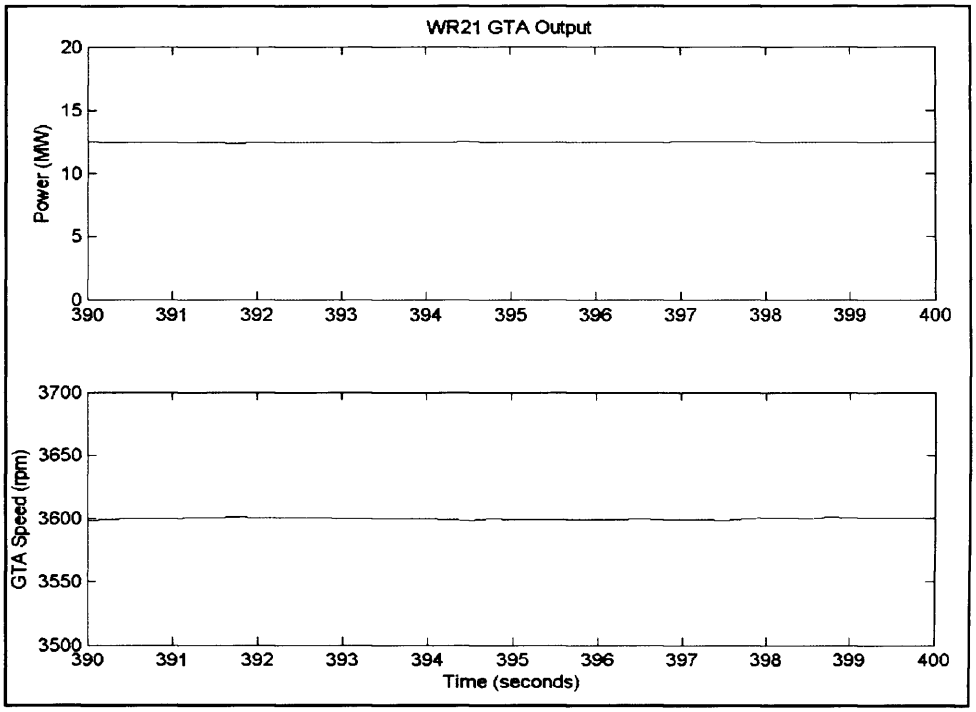

Figure 33: WR21 GTA output with control set at 80 rpm shaft speed and ship load

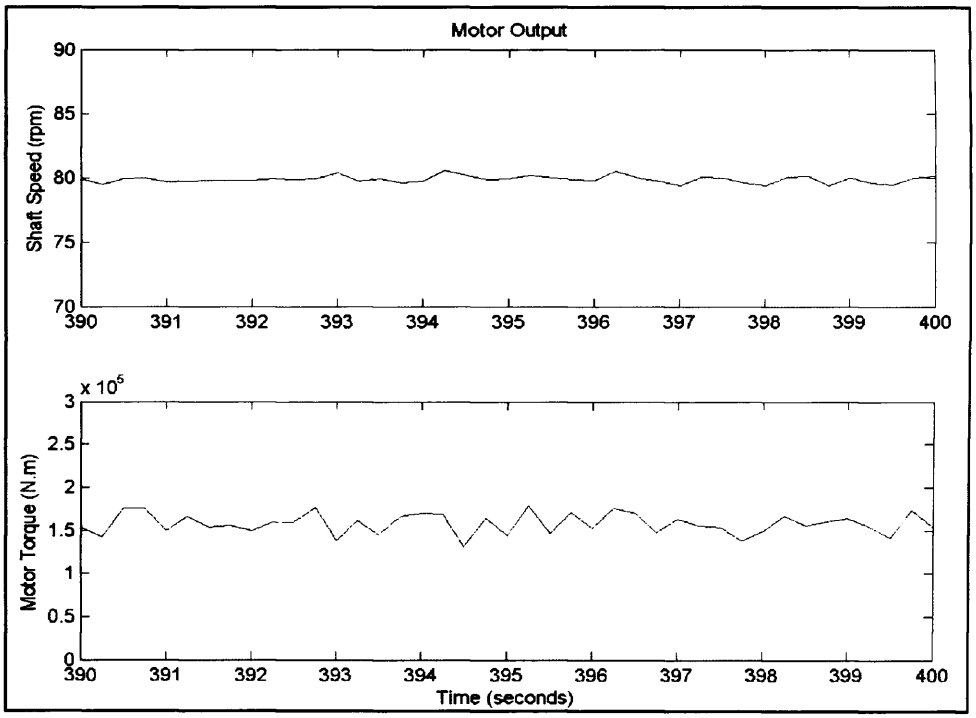

Figure 34: Motor Output with control set at 80 rpm shaft speed and ship load

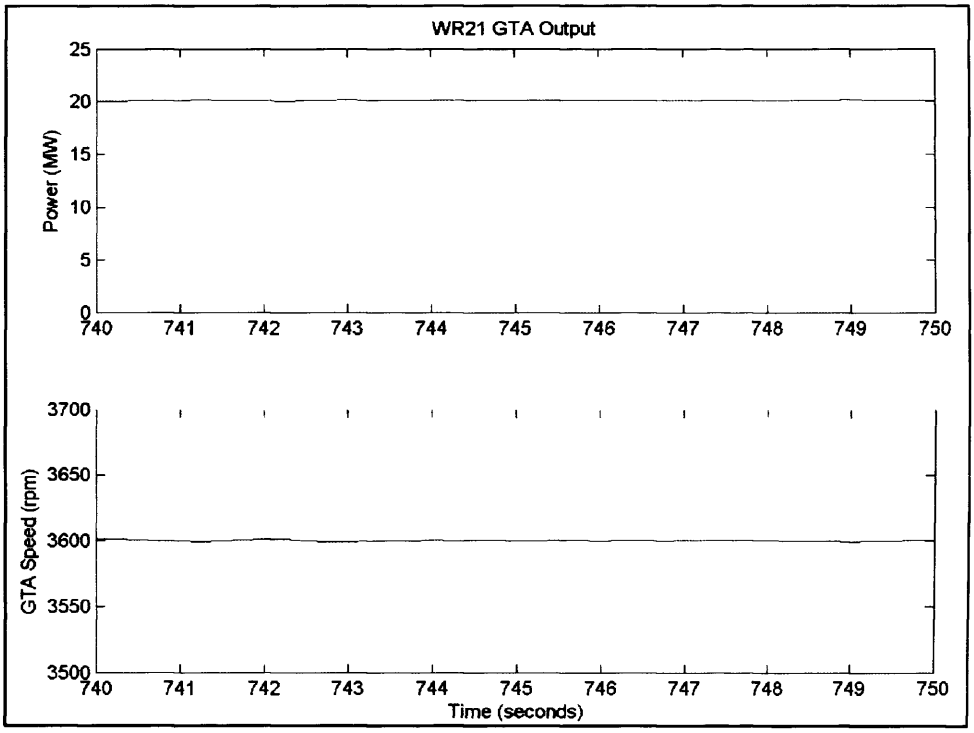

Figure 35: WR21 GTA output with control set at 130 rpm shaft speed and ship load

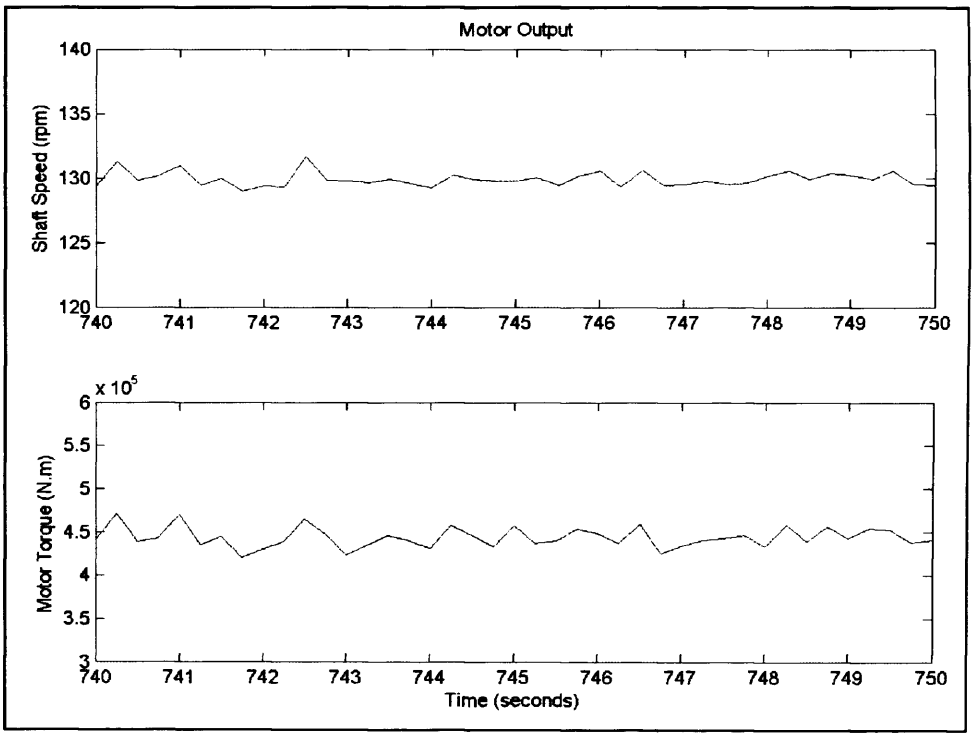

Figure 36: Motor Output with control set at 130 rpm shaft speed and ship load

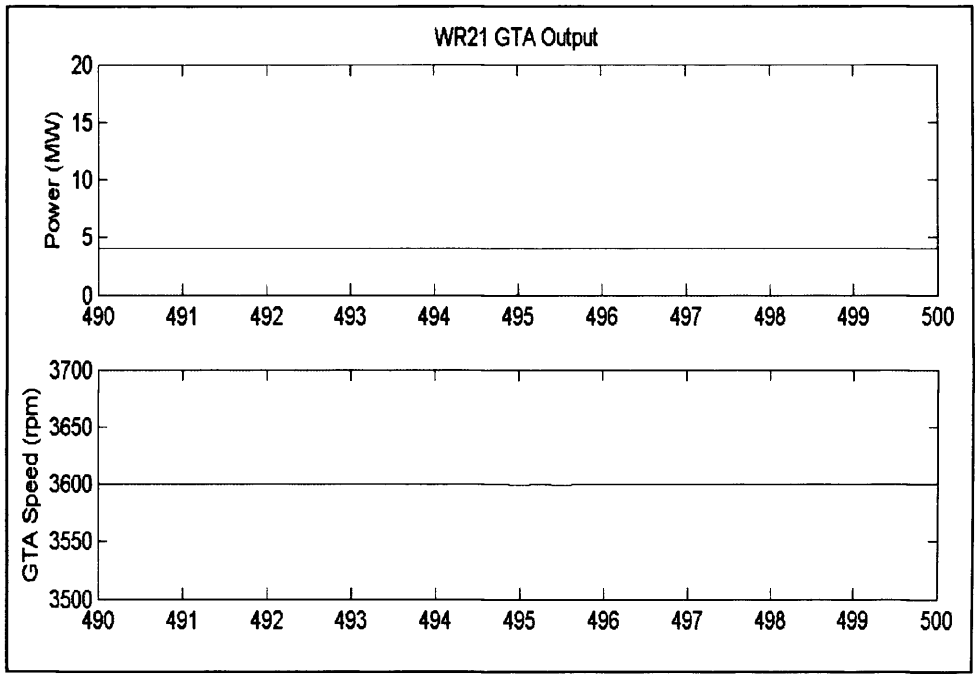

Figure 37: WR21 GTA output with control set at 80 rpm shaft speed and constant load

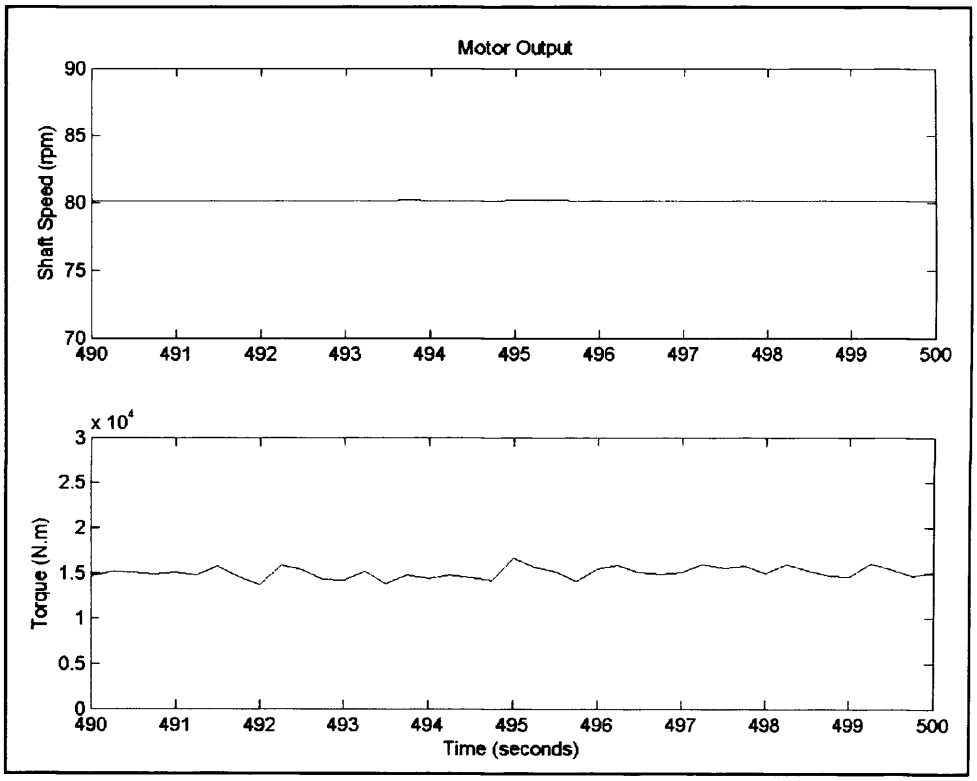

Figure 38: Motor Output with control set at 80 rpm shaft speed and constant load

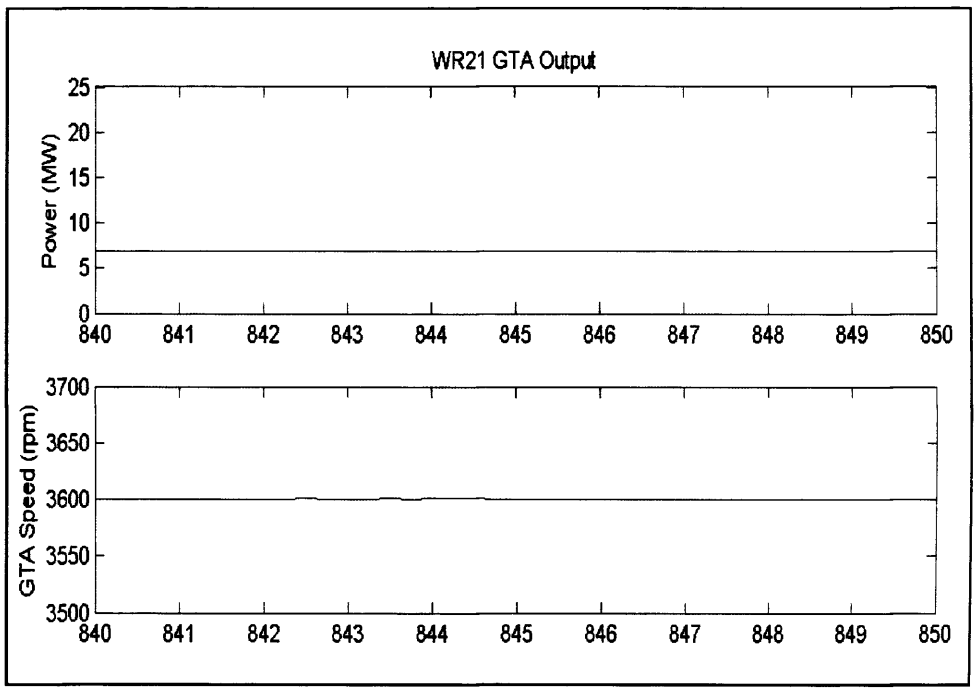

Figure 39: WR21 GTA output with control set at 130 rpm shaft speed and constant load

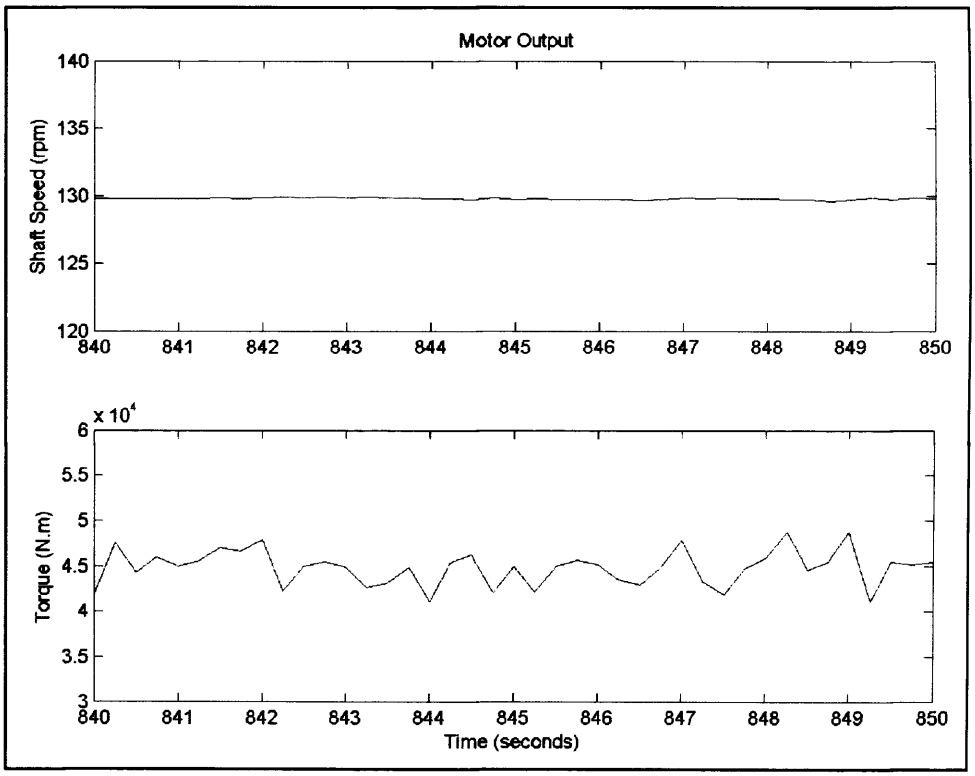

Figure 40: Motor Output with control set at 130 rpm shaft speed and constant load

8.2 Transient Analysis – Crash-stop Manoeuvre

One major convenience offered by the computational modelling is the simulation of dynamic behaviour of mechanic and electric systems, to allow the analysis of transient conditions. In the present context, the most important dynamic effect is that of the change in speed of the propeller shaft, and the consequential effect on torque [6].

One of the most severe transient conditions occurs during the crash-stop manoeuvre, which consists in bringing the ship from full speed ahead to standstill in the shortest time possible. It is a definitive test for the system and the control algorithm.

Figures 41, 42 and 43 shows the behaviour of some main variables during the crash-stop manoeuvre:

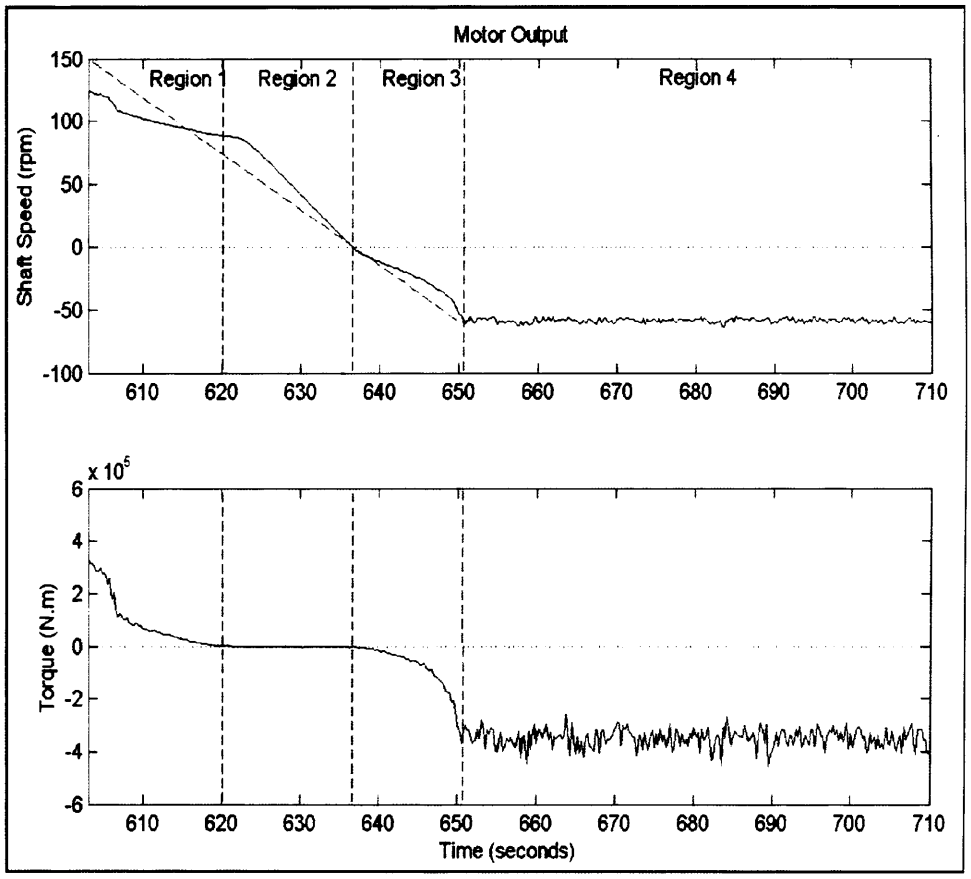

Figure 41: Motor output during crash-stop manoeuvre

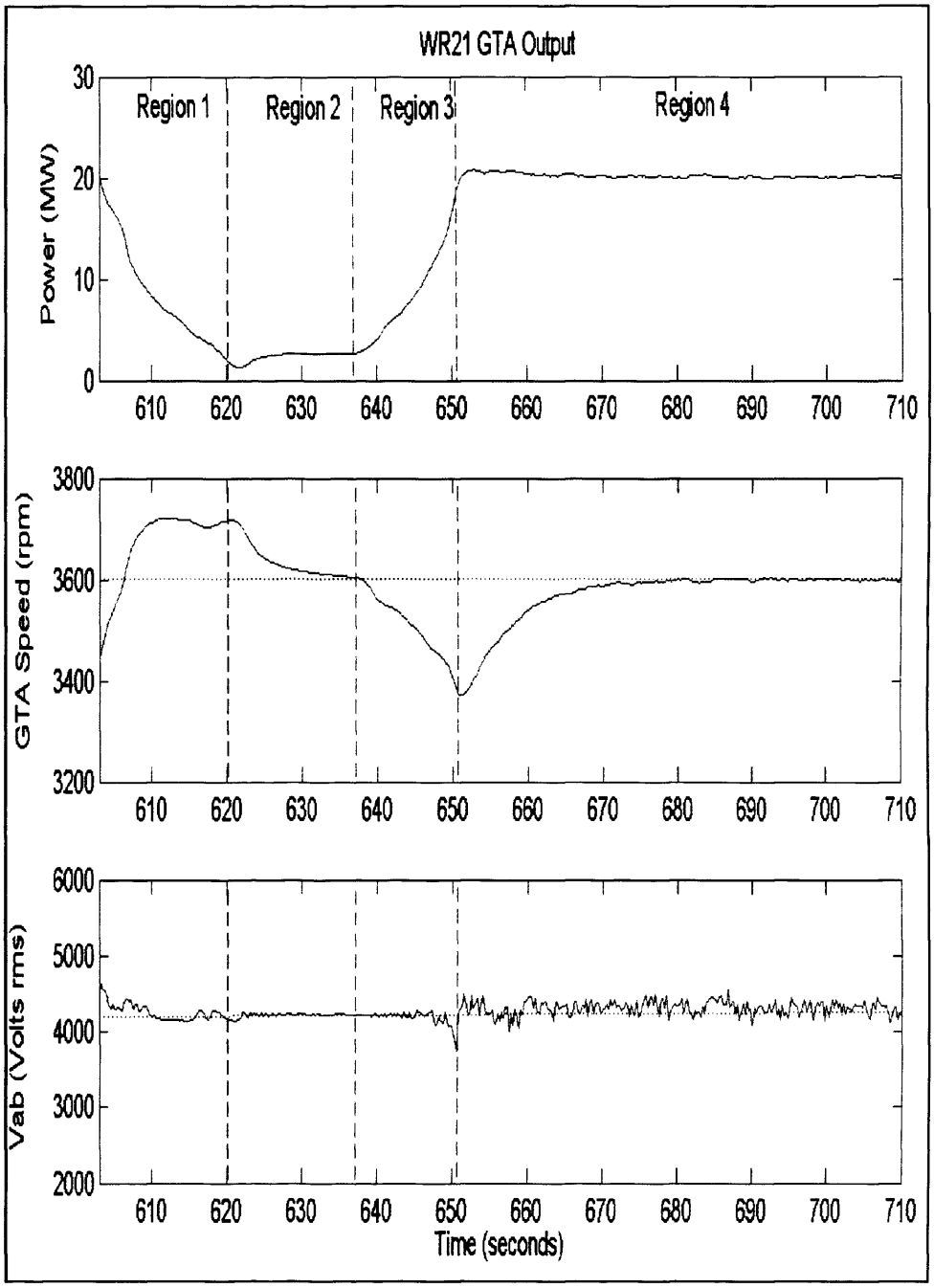

Figure 42: WR21 GTA output during crash-stop manoeuvre

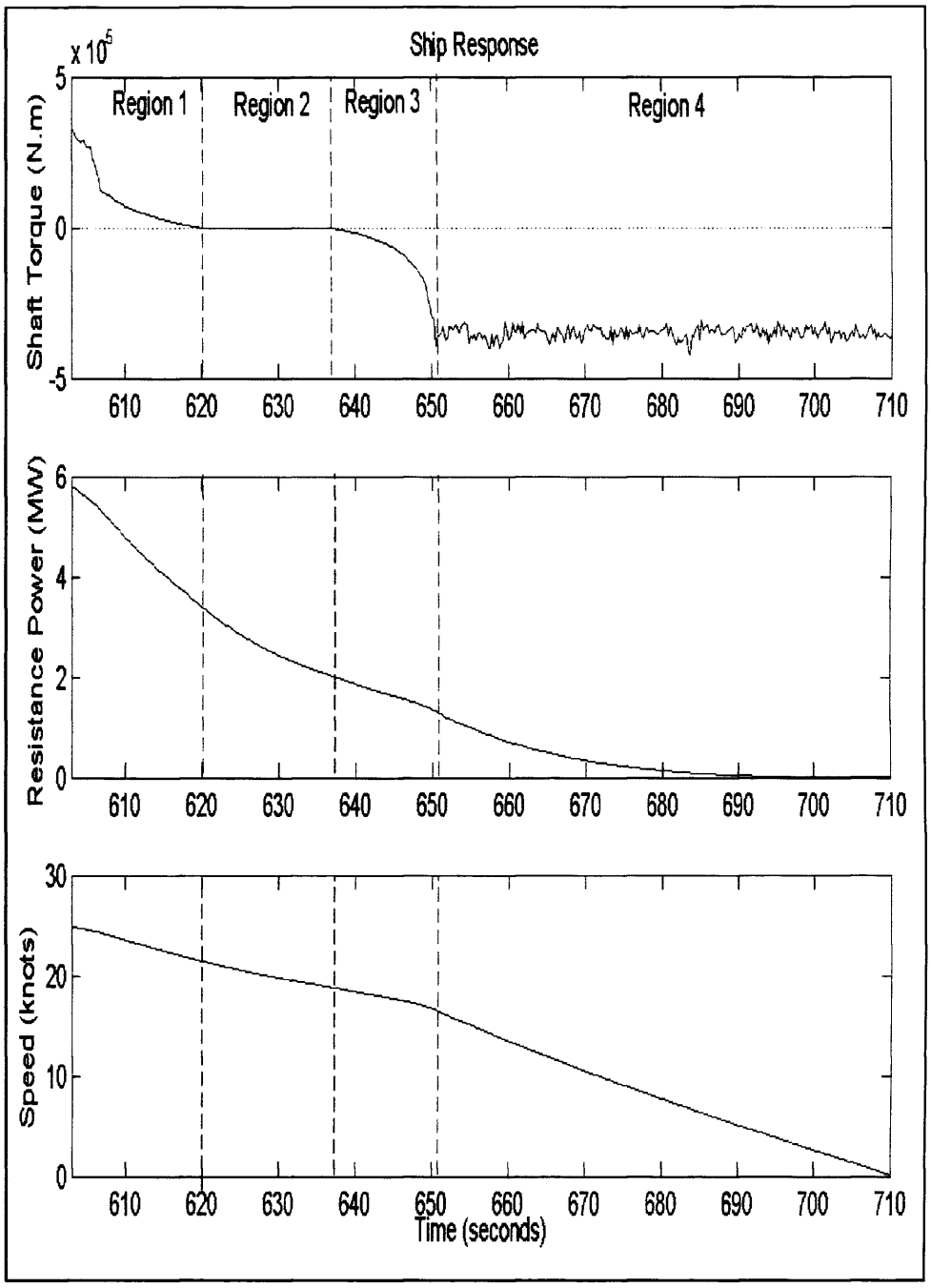

Figure 43: Ship response during crash-stop manoeuvre

- At region 1: Shaft speed decelerates, causing torque to decrease down to approximately zero, making the WR21 reduces the delivery of power to a minimum level.
- At region 2: Shaft speed decelerates down to zero; torque is kept to approximately zero and WR21 delivers minimum power.
- At region 3: Shaft speed accelerates with negative rotation; torque increases in magnitude (with negative signal) and WR21 increases delivery of power.
- At region 4: WR21 reaches maximum rated power delivery, causing the shaft speed and torque to oscillate around a constant value.

Simulation data of IFEP system behaviour during crash-stop manoeuvre is available in reference [6]. It can be used to compare and verify the coherence of the System Model results, but is inadequate to an accurate validation process, since 'the issue of validation is of paramount importance' and 'whatever technique is adopted for demonstration of model validity, plant data are required for direct comparison with model output [6].

The data from reference [6] is shown in figure 44 and consists of an example of output, obtained from a model developed by the MoD and MathWorks, for modelling IFEP power systems within the MATLAB/Simulink environment.

The parameters of the simulation are unknown; consequently it cannot be regarded as a precise point of reference. However, lacking of a better resource, it can be used to verify the consistency of the results generated by the System Model.

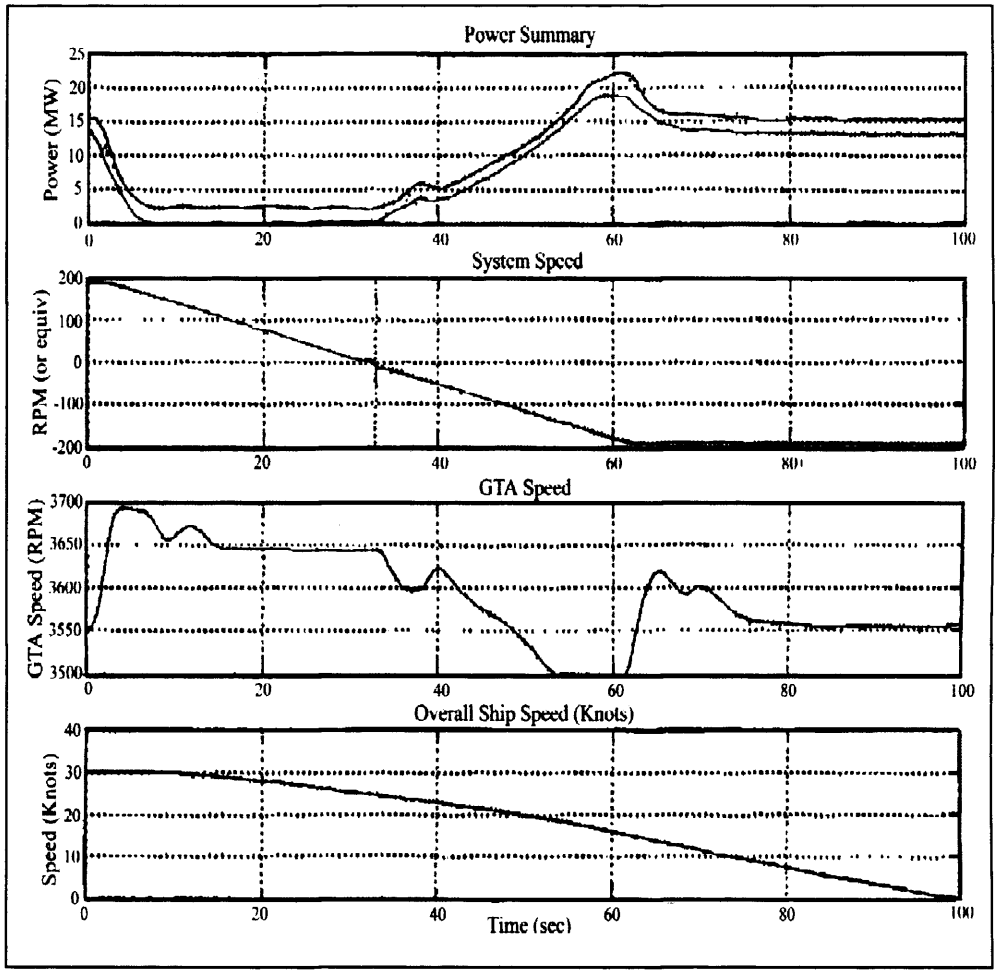

Figure 44: Example of crash-stop diagrams –source: MathWorks [6]

The main discrepancy between the System Model results and the MathWorks example concerns the shaft speed curve.

Figure 41 shows a shaft speed curve decelerating from approximately 130 rpm ahead to approximately 60 rpm astern in an uneven manner. There are several deviations from the reference speed (dashed line), which represents the rpm commanded by the control algorithm. At the beginning of region 4 (at Time = 651 seconds) the curve becomes a horizontal line, oscillating around 60 rpm astern.

Figure 44 shows a shaft speed curve smoothly decreasing from maximum speed of 180 rpm ahead to maximum speed of 180 rpm astern. Ripples and deviations are negligible.

The deviation from the reference speed, noted in regions 1,2 and 3 of figure 41, can possibly be caused by a difference in fidelity level between the models. The shaft speed profile will be strongly influenced by the load torque applied to the propeller. The actual load is particularly erratic, depending on sea waves and ship movements (heave, pitch and roll), just to mention a few factors. For that reason some divergence between the commanded speed and the actual one is expected.

The speed magnitude discrepancy, noted particularly in region 4 of figure 41, is explained by the parameter estimation method used for the System Model. The estimation was based on different bibliographic references for each subsystem. As a consequence the system as a whole resulted inevitably non-optimised. In such a situation the amount of losses produces sensible deterioration on the system performance, limiting the maximum shaft speed.

The parameters for the induction motor, for example, were taken from the IPS system (reference [24]), which specify a maximum rpm of 150. It is known that the Advanced Induction Motor – AIM – due to be fitted in the Type 45 Destroyer is rated at 180 rpm. It elucidates the poor performance of the motor of the System Model.

As a matter in fact the maximum speed astern of the new AIM is rated at 90 rpm, suggesting that the equipment doesn't achieve the maximum speed of 180 rpm astern, as portrayed in figure 44.

Another remarkable peculiarity observed when running the System Model, which is not visible in the resulting curves, is the difficulty to start the deceleration of the shaft at maximum speed steady state (which represents a situation of high stiff due to low slip) by actuating in the flux magnitude.

At this point, trying to reduce the shaft speed through decrement of flux magnitude could lead to an opposed result, if the decrement isn't large enough (since the motor stiffness tends to compensate the flux reduction by raising the shaft rpm, keeping the electromagnetic torque almost unchanged), or could result in motor stall, if the decrement is too large.

Consequently the flux variation must be fine tuned, and the initial move of the speed downwards is expected to be a little bit abrupt. This problem (and

the issue previously mentioned of deviation discrepancies) could be addressed by further development of the control system.

In conclusion, the crash-stop results obtained with the System Model are coherent, despite the differences compared to the crash-stop example provided by MathWorks. A further development of the control algorithm is advisable, to achieve a smoother change in shaft speed.

8.3 Faulted Operation

In three-phase motors the loss of one phase (open circuit) would cause an overwhelming unbalance, and therefore a devastating effect. A massive torque pulsation would be produced, the currents would exceed the maximum rates and the temperature would rise to the point of burnout, if the motor is kept running.

In the 15-phase motor the fault tolerance is expected to be much greater compared to the three-phase motor. Reference [37] states that 'immunity to an open-circuit fault increases with phase number, although there is clearly a diminishing return effect.' According to the same reference, after the open-circuit fault of one phase in the 15-phase motor it is expected a maximum torque decrement of 0.28% (at full load slip) and increase in stator loss of 7%.

The 15-phase induction motor was modelled in two different ways in this project: one using the *dq* reference frame, and other using matrix operations, with no reference frame transformation. Both models are to be tested for a faulted condition, in order to assess the different behaviours and the implications on the choice of motor model to be fitted in the System Model.

Figures 45 to 52 presents diagrams highlighting the instant in which the fault occur, both in the *dq* and in the matrix model, and its consequences for the stator currents:

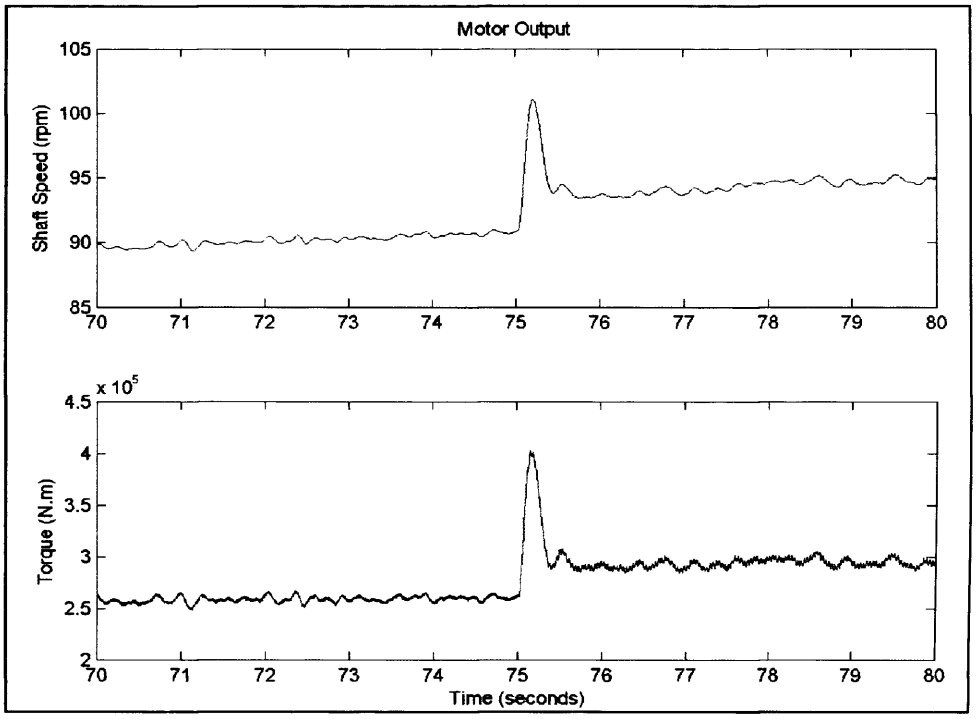

Figure 45: Motor faulted at the time of 75 seconds – *dq* model

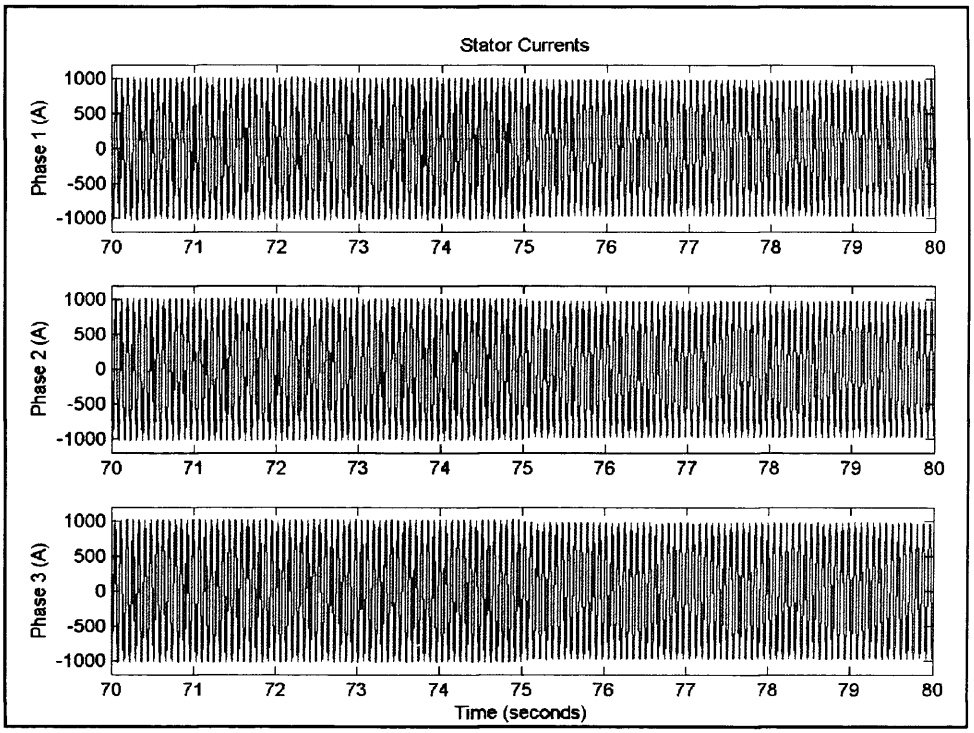

Figure 46: Stator currents – *dq* model

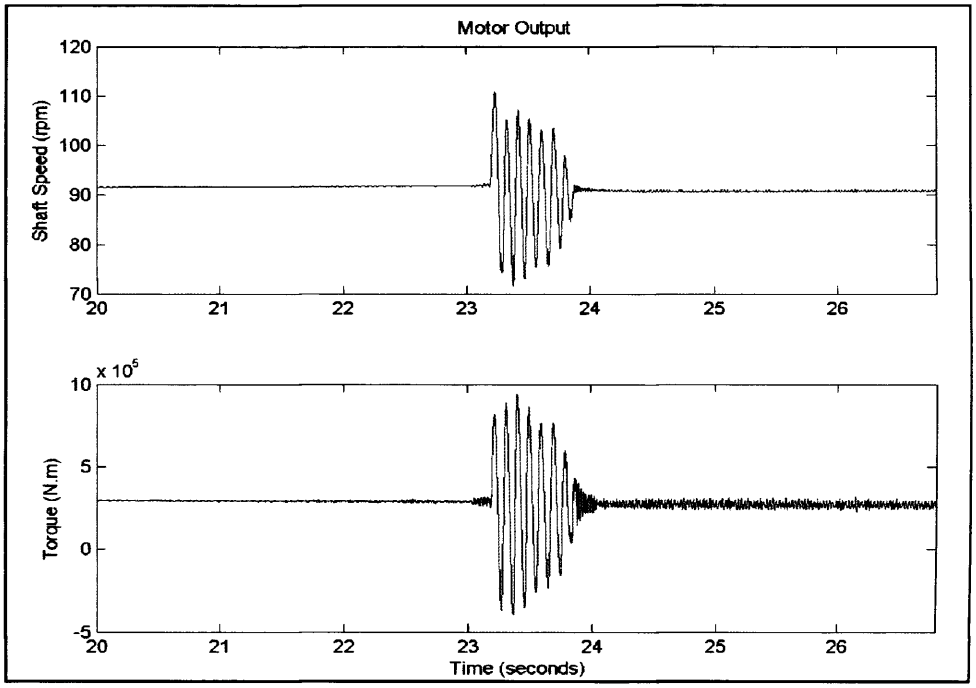

Figure 47: Motor faulted at the time of 23 seconds – 15x15 matrix model

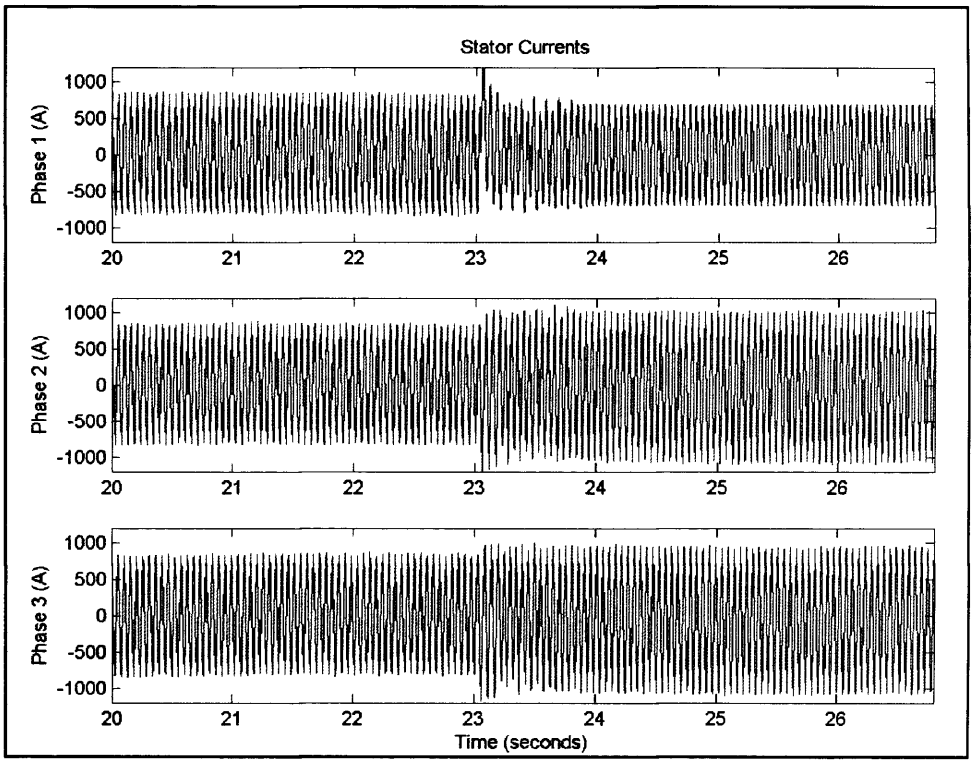

Figure 48: Stator currents – 15x15 matrix model

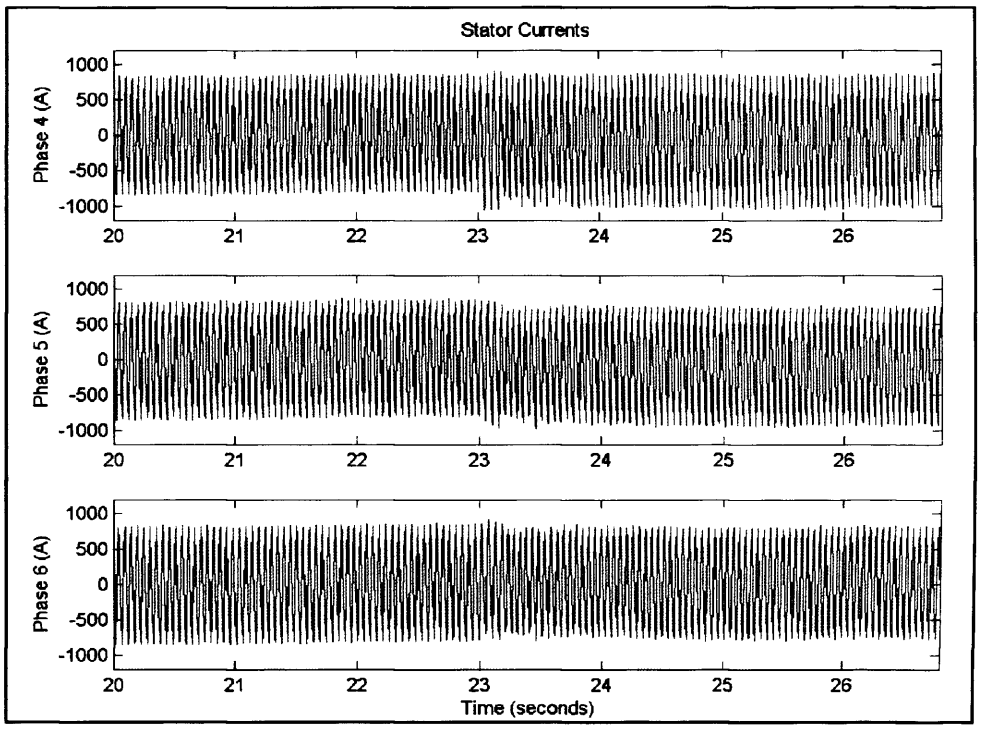

Figure 49: Stator currents – 15x15 matrix model

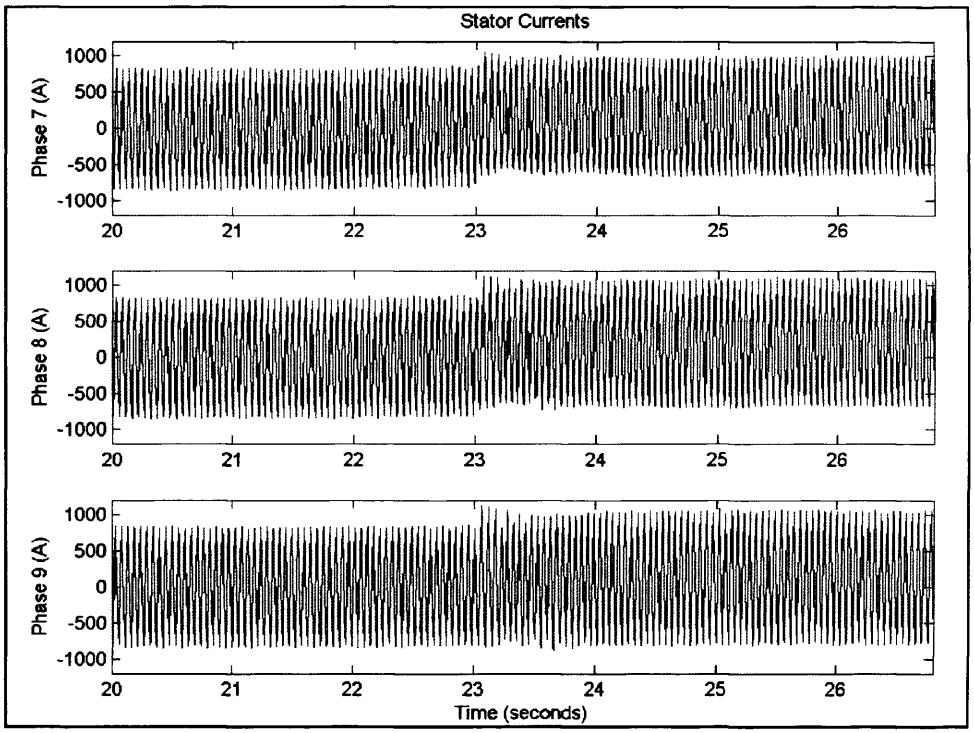

Figure 50: Stator currents – 15x15 matrix model

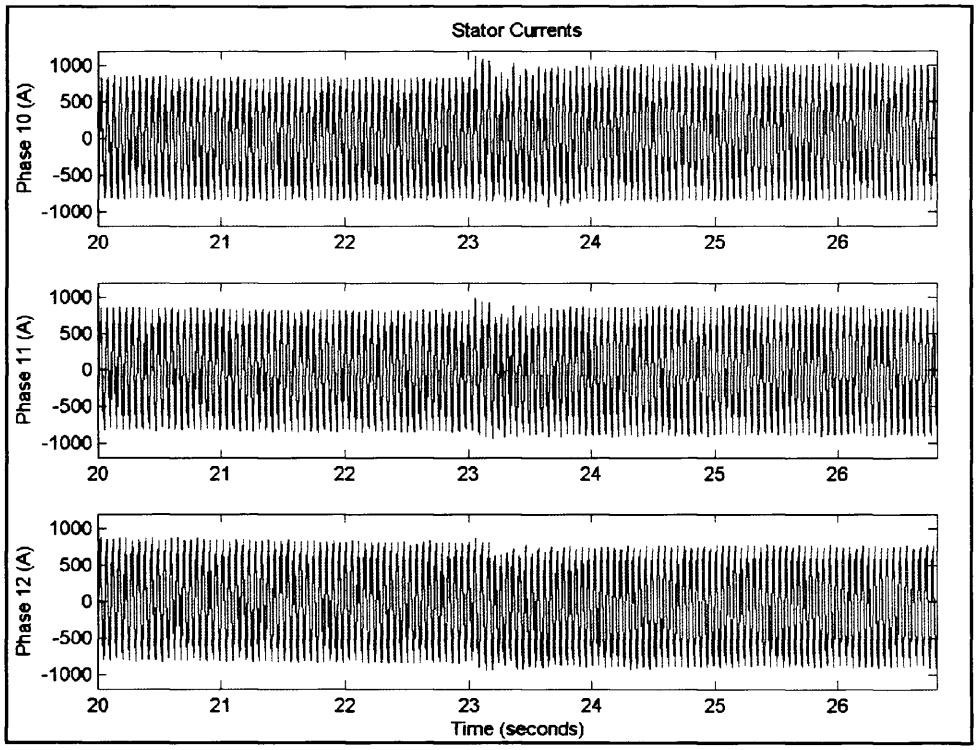

Figure 51: Stator currents – 15x15 matrix model

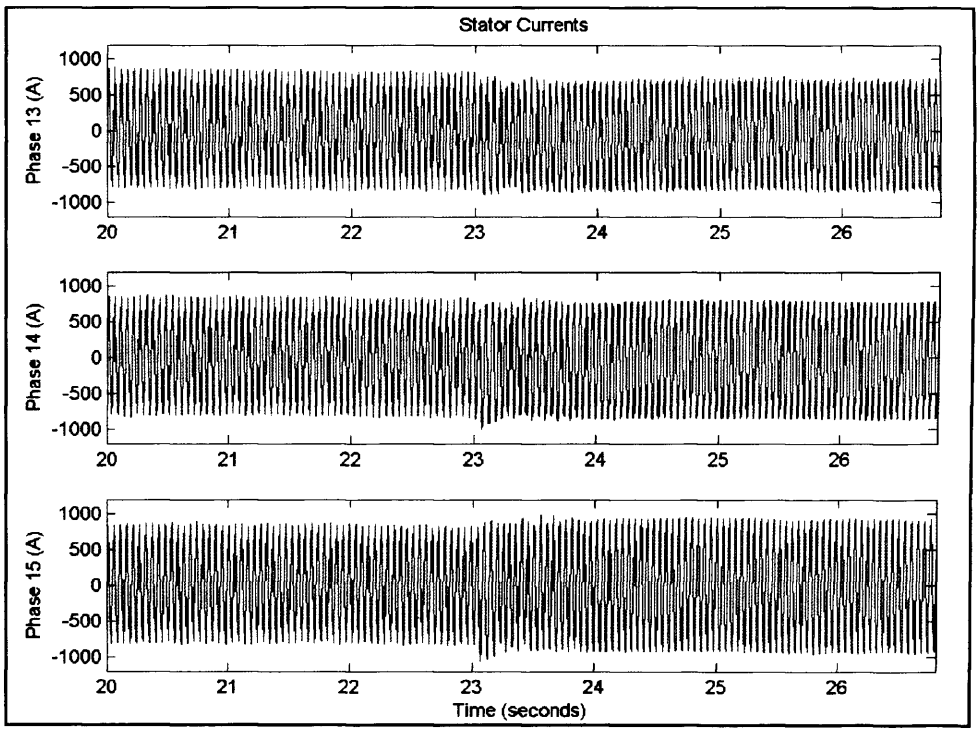

Figure 52: Stator currents – 15x15 matrix model

The *dq* model (figures 45 and 46) does not account for the unbalance in stator currents caused by the loss of one phase. Consequently, all the calculated stator currents have the same magnitude and after the fault there is a slight decrease in it, which causes some instability in the motor.

The response to this instability is an increase in shaft speed, trying to maintain the torque. The increase in shaft speed result in rise of shaft load torque, and consequently a new steady state is achieved after about 0.5 seconds at a higher shaft speed than before the fault, with a higher torque.

The matrix model algorithm (figures 47 to 52) accounts for the stator current unbalance, and therefore the magnitudes after the fault vary from 87% to 125% of the original value. This unbalance causes instability in the motor, which the control system struggles to fix by acting in the electromagnetic flux phasor.

After about 0.9 seconds, the control system manages to maintain the old rpm and torque. It is possible to realise that in faulted operation (after reaching of steady-state) there are larger torque ripples than in normal operation.

The effect of unbalance is rotor overheating without additional torque, resulting increased losses. The total motor loss is the sum of the losses calculated for each phase separately. To illustrate the severity of this condition, a simple calculation can estimate the percentage of temperature rise caused by unbalance, based on reference [15]:

Figure 4 shows the relationship between voltage and current unbalance in a three-phase induction motor. Through correlation it is possible to consider that the loss of one phase in a 15-phase machine can have similar consequences to the motor as a percentage of unbalance in a three-phase machine.

Evaluating the stator currents generate by the simulation, it is possible to verify that the maximum current unbalance generate would be:

$$Average\ current = \frac{\Sigma\, phase currents}{15} =$$

$$= \frac{704+1056+1021+915+831+810+824+880+901+915+859+796+775+810+915}{15}$$

$$Average\ current = 867.5\ A$$

$$Maximum\ current\ unbalance = \frac{Max\ difference}{Avg\ current} = \frac{1056 - 867.5}{867.5} = 0.217 = 21.7\%$$

Considering that maximum (full) load is:

$$Max load = \frac{Motor\ rating}{Max\ shaft\ speed} = \frac{20 \times 10^6}{\frac{2 \times \pi \times 15}{6}} = 1273\ kN.m$$

Therefore percentage of load delivered is:

$$\frac{Actual\ load}{Max\ load} = \frac{284}{1273} = 0.223 = 22.3\%$$

By entering the values in the diagram of figure 4 it is possible to say that the correspondent voltage unbalance that generates the same amount of current unbalance in a three-phase machine would be between 2 and 2.4% (say 2.2% approximately).

A small unbalanced phase voltage can cause a significant increase in motor temperature. Although there is no exact formula to determine the effect of voltage phase unbalance on temperature rise, laboratory tests indicate that the percentage increase in motor temperature is approximately equal to twice the square of the percentage voltage unbalance. This can be expressed by the following formula [15]:

$$\text{Temp. rise on unbalanced system} = \text{Temp. rise on balanced system} \times \left[1 + 2\,\frac{(\%\ \text{voltage unbalance})^2}{100}\right] \quad (23)$$

Therefore: $TRUS = TRBS * \left[1 + 2 * \frac{2.2^2}{100}\right] = 1.10$; the temperature rise would increase of about 10% for the case in study.

Obviously the formula and diagrams used are fitted for three-phase machines, and it is necessary availability of actual data to validate the method used above to infer the percentage of temperature rise.

Though the main objective of the previous calculations is to demonstrate a possible use of the matrix algorithm, which is capable of work out more precisely current unbalance in the 15-phase machine.

Usually the maximum voltage unbalance is set to 2% in standard motors; as a result the continuous operation of a 15-phase induction motor on only 14 phases (in the specific case studied) would rather be avoided. Hence, despite the negligible effect on torque decrement, there is a significant outcome in temperature rise due to the faulted phase.

8.4 Large and Small Generator Operating in Parallel

The main issue in parallel generation is synchronization. Before closing the breaker to connect a second generator to the main bus bar, it is necessary to guarantee that the voltage, frequency, and phase angle difference of the two sources are within a safe tolerance. Disregarding this requirement can result in mishap and damage to the equipment.

To promote the synchronization there are a number of methods. One of the most commons is the use of digital transducer with controller, like the Programmable Logic Controller – PLC, which increase or decrease the fuel supply slightly to force the generator into synchronism.

Figures 53 to 56 show the behaviour of the system when the emergency generator is connected to the bus bar out of synchronism.

The curves show the impact of connecting the small generator out of synchronism. In this particular case voltage and frequency were almost the same at GTA and DG; however the difference between phase angles was larger than the tolerance limit. The result is deterioration of system performance and instant decay of shaft speed and torque.

The Control System reacts to bring the shaft speed to its original value. The power delivered by the WR21 is at the maximum limit; therefore the consequence is loss of speed on the alternator, compromising the frequency of the voltage supplied to the system.

Motor torque and shaft speed are driven to values over the rated ones, bringing risk of damage to the equipment. The evident conclusion is that a controller (PLC type for example) has to be implemented.

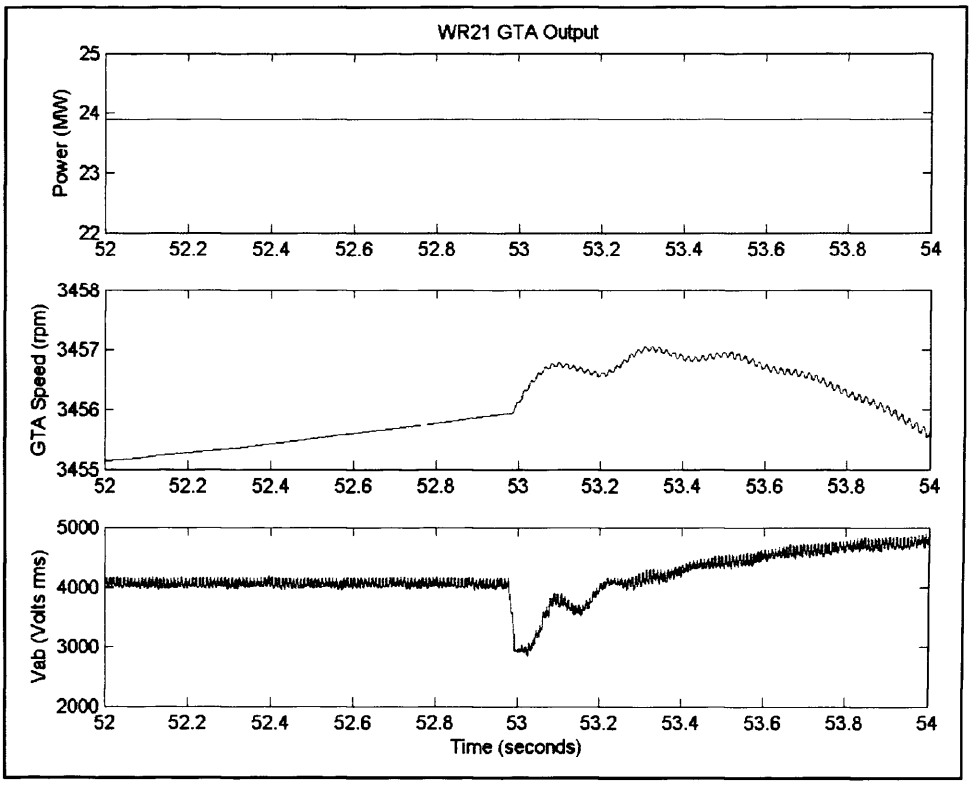

Figure 53: WR21 GTA output with DG connected out of synchronism at ~53 s

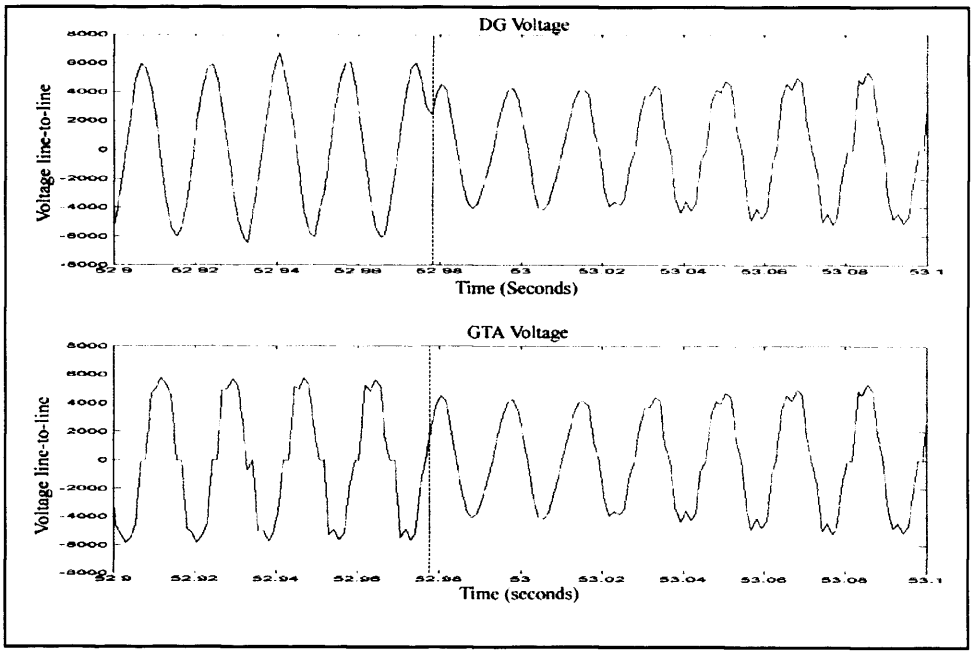

Figure 54: Generated voltages at DG and GTA in the moment they are connected out of synchronism at ~53 s

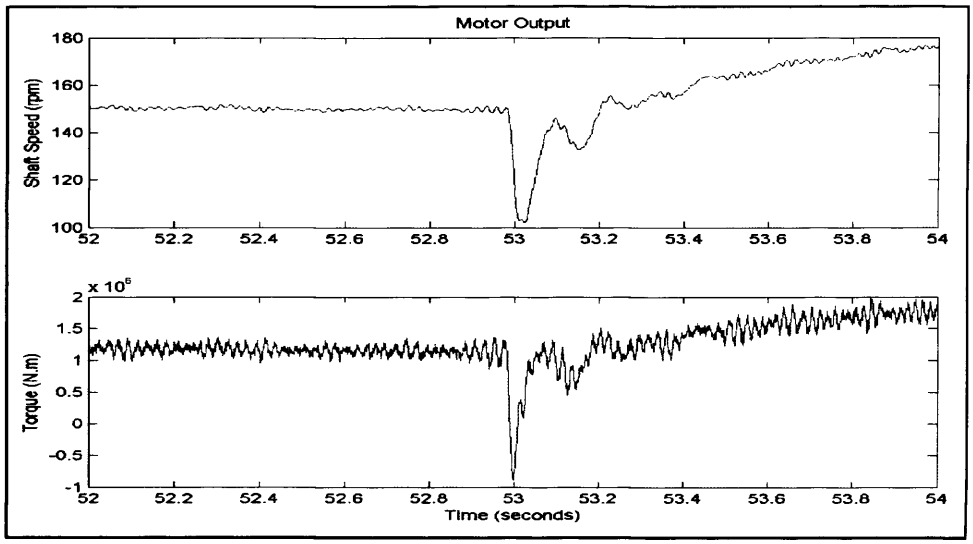

Figure 55: Motor output with DG connected out of synchronism at ~53 s

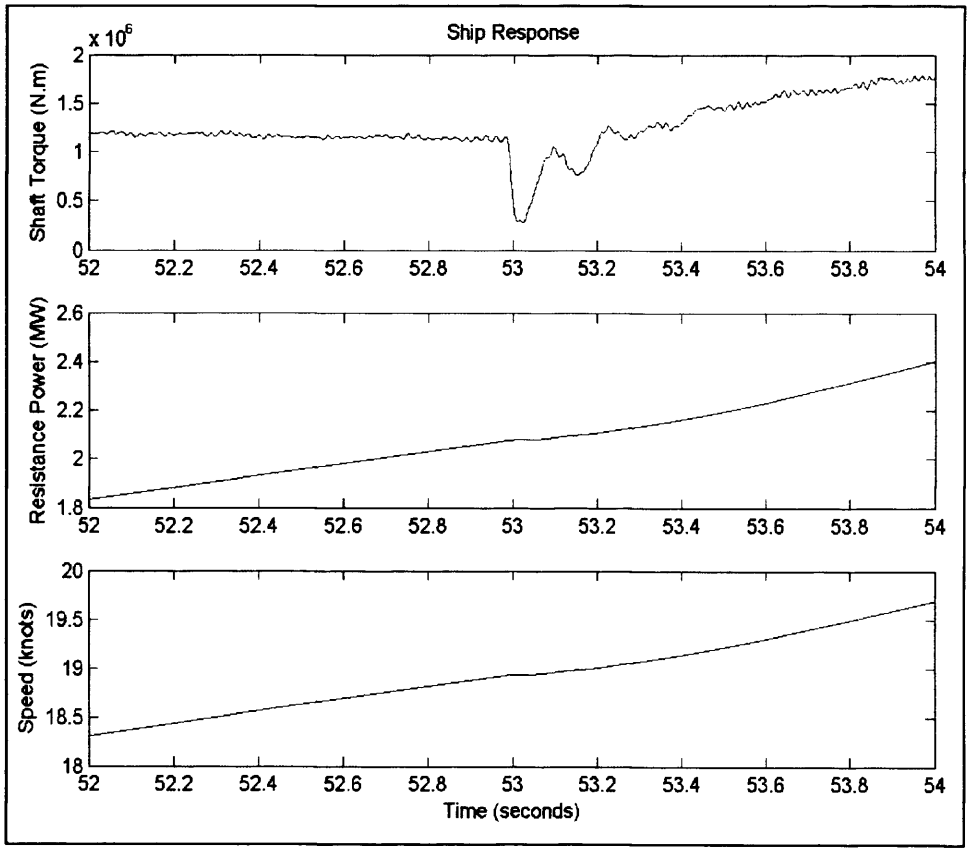

Figure 56: Ship response with DG connected out of synchronism at ~53 s

8.5 Conclusions

The System Model was tested under a number of important scenarios, and even though there are limitations to the model, it was possible to develop some conclusions regarding the likely behaviour of an actual IFEP system.

By performing steady-state analysis it was observed that the torque oscillation is always present, and the magnitudes of the torque and shaft speed oscillations are apparently proportional to the load torque applied to the induction motor. There are some means to minimise even more the torque ripples which can be incorporated in future works, although the effect on total harmonic distortion have to be assessed in parallel, to avoid increasing losses when restricting excessively the torque fluctuation.

By performing transient analysis (crash-stop manoeuvre) it was noticed a difficulty to start the deceleration of the shaft at maximum speed steady state (which represents a situation of high stiff due to low slip) by actuating in the flux magnitude. Consequently the control of flux variation by the DTFC algorithm must be fine tuned, to avoid abrupt changes in speed.

By applying a fault condition to one phase of the induction motor drive it was verified an unbalance in the resulting stator currents, which would lead to increasing the temperature rise rate of the windings. The consequence is the recommendation of avoiding prolonged operation of the system in faulted condition.

By connecting the emergency diesel generator out of synchronism it was realised the importance of a device to guarantee that the voltage, frequency, and phase angle difference of the two sources are within a safe tolerance. The synchronization is a matter that will have a greater significance in a future development, which is a System Model containing both shaft lines, having two WR21 gas turbines alternators connected to the same bus bar.

9.0 CHAPTER NINE – Conclusions and Recommendations

9.1 Conclusions

The aim of the project has been achieved: a System Model loosely based on the proposed Type 45 propulsion system has been built; the components validated and the whole system tested under a number of scenarios, such as:

- Steady-state operation;
- Crash-stop manoeuvre;
- Operation under faulted condition of the motor; and
- Operation of large and small generator in parallel.

The System Model is distant from having all the details that comprise an actual system. Nevertheless all the main features that have major influence in the dynamic behaviour are included, making the model thoroughly representative.

The strong points of the developed System Model are:

- It is user friendly: users with no knowledge of MATLAB/Simulink can run the model, change parameters and obtain simulation results (Appendix "L", page 175, provide a quick-start guide to the System Model user);
- It is adaptable: can be changed by incorporating new components or by updating the existing ones;
- It is controllable and stable: the Direct Torque and Flux Control method grant a simple and robust algorithm to the control system, allowing a wide range of manoeuvres and operational scenarios to be simulated;
- It is relatively fast in view of the complexity provided by the 15-phase advanced induction motor; and
- It can run in real-time applications, given an adequate hardware is used.

And the main weaknesses are:

- It is not completely validated: actual data measured from physical systems are essential; without this data a fully validated model is unachievable;
- It still has high losses due to Total Harmonic Distortion: a design effort still needed to incorporate means to reduce it; and
- It still has noticeable torque ripple: improvement of the control system and incorporation of harmonic filters should be able to provide further minimisation to it.

The obtained results were coherent and supported by the theory, which leads to the most important benefit provided by the project: its utility in a truthful and comprehensive assessment of different aspects of the dynamic performance of an advanced marine integrated electric propulsion system.

Examples of particular benefits are:

- Provide a cost-effective way of testing and de-risking new designs;
- Offer an environment for development, test and validation of new equipment models not included in the spectrum of this project; and
- Give students the opportunity to understand in greater depth the complexities of this novel technology, by applying the theory into practice through computer simulation.

Two main achievements of this project shall be highlighted:

- The construction of an algorithm for the 15-phase induction motor capable of processing the resulting stator and rotor currents in the machine more precisely than the traditional *dq*-algorithms, taking into account eventual unbalances and faults in the voltage supply; and
- The development of a Direct Torque and Flux Control

algorithm for the 15-phase system, capable of maintaining the stability of the induction motor under severe transients, such as the crash-stop manoeuvre.

Some considerations can be made about probable issues that will arise during the implementation of an actual IFEP design, which are:

- The torque oscillation is always present when operating the induction motor, but can be kept within a tolerable range;
- The magnitudes of the torque and shaft speed oscillations are apparently proportional to the load torque applied to the induction motor;
- There are means to minimise torque ripples which can be incorporated in the control system, although the effect on total harmonic distortion have to be assessed in parallel, to avoid increasing losses when restricting excessively the torque fluctuation;
- It could be difficult to start the deceleration of the shaft at maximum speed steady-state (which represents a situation of high stiff due to low slip) by actuating in the flux magnitude;
- A fault condition in one phase of the induction motor drive causes unbalance in the resulting stator currents, which increases the rate of temperature rise of the windings;
- The synchronization is a matter of major significance, especially in a system comprising two WR21 gas turbines alternators connected to the same bus bar.

9.2 Recommendations

Clearly there is potential for further developments of the present System Model, and work could be done in the following areas:

- Evaluation of THD: its causes and consequences to the system;
- Investigation on reduction of THD trough advanced techniques (active filters for example);

- Improvement of the control system, to reinforce the robustness and fault-tolerance of the algorithm;
- Adoption of a protection strategy, with the introduction in the design of fuses and breakers;
- Implementation of a subroutine in the algorithm of the control system to minimise the effects of 'negative impedance' in the DC Link, which is a major source of instabilities in the system;
- Evaluate potential of other software packages (such as 'Modelica') compared with the package currently in use (MATLAB SimPowerSystems); and
- Improvement of simulation speed, by assessing modern software and hardware for real-time simulation.

The processing speed is critical to fully appreciate the benefits of modelling and simulation. Real-time software was used in the present project nevertheless time still an issue.

To achieve real improvement in this area, it would be necessary a significant investment in hardware; although resources were not available at the time this project has finished.

In the future it is believed such equipments will be much more affordable, and simulation of complex and very heavy models will be a common trend. The consequence will be easier access to a range of new software and hardware, which will enable a consistent improvement in the simulation speed.

10.0 Reference List

[1] CNO Executive Board. *Excutive Summary Roadmap to an Electric Naval Force,* Naval Research Advisory Committee, USA - 2001.

[2] G M Jebsen. *Electric Warship Technology Overview,* Office of Naval Research, USA - 2001.

[3] S S Young, J M Newell and G T Little. *Electric Warship VII - The Reality,* Journal of Marine Design and Operations, London - 2001.

[4] "Type 45 Daring Class Anti-Air Warfare Destroyers, United Kingdom", http://www.naval-technology.com/projects/horizon/, UK – 2006.

[5] J Voyce. *Warship Electrical Power & Propulsion Systems - Ship Design Lecture,* University College London, UK - 2002.

[6] G Little and P Rottier. *A Modelling/Simulation Toolbox for Application to IFEP Naval Vessels,* INEC Conference Proceedings - IMAREST, London, UK - 2002.

[7] A R Greig, R A Patel and R W G Bucknall. *Development of Equipment Models for Marine Electrical Propulsion System Studies,* University College London, London, UK - 2000.

[8] H Elmqvist, S E Mattsson and K J Alström. *Evolution of Continuous-Time Modeling and Simulation,* The 12th European Simulation Multiconference, ESM'98, Manchester, UK - 1998.

[9] Ansoft. *Simplorer - The Multi-domain Simulation Package,* Ansoft, Pittsburgh, PA - 2002.

[10] M Beuschel. *A Uniform Approach for Modelling Electrical Machines,* Lund, Sweden, Modelica Workshop - 2000.

[11] G Sybille and others. *Power System Blockset User's Guide - Version 2,* TEQSIM International Inc., a sublicense of Hydro-Quebec, and The MathWorks, Inc, Quebec, Canada - 2001.

[12] TransEnergie Technologies. *SimPowerSys For Use with Simulink - User's Guide - Version 2,* TransEnergie Technologies Inc., HydroQuebec and The Mathworks Inc., USA - 2002 .

[13] C M Ong. *Dynamic Simulation of Electric Machinery,* Prentice Hall PTR, New Jersey, USA - 1998.

[14] J Smith and M J Chen. *Three-Phase Electrical Machine Systems - Computer Simulation,* Research Studies Press LTD./ John Wiley & Sons Inc, Somerset, UK - 1993.

[15] Siemens, "Application Manual for NEMA Motors - Section 2", 1998. Siemens Industries. Germany.

[16] U.S. Electrical Motors. *Unbalanced Voltage on Polyphase Induction Motors,* U.S. Electrical Motors, USA - 2000.

[17] Elecship 98. *International Conference on Electric Ship - Proceedings,* Middle East Technical University of Ankara, Turkey - 1998.

[18] R W G Bucknall. *Lectures from the MSc Course in Marine Engineering,* University College London, London, UK - 2001.

[19] ABB Industry Oy. *Technical Guide No. 1 - Direct Torque Control,* ABB, Helsinki, Finland - 2001.

[20] A M Trzynadlowski. *Control of Induction Motors,* Academic Press, San Diego, CA, USA - 2001.

[21] L Rollins. *Robust Control Theory,* Carnegie Mellon University, USA - 1999.

[22] M Staroswiecki, N E Wu and M Blanke. *Concepts and Methods in Fault-tolerant Control,* Tutorial at American Control Conference, USA - 2001.

[23] N Lechevin, S Aborida and M A Ouhrouche. *RT-Lab Based Real-Time Simulation of a Direct Field-Oriented Controller for an Induction Motor,* Electrimacs, USA - 2002.

[24] J T Alt, H J Hegner, H N Robey Jr and S D Sudhoff. *Control of a 15-Phase Induction Motor Drive System,* Proceedings of the 1997 Naval Symposium on Electric Machines, Newport, RI - 1997.

[25] K A Corzine, S F Glover, H J Hegner, H N Robey Jr. and S D Sudhoff. *DC Link Stabilized Field Oriented Control of Electric Propulsion Systems,* IEE Transactions on Energy Conversion, Vol. 13, No. 1, USA - 1998.

[26] P Vas. *Sensorless Vector and Direct Torque Control,* Oxford Science Publications, New York, USA - 1998.

[27] I Boldea and S A Nasar. *Electric Drives,* CRC Press, Florida, USA - 1999.

[28] IEEE Standards Board. *IEEE Recommended Practice for Excitation System Models for Power System Stability Studies - Std 421.5-1992,* Institute of Electrical and Electronics Engineers, Inc. , New York, USA - 1992.

[29] G F C Rogers, H I H Saravanamuttoo and H Cohen. *Gas Turbine Theory,* Logman Scientific and Technical, UK - 1987.

[30] R D Geertsma. *IFEP Warship Modelling,* University College London, London, UK - 1999.

[31] R D Geertsma, D Haynes and P Demers. *Ship Design Exercise 1999 - High Survivability Frigate,* University College London, London, UK - 1999.

[32] Wolfman. *Control Tutorial for Matlab and Simulink,* University of Guelph, Ontario, Canada - 2002.

[33] M Mikkola. *Simulation of Ship Network Behaviour During a Crash Stop Manouvre* , IMARE Conference All Electric Ship, London, UK - 1998.

[34] Allen-Bradley Company. *Dynamic Braking Resistor Calculator,* Rockwell Automation, Inc., USA - 2002.

[35] S D Round, R M Duke and J C Trounce. *Comparison by Simulation of Three-level Induction Motor Torque Control Schemes for Electric Vehicle Applications,* University of Canterbury, New Zealand - 2000.

[36] G Filliau, C J Saxby and P A Erskine. *Electric Warship VIII - Demonstrating the Electric Warship - IMarEST Evening Technical Meeting,* IMarEST, London, UK - 2002.

[37] S Smith, C Hodge and S Williamson. *Fault Tolerance in Multi-phase Propulsion Motors,* AES Conference - IMarEST, Edinburgh, UK - 2003.

Appendix 'A' - Reference Frame Theory

The three-phase induction motor, due to its own characteristics, has a natural mathematical representation on the *abc* reference frame, which is named in some technical literature "natural frame".

Usually, in order to simplify the modelling, it is possible to use mathematical transformation to adapt this representation to other reference frames, as:

- The $\alpha\beta$ reference frame, named also 'stationary' reference frame – using "Clarke" transformation; or
- The *dq* reference frame, named also 'rotating' reference frame, which can be referred to the rotor or synchronous speed – using "Park" transformation.

A very brief analyses of the mathematics involved in each reference frame is worthy, prior to a comparison being made between the performance of each reference frame in a simulation study. A detailed discussion about theory of reference frames is available in the Chapter 3 of reference [1].

abc reference frame

The three-phase voltages, currents and fluxes of AC motors can be analyzed in terms of complex space vectors.

The space vector for the stator currents can be defined, in the *abc* reference frame, as follows: Assuming that i_{as}, i_{bs} and i_{cs} are the instantaneous currents in the stator phases, then the complex stator current vector is defined by:

$$\underline{\mathbf{i}}_s = i_{as} + i_{bs}.\mathrm{a} + i_{cs}.\mathrm{a}^2 \qquad (1)$$

Where $\mathrm{a} = e^{j\frac{2}{3}\pi}$ and $\mathrm{a}^2 = e^{j\frac{4}{3}\pi}$ represent the spatial operators. The figure 4 shows the stator current complex space vector:

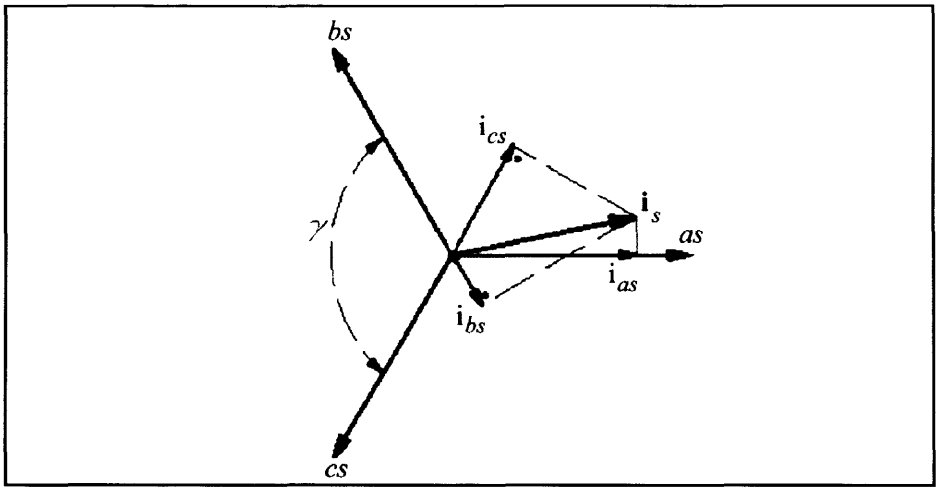

Figure 57: Relationship of stator current space vector and stator phase currents – *abc* reference frame

The problem in using this reference frame is that the inductances are time variant and the model designed using this method will have a more complex algorithm and consequently a longer simulation run time.

Mathematical transformations can facilitate the computation of the transient solution by transforming the differential equations, with time varying inductances, to differential equations with constant inductances [2].

$\alpha\beta$ reference frame [3]

Considering that the phase quantities are not independent variables for a three-phase, star-connected machine, then:

$$i_{as} + i_{bs} + i_{cs} = 0$$

$$v_{as} + v_{bs} + v_{cs} = 0$$

$$\omega_{as} + \omega_{bs} + \omega_{cs} = 0 \qquad (2)$$

Where i_s , v_s and ω_s denote stator phase currents, voltages and flux linkages, respectively.

As a result of this redundancy in the phase variable representation it is possible to transform the system to an equivalent two-phase representation. The transformation from three-phase to two-phase quantities is written in matrix form as:

$$\begin{bmatrix} i_{\alpha s} \\ i_{\beta s} \end{bmatrix} = \frac{2}{3}\begin{bmatrix} 1 & \cos(\gamma) & \cos(2\gamma) \\ 0 & \sin(\gamma) & \sin(2\gamma) \end{bmatrix}\begin{bmatrix} i_{as} \\ i_{bs} \\ i_{cs} \end{bmatrix} \tag{3}$$

Where $\gamma = 2\pi/3$. The transformation is equally valid for the voltages and flux linkages. The **stator current space vector** is defined as the complex quantity:

$$\mathbf{i}_s = \mathrm{i}_{\alpha s} + \mathrm{i}_{\beta s} = i_{\alpha s} + i_{\beta s} \cdot j \tag{4}$$

Where j is the complex operator.

The choice of the constant in the transformations of (3) is can be vary depending on criteria assumed. Here, the value of 2/3 adopted has the main advantage that magnitudes are preserved across the transformation. Therefore, sinusoidal phase currents with a peak magnitude of I_m, produce a current space vector with a peak magnitude of I_m.

For this transformation, the inverse relationship may be written:

$$\begin{bmatrix} i_{as} \\ i_{bs} \\ i_{cs} \end{bmatrix} = \begin{bmatrix} 1 & 0 \\ \cos(\gamma) & \sin(\gamma) \\ \cos(2\gamma) & \sin(2\gamma) \end{bmatrix}\begin{bmatrix} i_{\alpha s} \\ i_{\beta s} \end{bmatrix} \tag{5}$$

Transformation (3) and its counterpart (5) are denoted hereafter as the **Forward Clarke Transformation** and the **Reverse Clarke Transformation**, respectively.

The space vector may be viewed in the complex plane as shown in figure 5. The conventional magnetic axes of the three machine phases are separated by $\gamma = 2\pi/3$. The real or *as* axis of the new two-axis co-ordinate system is arbitrarily chosen to coincide with the *as* axis. Obviously, the imaginary or *jβs* axis lies in quadrature with the *as* axis. The current space vector is shown at an arbitrary location in the complex plane. The phase currents may be obtained by projecting the current space vector onto the respective phase axis.

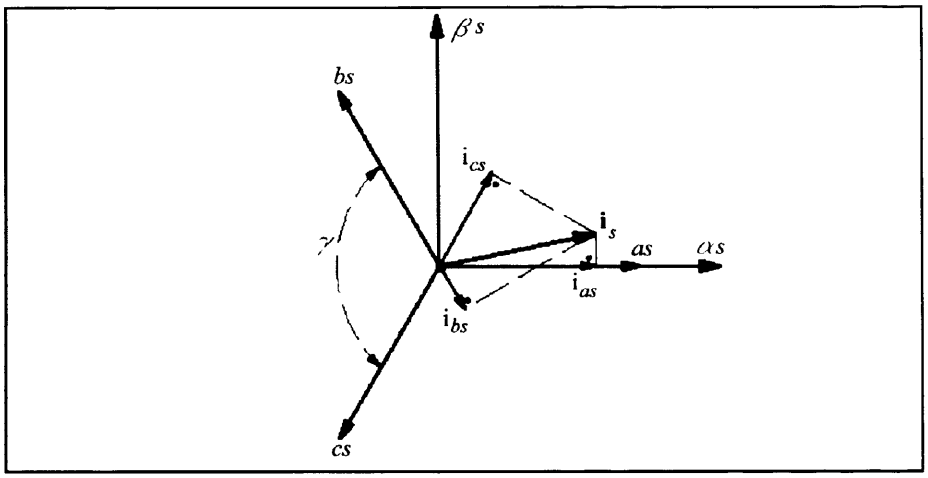

Figure 58: Relationship of stator current space vector and stator phase currents – *abc* and $\alpha\beta$ reference frame

Consider the case of a balanced set of three-phase stator currents:

$$i_{as} = I_m \sin(\upsilon - \omega)$$

$$i_{bs} = I_m \sin(\upsilon - \gamma - \omega)$$

$$i_{cs} = I_m \sin(\upsilon - 2\gamma - \omega) \qquad (6)$$

Where I_m is the magnitude of the phase currents, $\theta = \omega t$ is the angular position in radians and ω is the phase angle. Using (3) the currents of (8) may be transformed to the equivalent two-phase representation to give:

$$i_{\alpha s} = I_m \sin(\upsilon - \omega)$$

$$i_{\beta s} = I_m \cos(\upsilon - \omega) \qquad (7)$$

So that the current space vector of such a system may be written as:

$$\mathbf{i}_s = I_m \sin(\upsilon - \omega) - j.I_m \cos(\upsilon - \omega) = -j.I_m e^{j(\theta - \omega)} \qquad (8)$$

Which describes a circular trajectory in the space vector plane.

A balanced three-phase system may therefore be transformed to an equivalent two-axis representation. The radius of the circle is the peak magnitude of the phase quantities. The circular locus is described at a rate equal to the angular frequency of the phase quantities.

dq reference frame [3]

The stator current, voltage and flux linkage space vectors are complex quantities defined in a reference frame whose real axis is fixed to the magnetic axis *as* of stator winding. However, the corresponding quantities defined for the rotor circuit of a three-phase AC machine are similarly stated in a reference frame fixed to the rotor.

In the analysis of electrical machines, it is generally necessary to adopt a common reference frame for both the rotor and the stator. For this reason, a second transformation, known as a **vector rotation**, is formulated that rotates space vector quantities through a known angle.

In the space vector diagram of figure 5, the axes of the space vector plane are stationary. Meanwhile the space vectors of the current, voltage and flux linkages rotate about these axes at a rate equal to the angular frequencies of the corresponding phase quantities.

If instead a new reference frame is defined where the axes are made to rotate at the same rate as angular frequency of the phase quantities, stationary current, voltage and flux linkage space vector result.

Consider applying the vector rotation through an angle θ to the current space vector of (4). The current space vector in this new reference frame is given by:

$$\mathbf{i}_{dqs} = \mathrm{i}_{ds} + \mathrm{i}_{qs} = i_{ds} + i_{qs}.j = \mathbf{i}_s\, e^{-j\theta} \tag{9}$$

Which may also be written in matrix form as:

$$\begin{bmatrix} i_{ds} \\ i_{qs} \end{bmatrix} = \begin{bmatrix} \cos(\theta) & \sin(\theta) \\ -\sin(\theta) & \cos(\theta) \end{bmatrix} \begin{bmatrix} i_{\alpha s} \\ i_{\beta s} \end{bmatrix} \tag{10}$$

The real component of the current space vector in this new reference frame is the **direct axis component (*d*)** while the imaginary component is called the **quadrature axis component (*q*).**

The relationship of the real and imaginary components of the current space vector in the original stationary two-axis reference frame and the new rotating reference frame is shown in figure 6. Clearly, from the viewpoint of the stationary

($\alpha\beta$) frame, both the current space vector and the direct and quadrature axes are rotating at a speed ω.

However, when viewed from the rotating reference frame, the current space vector is stationary. The real axis of the rotating reference frame is located at an angle θ from the real axis of the stationary reference frame. The elimination of position dependency from the machine electrical variables is the main advantage of a vector rotation. This transformation will be referred to as the **Reverse Park Transformation**.

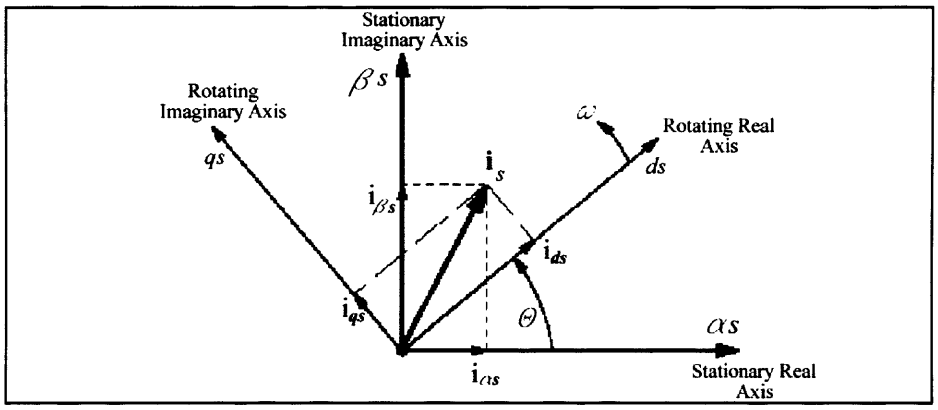

Figure 59: Relationship of current space vector components in stationary ($\alpha\beta$) and rotating (dq) reference frames

The inverse vector rotation, to transform from a rotating to a stationary reference frame, may be written:

$$\mathbf{i}_s = \mathbf{i}_{dqs}\, e^{j\theta} \tag{11}$$

Or in matrix form as:

$$\begin{bmatrix} i_{\alpha s} \\ i_{\beta s} \end{bmatrix} = \begin{bmatrix} \cos(\theta) & -\sin(\theta) \\ \sin(\theta) & \cos(\theta) \end{bmatrix} \begin{bmatrix} i_{ds} \\ i_{qs} \end{bmatrix} \tag{12}$$

This rotation is commonly called the **Forward Park Transformation**.

Consider application of the vector rotation to the current space vector of (8) derived for the balanced set of stator currents:

$$\mathbf{I}_{dq} = \mathbf{i}_s\, e^{-j\theta} = -j.I_m e^{\,j(\theta-\omega)}.e^{-j\theta} = -j.I_m e^{-j\omega} \tag{13}$$

So that:

$$i_{sd} = -I_m \cos(\omega)$$

$$i_{sq} = -I_m \sin(\omega) \tag{14}$$

Which are independent of the instantaneous angular position of the phase quantities.

A balanced three-phase system may therefore be transformed to an equivalent two-axis representation independent of angular position. This is achieved by applying a three-phase to two-phase transformation followed by a vector rotation by the angular position of the phase quantities.

Summary

For the previously mentioned reference frame transformations, a higher degree of simplification is obtained due to the assumption of having a balanced three-phase system, i.e. unbalance and the zero-sequence component is not considered. A more accurate analysis is often necessary, when unbalance is important. The transformation now becomes a little more complex by taking into account the zero-sequence component.

The complete form of the matrix equations of transformation (including the zero-sequence component) are:

Forward Clarke Transformation:

$$\begin{bmatrix} i_{\alpha s} \\ i_{\beta s} \\ i_{0s} \end{bmatrix} = \frac{2}{3} \begin{bmatrix} 1 & \cos(\gamma) & \cos(2\gamma) \\ 0 & \sin(\gamma) & \sin(2\gamma) \\ 1/2 & 1/2 & 1/2 \end{bmatrix} \begin{bmatrix} i_{as} \\ i_{bs} \\ i_{cs} \end{bmatrix} \tag{15}$$

Reverse Clarke Transformation:

$$\begin{bmatrix} i_{as} \\ i_{bs} \\ i_{cs} \end{bmatrix} = \begin{bmatrix} 1 & 0 & 1 \\ \cos(\gamma) & \sin(\gamma) & 1 \\ \cos(\gamma) & \sin(2\gamma) & 1 \end{bmatrix} \begin{bmatrix} i_{\alpha s} \\ i_{\beta s} \\ i_{0s} \end{bmatrix} \tag{16}$$

Reverse Park Transformation:

$$\begin{bmatrix} i_{ds} \\ i_{qs} \\ i_{0s} \end{bmatrix} = \begin{bmatrix} \cos(\theta) & \sin(\theta) & 0 \\ -\sin(\theta) & \cos(\theta) & 0 \\ 0 & 0 & 1 \end{bmatrix} \begin{bmatrix} i_{\alpha s} \\ i_{\beta s} \\ i_{0s} \end{bmatrix} \tag{17}$$

Forward Park Transformation:

$$\begin{bmatrix} i_{\alpha s} \\ i_{\beta s} \\ i_{0s} \end{bmatrix} = \begin{bmatrix} \cos(\theta) & -\sin(\theta) & 0 \\ \sin(\theta) & \cos(\theta) & 0 \\ 0 & 0 & 1 \end{bmatrix} \begin{bmatrix} i_{ds} \\ i_{qs} \\ i_{0s} \end{bmatrix} \tag{18}$$

Applying Clarke and Park transformations to obtain a generic set of equations to be used in the model's algorithm (which can be applied to stator and rotor voltages or stator and rotor currents) will result [4]:

$$i_{ds} = \frac{2}{3}(i_{as}\sin(\omega t) + i_{bs}\sin(\omega t - \frac{2\pi}{3}) + i_{cs}\sin(\omega t + \frac{2\pi}{3}))$$

$$i_{qs} = \frac{2}{3}(i_{as}\cos(\omega t) + i_{bs}\cos(\omega t - \frac{2\pi}{3}) + i_{cs}\cos(\omega t + \frac{2\pi}{3}))$$

$$i_{0s} = \frac{1}{3}(i_{as} + i_{bs} + i_{cs}) \tag{19}$$

And for transformation *dq0* to *abc* will be:

$$i_{as} = i_{ds}\sin(\omega t) + i_{qs}\cos(\omega t) + i_{0s}$$

$$i_{bs} = i_{ds}\sin(\omega t - \frac{2\pi}{3}) + i_{qs}\cos(\omega t - \frac{2\pi}{3}) + i_{0s}$$

$$i_{cs} = i_{ds}\sin(\omega t + \frac{2\pi}{3}) + i_{qs}\cos(\omega t + \frac{2\pi}{3}) + i_{0s} \tag{20}$$

Where $\theta = \omega t$, $\gamma = 2\pi/3$, and ω=rotation speed, in rad/s, of the rotating frame.

The stationary reference frame ($\alpha\beta$) can be considered as a particular case of the equations (19) and (20), where ω=0. The synchronous reference frame will be used when ω = synchronous speed and the rotor reference frame when ω=rotor speed.

The following reference frames can therefore be used to build the model:

- *abc* (or natural) reference frame;
- $\alpha\beta$ (or stationary) reference frame;
- $\alpha\beta 0$ (or stationary) reference frame with zero-sequence;

- *dq* reference frame, subdivided in:

  i.Synchronous speed referred; and

  ii.Rotor speed referred.

- *dq0* reference frame with zero-sequence, subdivided in:

  i.Synchronous speed referred; and

  ii.Rotor speed referred.

Reference List for Appendix "A"

[1] O Wasynczuk, S D Sudhoff and P C Krause. *Analysis of Electric Machinery and Drive Systems,* IEEE Press Power Engineering Series, John Wiley & Sons, INC Publication, New York, USA - 2002.

[2] C M Ong. *Dynamic Simulation of Electric Machinery,* Prentice Hall PTR, New Jersey, USA - 1998.

[3] Analog Devices Inc., "ADSP-21990: Reference Frame Conversions", no. AN21990-11, 2002. Analog Devices Inc. USA.

[4] TransEnergie Technologies. *SimPowerSys For Use with Simulink - User's Guide - Version 2,* TransEnergie Technologies Inc., HydroQuebec and The Mathworks Inc., USA - 2002.

Appendix "B" - dq_im_model / dq0_im_model / matrix_im_model

"dq_im_model" - Using *dq* reference frame (built with PSB components):

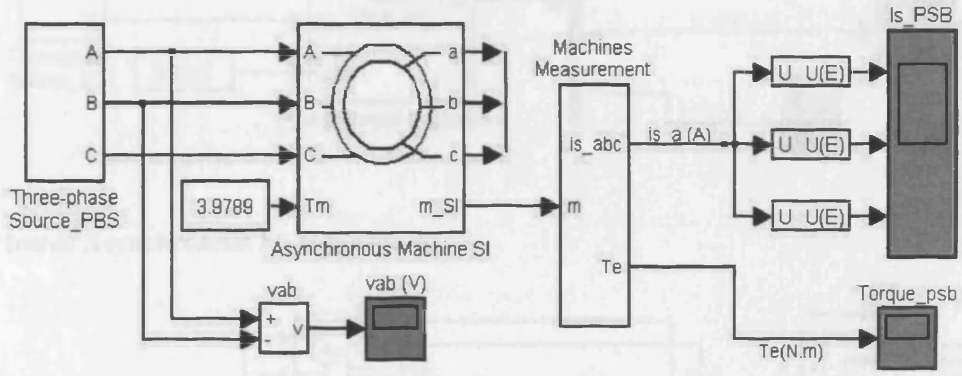

Inside Asynchronous Machine block*:

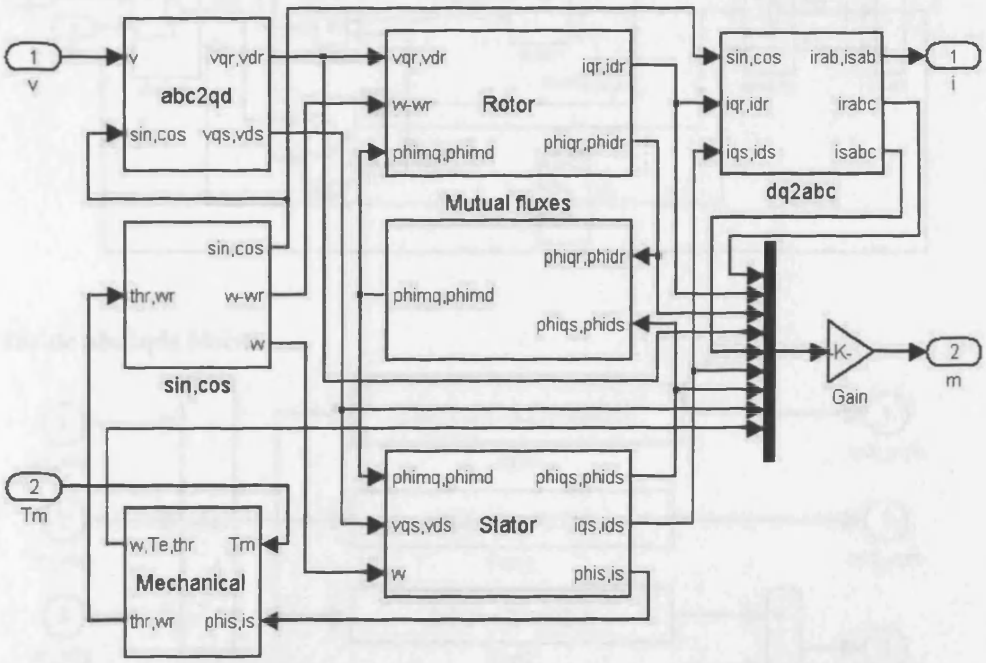

* It is part of the standard library of Power System Blockset – more detail can be found in **powerlib_models.mdl** file of PSB.

"dq0_im_model" - Using *dq0* reference frame (built with Simulink blocks):

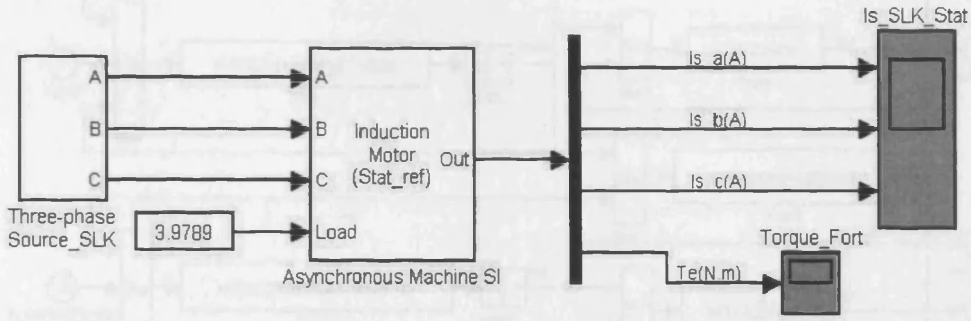

Inside Asynchronous Machine block:

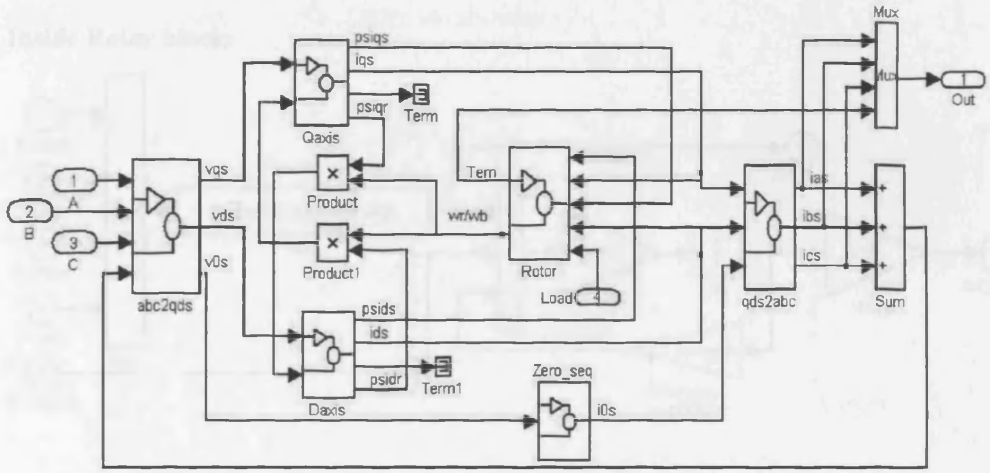

Inside abc2qds block:

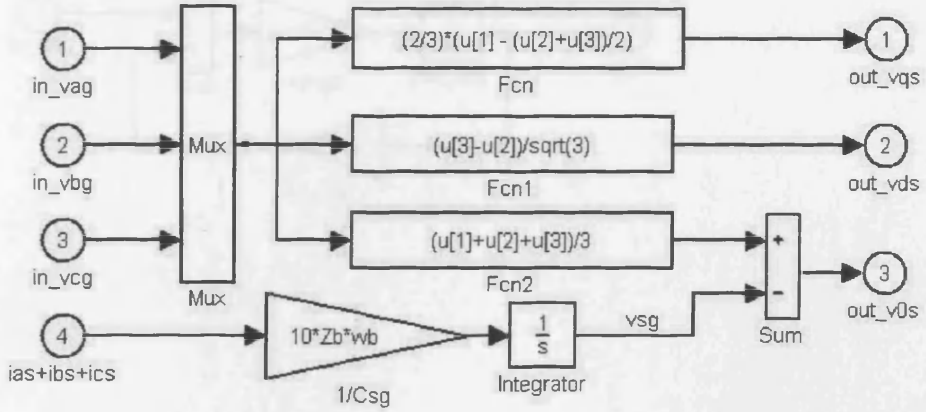

Inside Q axis block (D axis block is similar):

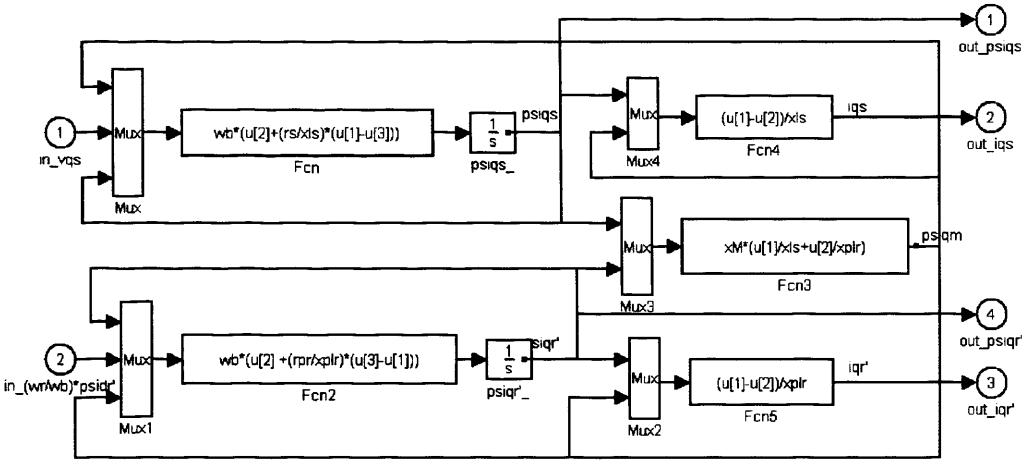

Inside Rotor block:

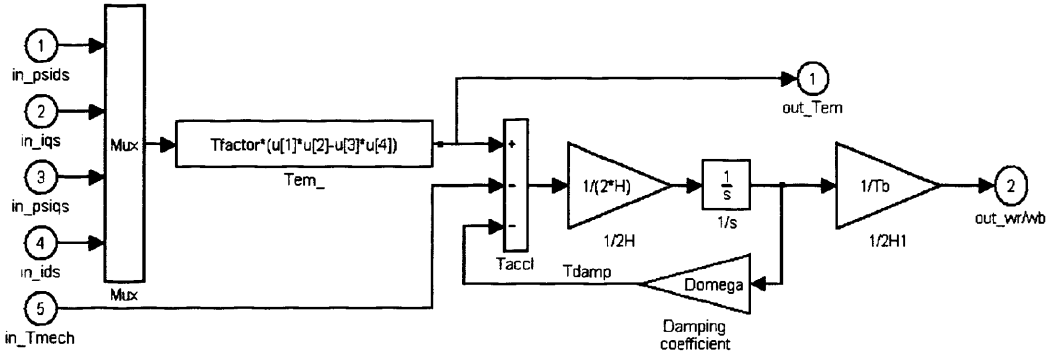

Inside Zero_seq block:

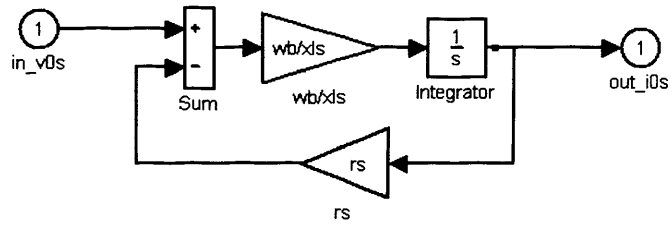

Inside qds2abc block:

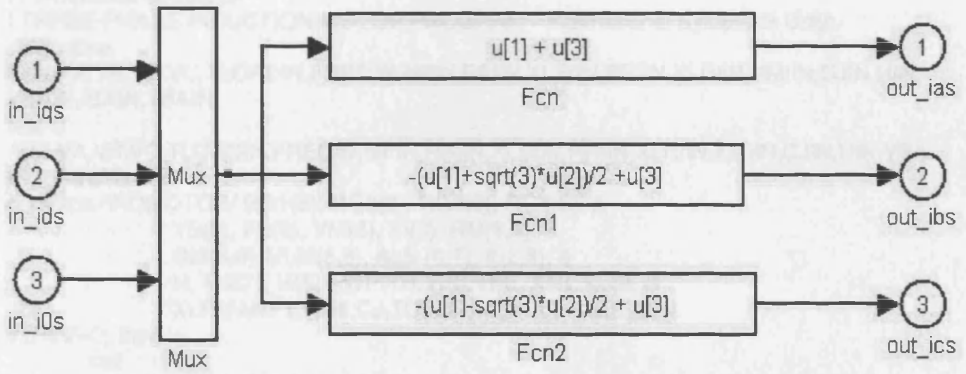

"matrix_im_model" - Using *abc* reference frame (built with Simulink blocks and Fortran subroutine):

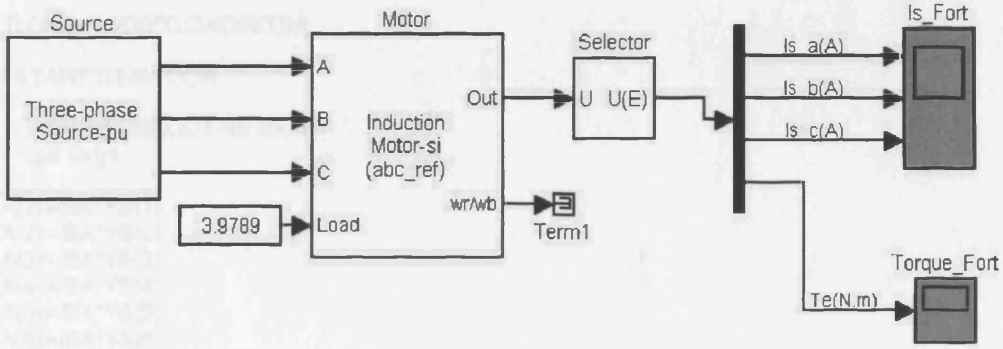

Inside Motor block:

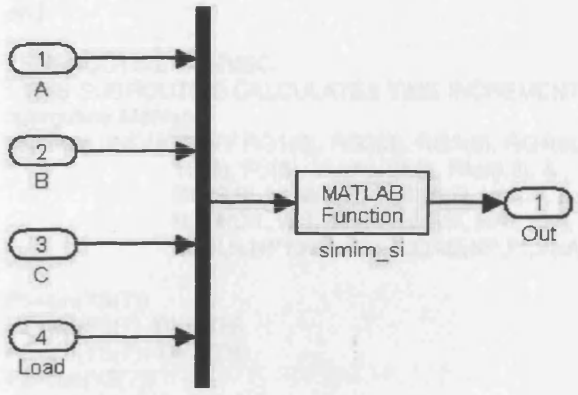

FORTRAN subroutine:

```
! PROGRAM SIMIM_SI
! THREE-PHASE INDUCTION MOTOR PROGRAM - International System of Units
subroutine
Motor(A,VA,VB,VC,TLOADIN,FREQIN,NPIN,RSIIN,XLSIIN,RRIIN,XLRIIN,XMIIN,CJIN,HIN,
VBAIN,IBAIN,TBAIN)
real*8
A(6),VA,VB,VC,TLOADIN,FREQIN,NPIN,RSIIN,XLSIIN,RRIIN,XLRIIN,XMIIN,CJIN,HIN,VBA
IN,IBAIN,TBAIN
common /INDMOTOR/ RG1(8), RG2(8), RG3(8), RG4(8), &
                   YS(8), FS(8), VM(6), SI(3), RM(6,6), &
                   GM(6,6), VLM(6,6), ALS (6,7), V(2,3), &
                   H, TMOT, WS, TWPITH, RSI, RRI, XMI, XLSI, &
                   XLRI,N,NP1,NM1,CJ,TLOAD,NP,PI,VBA,IBA,TBA
if (HIN/=0) then
        call
Parim(FREQIN,NPIN,RSIIN,XLSIIN,RRIIN,XLRIIN,XMIIN,CJIN,HIN,VBAIN,IBAIN,TBAIN)
        else
V(1,1)=V(2,1)
V(1,2)=V(2,2)
V(1,3)=V(2,3)
V(2,1)=1.0D0*VA/VBA
V(2,2)=1.0D0*VB/VBA
V(2,3)=1.0D0*VC/VBA

TLOAD=1.0D0*TLOADIN/TBA

! START ITERATION

   ! CALL SUBROUTINE RKG1
   call Rkg1

A(1)=IBA*YS(1)
A(2)=IBA*YS(2)
A(3)=IBA*YS(3)
A(4)=IBA*YS(4)
A(5)=IBA*YS(5)
A(6)=IBA*YS(6)
A(7)=WS*60*YS(8)/(PI*NP)
A(8)=TBA*TMOT
end if
return
end

! SUBROUTINE MOTVEC
! THIS SUBROUTINE CALCULATES TIME INCREMENTS OF MACHINE VARIABLES
subroutine Motvec
common /INDMOTOR/ RG1(8), RG2(8), RG3(8), RG4(8), &
                   YS(8), FS(8), VM(6), SI(3), RM(6,6), &
                   GM(6,6), VLM(6,6), ALS (6,7), V(2,3), &
                   H, TMOT, WS, TWPITH, RSI, RRI, XMI, XLSI, &
                   XLRI,N,NP1,NM1,CJ,TLOAD,NP,PI,VBA,IBA,TBA

F1=sin(YS(7))
F3=sin(YS(7)-TWPITH)
F5=sin(YS(7)+TWPITH)
F2=cos(YS(7))
F4=cos(YS(7)-TWPITH)
F6=cos(YS(7)+TWPITH)
! Ra, Rr
```

```
RM(1,1)=RSI
RM(2,2)=RSI
RM(3,3)=RSI
RM(4,4)=RRI
RM(5,5)=RRI
RM(6,6)=RRI
! Lss
HXMI=-XMI/2
VLM(1,1)=XLSI+XMI
VLM(1,2)=HXMI
VLM(1,3)=HXMI
VLM(2,1)=HXMI
VLM(2,2)=XLSI+XMI
VLM(2,3)=HXMI
VLM(3,1)=HXMI
VLM(3,2)=HXMI
VLM(3,3)=XLSI+XMI
! Lrr
VLM(4,4)=XLRI+XMI
VLM(4,5)=HXMI
VLM(4,6)=HXMI
VLM(5,4)=HXMI
VLM(5,5)=XLRI+XMI
VLM(5,6)=HXMI
VLM(6,4)=HXMI
VLM(6,5)=HXMI
VLM(6,6)=XLRI+XMI
! Lsr
TXMI=XMI
VLM(1,4)=TXMI*F2
VLM(1,5)=TXMI*F6
VLM(1,6)=TXMI*F4
VLM(2,4)=TXMI*F4
VLM(2,5)=TXMI*F2
VLM(2,6)=TXMI*F6
VLM(3,4)=TXMI*F6
VLM(3,5)=TXMI*F4
VLM(3,6)=TXMI*F2
! Gsr
GM(1,4)=-TXMI*F1
GM(1,5)=-TXMI*F5
GM(1,6)=-TXMI*F3
GM(2,4)=-TXMI*F3
GM(2,5)=-TXMI*F1
GM(2,6)=-TXMI*F5
GM(3,4)=-TXMI*F5
GM(3,5)=-TXMI*F3
GM(3,6)=-TXMI*F1
! Lra, Grs
do 10 I1=4,6
do 20 J1=1,3
GM(I1,J1)=GM(J1,I1)
VLM(I1,J1)=VLM(J1,I1)
20 continue
10 continue

! CALCULATE ELECTRO-MAGNETIC TORQUE
do 30 I1=1,6
TMP=0
do 40 J1=1,6
```

```
TMP=TMP+(RM(I1,J1)+WS*YS(8)*GM(I1,J1))*YS(J1)
ALS(I1,J1)=VLM(I1,J1)
40 continue
ALS(I1,NP1)=VM(I1)-TMP
30 continue

   ! CALL SUBROUTINE GAUSS
   call Gauss

do 50 I1=1,6
FS(I1)=ALS(I1,NP1)
50 continue

FS(7)=YS(8)*WS

do 60 I1=1,3
SI(I1)=0
   do 70 J1=1,6
   SI(I1)=SI(I1)+VLM(I1,J1)*YS(J1)
   70 continue
60 continue

TMOT=(SI(1)*(YS(2)-YS(3))+SI(2)*(YS(3)-YS(1))+SI(3)*(YS(1)-
YS(2)))*WS*2.0D0/(3.0D0*1.732050808D0)
FS(8)=(TMOT-TLOAD)/(2.0D0*CJ)
return
end


! SUBROUTINE RKG1
! RUNGE-KUTTA-GILL SUBROUTINE
subroutine Rkg1
common /INDMOTOR/ RG1(8), RG2(8), RG3(8), RG4(8), &
                   YS(8), FS(8), VM(6), SI(3), RM(6,6), &
                   GM(6,6), VLM(6,6), ALS (6,7), V(2,3), &
                   H, TMOT, WS, TWPITH, RSI, RRI, XMI, XLSI, &
                   XLRI,N,NP1,NM1,CJ,TLOAD,NP,PI,VBA,IBA,TBA
do 80 I=1,8
RG4(I)=YS(I)
80 continue


do 85 JJ=1,4

   ! CALL SUBROUTINE MOTVEC
   call Motvec

      do 90 J=1,8
         if (JJ==1) then
         RG1(J)=H*FS(J)
         YS(J)=RG4(J)+0.5D0*RG1(J)
         elseif (JJ==2) then
         RG2(J)=H*FS(J)
         YS(J)=RG4(J)+0.2071067D0*RG1(J)+0.29289325D0*RG2(J)
         elseif (JJ==3) then
         RG3(J)=H*FS(J)
         YS(J)=RG4(J)-0.7071087D0*RG2(J)+1.7071067D0*RG3(J)
         else
         AUX=RG4(J)
         RG4(J)=H*FS(J)
```

```
YS(J)=AUX+RG1(J)/6.0D0+(0.29289326D0*RG2(J))/3.0D0+(1.7071067D0*RG3(J))/3.0D0+
RG4(J)/6.0D0
        end if
      90 continue
   if (JJ==1) then
   VM(1)=(V(1,1)+V(2,1))/2
        VM(2)=(V(1,2)+V(2,2))/2
        VM(3)=(V(1,3)+V(2,3))/2
   elseif (JJ==2) then
   VM(1)=(V(1,1)+V(2,1))/2
        VM(2)=(V(1,2)+V(2,2))/2
        VM(3)=(V(1,3)+V(2,3))/2
   else
   VM(1)=V(2,1)
        VM(2)=V(2,2)
        VM(3)=V(2,3)
   end if
85 continue
return
end


! SUBROUTINE GAUSS
! THIS SUBROUTINE SOLVES N REAL SIMULTANEOUS LINEAR EQUATIONS BY
! GAUSSIAN ELIMINATION (N+1) COLUMN OF (ALS) CONTAINS THE SOLUTIONS
subroutine Gauss
common /INDMOTOR/ RG1(8), RG2(8), RG3(8), RG4(8), &
                  YS(8), FS(8), VM(6), SI(3), RM(6,6), &
                  GM(6,6), VLM(6,6), ALS (6,7), V(2,3), &
                  H, TMOT, WS, TWPITH, RSI, RRI, XMI, XLSI, &
                  XLRI,N,NP1,NM1,CJ,TLOAD,NP,PI,VBA,IBA,TBA
EPS=1.0E-20
! FORWARD ELIMINATION AND SEARCH FOR PIVOT ROW
IC=1
IR=1

500 if (IR<=N) then
PIVOT=ALS(IR,IC)
IPIVOT=IR
   do 100 I2=IR,N
   if (abs(ALS(I2,IC))>abs(PIVOT)) then
   PIVOT=ALS(I2,IC)
   IPIVOT=I2
   end if
   100 continue
      if (abs(PIVOT)<=EPS) then
      stop
      end if
   if (IPIVOT/=IR) then
   do 110 K2=IC,NP1
   B=ALS(IPIVOT,K2)
   ALS(IPIVOT,K2)=ALS(IR,K2)
   ALS(IR,K2)=B
   110 continue
   end if

do 120 K2=IC,NP1
ALS(IR,K2)=ALS(IR,K2)/PIVOT
120 continue
```

```
IRP1=IR+1
   do 140 IP=IRP1,N
   B=ALS(IP,IC)
      if (abs(B)>EPS) then
      do 130 K2=IC,NP1
      ALS(IP,K2)=ALS(IP,K2)-ALS(IR,K2)*B
      130 continue
      end if
   140 continue
IR=IR+1
IC=IC+1
goto 500
end if

   do 150 K2=1,NM1
   NMK=N-K2
      do 160 J2=1,K2
      NP1MJ=N+1-J2
      ALS(NMK,NP1)=ALS(NMK,NP1)-ALS(NMK,NP1MJ)*ALS(NP1MJ,NP1)
      160 continue
   150 continue
return
end

! SUBROUTINE PARIM
! PARAMETERS
subroutine
Parim(FREQIN,NPIN,RSIIN,XLSIIN,RRIIN,XLRIIN,XMIIN,CJIN,HIN,VBAIN,IBAIN,TBAIN)
real*8 FREQIN,NPIN,RSIIN,XLSIIN,RRIIN,XLRIIN,XMIIN,CJIN,HIN,VBAIN,IBAIN,TBAIN
common /INDMOTOR/ RG1(8), RG2(8), RG3(8), RG4(8), &
                  YS(8), FS(8), VM(6), SI(3), RM(6,6), &
                  GM(6,6), VLM(6,6), ALS (6,7), V(2,3), &
                  H, TMOT, WS, TWPITH, RSI, RRI, XMI, XLSI, &
                  XLRI,N,NP1,NM1,CJ,TLOAD,NP,PI,VBA,IBA,TBA

do 200 I=1,6
do 210 J=1,6
RM(I,J)=0.0D0
GM(I,J)=0.0D0
VLM(I,J)=0.0D0
ALS(I,J)=0.0D0
210 continue
200 continue
ALS(6,7)=0.0D0

do 220 I=1,8
RG1(I)=0.0D0
RG2(I)=0.0D0
RG3(I)=0.0D0
RG4(I)=0.0D0
YS(I)=0.0D0
FS(I)=0.0D0
220 continue

V(2,1)=0.0D0
V(2,2)=0.0D0
V(2,3)=0.0D0
VM(1)=0.0D0
VM(2)=0.0D0
```

```
VM(3)=0.0D0

VBA=1.0D0*VBAIN
IBA=1.0D0*IBAIN
TBA=1.0D0*TBAIN
ZBA=VBA/IBA

FREQ=1.0D0*FREQIN
NP=1.0D0*NPIN
RSI=1.0D0*RSIIN/ZBA
XLSI=1.0D0*XLSIIN/ZBA
RRI=1.0D0*RRIIN/ZBA
XLRI=1.0D0*XLRIIN/ZBA
XMI=1.0D0*XMIIN*2.0D0/(3.0D0*ZBA)
CJ=1.0D0*CJIN
H=1.0D0*HIN
PI=4.0D0*DATAN(1.0D0)
TWTHRD=2.0D0/3.0D0
TWPITH=PI*TWTHRD
N=6
NP1=N+1
NM1=N-1
WS = 2.0D0*PI*FREQ
TMOT=0.0D0
return
end
```

Appendix "C"- FORTRAN subroutine for 15-Phase Induction Motor model

```
! PROGRAM SIMIM15
! 15-PHASE INDUCTION MOTOR PROGRAM - International System of Units
subroutine Motor(A,DIN)
real*8 A(32),DIN(17)
common /INDMOTOR/ RG1(32), RG2(32), RG3(32), RG4(32), &
                  YS(32), FS(32), VM(30), SI(15), RM(30,30), &
                  GM(30,30), VLM(30,30), ALS (30,31), V(2,15), &
                  H, TMOT, WS, TWPITH, RSI, RRI, XMI, XLSI, &
                  XLRI,N,NP1,NP2,NM1,ND2,CJ,TLOAD,POL,PI,VBA,IBA,TBA
if (DIN(17)/=0) then
        call Parim(DIN)
        else
        do 10 I=1,ND2
        V(1,I)=V(2,I)
        V(2,I)=1.0D0*DIN(I)/VBA
        10 continue
        TLOAD=1.0D0*DIN(ND2+1)/TBA

        ! START ITERATION
                ! CALL SUBROUTINE RKG1
                call Rkg
        do 20 I=1,N
        A(I)=IBA*YS(I)
        20 continue
        A(NP1)=WS*60*YS(32)/(PI*POL)
        A(NP2)=TBA*TMOT
end if
return
end

! SUBROUTINE RKG
! RUNGE-KUTTA-GILL SUBROUTINE
subroutine Rkg
common /INDMOTOR/ RG1(32), RG2(32), RG3(32), RG4(32), &
                  YS(32), FS(32), VM(30), SI(15), RM(30,30), &
                  GM(30,30), VLM(30,30), ALS (30,31), V(2,15), &
                  H, TMOT, WS, TWPITH, RSI, RRI, XMI, XLSI, &
                  XLRI,N,NP1,NP2,NM1,ND2,CJ,TLOAD,POL,PI,VBA,IBA,TBA
do 30 I=1,NP2
RG4(I)=YS(I)
30 continue
do 40 I=1,4
   ! CALL SUBROUTINE MOTVEC
   call Motvec
        do 50 J=1,32
        if (I==1) then
        RG1(J)=H*FS(J)
        YS(J)=RG4(J)+0.5D0*RG1(J)
        elseif (I==2) then
        RG2(J)=H*FS(J)
        YS(J)=RG4(J)+0.2071067D0*RG1(J)+0.29289325D0*RG2(J)
        elseif (I==3) then
        RG3(J)=H*FS(J)
        YS(J)=RG4(J)-0.7071087D0*RG2(J)+1.7071067D0*RG3(J)
        else
        AUX=RG4(J)
```

```
        RG4(J)=H*FS(J)
YS(J)=AUX+RG1(J)/6.0D0+(0.29289326D0*RG2(J))/3.0D0+(1.7071067D0*RG3(J))/3.0D0+
RG4(J)/6.0D0
        end if
      50 continue
   if ((I==1).or.(I==2)) then
                do 60 K=1,ND2
                VM(K)=(V(1,K)+V(2,K))/2
                60 continue
   else
                do 70 K=1,ND2
                VM(K)=V(2,K)
                70 continue
   end if
40 continue
return
end

! SUBROUTINE MOTVEC
! THIS SUBROUTINE CALCULATES TIME INCREMENTS OF MACHINE VARIABLES
subroutine Motvec
real*8 F(30),FF1,FF2,ANG
common /INDMOTOR/ RG1(32), RG2(32), RG3(32), RG4(32), &
                YS(32), FS(32), VM(30), SI(15), RM(30,30), &
                GM(30,30), VLM(30,30), ALS (30,31), V(2,15), &
                H, TMOT, WS, TWPITH, RSI, RRI, XMI, XLSI, &
                XLRI,N,NP1,NP2,NM1,ND2,CJ,TLOAD,POL,PI,VBA,IBA,TBA
K=-7.0D0
do 80 I=1,NM1,2
IP=I+1
ANG=1.0D0*(YS(NP1)-K*TWPITH)
F(I)=dsin(ANG)
F(IP)=dcos(ANG)
K=K+1.0D0
80 continue
! Lsr, Gsr
TXMI=XMI
do 110 I=1,ND2
K=ND2
        do 120 J=1,NM1,2
        K=K+1
        JP=J+1
        VLM(I,K)=TXMI*F(JP)
        GM(I,K)=-TXMI*F(J)
        120 continue
FF1=F(NM1)
FF2=F(N)
        do 130 L=NM1,3,-2
        LP=L+1
        F(L)=F(L-2)
        F(LP)=F(LP-2)
        130 continue
F(1)=FF1
F(2)=FF2
110 continue
! Lrs, Grs
do 140 I=ND2+1,N
        do 150 J=1,ND2
        GM(I,J)=GM(J,I)
        VLM(I,J)=VLM(J,I)
```

```
        150 continue
140 continue

! CALCULATE ELECTRO-MAGNETIC TORQUE
do 160 I=1,N
TMP=0
        do 170 J=1,N
        TMP=TMP+(RM(I,J)+WS*YS(NP2)*GM(I,J))*YS(J)
        ALS(I,J)=VLM(I,J)
        170 continue
ALS(I,NP1)=VM(I)-TMP
160 continue
  ! CALL SUBROUTINE GAUSS
  call Gauss
do 180 I=1,N
FS(I)=ALS(I,NP1)
180 continue
FS(NP1)=YS(NP2)*WS
do 190 I=1,ND2
SI(I)=0
  do 200 J=1,N
  SI(I)=SI(I)+VLM(I,J)*YS(J)
  200 continue
190 continue
TMOT=(SI(1)*(YS(9)-YS(8))+SI(2)*(YS(10)-YS(9))+SI(3)*(YS(11)-YS(10))+SI(4)*(YS(12)-
YS(11))+SI(5)*(YS(13)-YS(12))+ &
        SI(6)*(YS(14)-YS(13))+SI(7)*(YS(15)-YS(14))+SI(8)*(YS(1)-YS(15))+SI(9)*(YS(2)-
YS(1))+ &
        SI(10)*(YS(3)-YS(2))+SI(11)*(YS(4)-YS(3))+SI(12)*(YS(5)-YS(4))+SI(13)*(YS(6)-
YS(5))+ &
        SI(14)*(YS(7)-YS(6))+SI(15)*(YS(8)-YS(7)))*WS/(3.0D0*0.20791169D0)

FS(NP2)=(TMOT-TLOAD)/(2.0D0*CJ)
return
end

! SUBROUTINE GAUSS
! THIS SUBROUTINE SOLVES N REAL SIMULTANEOUS LINEAR EQUATIONS BY
! GAUSSIAN ELIMINATION (N+1) COLUMN OF (ALS) CONTAINS THE SOLUTIONS
subroutine Gauss
common /INDMOTOR/ RG1(32), RG2(32), RG3(32), RG4(32), &
                   YS(32), FS(32), VM(30), SI(15), RM(30,30), &
                   GM(30,30), VLM(30,30), ALS (30,31), V(2,15), &
                   H, TMOT, WS, TWPITH, RSI, RRI, XMI, XLSI, &
                   XLRI,N,NP1,NP2,NM1,ND2,CJ,TLOAD,POL,PI,VBA,IBA,TBA
EPS=1.0E-20
! FORWARD ELIMINATION AND SEARCH FOR PIVOT ROW
IC=1
IR=1
300 if (IR<=N) then
PIVOT=ALS(IR,IC)
IPIVOT=IR
  do 210 I2=IR,N
  if (abs(ALS(I2,IC))>abs(PIVOT)) then
  PIVOT=ALS(I2,IC)
  IPIVOT=I2
  end if
  210 continue
    if (abs(PIVOT)<=EPS) then
    stop
```

```
      end if
   if (IPIVOT/=IR) then
   do 220 K2=IC,NP1
   B=ALS(IPIVOT,K2)
   ALS(IPIVOT,K2)=ALS(IR,K2)
   ALS(IR,K2)=B
   220 continue
   end if

do 230 K2=IC,NP1
ALS(IR,K2)=ALS(IR,K2)/PIVOT
230 continue
IRP1=IR+1
   do 240 IP=IRP1,N
   B=ALS(IP,IC)
      if (abs(B)>EPS) then
      do 250 K2=IC,NP1
      ALS(IP,K2)=ALS(IP,K2)-ALS(IR,K2)*B
      250 continue
      end if
   240 continue
IR=IR+1
IC=IC+1
goto 300
end if
   do 260 K2=1,NM1
   NMK=N-K2
      do 270 J2=1,K2
      NP1MJ=N+1-J2
      ALS(NMK,NP1)=ALS(NMK,NP1)-ALS(NMK,NP1MJ)*ALS(NP1MJ,NP1)
      270 continue
   260 continue
return
end

! SUBROUTINE PARIM
! PARAMETERS
subroutine Parim(DIN)
real*8 DIN(17),G(15),GG1,ANG
! real*8 FREQIN,NPIN,RSIIN,XLSIIN,RRIIN,XLRIIN,XMIIN,CJIN,HIN,VBAIN,IBAIN,TBAIN
common /INDMOTOR/ RG1(32), RG2(32), RG3(32), RG4(32), &
                   YS(32), FS(32), VM(30), SI(15), RM(30,30), &
                   GM(30,30), VLM(30,30), ALS (30,31), V(2,15), &
                   H, TMOT, WS, TWPITH, RSI, RRI, XMI, XLSI, &
                   XLRI,N,NP1,NP2,NM1,ND2,CJ,TLOAD,POL,PI,VBA,IBA,TBA
N=30
NP1=N+1
NP2=N+2
NM1=N-1
ND2=N/2

do 310 I=1,N
         do 320 J=1,N
         RM(I,J)=0.0D0
         GM(I,J)=0.0D0
         VLM(I,J)=0.0D0
         ALS(I,J)=0.0D0
         320 continue
ALS(I,NP1)=0.0D0
310 continue
```

```
do 330 I=1,NP2
RG1(I)=0.0D0
RG2(I)=0.0D0
RG3(I)=0.0D0
RG4(I)=0.0D0
YS(I)=0.0D0
FS(I)=0.0D0
330 continue

do 340 I=1,ND2
V(2,I)=0.0D0
VM(I)=0.0D0
340 continue

VBA=1.0D0*DIN(9)
IBA=1.0D0*DIN(10)
TBA=1.0D0*DIN(11)
ZBA=VBA/IBA
FREQ=1.0D0*DIN(1)
POL=1.0D0*DIN(2)
RSI=1.0D0*DIN(3)/ZBA
XLSI=1.0D0*DIN(4)/ZBA
RRI=1.0D0*DIN(5)/ZBA
XLRI=1.0D0*DIN(6)/ZBA
XMI=2.0D0*DIN(7)/(15.0D0*ZBA)
CJ=1.0D0*DIN(8)
H=1.0D0*DIN(17)
PI=4.0D0*datan(1.0D0)
TWPITH=2.0D0*PI/15.0D0
WS = 2.0D0*PI*FREQ
TMOT=0.0D0
K=0
do 350 I=1,ND2
ANG=1.0D0*(K*TWPITH)
G(I)=dcos(ANG)
K=K+1
350 continue

do 360 I=1,ND2
IP=I+ND2
        do 370 J=1,ND2
        ! Lss / Lrr
        JP=J+ND2
        VLM(I,J)=G(J)*XMI
        VLM(IP,JP)=G(J)*XMI
        370 continue
VLM(I,I)=XLSI+XMI
VLM(IP,IP)=XLRI+XMI
! Ra / Rr
RM(I,I)=RSI
RM(IP,IP)=RRI
GG1=G(ND2)
        do 380 L=ND2,2,-1
        G(L)=G(L-1)
        380 continue
G(1)=GG1
360 continue
return
end
```

Appendix "D" – 15-Phase *dq* Induction Motor model

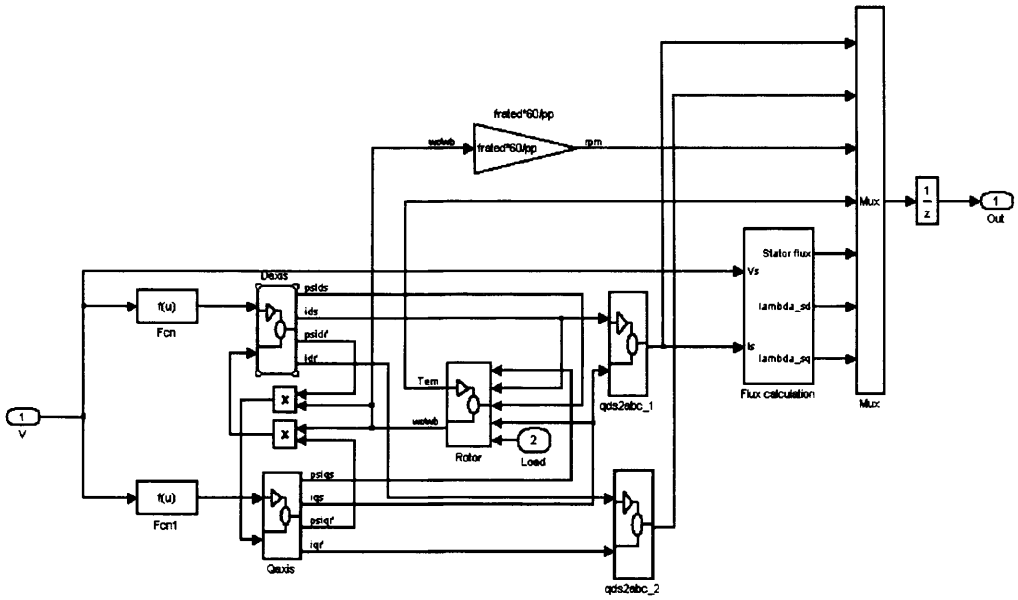

Inside Fcn block:

(2/15)*(u[1]+0.9135*u[2]+0.6691*u[3]+0.3090*u[4]-0.1045*u[5]-0.5*u[6]-
0.8090*u[7]-0.9781*u[8]-0.9781*u[9]-0.8090*u[10]-0.5*u[11]-
0.1045*u[12]+0.3090*u[13]+ 0.6691*u[14]+0.9135*u[15])

Inside Fcn1 block:

-(2/15)*(-0.4067*u[2]-0.7431*u[3]-0.9511*u[4]-0.9945*u[5]-0.8660*u[6]-
0.5878*u[7]-
0.2079*u[8]+0.2079*u[9]+0.5878*u[10]+0.8660*u[11]+0.9945*u[12]+0.9511*u[13
]+0.7431*u[14]+0.4067*u[15])

Inside Daxis block:

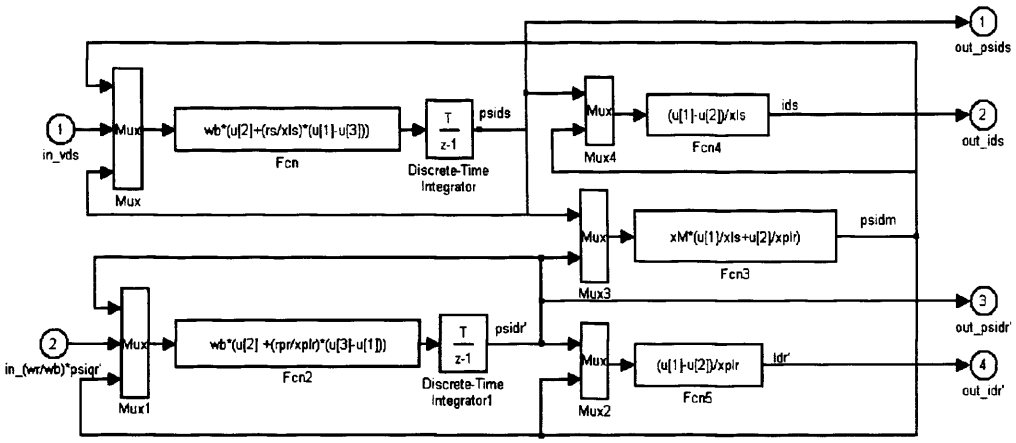

Inside Qaxis block:

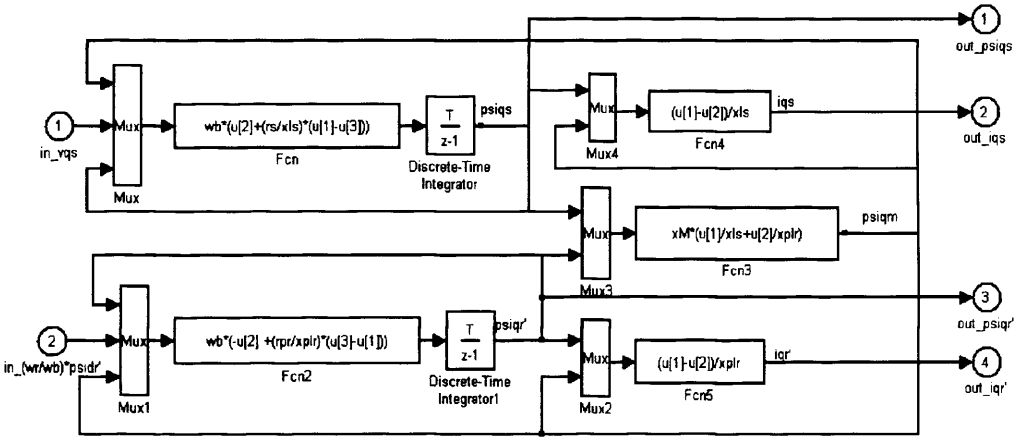

Inside Rotor block:

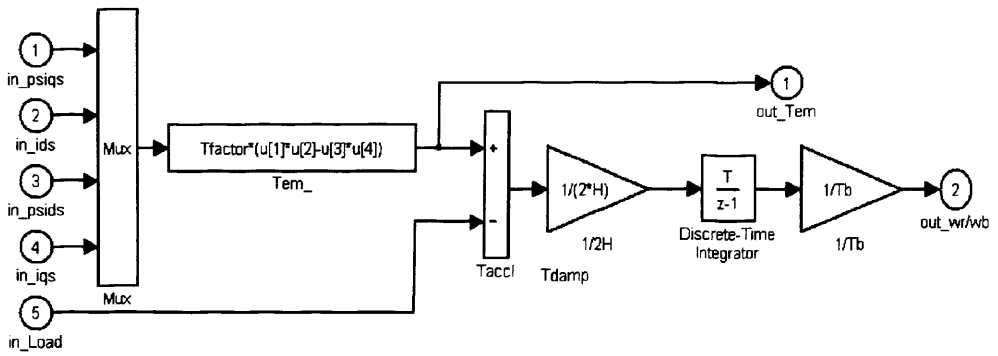

Inside Flux calculation block:

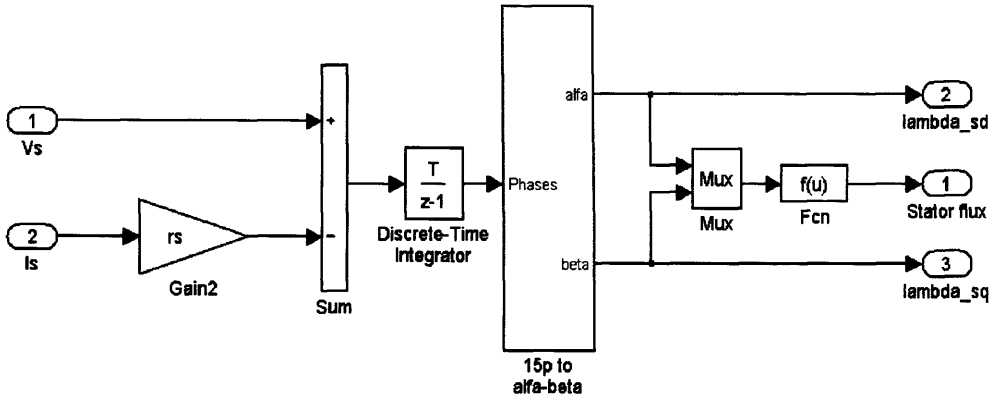

Inside qds2abc_1 block:

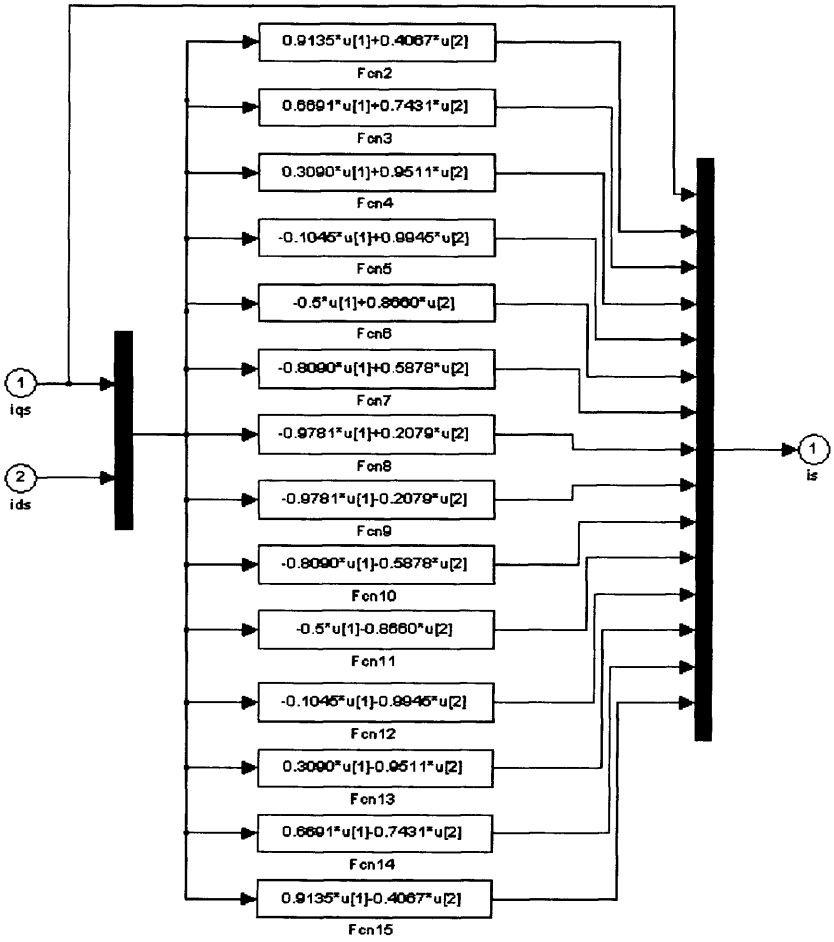

Inside Daxis block:

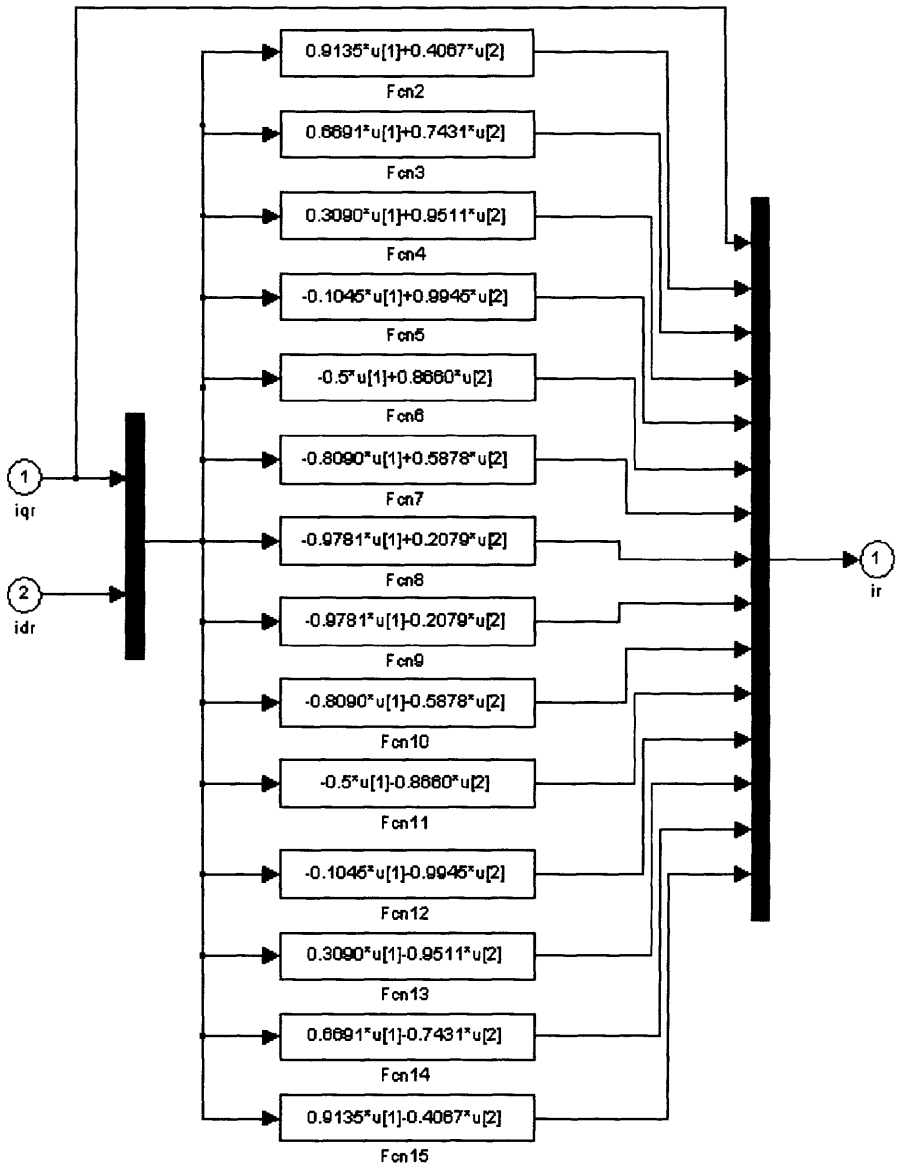

Appendix "E" – Fifteen-phase PWM Converter

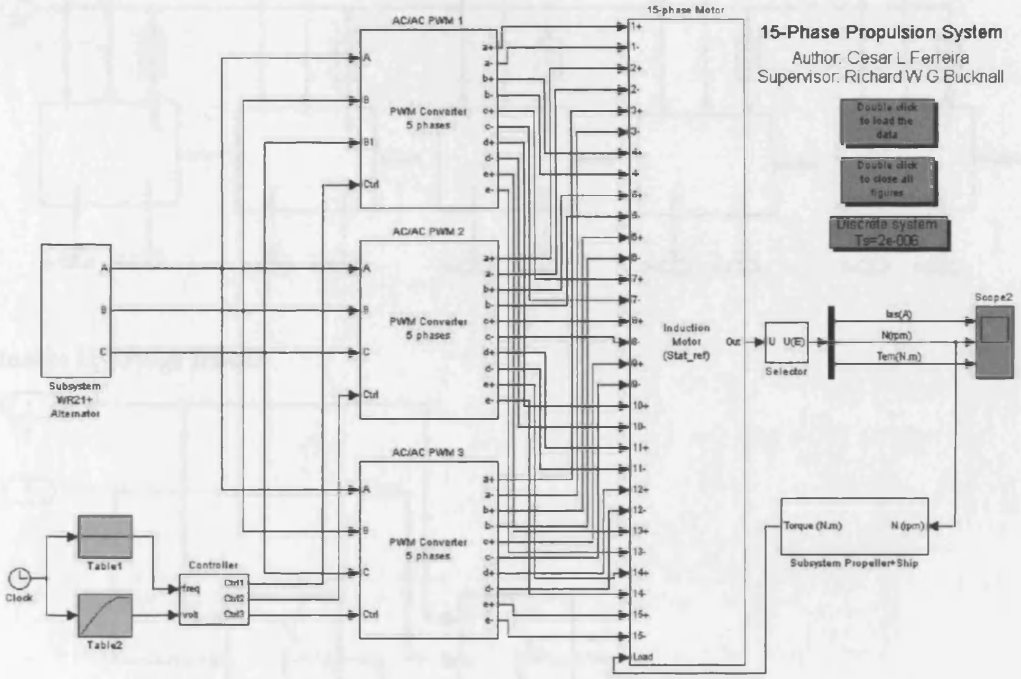

Inside AC/AC PWM block:

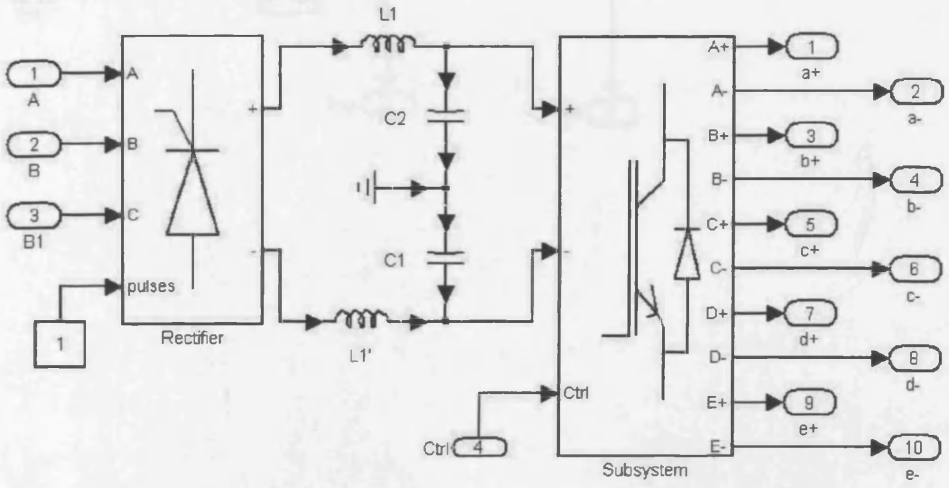

Inside Inverter block:

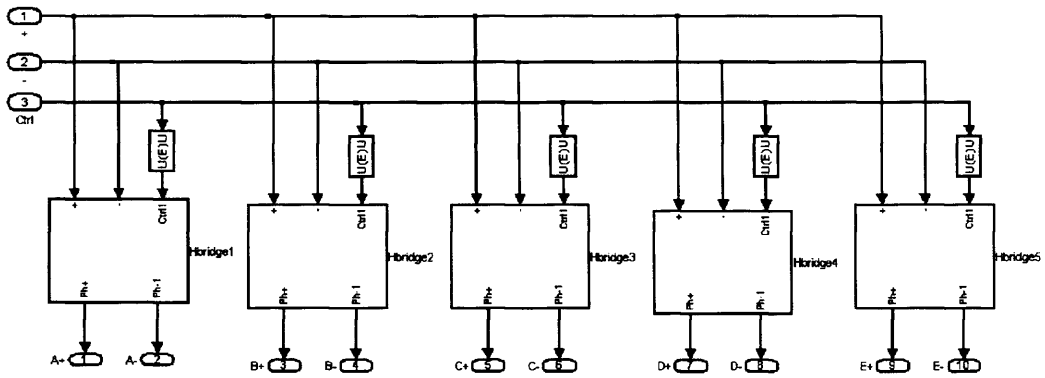

Inside H Bridge block:

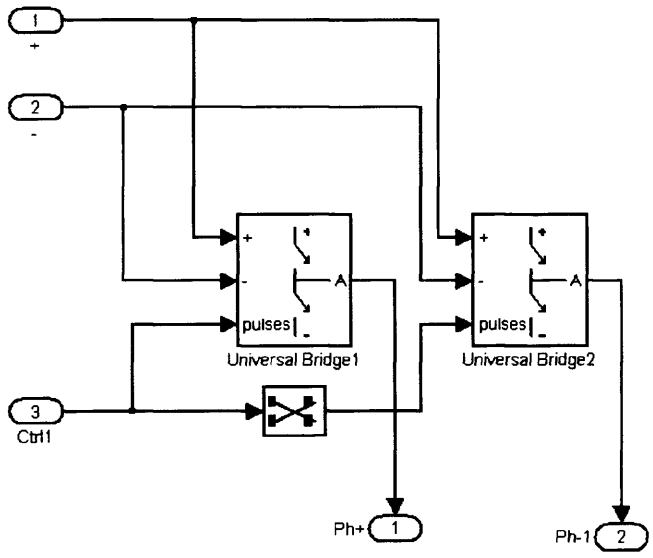

Appendix "F" – 3-Phase Field-oriented Control model

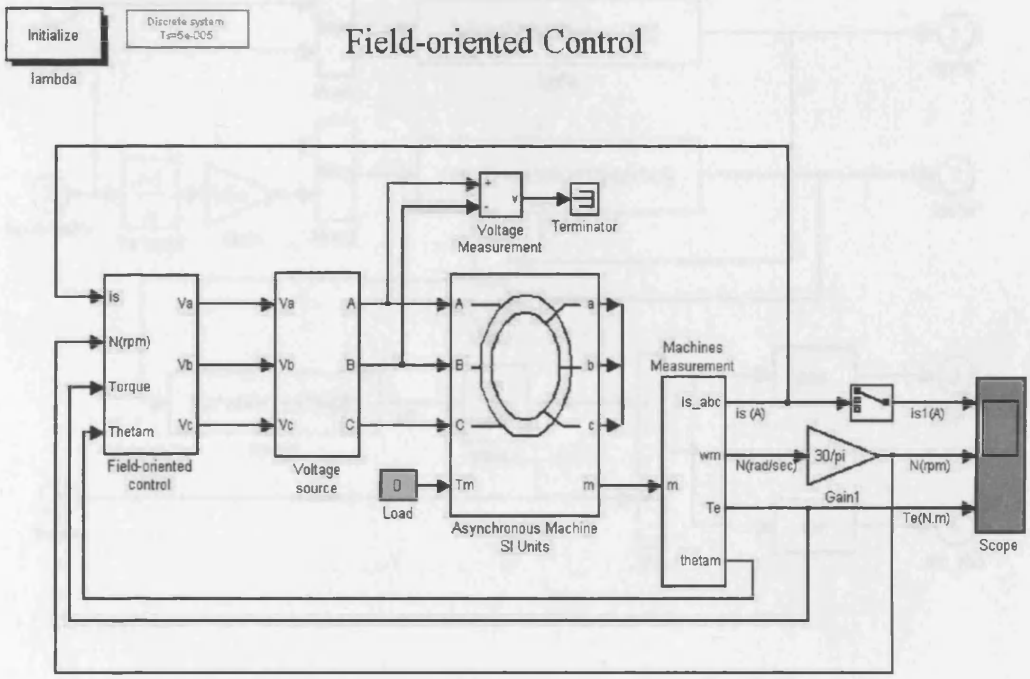

Inside Field-oriented Control block:

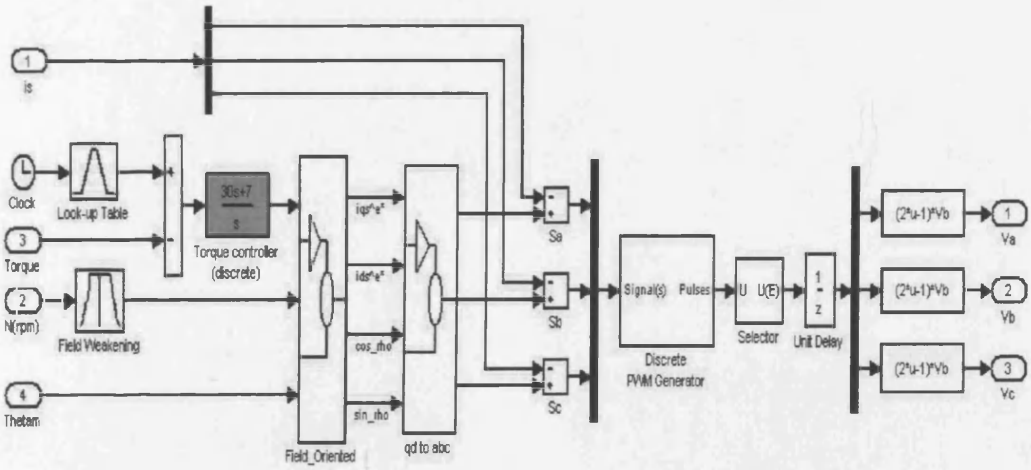

Inside Field-Oriented block:

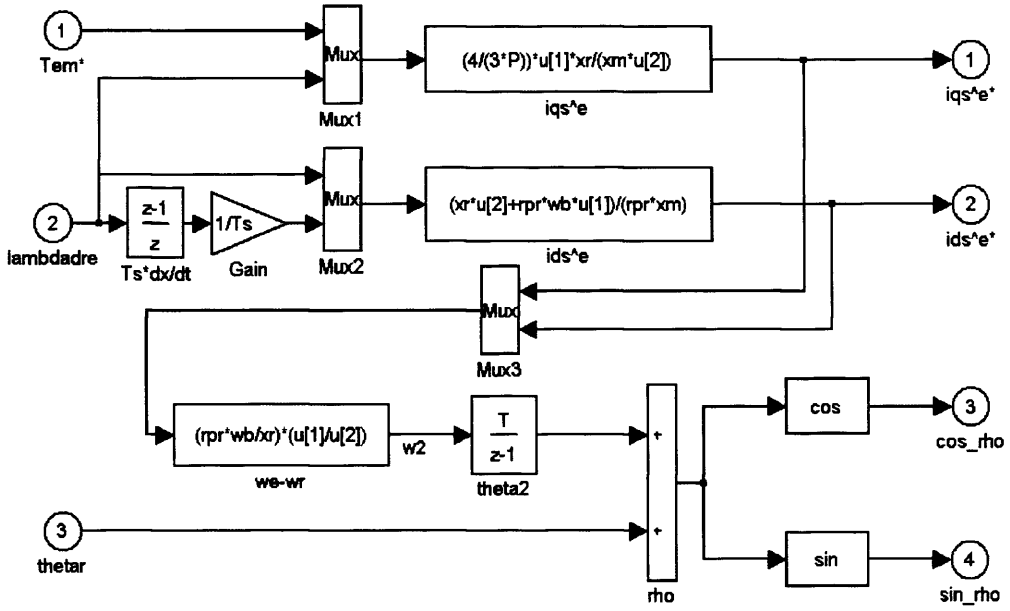

Appendix "G" – 3-Phase Direct Torque and Flux Control model

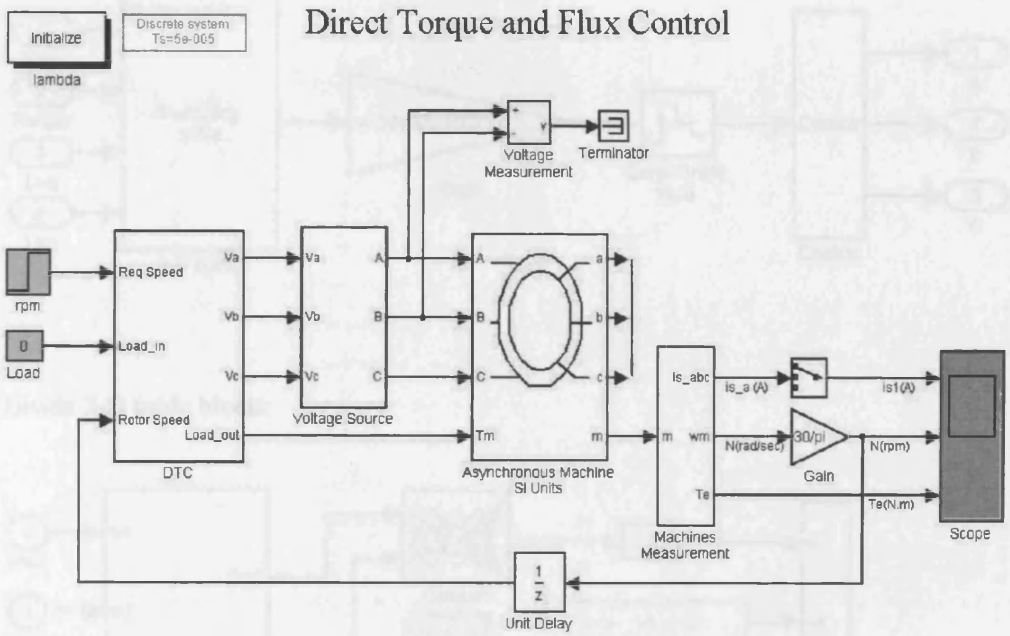

Inside DTC block:

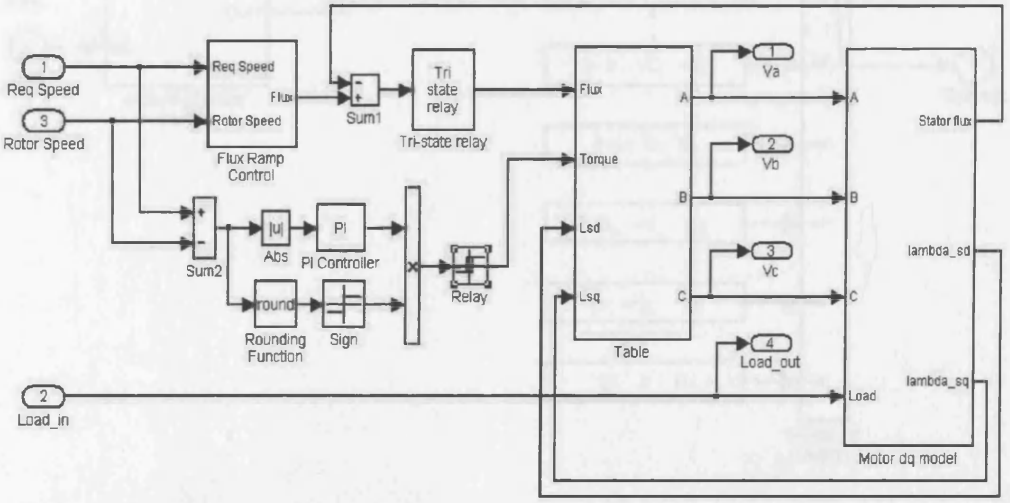

Inside Table block:

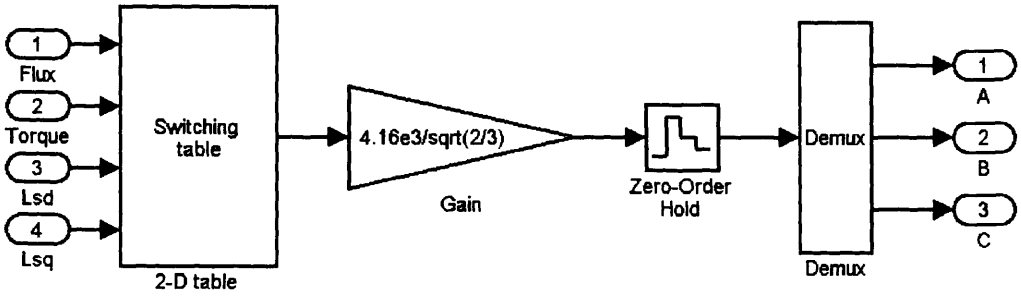

Inside 2-D table block:

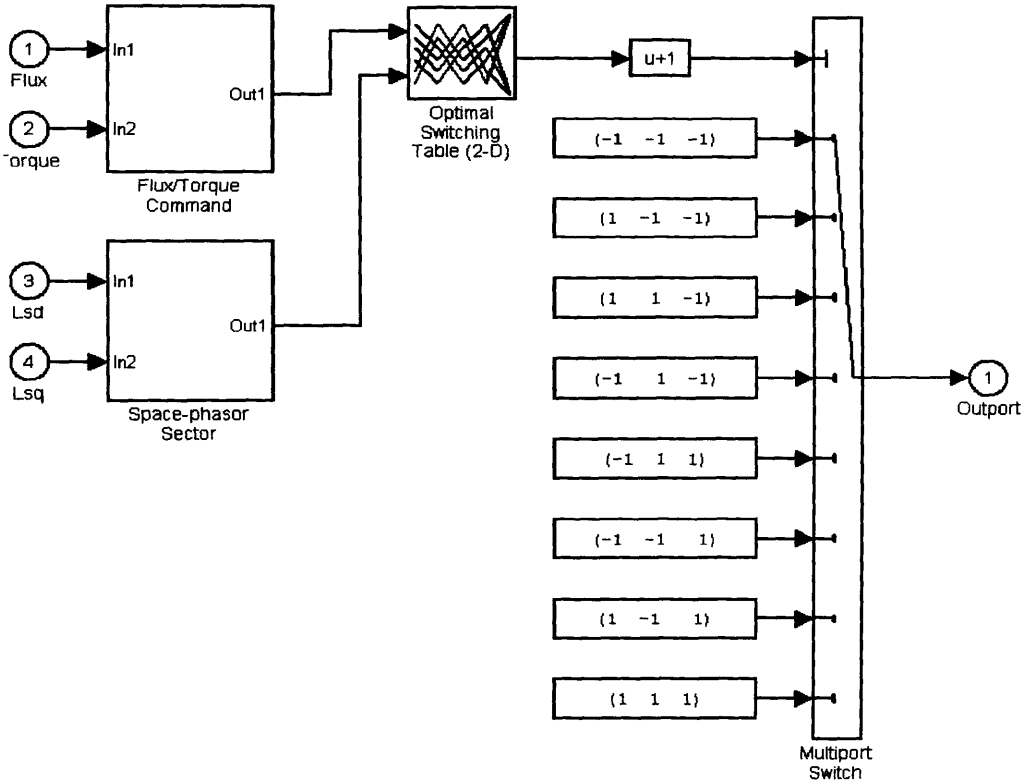

Appendix "H" – 15-Phase Direct Torque and Flux Control model

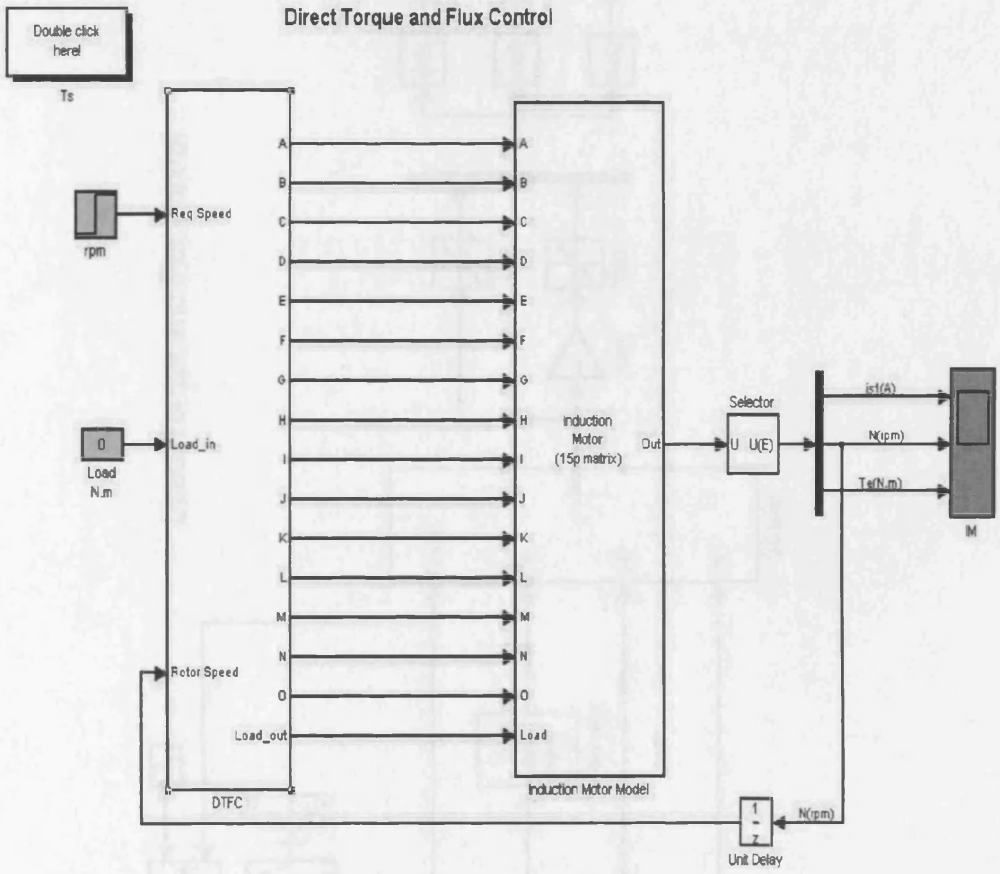

Inside DTFC block:

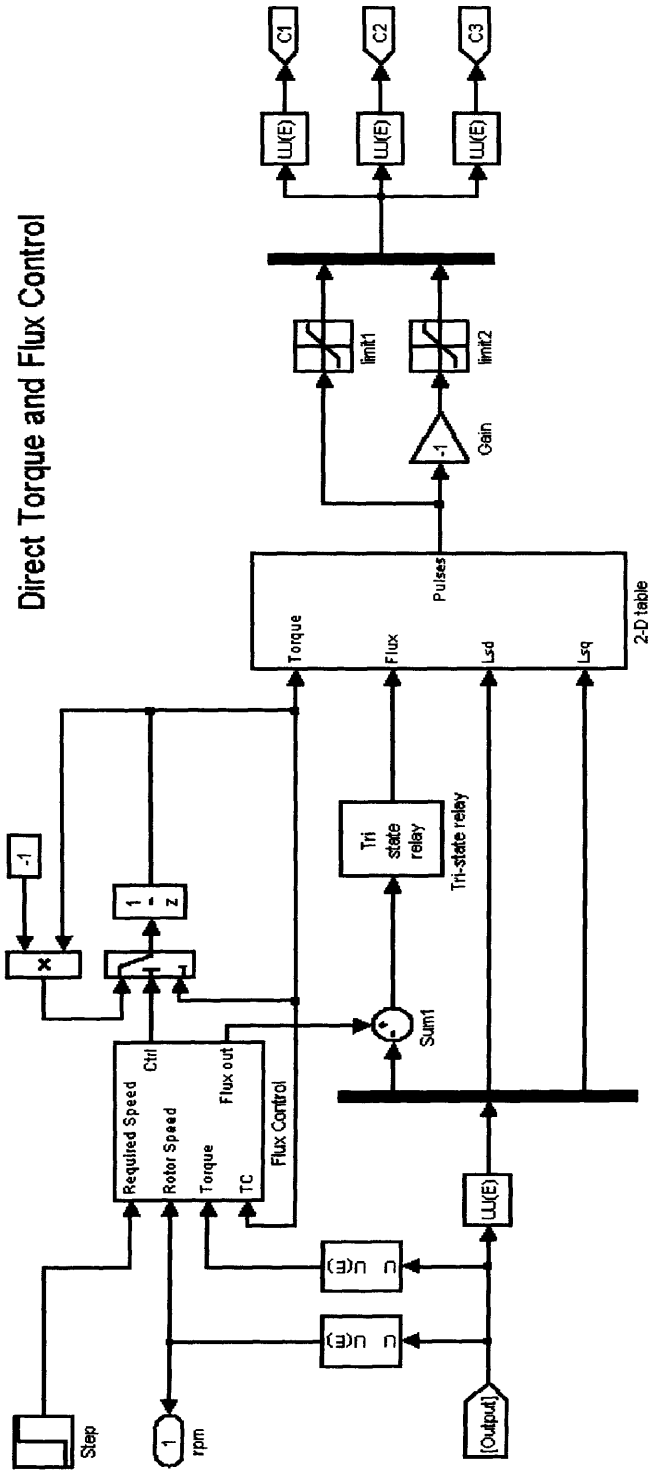

Inside 2-D table block:

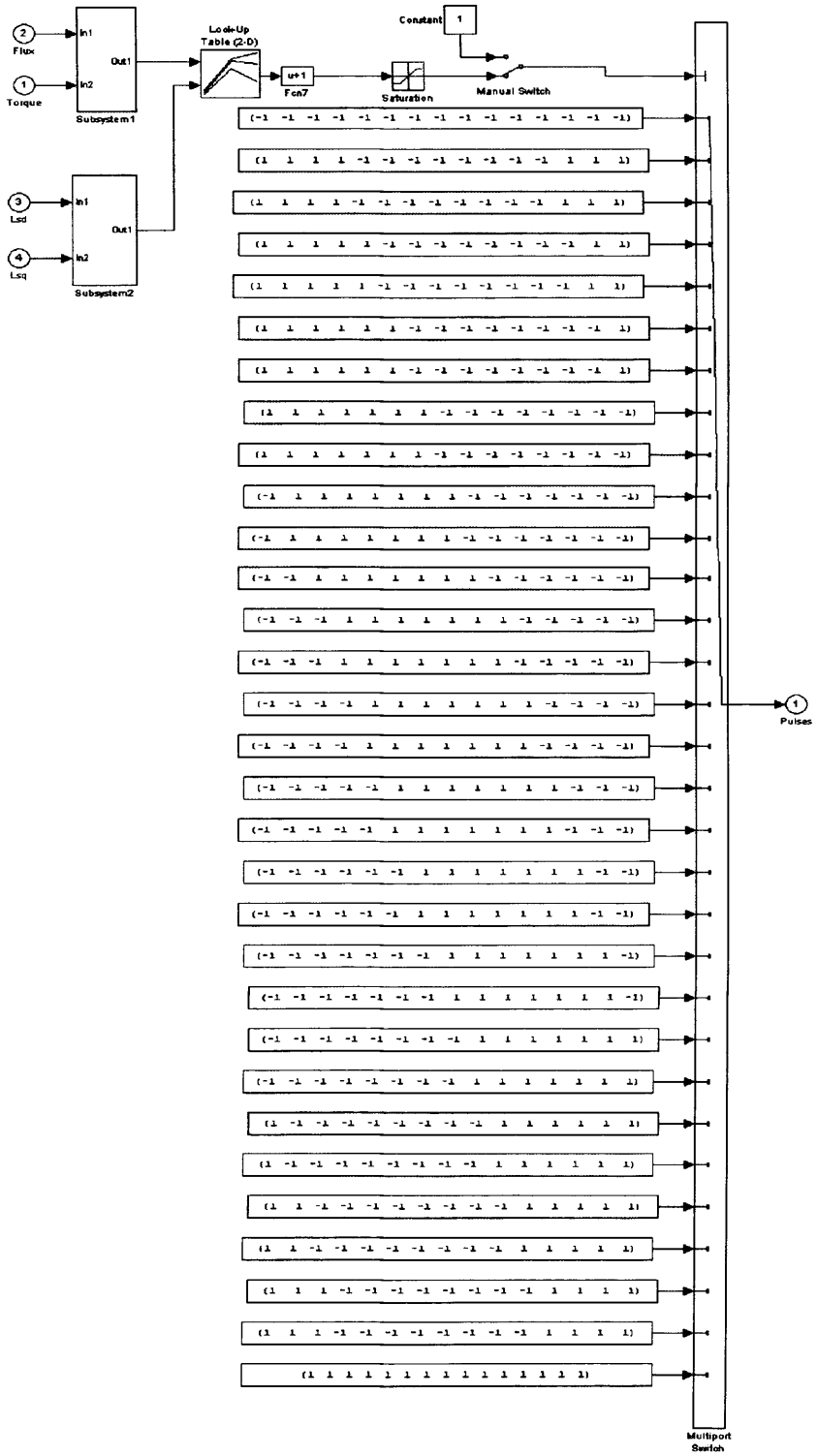

Inside Flux Control block:

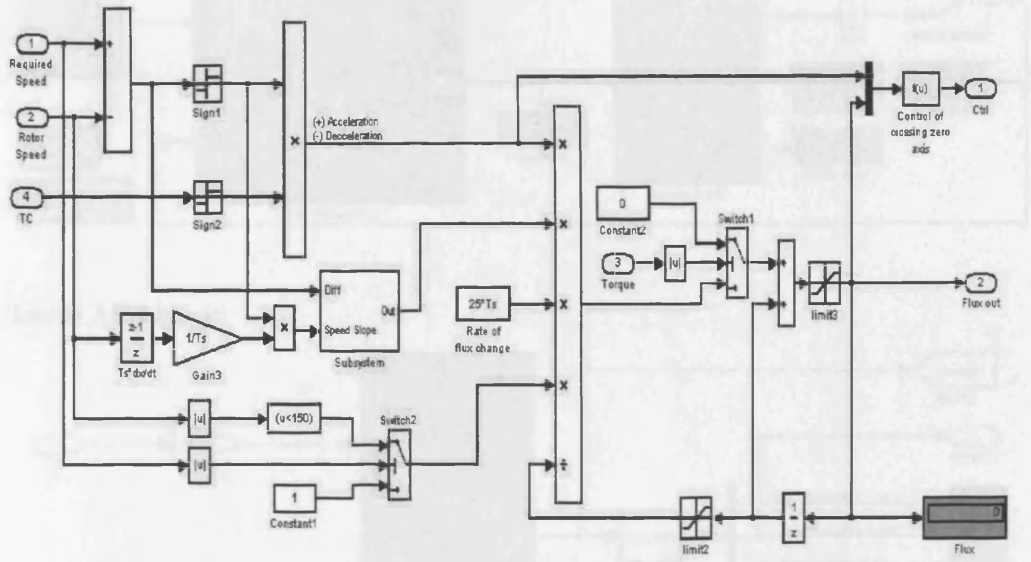

Inside Subsystem block:

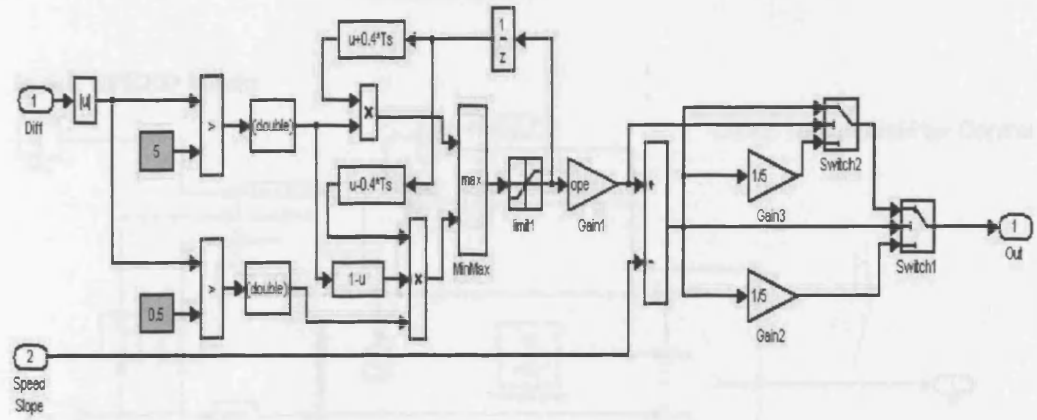

Appendix "I" – Model for validation of 15-Phase Control System

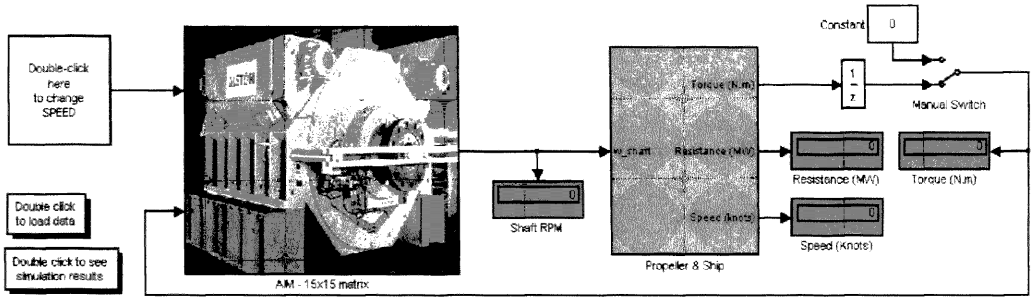

Inside AIM block:

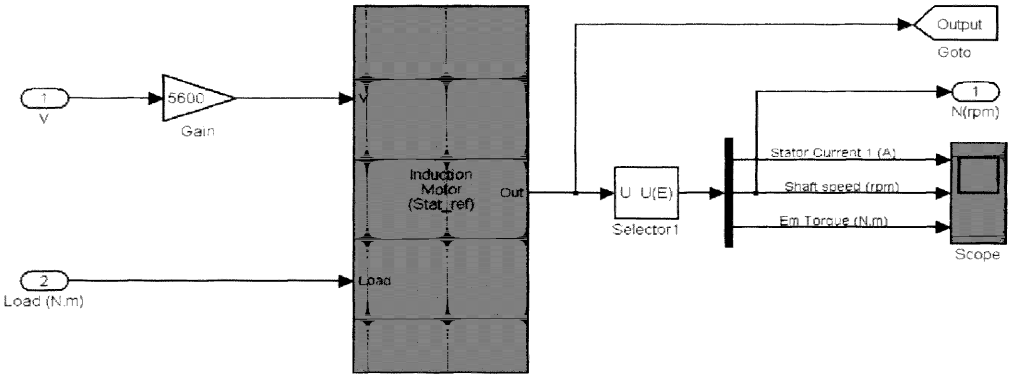

Inside SPEED block:

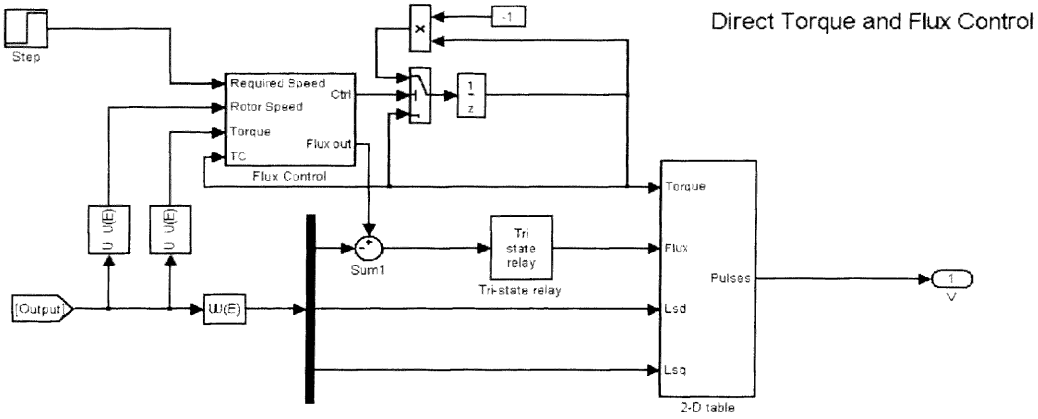

Appendix "J" – Characteristic curves of WR21 Gas Turbine

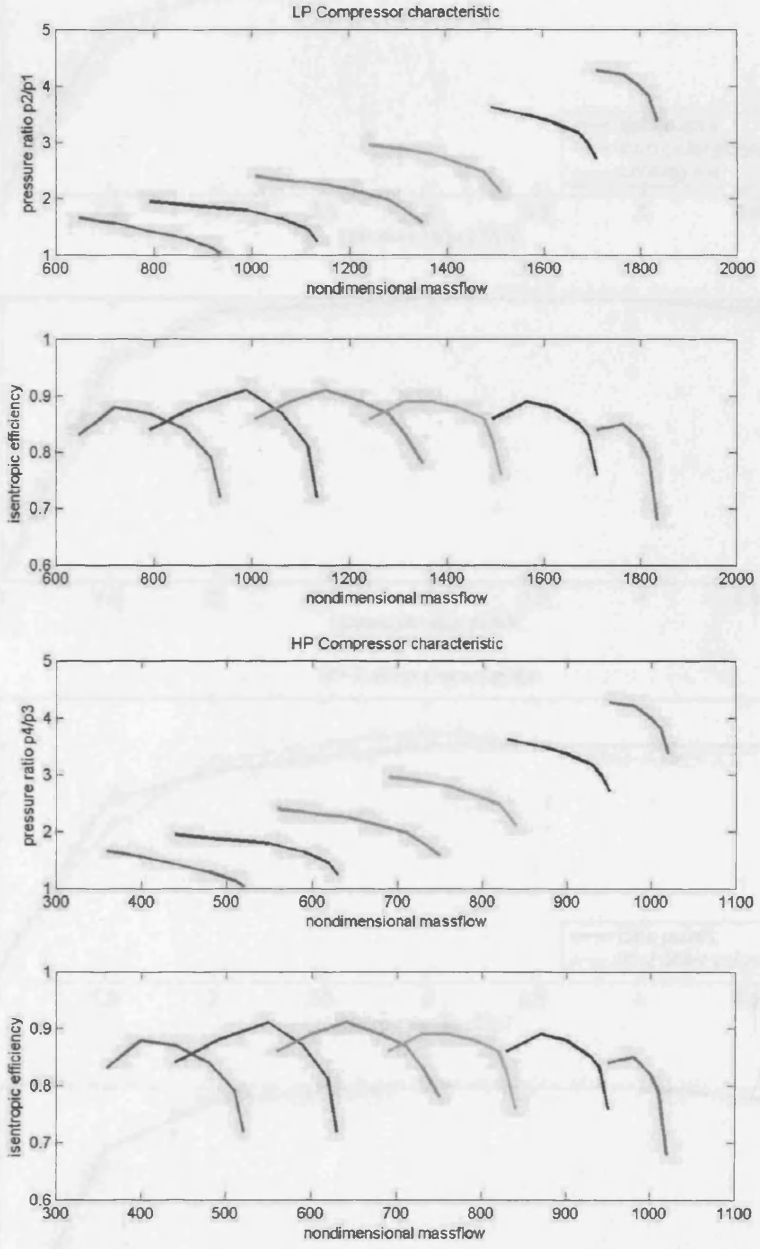

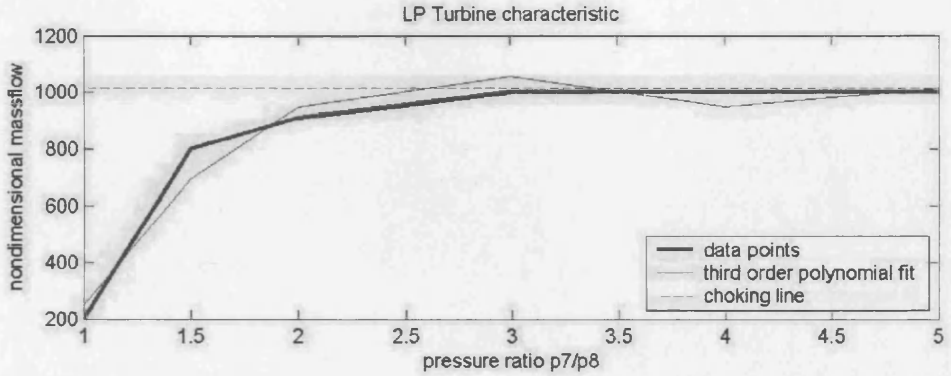
LP Turbine characteristic
nondimensional massflow
pressure ratio p7/p8
data points
third order polynomial fit
choking line

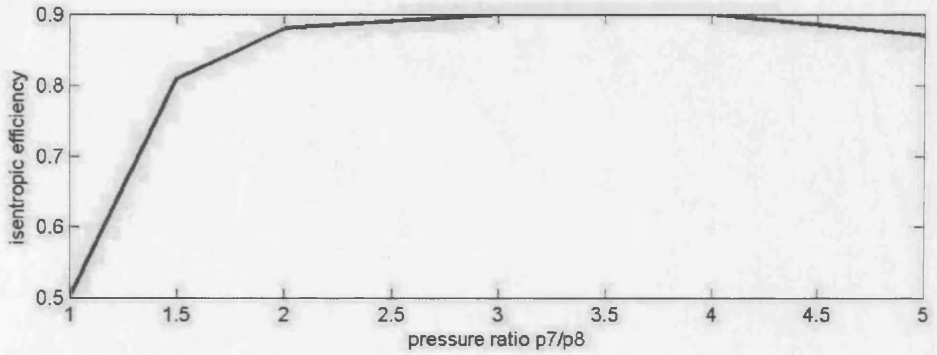
isentropic efficiency
pressure ratio p7/p8

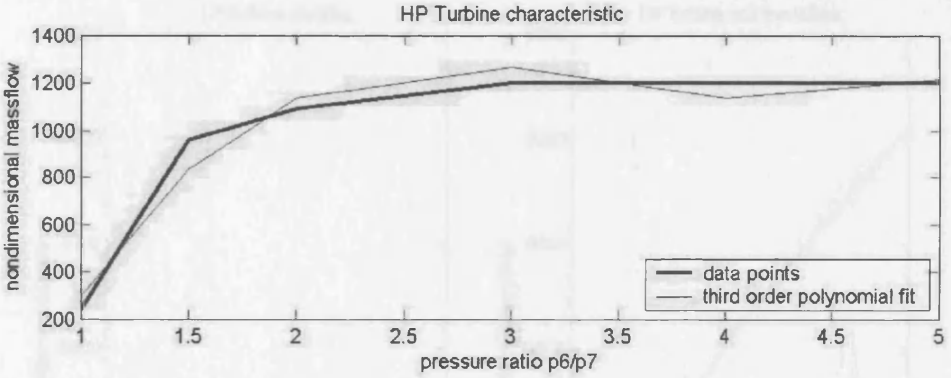
HP Turbine characteristic
nondimensional massflow
pressure ratio p6/p7
data points
third order polynomial fit

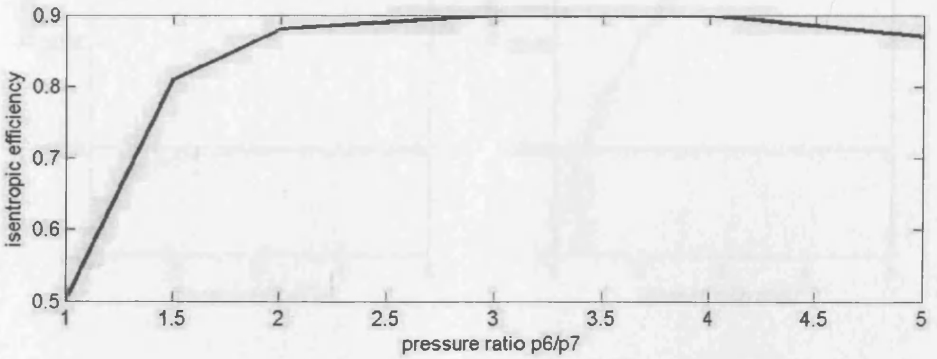
isentropic efficiency
pressure ratio p6/p7

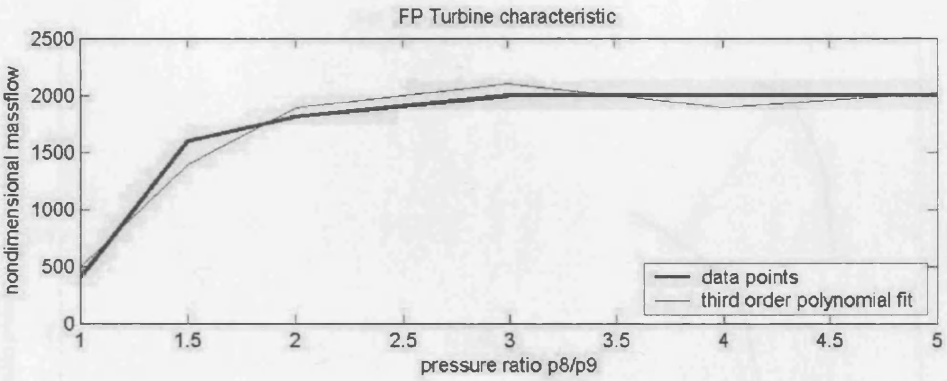
FP Turbine characteristic
nondimensional massflow
pressure ratio p8/p9
data points
third order polynomial fit

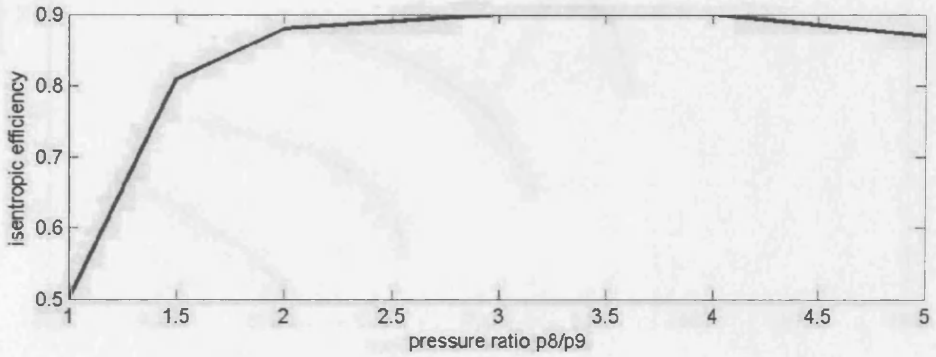
isentropic efficiency
pressure ratio p8/p9

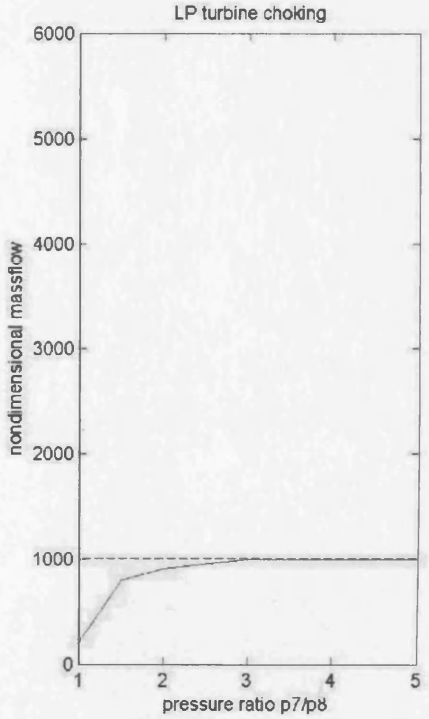
LP turbine choking
nondimensional massflow
pressure ratio p7/p8

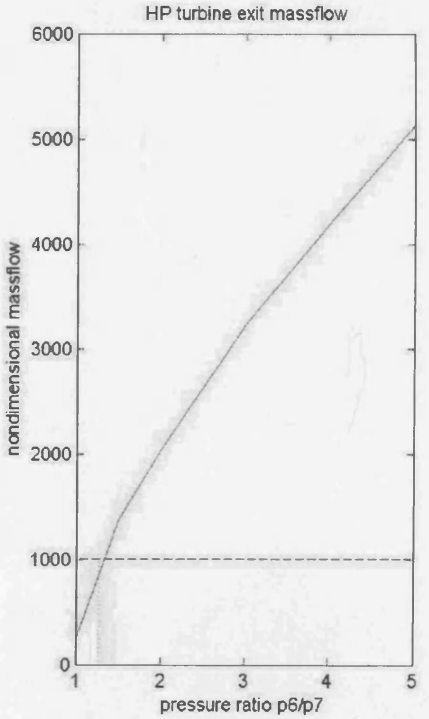
HP turbine exit massflow
nondimensional massflow
pressure ratio p6/p7

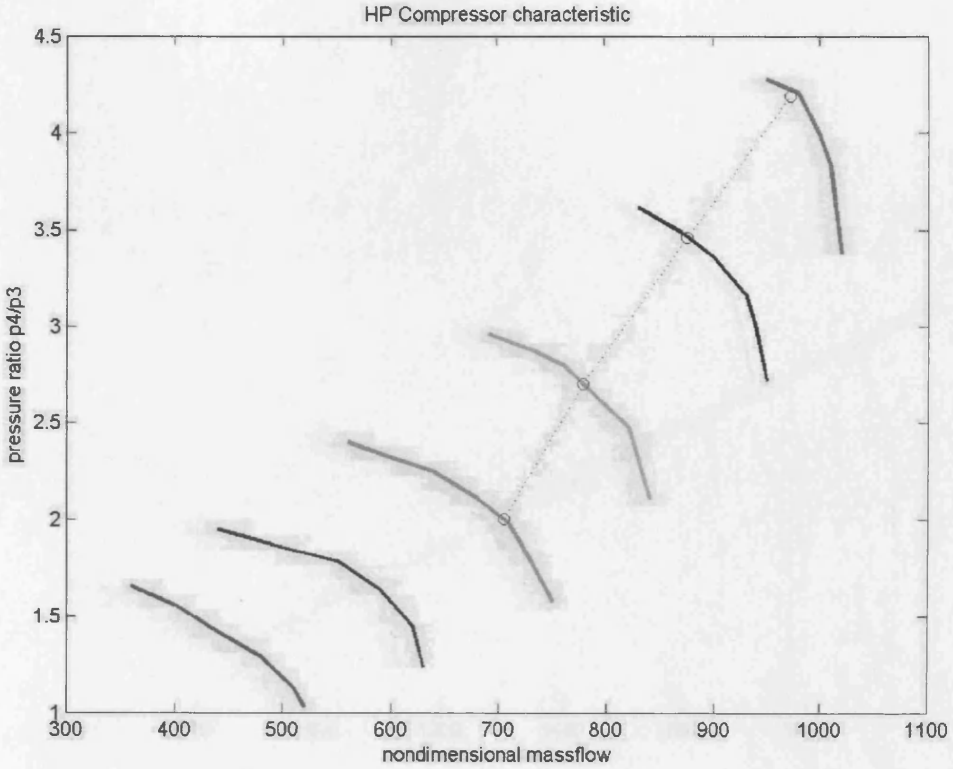
HP Compressor characteristic
pressure ratio p4/p3
nondimensional massflow
4.5
4
3.5
3
2.5
2
1.5
1
300
400
500
600
700
800
900
1000
1100

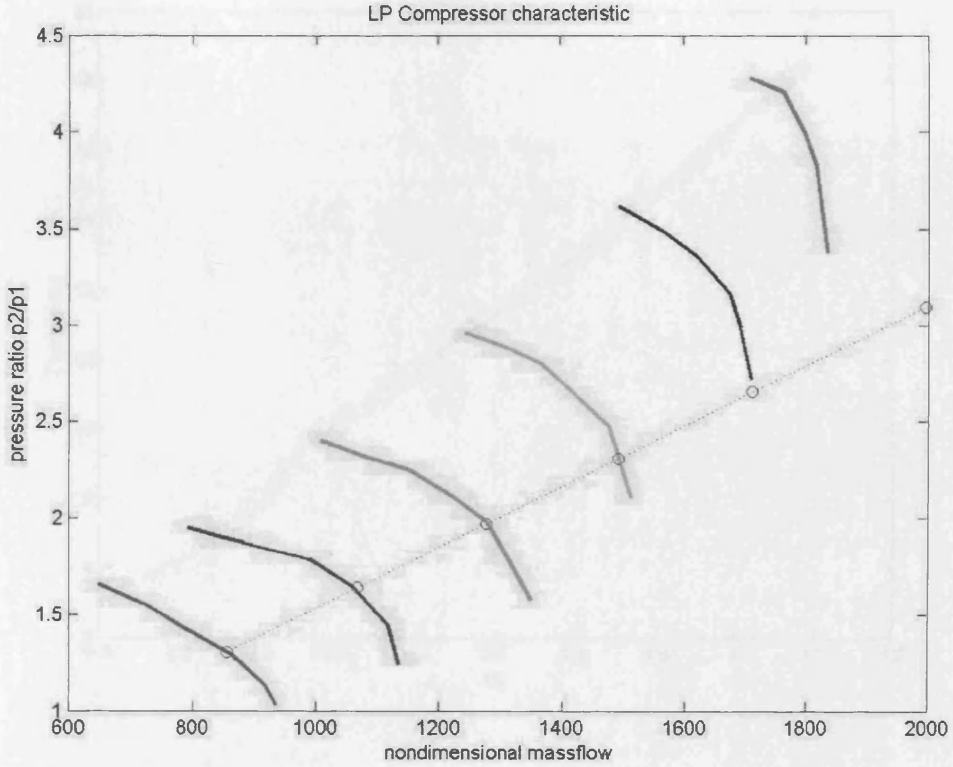
LP Compressor characteristic
pressure ratio p2/p1
nondimensional massflow
4.5
4
3.5
3
2.5
2
1.5
1
600
800
1000
1200
1400
1600
1800
2000

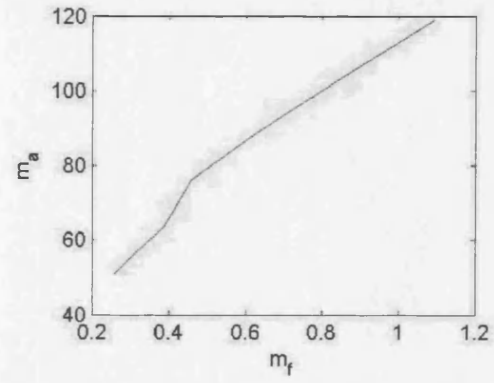
m_a
m_f
120
100
80
60
40
0.2
0.4
0.6
0.8
1
1.2

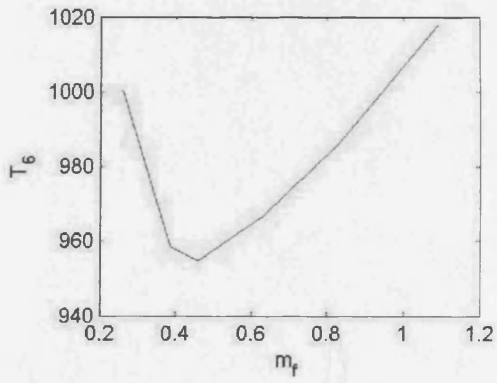
T_6
m_f
1020
1000
980
960
940
0.2
0.4
0.6
0.8
1
1.2

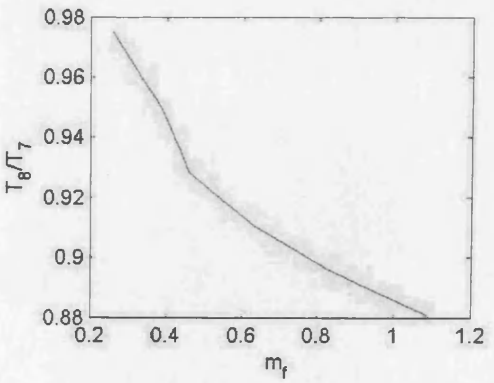
T_8/T_7
m_f
0.98
0.96
0.94
0.92
0.9
0.88
0.2
0.4
0.6
0.8
1
1.2

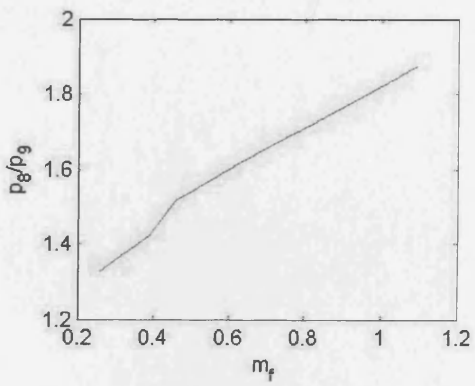
p_8/p_9
m_f
2
1.8
1.6
1.4
1.2
0.2
0.4
0.6
0.8
1
1.2

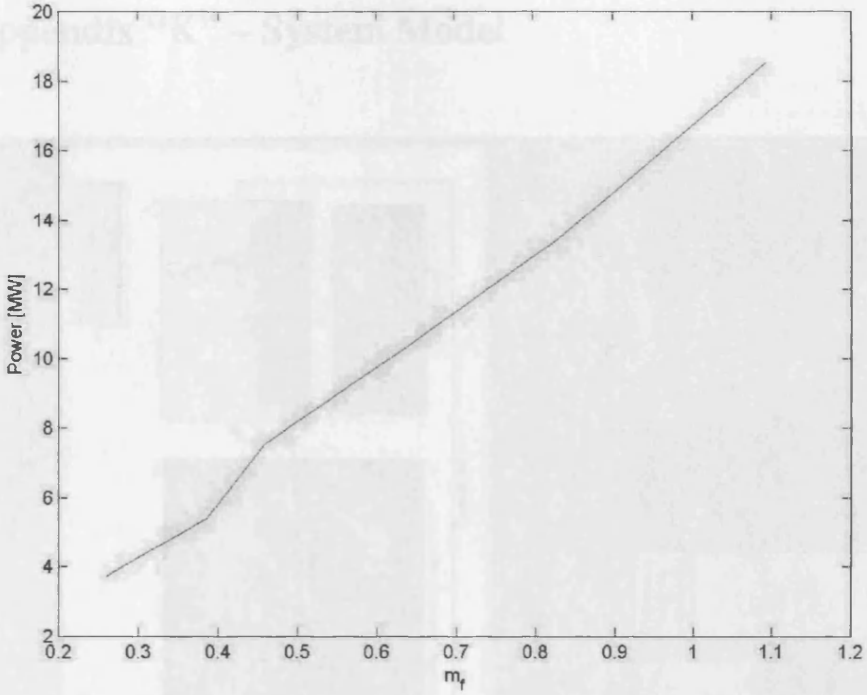
Power [MW]
20
18
16
14
12
10
8
6
4
2
0.2
0.3
0.4
0.5
0.6
0.7
0.8
0.9
1
1.1
1.2
m_f

Appendix "K" – System Model

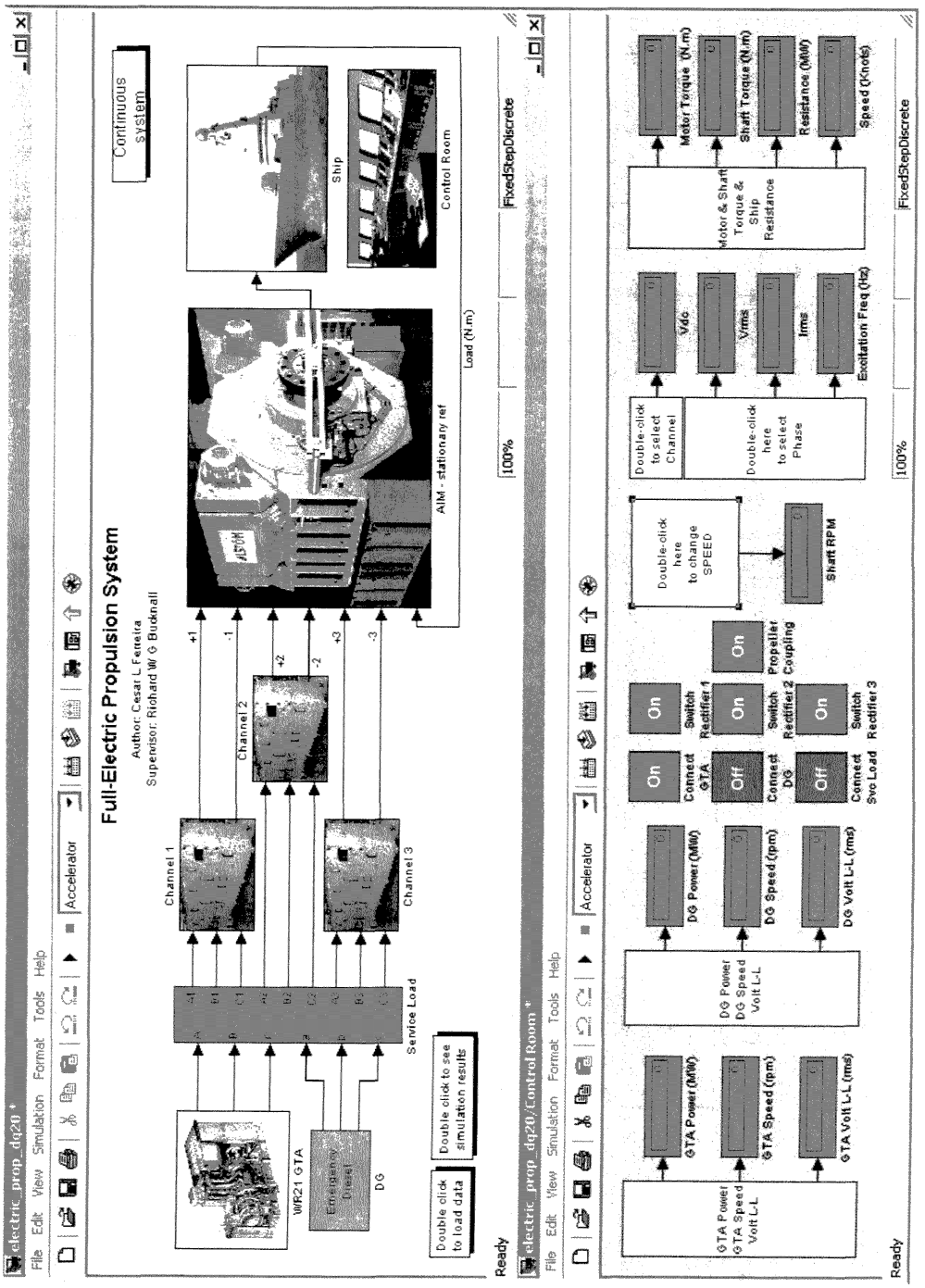

Inside WR21 GTA block:

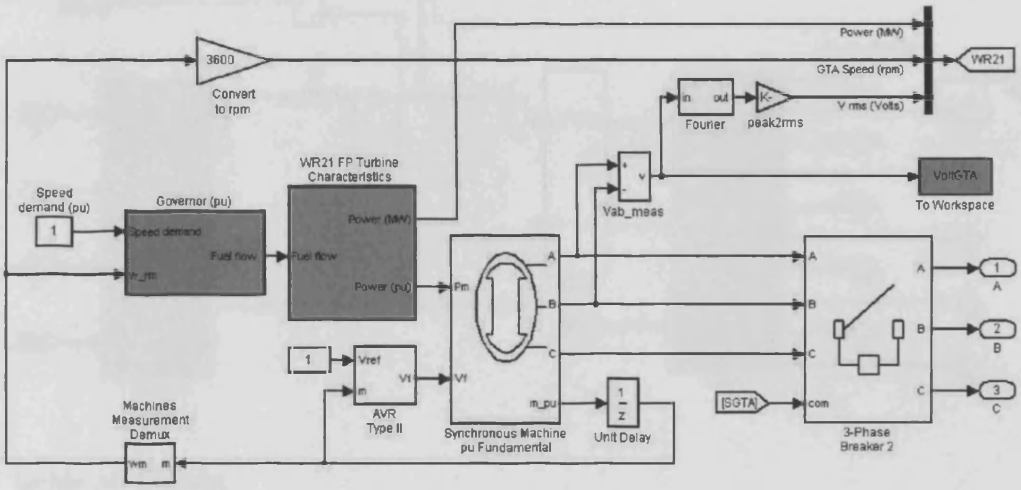

Inside Service Load block:

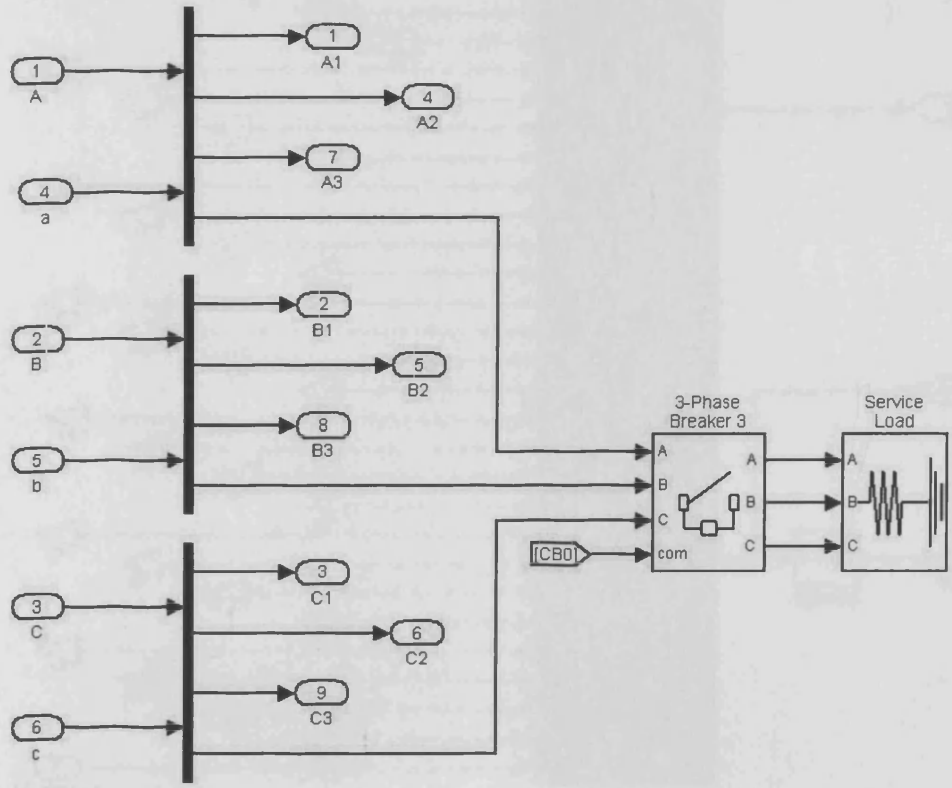

Inside Channel 1 (same as Cannel 2 and 3) block:

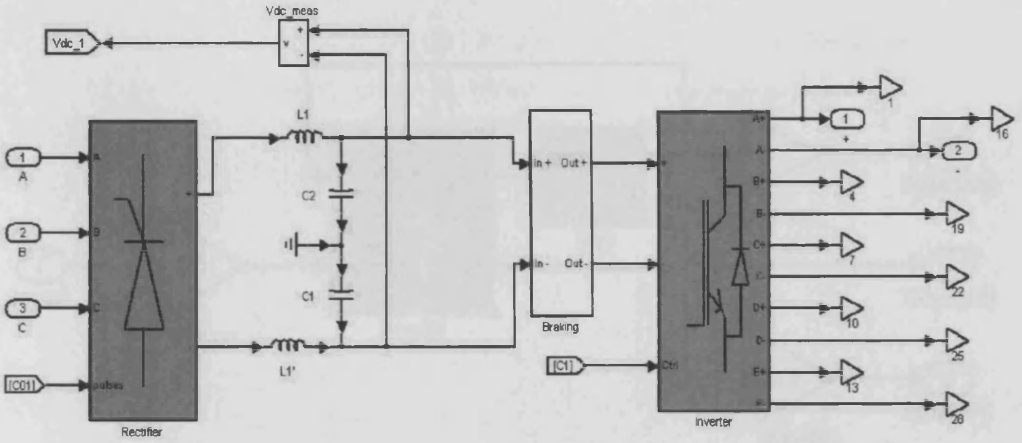

Inside AIM block:

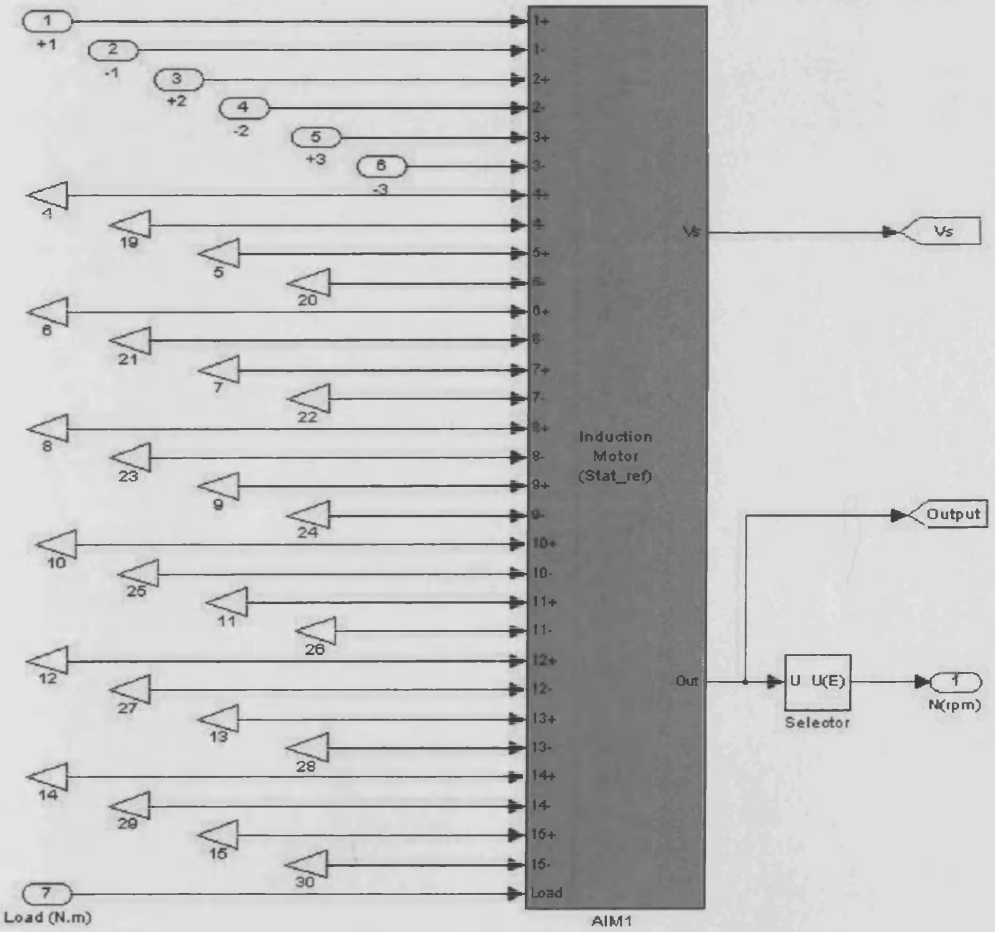

Inside Ship block:

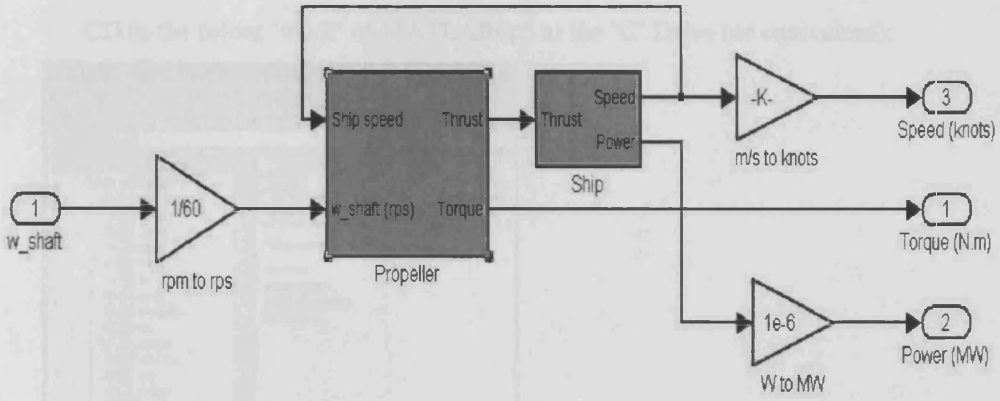

Appendix "L" – Quick-start Guide to the System Model User

1. Install System Model by copying folder 'SystemModel' from the provided CD to the folder 'work' of MATLAB6p5 at the 'C' Drive (or equivalent):

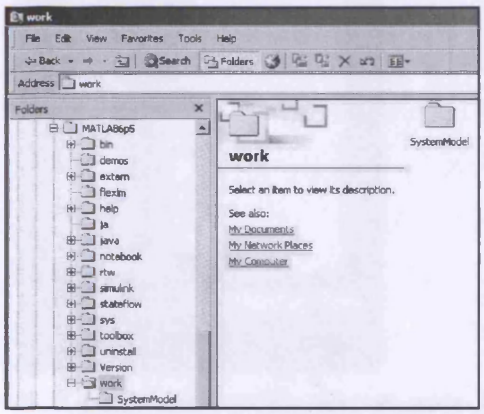

2. Open MATLAB 6.5 Release 13 (or more recent) with Simulink and SimPowerSystems Toolbox available.
3. Set path to new folder:

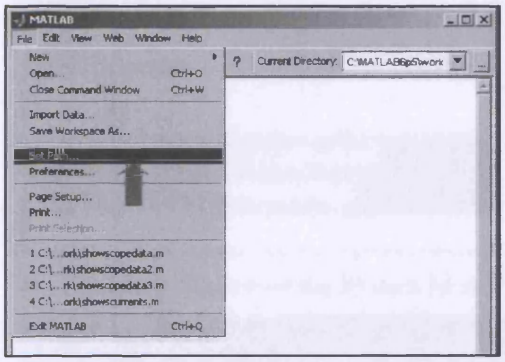

4. Add folder with subfolders:

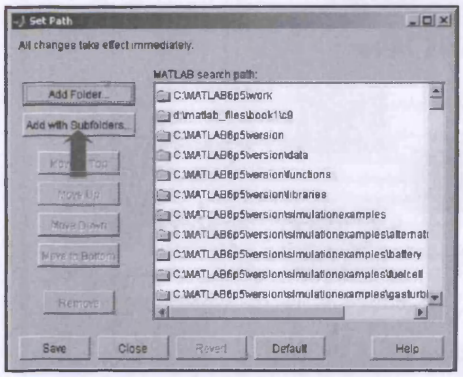

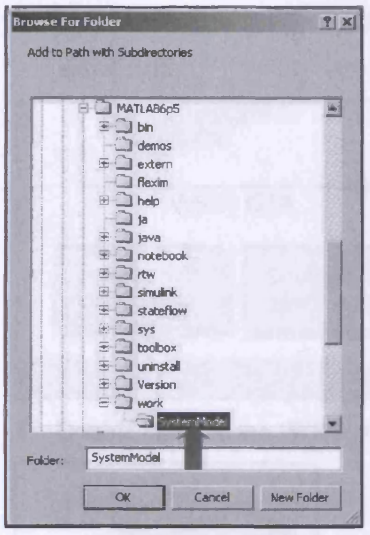

5. Open model from file **electric_prop_dq20.mdl**:

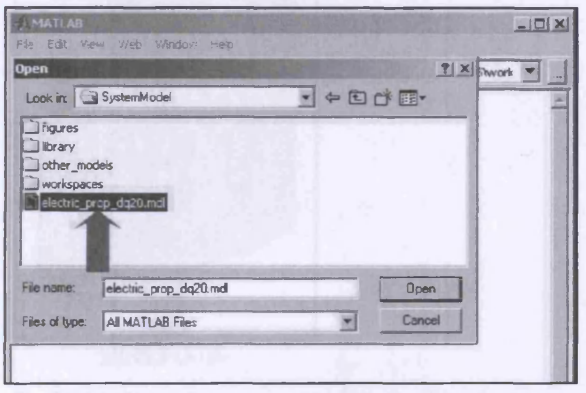

6. The main window of the System Model will pop-up on the screen:

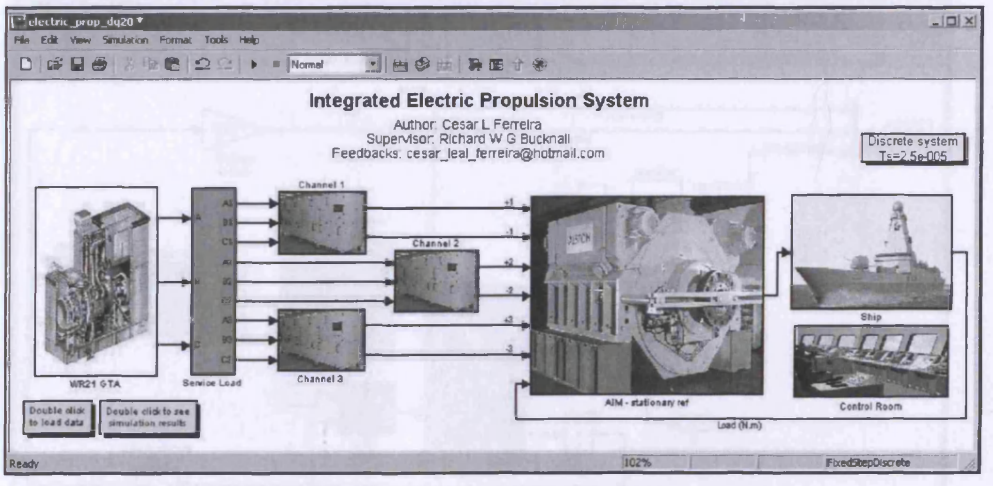

7. Double click on the first yellow box on the left corner of the window to load initial data:

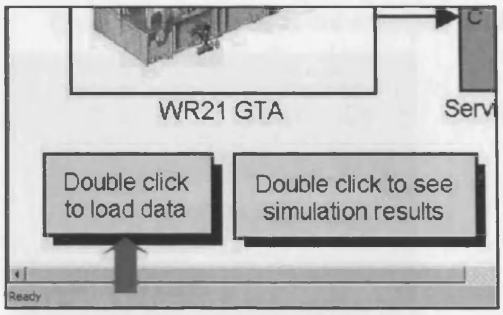

8. Double click on the 'WR21 GTA' box to open subsystem:

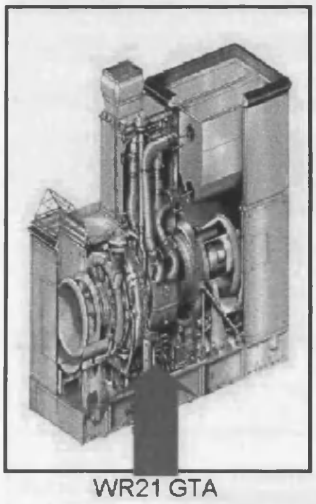

9. Inside the subsystems identify the blocks in magenta colour:

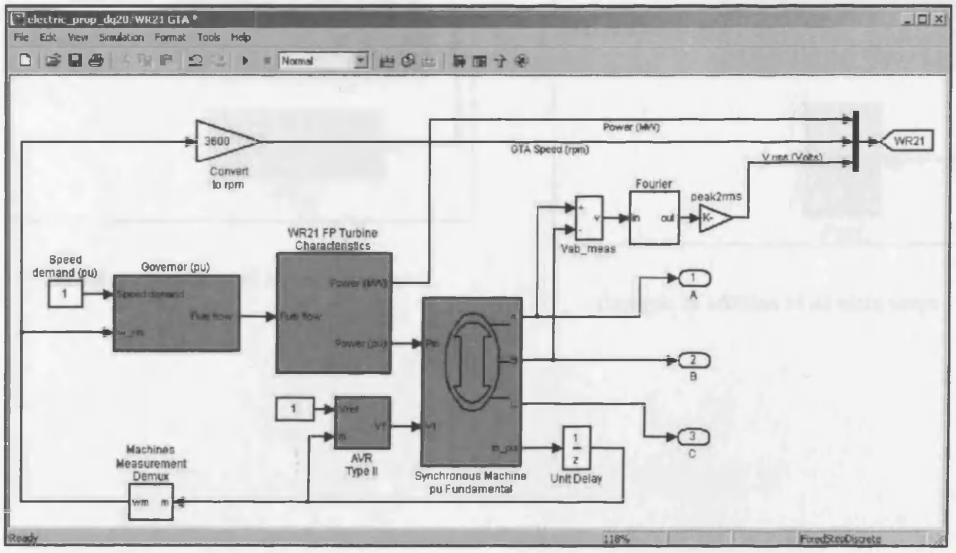

10. These blocks in magenta have tuneable parameters, which can be changed by double clicking on the block. After double clicking on one of the blocks (Synchronous Machine for example), a dialog box will pop-up:

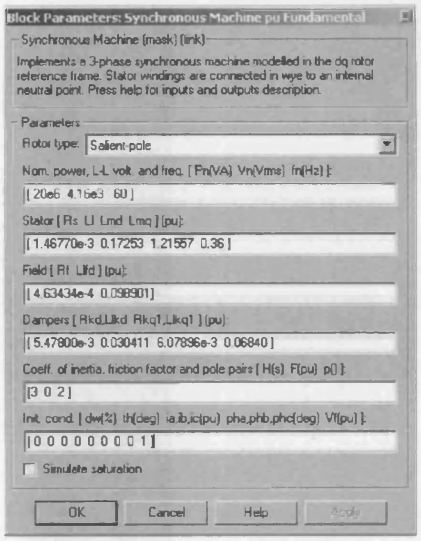

11. Make any changes to parameters (if wished) and click 'OK' to close the dialog box.
12. It is also possible to make changes to the subsystem, by adding or modifying blocks (if wished):

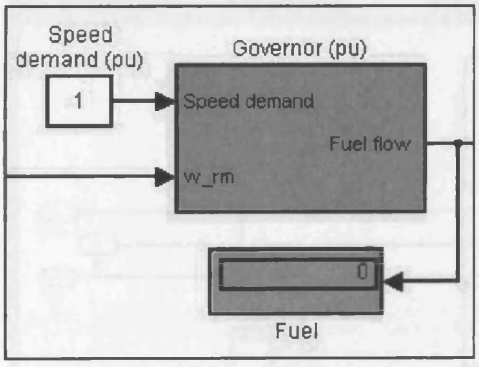

- Example of addition of an extra display

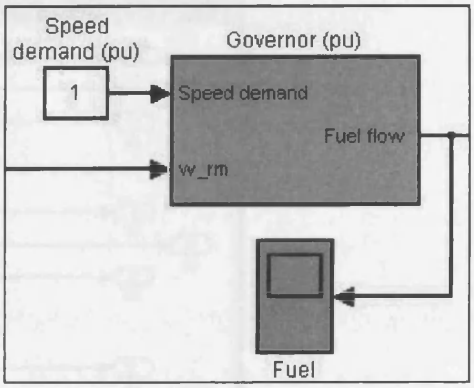

- Example of addition of an extra scope

13. After tuning parameters and changing the 'WR21' subsystem (if wished), close subsystem window and save modified model.
14. Double click on the 'Service Load' box to open subsystem:

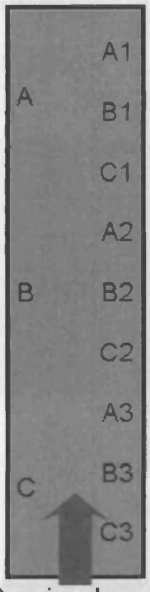

Service Load

15. Identify magenta box, double click on it and change parameters (if wished):

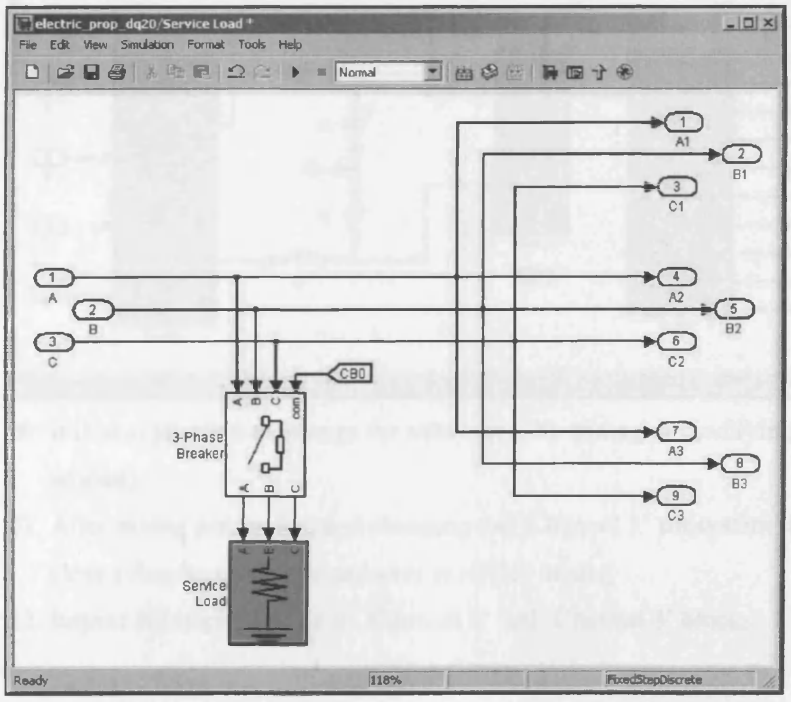

16. It is also possible to change the subsystem, by adding or modifying blocks (if wished).
17. After tuning parameters and changing the 'Service Load' subsystem (if wished), close subsystem window and save modified model.
18. Double click on the 'Channel 1' box to open subsystem:

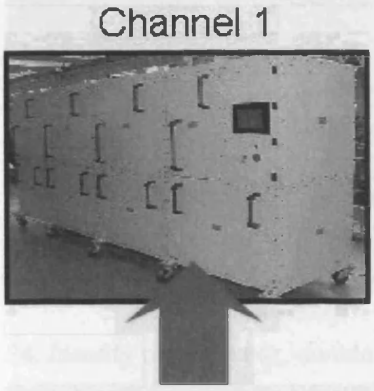

19. Identify magenta boxes, double click on them and change parameters (if wished):

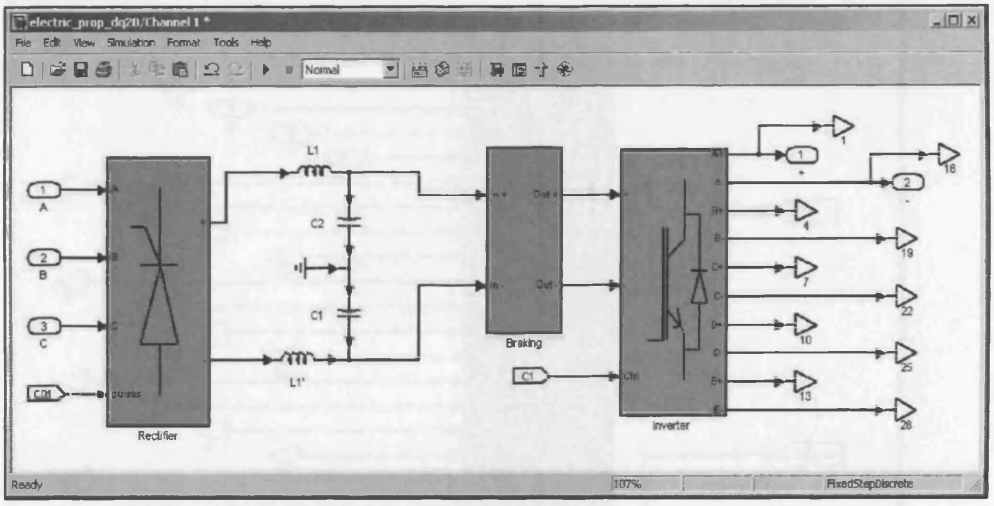

20. It is also possible to change the subsystem, by adding or modifying blocks (if wished).
21. After tuning parameters and changing the 'Channel 1' subsystem (if wished), close subsystem window and save modified model.
22. Repeat the steps 18 to 21 to 'Channel 2' and 'Channel 3' blocks.

23. Double click on the 'AIM' – Advanced Induction Motor box to open subsystem:

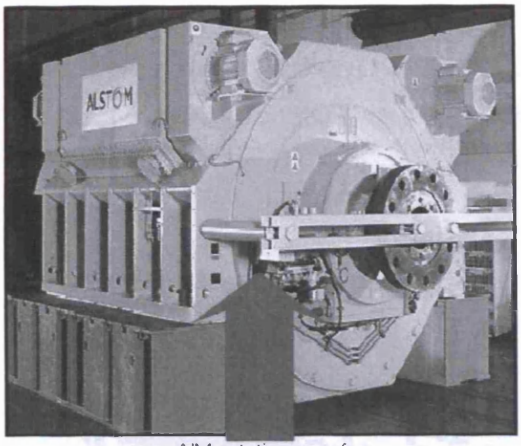

AIM - stationary ref

24. Identify magenta box, double click on it and change parameters (if wished):

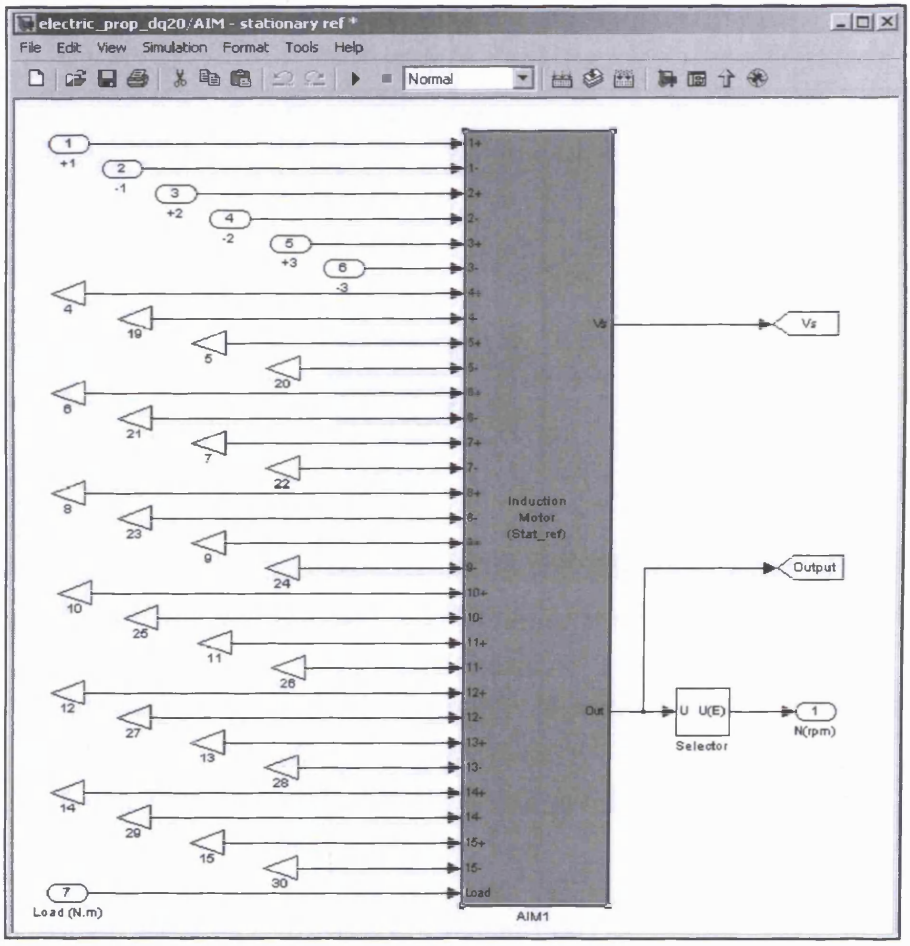

25. It is also possible to change the subsystem, by adding or modifying blocks (if wished).
26. After tuning parameters and changing the 'AIM' subsystem (if wished), close subsystem window and save modified model.
27. Double click on the 'Ship' box to open subsystem:

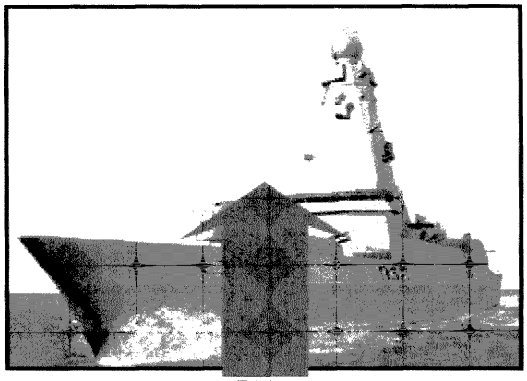

28. Identify magenta box, double click on it and change parameters (if wished):

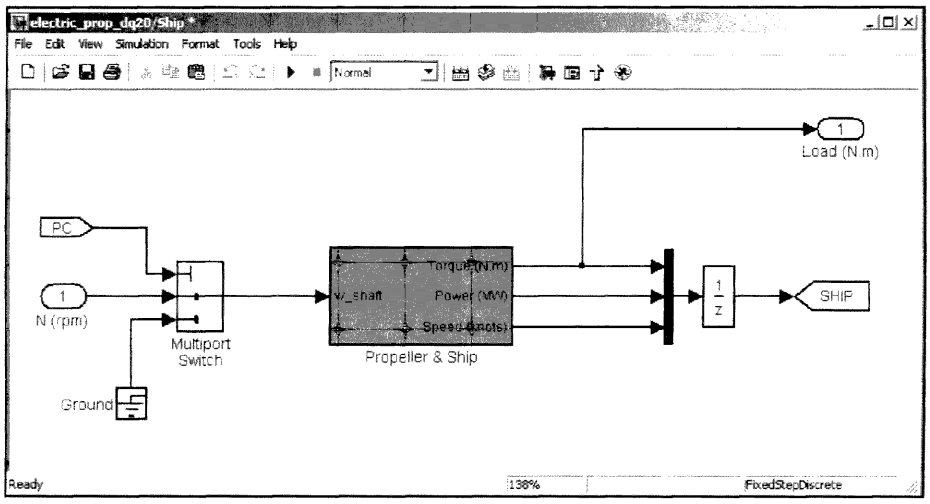

29. It is also possible to change the subsystem, by adding or modifying blocks (if wished).
30. After tuning parameters and changing the 'Ship' subsystem (if wished), close subsystem window and save modified model.
31. Double click on the 'Control Room' box to open subsystem:

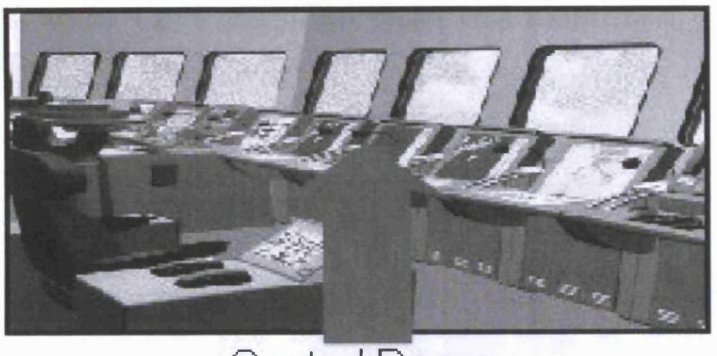

Control Room

32. The window of the 'Control Room' subsystem will pop-up on the screen:

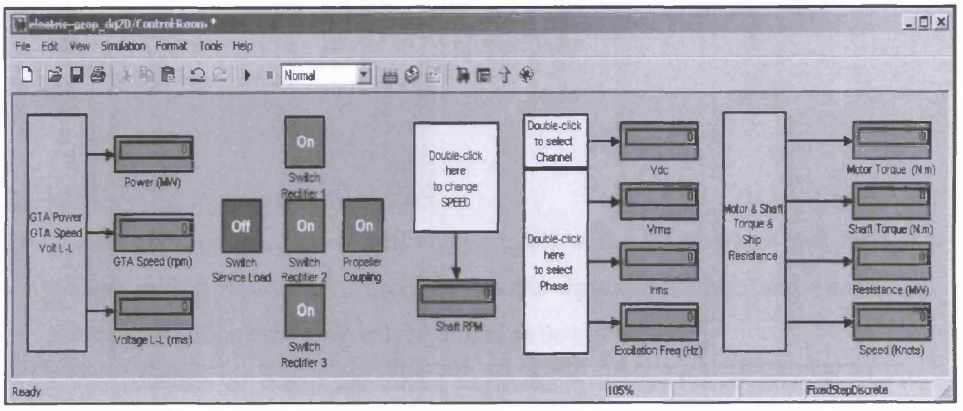

33. Double click on the switch boxes to connect/disconnect service load, switch on/off rectifiers and couple/uncouple propeller:

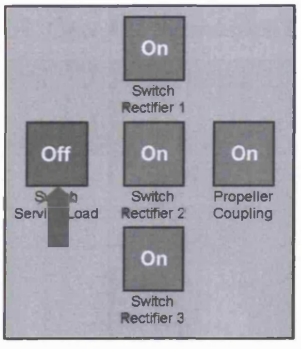

34. Double click on the 'SPEED' yellow box to set shaft rpm.

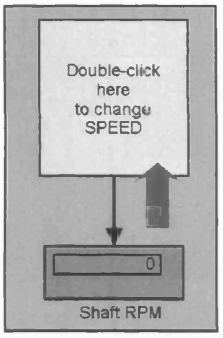

35. Double click on the 'Channel' yellow box to select the Channel which will have voltage visualized on the display; voltage and current curves of the selected Channel will be stored to be plotted later.

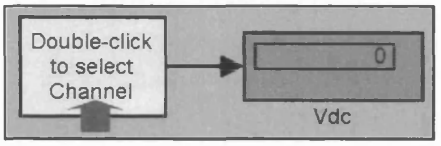

36. Double click on the 'Phase' yellow box to select the Phase which will have voltage and current rms* visualized on the displays; voltage and current curves of the selected Phase will be stored to be plotted later.

* The calculation of voltage and current magnitudes is through Fourier series. Due to imprecise measurement of frequency, these values are not strongly reliable, and consequently must be used only as reference. For precise values refer to curves which are stored during simulation.

37. Open the 'Simulation parameters' box:

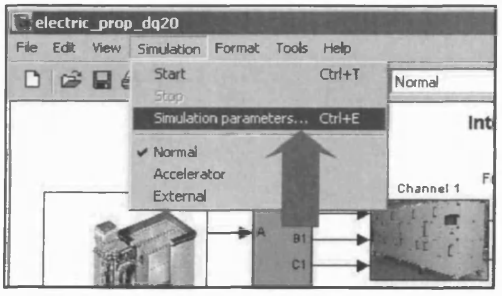

38. Select the simulation time, by entering start time and stop time; stop time can be set **inf** (infinity), and then the simulation will keep running until stopped manually:

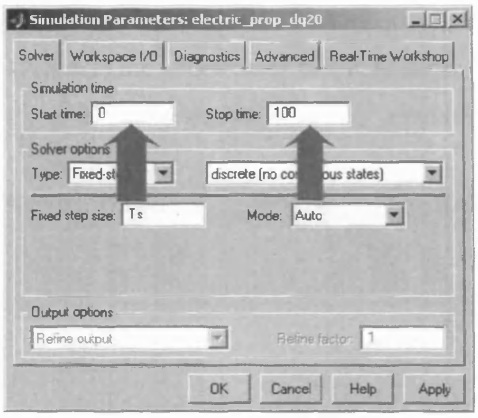

39. Make sure that the solver option is **fixed-step** type – **discrete (no continuous states)**, the step is set to **Ts** and the mode is set to **auto**.

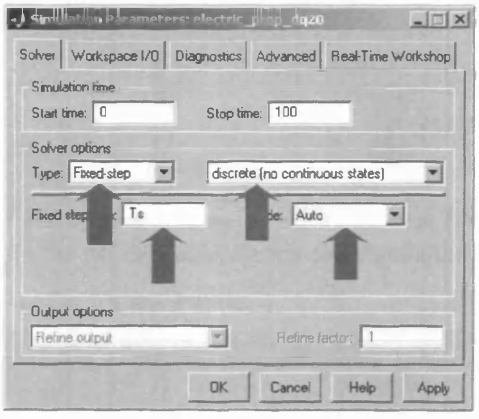

40. It is possible to save the final states for the current simulation to apply them subsequently, in a second simulation, resuming from the point it stopped in the first one. To enable this feature check the **'save to workspace – final state'** box and select **structure with time** format.

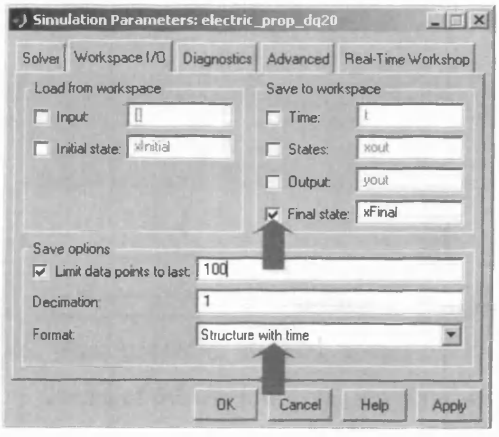

41. Close the Simulation Parameters window by clicking on the 'OK' button.
42. Select the **accelerator** mode, to allow pre-compilation of the model, resulting in a faster simulation (only available if Real-Time Workshop add-on is installed):

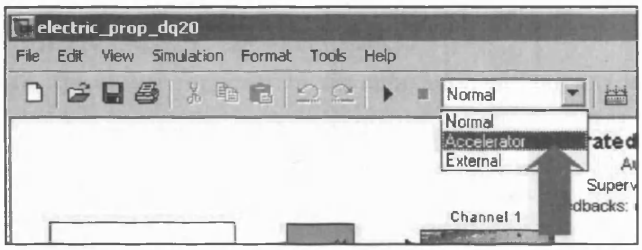

43. Start the simulation, by clicking the 'play' button:

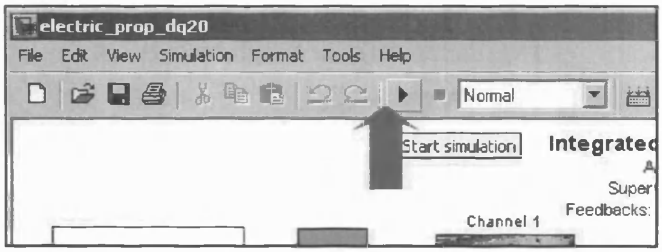

44. At any moment during the simulation it is possible to pause, by clicking on the 'pause' button:

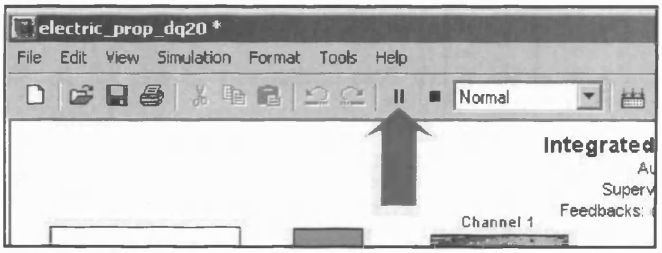

45. At any moment during the simulation it is possible to stop, by clicking on the 'stop' button:

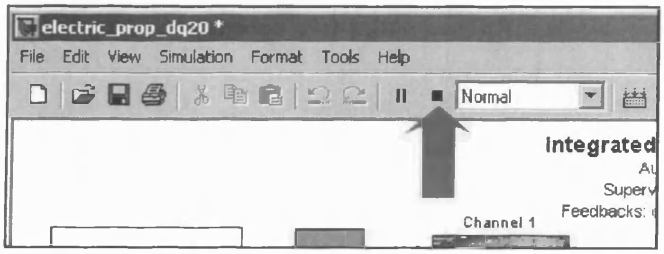

46. When paused or stopped, double click on the second yellow box on the left corner of the window to see the simulation results (partial or final):

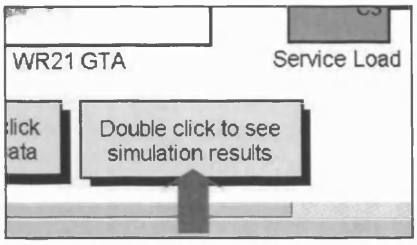

47. The curves generated by the simulation will pop-up on the screen:

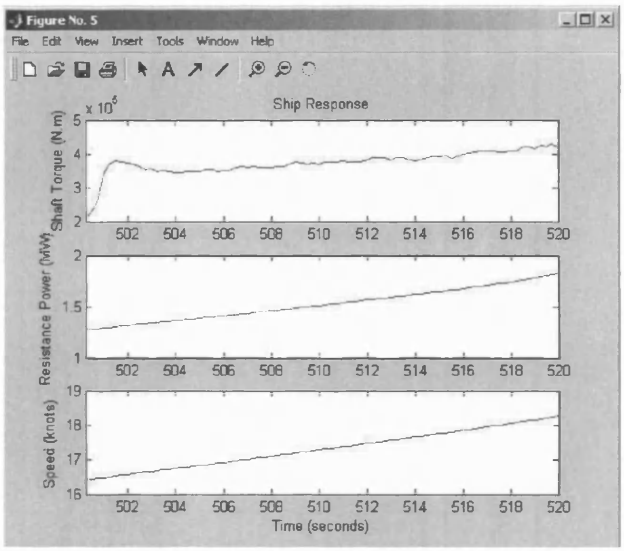

48. At the end of simulation, save the resulting workspace in the appropriate folder.